OLLSCOIL NA GAILLIMHE
UNIVERSITY OF GALWAY

Mediated glucose biosensors for application in continuous glucose monitoring

Submitted by:

Kavita Jayakumar, MSc.

Thesis is submitted for the Doctor of Philosophy (PhD) degree by research of the University of Galway

School of Biological and Chemical Sciences

Supervisor: Professor Dónal Leech

December, 2022

Declaration

The contents of this thesis, except where otherwise stated, are based entirely on my own research which was carried out in the Biomolecular Electronics Research Laboratory based in the School of Biological and Chemical Sciences and Ryan Institute, University of Galway, Ireland. I have not obtained a degree at University of Galway or any other university on the basis of this research.

Kavita Jayakumar

December 2022

Acknowledgments

I would like to express my gratitude to all those who helped me throughout my PhD.

First, all work presented in this thesis was supported by funding from the European Union's Horizon 2020 research and innovation programme under grant agreement Nº813006.

I would like to thank my supervisor, Prof Dónal Leech, for selecting me to be a part of his research group and offering me the position of ESR 5 in the ImplantSens ITN. I was a young inexperienced student at the beginning of this journey and appreciate the chance you took on me. You always allowed me to investigate my interests even when they took me down a path far from electrochemistry and used your connections to reach out to collaborators for me. You pushed me to my limits and made me strive to fully realise my ambitions.

Thank you Prof. Wolfgang Schuhmann, director of ImplantSens for all your help. For being open to virtual collaborations during COVID-19, and always finding unique methods to reach our goals and deadlines despite the interruption of a global pandemic.

I must mention the ImplantSens network, with its training programmes and network meetings – educational but fun at the same time. A special mention to Sabine Seisel, the administrative coordinator of ImplantSens for all her help, especially with visas and planning.

I am exceedingly grateful to all my colleagues from ImplantSens. It's truly been an experience to go through a PhD together. Merve, thank you for all the conversations, coffees and sangria nights on every visit to Madrid for vacation. Anna L, my favourite collaborator – I loved going down research spirals with you, during your visit to Galway and mine to Bochum. It's not often you find someone who is on the same wavelength as you and I was thrilled to find a partner in crime. You made all the deliverables and deadlines enjoyable. Carolin Psotta, thank you for all your help during

my trip to Malmo. But mostly for all the memes and commiseration during every roadblock during this journey.

I must also take the time to thank Garry Duffy for all the advice. For taking the time to explain what goes on in the body to a novice like me, and all the ideas on how to mimic that *in vitro* for testing. For allowing me into your lab to test some theories. Ruth Levey for all her help with the actual tests and for always catching up with coffees or beers at the college bar.

Marta and Lorenzo, lovely friends that gave me a mountain of support and helped me create many fond memories here in Galway. Finally, to my partner Dani. When we made the decision to move here to Ireland for our respective PhDs, we had no idea what to expect. We knew it would be hard and stressful, but life has a way of surprising you. After all, no one could predict a global pandemic. Out of all the things I've learned during this PhD, one of the best is that I've found a partner for life. My best friend, the person I want to share everything and can rely on, the one who makes every day better than the last. You have been a superstar- an endless source of support and my best friend, all the while dealing with your own struggles and successes. You always managed to make me laugh, even when science made me want to cry. It's even more poignant knowing that there were a few times where you spent hours cheering me up even when you had a terrible day yourself. There are not enough words to describe how much I appreciate everything you've done in the last few years and how grateful I am that we could experience this together.

Table of Contents

Abstract

Diabetes affects 1 in 11 people globally and requires monitoring of blood glucose levels as a part of its treatment. Initial blood glucose monitoring devices involved finger prick testing at regular intervals daily, a self-monitoring strategy reliant on patient compliance. Advances in technology have facilitated continuous glucose monitors (CGMs), (semi-) implantable devices that can monitor glucose levels in vivo and transmit the data to mobile applications. Majority of commercial CGMs are electrochemical in nature and meet the requirements for a commercial sensing implant. There are three main factors that limit CGMs for in vivo use – namely oxygen dependence, low molecular weight (LMW) materials and foreign body response (FBR) – which negatively affect the lifetime and accuracy of CGMs. This thesis aims to detail strategies to combat these issues, building on previous work performed in the field of enzymatic electrochemical glucose sensors.

Chapter 2 details the use of design of experiments (DoE) to optimise enzyme electrode components – Osmium complex-based redox polymer, commercial glucose oxidising enzyme (glucose oxidase, GOx) and crosslinker (polyethylene glycol diglycidyl ether, PEGDGE). Previous work established high current and stability of a similar system which also incorporated acid treated multiwalled carbon nanotubes (MWCNTs) as a nanosupport. The MWCNTs enable high currents and surface coverages, but the quantities required were quite high, which can be detrimental for in vivo applications. In this chapter, the grafting of enzyme to nanosupport was carried out to allow minimisation of MWCNT amounts while retaining high currents and operational stability. DoE facilitated the determination of electrode component amounts for optimal current density and stability. The optimised enzyme electrodes show a current density of 3.18 ± 0.30 mA cm^{-2}, representing a 146% increase in current density in 50 mM phosphate-buffered saline at 37 °C containing 5 mM glucose when compared to similar systems where enzyme and nanosupport are not grafted to each other. Using the predictive DoE model, component amounts were then modified to minimise the quantity of the enzyme-MWCNT nanoconjugate, resulting in a biosensor which showed similar electrochemical behaviour and current density to the optimised system while using 93% less of the nanoconjugate.

Commercial GOx shows excellent behaviour for glucose oxidation but uses oxygen in its half reaction to regenerate. This is problematic as in vivo oxygen levels can fluctuate resulting in errors in measurement. Additionally, enzyme regeneration by oxygen reduction gives hydrogen peroxide as a product. Peroxide can cause enzyme instability as it oxidises the methionine residues of the enzyme, decreasing its activity. To combat this use, GOx was replaced with engineered cellobiose dehydrogenase (CDH) in Chapter 3. CDH is a dehydrogenase and thus does not use oxygen in its half reactions and has been modified to selectively choose glucose as its substrate. The enzyme electrodes comprising osmium complex-based redox polymer, CDH and PEGDGE were optimised with DoE, while a direct electron transfer (DET) based system was also optimised through conventional methods. The resulting sensors had sensitivities in the same order of magnitude as those in literature. Most importantly, sensor signals showed no difference in the presence and absence of oxygen. The sensors derived from CDH were shown to be specific to glucose over other clinically relevant in vivo sugars and selective, i.e., capable of glucose sensing in the presence of interfering species present in complex media.

While no individual species is classified as an interferent in complex media they seemed to exhibit a cooperative effect resulting in a minimisation of current (43%). This is usually overcome with the use of polymer coatings. However, polymer coatings themselves lead to reduced sensor signals on their application, due to the formation of a diffusion barrier. Chapter 4 focuses on the design of polymer coatings to enable protection against biofouling while retaining current density. This was done by designing polymer coatings with a compatible epoxy crosslinking moiety on the polymer backbone that could crosslink with the redox polymer used in the sensing layer. The polymers selected in this study were zwitterionic in nature because of their inherent ability to minimise biofouling. Protein adsorption and cell adhesion studies, using fibrinogen and fibroblasts respectively, allowed a screening to select the most effective of the synthesised polymers for biofouling resistance. This poly(2-methacryloyloxyethyl phosphorylcholine-*co*-glycidyl methacrylate (MPC)-type polymer showed similar biofouling resistance compared to commercial polymer Lipidure with ~50% reduction in fibrinogen adsorption and ~80% reduction in fibroblast adhesion. When used as coatings for glucose biosensors fabricated in

Chapter 3, MPC showed ability to resist protein adsorption while retaining current density similar to a non-coated system with 1.5-fold increase in sensitivity.

MPC polymers showed ability to impart biofouling resistance while maintaining current signals. Nevertheless, their ability to resist LMW materials was not proved. In Chapter 5, a series of different protective strategies were explored to determine which approach would be the best to protect from biological and LMW interferences. Enzymatic scavenging using enzymes that target LMW species was investigated but showed inefficient scavenging, likely due to low enzymatic activity. Polymer multilayer approach with successive anionic and MPC polymer layers was utilised and showed the best potential. MPC as the outerlayer showed biofouling resistance whereas an anionic interlayer ([Poly(1-vinylimidazole-co-4-styrene sulfonic acid sodium salt hydrate], P(VI^1-$SSNa^1$)) inhibited anionic LMW species such as uric acid and ascorbic acid which cause interference. Moreover, due to the compatible crosslinking sites, the layers intermix at the boundary between them, minimising diffusional barrier and allowing current signals similar to a non-coated system. This multilayer protection system extends linear range and enables higher current and stability than a non-coated system in 50 mM phosphate-buffered saline and artificial plasma. Chapter 6 summarises the results from Chapter 2-5 and highlights the significant conclusions that can be drawn from these results. Future directions that can improve on the strategies in this thesis are also discussed

Chapter 1: Introduction

1.1 Diabetes

Diabetes is a chronic metabolic disease occurring due to a disturbance in insulin secretion and/or action. Type 1 diabetes (T1D) is characterised by deficient insulin secretion by the pancreas due to autoimmune destruction of insulin-producing ß-cells and can be treated by exogenous administration of insulin, whereas type 2 diabetes (T2D), the onset of which is often facilitated by poor daily habits such as physical inactivity and unhealthy diet, is characterised by inefficient insulin action[1]. In diabetics, blood glucose concentrations tend to exceed the safe range leading to hyperglycaemic events that can cause severe long-term damage such as retinopathy and cardiovascular diseases, mitigated by insulin injections. Diabetes can be managed by exogenous administration of insulin, aiming to improve the control of the patient's blood glucose levels. However, incorrect administration can be dangerous in the short term and can lead to coma or even death [1,2]. Therefore, it is important to monitor blood glucose levels in conjunction with insulin treatment to mitigate the effects of diabetes without causing adverse side effects. According to the latest World Health Organisation report, the number of people with diabetes has increased from 108 million in 1980 to 537 million in 2021. This means that about 8.5% of adults aged 18 years and older had diabetes, and this number is expected to rise to 783 million by 2045[3]. Research efforts over the past decades, focused on improving glucose monitoring techniques in conjunction with technological advances, have enabled the evolution of glucose monitoring from rudimentary finger prick tests, requiring patients to self-measure their blood glucose 3 to 4 times a day, to (semi-)implantable continuous glucose monitors (CGMs) paired with mobile applications where algorithms and wireless transmission facilitate glucose monitoring without burden to the patient. Such feedback on changes in body chemistry has far-reaching implications for the treatment of various diseases. The treatment of diabetes is thus the first example of individualised (personalised) medicine[4].

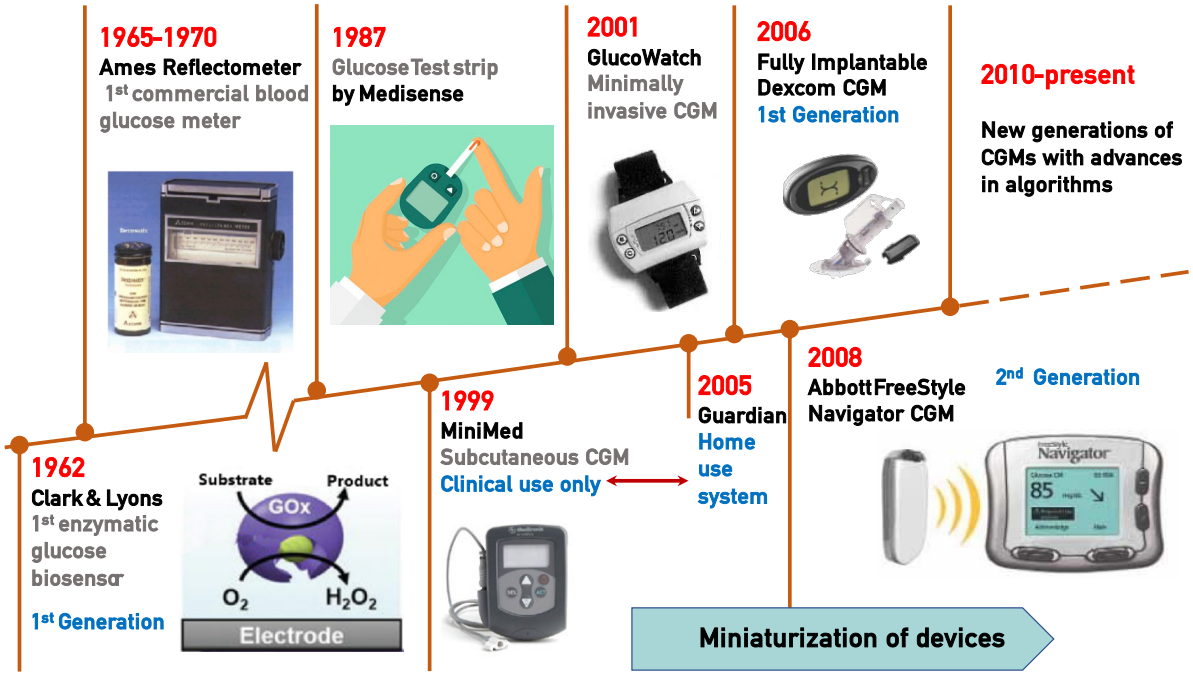

Figure 1.1: History of a few key achievements in glucose sensing

Clark and Lyons first introduced the concept of an electrochemical glucose sensor based on the oxidation of glucose to gluconolactone by oxygen, catalysed by glucose oxidase, producing hydrogen peroxide as a by-product [5]. Since oxygen is ubiquitous in both tissues and the atmosphere, it is ideal as the natural co-substrate for regeneration of the enzyme. The original concept was that monitoring oxygen consumption by reducing oxygen at a platinum electrode would detect a current proportional to the glucose concentration. This method of indirect glucose monitoring forms the first generation of glucose sensors. An advantage of these first-generation electrochemical sensors is the relatively simple technology required for the readout electronics and miniaturisation. The concept of electrochemical biosensors based on Clark's original work took two routes: glucose strips for self-monitoring of blood glucose (SMBG) and continuous glucose monitoring (CGM) systems. Shichiri *et al.* took the first step towards CGM by implanting a subcutaneous glucose sensor in dogs for 7 days [6] and used the oxidation of hydrogen peroxide, which is produced during the regeneration of the enzyme, as the target electrochemical reaction for detection of glucose.

In 1965, Ames developed the first blood glucose test strip[7], called Dextrostix, which used glucose oxidase and detected colorimetric changes. This early strip was intended for clinical use. To convert it into a self-monitoring device for home use, Anton Clemens [8] filed the first patent in the United States in 1971 for the Ames Reflectance Metre (AMF), which was intended for reliable point-of-care use by diabetics. This glucose metre was used in conjunction with Dextrostix and required a small volume of blood (about 50-100 μL). Blood glucose was calculated from a table by interpreting the visible colour change. In 1987, Medisense launched a series of glucose test strips based on glucose oxidase combined with a ferrocene mediator as electrochemical SMBGs to compete with Dextrostix[9,10]. These strips, where an organometallic mediator replaced oxygen/hydrogen peroxide, forms the second generation of glucose sensors.

MiniMed (later acquired by Medtronic) produced the first approved CGM for clinical use in 1999. Subsequently, Medtronic developed a home use CGM (Guardian), based on the same technology, which was launched in 2005[11]. The GlucoWatch biographer by Cygnus, which is considered "minimally invasive" because it did not pierce the skin [12], was introduced in 2001. However, the reverse iontophoresis sampling method caused significant skin irritation. In addition, the system was designed to shut down if excessive sweating was detected, which is common in hypoglycaemia. These two factors resulted in a commercially unviable product and this model was withdrawn from the market. Dexcom, a company founded on the basis of peroxide oxidation for blood glucose monitoring, released a transcutaneously implanted sensor that was approved for home use in 2006[13]. Adam Heller founded Therasense with his "wired" osmium complex-mediated technology and developed a glucose strip system while working on a CGM system. Abbott bought Therasense and acquired both the strips and the CGM technology and released their Navigator CGM in 2008[14]. Later generations of Guardian and Navigator CGMs with improved algorithms have since joined the market. There are currently seven CGMs on the market, six of which are based on enzymatic glucose conversion and electrochemical detection [14–19].

1.2 The generations of glucose biosensors

One of the main concerns in the selection of enzyme catalysts for biosensors is efficient electron transfer between the active site of enzyme and the electrode surface. There are three generations in the development of glucose biosensors. The first generation relies on the use of the natural co-substrate of glucose oxidase (GOx), oxygen, and the production and detection of hydrogen peroxide. This technology was the basis for the first glucose test strips, subcutaneous[6] and fully implanted glucose meters [11].

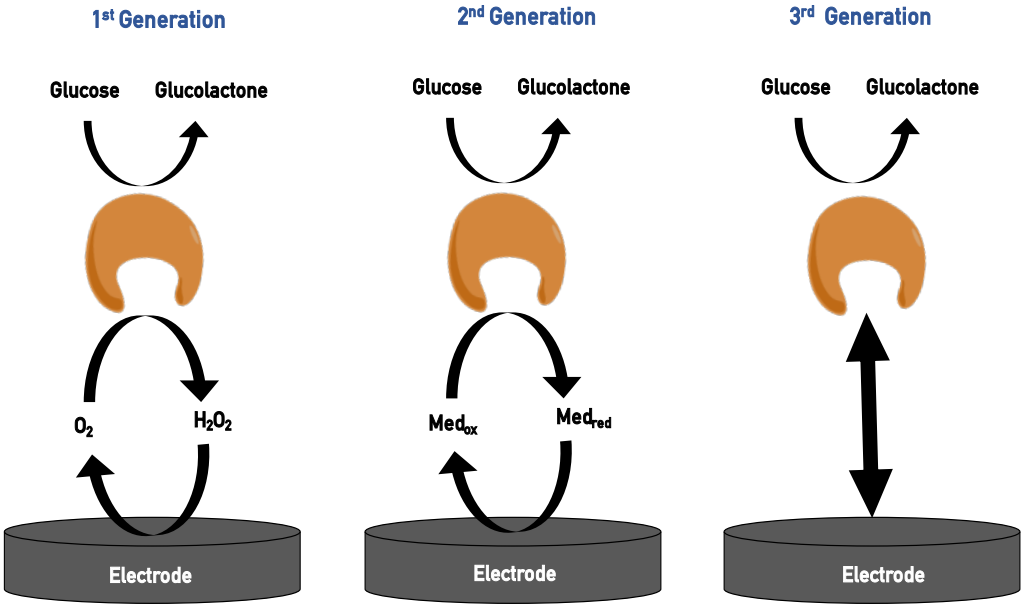

Figure 1.2: Generations of electrochemical glucose sensors and their mechanism of action.

If we take an example of a general glucose-oxidising enzyme, it oxidises glucose to glucolactone, undergoing reduction in the process (Equation 1.1). In the case of a first generation sensor and if the enzyme is an oxidase, the enzyme is regenerated or re-oxidised in the presence of oxygen (O_2) (Equation 1.2), forming hydrogen peroxide (H_2O_2) in the process (Equation 1.3).

$$\text{Glucose} + \text{Enzyme}_{ox} \rightarrow \text{Glucolactone} + \text{Enzyme}_{red} \qquad \text{Equation 1.1}$$

$$\text{Enzyme}_{red} + O_2 \rightarrow \text{Enzyme}_{ox} + H_2O_2 \qquad \text{Equation 1.2}$$

$$H_2O_2 \rightarrow 2H^+ + O_2 + \text{Enzyme}_{ox} \qquad \text{Equation 1.3}$$

The preliminary versions of first-generation sensors actually measured the consumption of oxygen (i.e., the decrease in O_2 concentration). To ameliorate the sensor performance, the oxidation/production of H_2O_2 (Equation 1.3) was measured at the electrode, as it has a proportional relationship to concentration of glucose. However, there are two major limitations to these first generation sensors. First, oxygen concentrations may vary *in vitro* and *in vivo*, leading to errors in measurement. Second, the high polarisation voltage (0.6 V vs Ag/AgCl) required to oxidise H_2O_2 can trigger co-oxidation of other endogenous or exogenous species such as ascorbic acid (AA), uric acid (UA) or acetaminophen, which can interfere with the sensor response. To overcome these selectivity issues, the second-generation sensors employ a non-physiological, 'artificial', electron acceptor, classified as a mediator (Med), to transport electrons and solve the issues of oxygen deficiency and co-oxidation. This is achieved with a general mediated reaction shown in Figure 1.2 and Equation 1.4. This was the basis for the MediSense glucose test strips[9].

$$\text{Enzyme}_{red} + \text{Med}_{ox} \rightarrow \text{Enzyme}_{ox} + \text{Med}_{red} \qquad \text{Equation 1.4}$$

$$\text{Med}_{red} \xrightarrow{\text{Electrode}} \text{Med}_{ox} + e^- \qquad \text{Equation 1.5}$$

In second-generation sensors, a mediated electron transfer (MET) pathway is followed. The mediator replaces oxygen. The enzyme-substrate reaction (Equation 1.1) remains the same. The reduced enzyme is regenerated by the mediator, which undergoes reduction in the process (Equation 1.4). The reduced mediator (Med_{red}) transfers electrons to the electrode (detected as current) and is regenerated according to Equation 1.5. Thus, the mediator acts as an electron transfer relay between the enzyme and the electrode, enabling sensing of glucose oxidation as current at lower polarisation voltages. Producing a system for implantable sensors that is safe and effective proves difficult because of the mediator's tendency to leach out of the sensor system. However, the market-leading methods are based on second-generation sensor technology.

The design of third-generation glucose sensors aims to get rid of the leachable artificial mediators by facilitating direct electrical contact between the enzyme active site and the electrode. In direct electron transfer (DET) systems, electrons are transferred directly from the active site of the enzyme to the electrode surface (Figure 1.2, Equation 1.6). For this to occur, the active site of the enzyme must be at an appropriate distance from the electrode surface, with rapid electron transfer limited to distances of less than 0.8 nm[20].

$$\text{Enzyme}_{red} \xrightarrow{\text{Electrode}} \text{Enzyme}_{ox} + e^- \qquad \text{Equation 1.6}$$

While evaluating DET using cytochrome c and a zinc-substituted cytochrome c as a model system, it was shown that the electron transfer rate decreases by about 10^4 when this distance is increased from 0.8 nm to 1.7 nm[21,22]. This places a limit on the number of enzymes that can be directly wired to the electrode surface and the type of enzymes that can be wired, as not all enzymes can undergo DET. An important consideration for DET systems is the orientation of the enzyme on the electrode surface. Random positioning of enzymes on an electrode surface leads to inefficient direct wiring. Therefore, orientation strategies based on chemical bonding and surface treatments are required[23]. This complicates the assembly of enzyme electrodes and is often difficult to achieve, while the currents generated are low compared to MET based enzyme electrodes[24]. While research has been ongoing into enzymes capable of undergoing DET, enzyme engineering efforts for the same and integration into biosensors, glucose strips and CGM technology comparable to those commercially available are yet to be achieved[4,25,26].

1.3 Enzymes as catalysts

1.3.1 Glucose oxidase

Glucose oxidase is a glucose oxidising enzyme with a molecular weight of 160 kDa. It is a dimeric glycoprotein consisting of two subunits, each weighing 80 kDa, (Figure 1.3). The flavin adenine dinucleotide (FAD) in the active site is buried about 1.5 nm inside the protein shell and acts as an initial electron acceptor. When glucose is

oxidised to form gluconolactone, if GOx is the enzyme in Equation 1.1, the co-factor FAD is reduced to $FADH_2$, which in turn is oxidised back to FAD by the final electron acceptor [27–29]. Molecular oxygen acts as a natural co-substrate and final electron acceptor for the enzyme. If O_2 acts as the electron acceptor and either O_2 consumption or H_2O_2 production is the reaction measured, a first generation sensor is formed. The reduction and oxidation of FAD in this case is represented by equations 1.7 and 1.8 below. However, if the MET pathway is followed the second-generation sensor still shows reduction of enzyme according to Equation 1.7 but the regeneration follows Equation 1.9 wherein the mediator shuttles electrons between enzyme co-factor and electrode surface.

$$GOx(FAD) + 2e^- + 2H^+ \rightarrow GOx(FADH_2) \qquad \text{Equation 1.7}$$

$$GOx(FADH_2) + O_2 \rightarrow GOx(FAD) + H_2O_2 \qquad \text{Equation 1.8}$$

$$GOx(FADH_2) + Med_{ox} \rightarrow GOx(FAD) + Med_{red} \qquad \text{Equation 1.9}$$

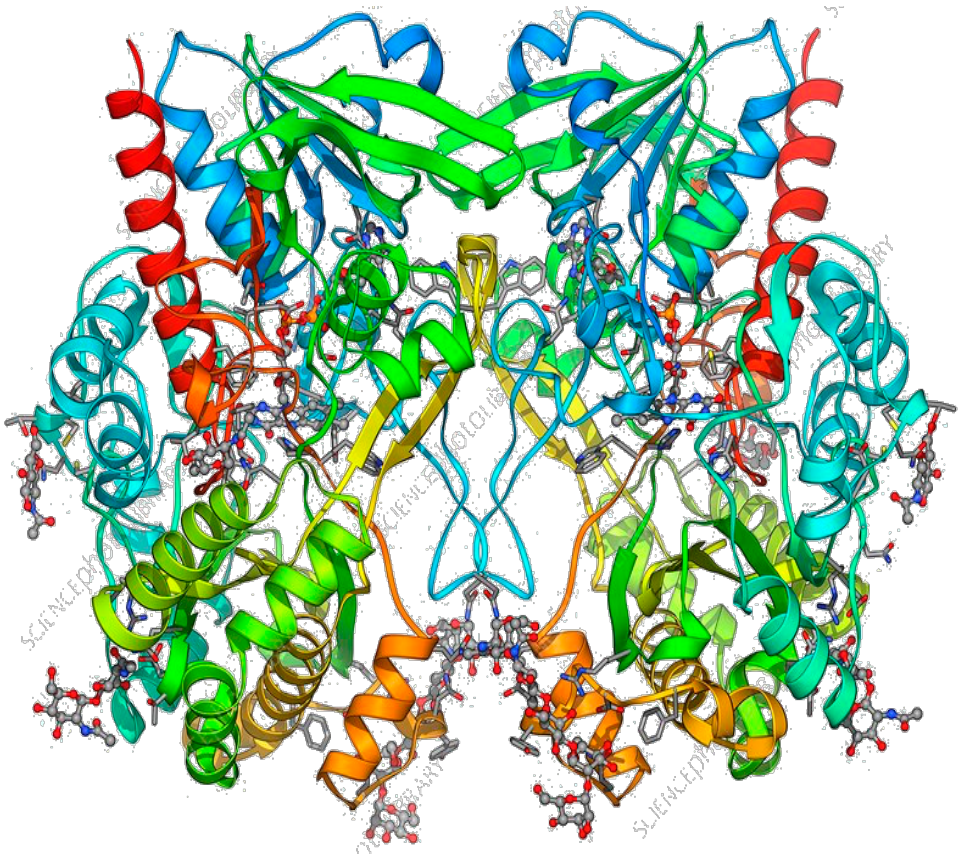

Figure 1.3: Crystal structure of the Aspergillus niger glucose oxidase. Image prepared using UCFS Chimera version 1.13.1.

Glucose oxidase cannot perform direct electron transfer to donate electrons to a solid electrode, despite multiple publications claiming that it can[20]. GOx has a bulky shell surrounding its active site FAD that acts as a catalyst in a ping-pong mechanism, making DET impossible with GOx[30,31]. A redox mediator is therefore required to facilitate electron transfer between the active site and the electrode. Redox mediators can compete with oxygen to accept electrons from the enzyme active site for wiring the enzyme active site to the electrode surface. This mediated electron transfer occurs at lower overpotential than the oxidation of the enzyme co-product peroxide or the reduction of the enzyme co-substrate oxygen (equation 1.4). However, this competition means that there is a parasitic effect due to oxygen presence, leading to lower electricity production at a GOx anode or sensor. The second problem is the production of hydrogen peroxide as a by-product when oxygen is the final electron acceptor. Peroxide affects the performance of enzyme electrodes because it is harmful to these biological macromolecules[32]. For these reasons, it is desirable to replace GOx

as a glucose-oxidising enzyme with an oxygen-insensitive enzyme, such as a dehydrogenase. However, because GOx is commercially available, relatively stable and substrate specific, it is a useful benchmark for evaluating the performance of alternative enzyme electrodes[28,33].

1.3.2 Engineered Cellobiose dehydrogenase

Cellobiose dehydrogenase (CDH, EC 1.1.99.11) is an oxidoreductase enzyme capable of oxidising cellobiose, with the formation of the corresponding δ-lactones, and structurally similar disaccharides which have a β-1-4-linkage with a β-glucose at the reducing end (e.g. lactose) and even monosaccharides (e.g. glucose)[34–37]. Biosensors using dehydrogenases have gained importance in recent years because these enzymes do not donate electrons to oxygen as a co-substrate and therefore do not generate hydrogen peroxide as a co-product. CDH is a monomeric protein with two domains, a heme b-containing cytochrome domain (CDH_{CYT}) linked to a flavin-containing dehydrogenase domain (CDH_{DH})[36]. The large (~65 kDa), catalytically active, saccharide oxidising CDH_{DH} domain (Figure 1.4A, yellow) shares protein folding and cofactor with GOx. CDH is produced by many fungi and forms a diverse family within the glucose- methanol- choline oxidoreductases with differences in substrate specificity, pH optimum, stability and DET efficiency[34,35,38]. Heterologous expression of CDH in *Pichia pastoris* enables protein engineering and rapid and reliable enzyme production. GOx also belongs to the glucose-methanol-choline oxidoreductase superfamily, but the difference between CDH and GOx is that the mobile CDH_{CYT} of CDH (25 kDa) acts as a "built-in mediator", accepting electrons from the reduced $FADH_2$ cofactor[34,39] (Figure 1.4B) via interdomain electron transfer (IET). The CDH_{CYT} can then transfer electrons directly to different electrode surfaces, enabling DET. The CDH is thus one of the limited number of enzymes that, in its native form, can perform efficient DET between the enzyme active site and electrode surface. The CDHs have been tested in combination with various electrode materials to utilise and enhance DET and increase the current density of CDH bioelectrodes[36,40–47].

When CDH is immobilised on the surface of an electrode and in contact with a substrate (e.g. cellobiose)-containing solution, CDH will catalyse the oxidation of the

substrate, whereby two electrons are transferred from the substrate to the oxidised FAD cofactor (F_o) of CDH_{DH} and will convert F_o into its fully reduced state F_R[Equation 1.10]:

$$CDH(F_OH_O). + 2e^- + 2H^+ \rightarrow CDH(F_RH_O). \qquad \text{Equation 1.10}$$

In the absence of any electron acceptor in the solution, the electron transfer from the reduced CDH_{DH} to the electrode will occur sequentially through an initial reoxidation of the fully reduced CDH_{DH}, F_R, via an interdomain electron transfer (IET) mechanism occurring in two consecutive single-electron-transfer steps to form the reduced heme cofactor (H_r) of CDH_{CYT}, with Equation 1.11 being the first one:

$$CDH(F_RH_O) \xrightarrow{IET} CDH(F_rH_R) + H^+ \qquad \text{Equation 1.11}$$

The transfer of the first electron from F_R to H_O results in the formation of a semiquinone radical of the FAD cofactor, $F_{r^{\cdot}}$, as shown in Equation 1.11. However, before the second electron from $F_{r^{\cdot}}$ can be transferred to CDH_{CYT}, the fully reduced heme (H_R) formed in Equation 1.11 must be re-oxidised and that takes place via a DET from H_r of CDH_{CYT} to the electrode (Equation 1.12):

$$CDH(F_rH_R) \xrightarrow{Electrode} CDH(F_rH_O) + e^- \qquad \text{Equation 1.12}$$

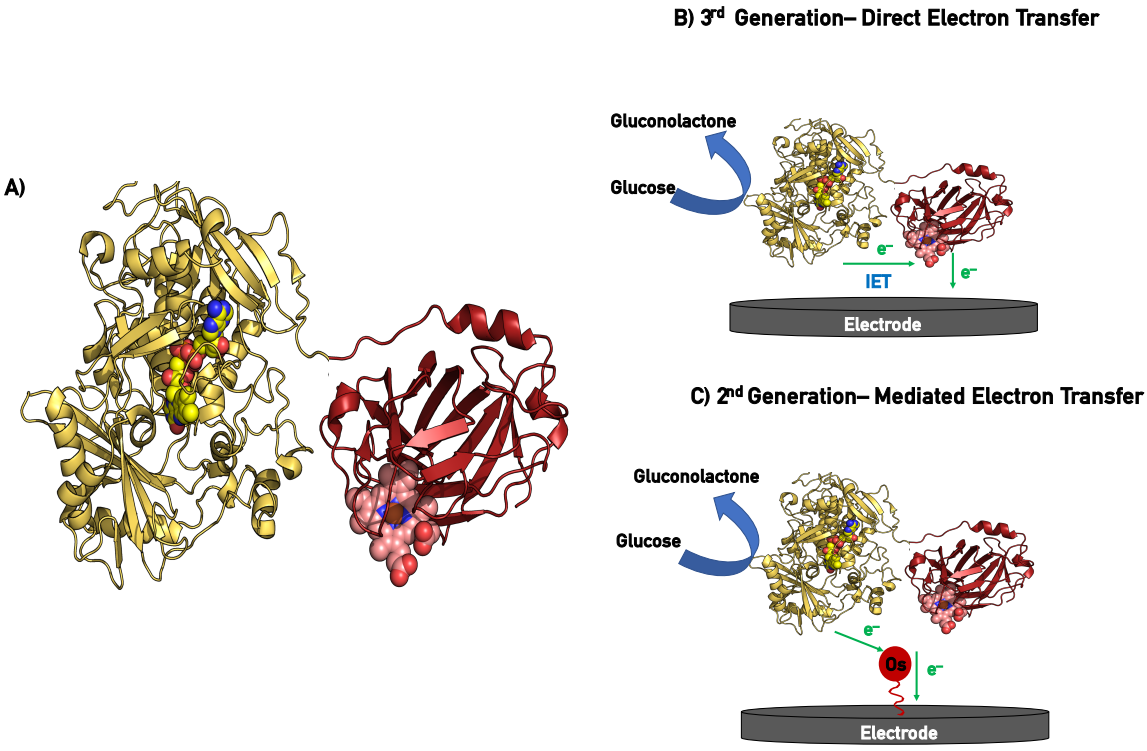

Figure 1.4: A) Crystal structure of cellobiose dehydrogenase from *C.hotsonii* with CDH_{DH} (yellow) capable of oxidising glucose and CDH_{CYT} (red) able to act as an in-built mediator and its mechanism to follow a B) DET pathway and C) MET pathway. Image prepared using UCFS Chimera version 1.13.1,

Once CDH_{CYT} is oxidised, as seen in Equation 1.12, only then does the transfer of the second electron from $F_{r}^{\cdot}$ to H_O take place through a second IET reaction (Equation 1.13) and finally this electron is transferred to the electrode in a reaction similar to Equation 1.14. In CDH, Equation 1.6 is split into two steps (Equations 1.12 and 1.14) as CDH_{CYT} must pass the electron to the electrode surface before accepting another electron and cannot proceed by a 2 electron redox reaction.

$$CDH(F_RH_O) \xrightarrow{IET} CDH(F_OH_R) + H^+ \qquad \text{Equation 1.13}$$

$$CDH(F_OH_R) \xrightarrow{Electrode} CDH(F_OH_O) + e^- \qquad \text{Equation 1.14}$$

In an alternative mediated reaction pathway, the reduced $FADH_2$ is re-oxidized to FAD in the oxidative cycle and can proceed either through a 2 e− acceptor or two equivalents of a 1 e− acceptor [34,48,49]. A 1 e^- acceptor, here exemplified by an Os^{3+} complex, directly picks up 1 e^- at a time and, as in Equation 1.11, initially a semiquinone radical of the FAD cofactor, $F_r^{\cdot}$, is formed (Equation 1.15):

$$CDH(F_RH_O) + Med_{ox} \rightarrow CDH(F_rH_O) + Med_{red} \qquad \text{Equation 1.15}$$

The second e^- can then be picked up by a second Os^{3+} complex (Equation 1.16) and finally the two reduced 1 e^-acceptor (mediator) equivalents are electrochemically re-oxidised according to Equation 1.5 and as depicted in Figure 1.4C.

$$CDH(F_rH_O) + Med_{ox} \rightarrow CDH(F_OH_O) + Med_{red} \qquad \text{Equation 1.16}$$

The structure of this enzyme allows for efficient direct and mediated electron transfer (DET and MET respectively) at various electrode materials, making it very attractive for promising applications in the field of biosensors. A cellobiose dehydrogenase will be evaluated in this thesis as an oxygen independent alternative to GOx. The CDH used in Chapter 3,4 and 5 was donated, as part of the Implantsens research consortium, by DirectSens. It was initially isolated from *Crassicarpon hotsonii* and then genetically engineered to equip it with glucose activity-enhancing mutations C291Y and W295R. It was then recombinantly produced in *Komagatella phaffii* as described previously[50]. It is referred to as wild-type *Ch*CDH (WT*Ch*CDH) in Chapter 3 and CDH in Chapter 4 and 5.

1.4 Mediators for 2nd generation sensors

Historically GOx-based enzyme electrodes for sensing of glucose focused on the oxidation of hydrogen peroxide at an electrode surface to monitor blood glucose levels. These sensors operated at high potentials (0.6 V vs. Ag/AgCl) as they use oxygen as a physiologically available mediator and suffered from interference through direct

oxidation of compounds such as UA and AA present in blood[4,51]. The introduction of artificial redox mediators to shuttle electrons from active site to the electrode surface allowed for glucose sensors to operate at lower potentials [52], limiting the effect of interfering compounds. Electrode assembly can be more straightforward when including the mediator due to wiring of the active site to the electrode surface such that proximity and orientation of the enzyme is not important, as it is to achieve DET. There are a few characteristics to keep in mind during the selection of an artificial mediator for a sensor. For effective electron transfer to occur between the active site and the artificial mediator an appropriate redox potential for the mediator is required to make the transfer thermodynamically favourable[29,53,54]. Furthermore, for the mediator to operate over long timeframes, it needs to be stable in both oxidised and reduced states. This is to allow for continuous regeneration of the oxidised form of the mediator for shuttling of electrons from enzyme to active site.

The first demonstration of mediated electron transfer using GOx was by Cass *et al*. who used ferrocene-based compounds as mediators. GOx was co-immobilised on a pyrolytic graphite electrode with ferrocene to produce a glucose sensor which operated at 0.35 V vs. Ag/AgCl [9]. As this technology was used in the glucose strip industry, ferrocene derivatives were extensively studied as mediators for glucose sensing. For example, Updike *et al*. developed a ferrocene derivative-mediated system for implanted sensors[55,56] and Meredith *et al*. reported that GOx crosslinked with ferrocene modified linear poly(ethyleneimine) polymer on electrodes produces 2 mA cm^{-2} in the presence of 100 mM glucose at 0.13 V vs. Ag/AgCl in phosphate buffered saline (PBS) [57]. Despite improvements to ferrocene mediated GOx enzyme electrodes, issues remain with the use of ferrocene derivatives such as the fact that ferrocene in its oxidised form (ferricenium) is unstable in aqueous solution and that ferrocene derivatives are not readily soluble leading to complications with electrode assembly[53]. This resulted in the introduction of a range of alternative metal-based mediators to overcome the limitations of ferrocene and its derivatives. For example, Zakeeruddin *et al*. synthesised a range of tris-(4,4′-substituted-2,2′-bipyridine) complexes of iron (II), ruthenium (II) and osmium (II) mediator compounds for application as mediators in GOx-based enzyme electrodes[58]. Osmium-based polypyridyl redox complexes and polymers are attractive candidates as mediators due to their stability in oxidised and reduced forms, tunable redox potential, ease of co-

immobilisation and ability to operate at low potentials [59–62]. The tunable nature of the osmium redox potential allows for inclusion of osmium-based mediators in both anodic and cathodic processes[54,63]. Osmium-based polypyridyl redox centres connected to polymer backbones allow the formation of redox hydrogels wherein the redox centres are tethered to an insoluble but water-swollen crosslinked polymer network of the gel[59,64]. Because the redox hydrogels envelope the redox enzymes, they electrically connect the enzymes' reaction centres to electrodes irrespective of the spatial orientation of the enzyme at the electrode surface and also connect multiple enzyme layers. Hence, the attained current densities are usually about 10-fold higher, and in some cases 100-fold higher, than they are when enzyme monolayers are packed onto electrode surfaces and when most of their redox centres are electrically connected to the electrode surfaces.

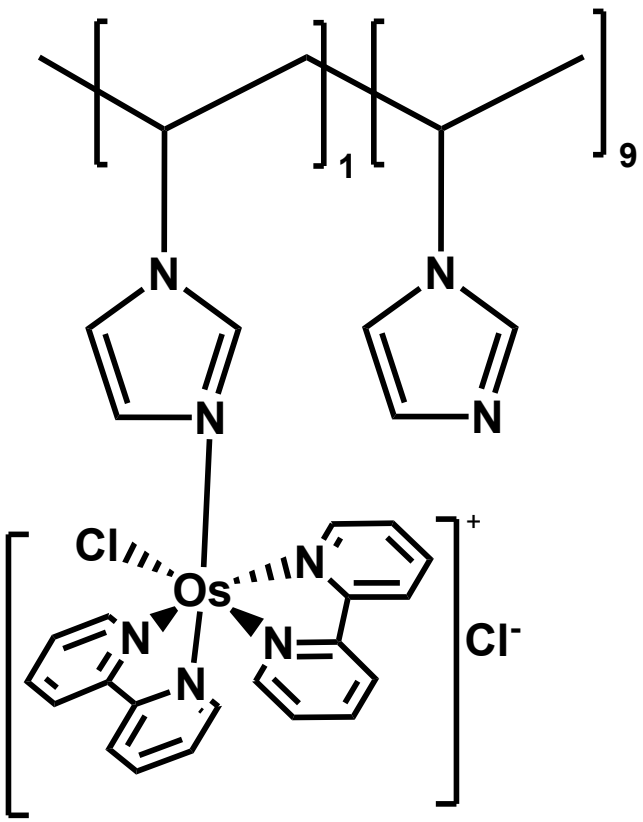

Figure 1.5: Structure of the redox polymer $[Os(2,2'\text{-bipyridine})_2(\text{poly-vinylimidazole})_{10}Cl]^{+}$ (Os(bpy)PVI)

From the initial development of mediated glucose oxidising electrodes by Cass *et al*. to the development of tris-substituted polypyridyl-osmium, ruthenium and iron complexes by Zakeeruddin *et al*. there has been much interest in the field of mediator development for glucose oxidising electrodes[9,58]. Osmium-based redox hydrogels are advantageous as they operate at lower potentials (-0.2–0.6 V vs Ag/AgCl) and have faster electron self-exchange rates[58,65,66]. The structure of one of the most widely used redox polymers, $[Os(2,2'\text{-bipyridine})_2(\text{poly-vinylimidazole})_{10}Cl]^+$ (Os(bpy)PVI), is presented in Figure 1.5. The basis of research in this thesis is the improvement of glucose oxidising electrodes using the Os(bpy)PVI redox polymer (Chapters 2-5), so alternative mediators are not discussed further.

1.5 Sensor fabrication strategy

There are numerous approaches for immobilising components on the electrode surface, such as covalent bonding, physisorption, entrapment and crosslinking, all with the aim of enhancing operational stability by minimising leaching[67].

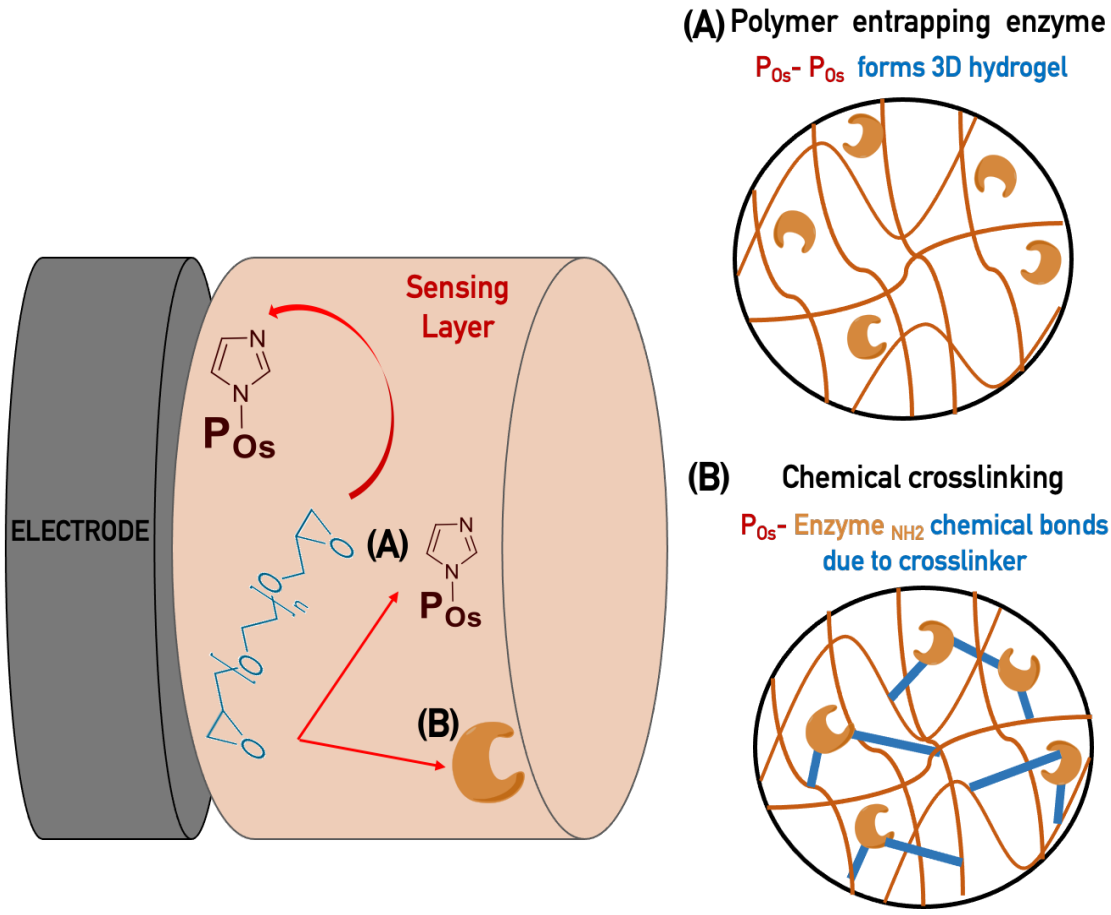

Figure 1.6: Scheme of formation of redox hydrogel by imidazole-epoxy reaction at ambient temperature resulting in immobilisation of enzyme in hydrogel due to A) entrapment and/or B) crosslinking.

Gregg and Heller developed a strategy for entrapment of enzymes and mediators using epoxy-based cross-linking agents to assemble three-dimensional redox hydrogels[68]. These three-dimensional redox hydrogels are inherently hydrophilic and swell when immersed in a solution, enhancing self-exchange redox conduction and aiding mass transport[69]. Redox hydrogels have an advantage over freely diffusing redox mediators as they have no leachable components. Heller's group synthesised a redox hydrogel of poly[(vinylpyridine)] or poly[(vinylimidazole)] with an osmium (bipyridine) centre and co-deposited this with GOx[68]. A commercialised version of this "wired" chemistry is included in glucose monitoring systems sold by Abbott[14]. Heller proved that nitrogen in N-heterocycles and amines can react with epoxy groups at ambient temperatures, crosslinking to form hydrogels[70]. O'Hara *et al*. fabricated crosslinked enzyme electrodes consisting of Os(bpy)PVI, GOx and the crosslinker poly (ethylene

glycol) diglycidyl ether (PEGDGE) (Figure 1.6) [71] based on this principle. The same mechanism was used to fabricate enzyme electrodes in this thesis, based on Os(bpy)PVI redox polymer (Figure 1.5), glucose-oxidising enzyme and PEGDGE crosslinker. The epoxy group of PEGDGE can react with the imidazole in the redox polymer backbone at ambient temperature [70]. Simultaneously, due to bifunctionality of PEGDGE, the other epoxy group can crosslink with another Os(bpy)PVI moiety or the amino groups in the redox enzyme, enabling formation of polymer films with the entrapment and/or cross-linking of redox-active enzymes (Figure 1.6), while preventing leaching from the surface[59,72]. Electron transfer through these hydrogels is proposed to occur by self-exchange between oxidised and reduced osmium moieties along the polymer backbone and/or between moieties on adjacent polymer strands. Here a reduced redox-species collides with an oxidized redox-species, the reduced species transferring its electron, or the oxidized species transferring its hole (Figure 1.7)[73].

While this immobilisation method results in a redox hydrogel, minimising probability of leaching, optimisation is required to determine the component amounts used. Through optimisation strategies, the component ratios required to yield high current densities and/or operational stabilities can be determined. In Chapter 2 and 3, a design of experiments approach has been used for this purpose. The optimised sensor from Chapter 3, using the immobilisation strategy described here, is used in Chapter 4 and 5.

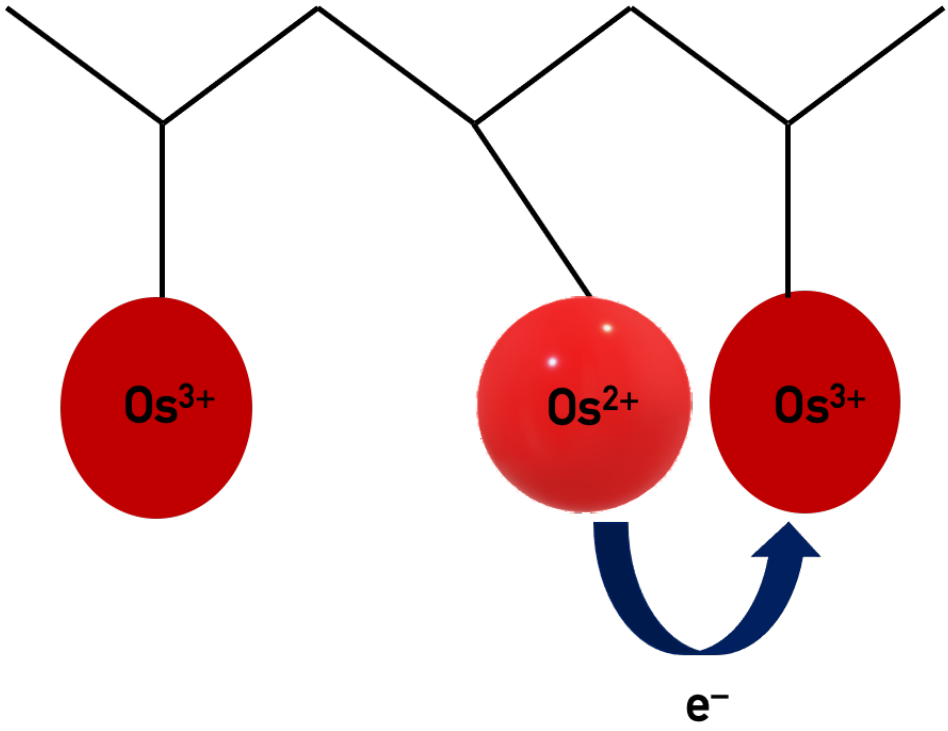

Figure 1.7: Scheme showing electron transfer in redox hydrogels through collision of reduced and oxidised redox centres on polymer backbone.

1.6 Design of Experiments Optimisation

Traditionally, optimisation of a reaction or process is achieved by focussing on one variable or factor at a time (OVAT/OFAT). Consider an example of a synthetic reaction, where two factors that affect the yield of the synthesis are concentration of a reactant and temperature of the reaction mixture. Conventional optimisation can be attempted by setting a concentration and varying the temperature until the greatest yield is achieved, then holding that temperature constant and varying the concentration to see if there is an effect. Based on the variation of these two factors, an optimum is determined (Figure 1.8A). Unfortunately, the majority of the reaction space is discarded during this OFAT optimisation and only a cross-section of the reaction space is investigated. There is a large probability that a false optimum has been discovered. Additionally, a true optimisation is never achieved when experimenting in this fashion as interactions between factors are disregarded and the full potential of the system will not be uncovered.

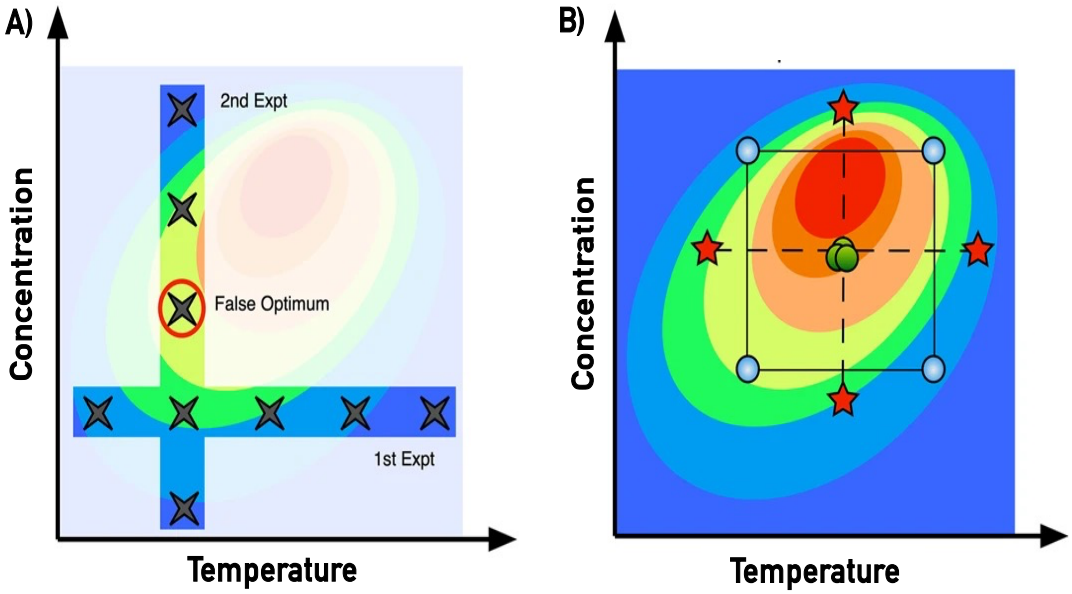

Figure 1.8: Schematic depicting the difference between A) OFAT and B) DoE approaches to finding an optimum yield for a synthetic reaction

Design of experiments (DoE) is a more effective experimental technique that involves planning, conducting and interpreting a series of controlled experiments in which multiple factors (affecting the response to be optimised) are varied simultaneously [74,75]. It permits the effect of each factor on a measured response to be studied and is able to interpret the combined effect of 2 or more factors (i.e., their interaction) on the response. This knowledge is gained through the use of statistics using mathematical models created to fit the experimental data. These models can be used to determine which factors have the greatest influence on a desired response, what interactions are at play, and how to optimise the response based on the factors involved. To create a successful experimental design, all possible factors for the reaction in question must be considered and then trimmed down to those that are expected to influence the outcome. This can be done through prior knowledge or knowledge of the literature, and confirmed through preliminary experiments. Once the important factors are selected, the levels at which they will be studied are chosen. The factors are all investigated at high and low levels to cover a wide range of experimental space (Figure 1.8B). A set of experiments where factors are varied between their pre-set range allows the creation of a model across the experimental space. This model results in a heat map or contour plot showing the potential areas of greatest response. Re-visiting the

example of a synthetic reaction where the concentration of a reactant and the temperature of the reaction mixture affect the yield of the product, a DoE can provide a clear contour plot where the red areas indicate the highest yield and the design can be used to extract optimal experimental values for each factor (Figure 1.8B) [74,75].

The statistical optimisation process offered by DoE has gained popularity in a variety of industries for optimising a range of scientific processes. For example, Kumar and Lahann employed a DoE approach to identify operating limits within which four gel architectures can be realised, including a new regime of associated brushes in thin films[76]. Similarly, Bowden *et al*. used DoE to optimise copper-mediated ^{18}F fluorination reactions of arylstannanes [77]. Considering the field of biosensors, Flexer *et al*. focused on the use of DoE for optimising the preparation of enzyme electrodes and described its implementation for optimising the experimental parameters of electrodes composed of osmium redox polymer and GOx. The obtained results showed an excellent correlation between the experimental and simulated results and allowed the optimisation of film thickness and the concentration of the redox mediator[78]. Babanova *et al*. used DoE to improve the performance of a bilirubin oxidase-based air-breathing cathode. The key factors associated with improved performance were identified and an improved cathode was assembled based on the DoE results. This cathode produced current densities that were 2-5 times higher than the highest reported current density of a similar cathode to date[79]. Recently, Kumar and Leech, and Bennett *et al*. described a DoE approach to optimise the current density of a glucose oxidising electrode based on GOx and an FAD-dependent glucose dehydrogenase (FADGDH) with osmium-based redox mediators[80,81]. The glucose oxidation currents were 32% and 52% higher than the currents optimised by using OFAT[76,78]. In Chapter 2, a Box-Behnken design is used to optimise the current signal for glucose oxidising electrodes based on a combination of redox polymer, GOx grafted onto multi-walled carbon nanotubes (CNTs) and PEGDGE as crosslinker. In Chapter 3, DoE is utilised to optimise the current density when the GOx grafted on CNT was replaced by the engineered glucose-oxidising WT*Ch*CDH enzyme.

1.7 Glucose Biosensor Performance: the good, the bad and the ugly

A biosensor consists of three components: (i) a biological recognition element capable of distinguishing the target analyte in the presence of various chemicals, (ii) a transducer capable of converting the biorecognition event into a measurable signal, and (iii) a signal processing system responsible for converting the signal into a readable format[83]. Most glucose biosensors rely on enzymes as the biorecognition element in combination with an electrochemical transduction method. A biosensor requires certain fundamental performance characteristics to be effective and commercially viable. It must be sensitive (with linearity within a biologically relevant range (3-20 mM)), selective and specific, while ensuring accuracy and precision[4,25,84]. These properties usually depend on the biorecognition element. Sensitivity means that the sensor can easily distinguish the signal on changing the concentration of the analyte. Specificity is the ability of the enzyme to recognise the selected target analyte over other molecules with similar structure, i.e., glucose over other clinically relevant sugars[85]. Selectivity implies that the enzyme can oxidise glucose in the presence of interfering species that are oxidised in the same potential range[85]. This is what limits first-generation glucose biosensors [4,84]. Consider the single-use glucose strip technology, which is based on finger prick testing, a common method to gain insight into blood glucose levels. It is enzyme-based and analysed with *in vitro* methods using test strips and a glucose metre[86,87]. It meets the requirements for an effective biosensor and has already been commercialised but has a significant drawback. The effectiveness of this method depends on strict patient compliance, which can be compromised by time constraints or pain[88]. In addition, it is not a continuous monitoring method as tests must be performed several times a day to check for elevated glucose levels [89,90], especially after exercise, meals and insulin doses. Furthermore, due to this non-continuity, periods of hyper- or hypoglycaemia may be missed[88]. Although the requirements for a commercial sensor are met, disregarding the burden self-monitoring places on patient compliance limits its long-term usage and effectiveness.

In contrast, CGM devices minimise or eliminate this burden of self-monitoring and patient compliance, while incorporating several features that allow decisions about therapeutic interventions to be made based on continuous monitoring of glucose

levels[91]. For example, based on real-time information, a snack can be consumed to compensate for hypoglycaemia, or medication or exercise used to treat hyperglycaemia. Modern CGM devices can also display the blood glucose level and its trend in real time and give audio and visual warnings in case of hypo/hyperglycaemia to encourage these interventions[92]. To function accurately *in vivo* over an extended period of time (one week to several months), a CGM sensor must meet the fundamental performance characteristics of glucose strips. As it is no longer a single-use technology and is embedded in biological tissue, lifetime must also be considered. The accuracy levels of commercially available sensors in CGMs are still significantly worse than SMBG systems (which have a MARD of between 5 and 10%), so they still often need to be calibrated with finger prick tests[92]. Due to *in vivo* use, precision and accuracy of CGM systems are compromised by biological processes such as biofouling, fibrous encapsulation of the implanted electrode, inflammation and loss of host vessels [93–95]. Another obstacle is sensor lifetime, as most implantable electrodes lose their function within 7 days and calibration would also cause numerous problems such as cost, inconvenience and discomfort[15].

Glucose sensor instability depends on many environmental and internal factors. Environmental factors occur *in vivo* due to lack of biocompatibility and include membrane biofouling, electrode passivation and fibrous encapsulation. Internal factors result from both external penetrants (low molecular weight (LMW) materials) and internal sensor problems. Internal factors include lead detachment, electrical shorting, membrane delamination, membrane degradation and sensing enzyme degradation[96]. For glucose sensors implanted in biological tissue, the obstacles to meeting performance characteristics are 1) oxygen dependence 2) interfering substances and 3) biocompatible function. A summary of these processes and their effect in sensor performance is depicted in Figure 1.9 and is discussed further below.

1.7.1 Oxygen dependence

Oxidase-based devices that rely on the use of oxygen as a physiological electron acceptor are subject to errors resulting from variations in oxygen tension and the stoichiometric limitation of oxygen[4]. Blood oxygen levels can fluctuate, especially due to changes in altitude, health complications such as asthma, sleep apnea, etc.,

leading to errors in glucose measurement[25,84]. This can lead to inaccurate insulin administration, which can cause significant hypoglycaemia events leading to coma or even death in extreme cases[2,25]. This limits use of first generation glucose sensors. In addition, oxygen concentration *in vivo* is an order of magnitude lower than that of glucose, creating a stoichiometric limitation known as “oxygen deficit”. While this can be overcome using permselective membranes to limit the flux of the analyte[84], this does not address the wide-ranging complications that can arise from variations in oxygen levels in the body.

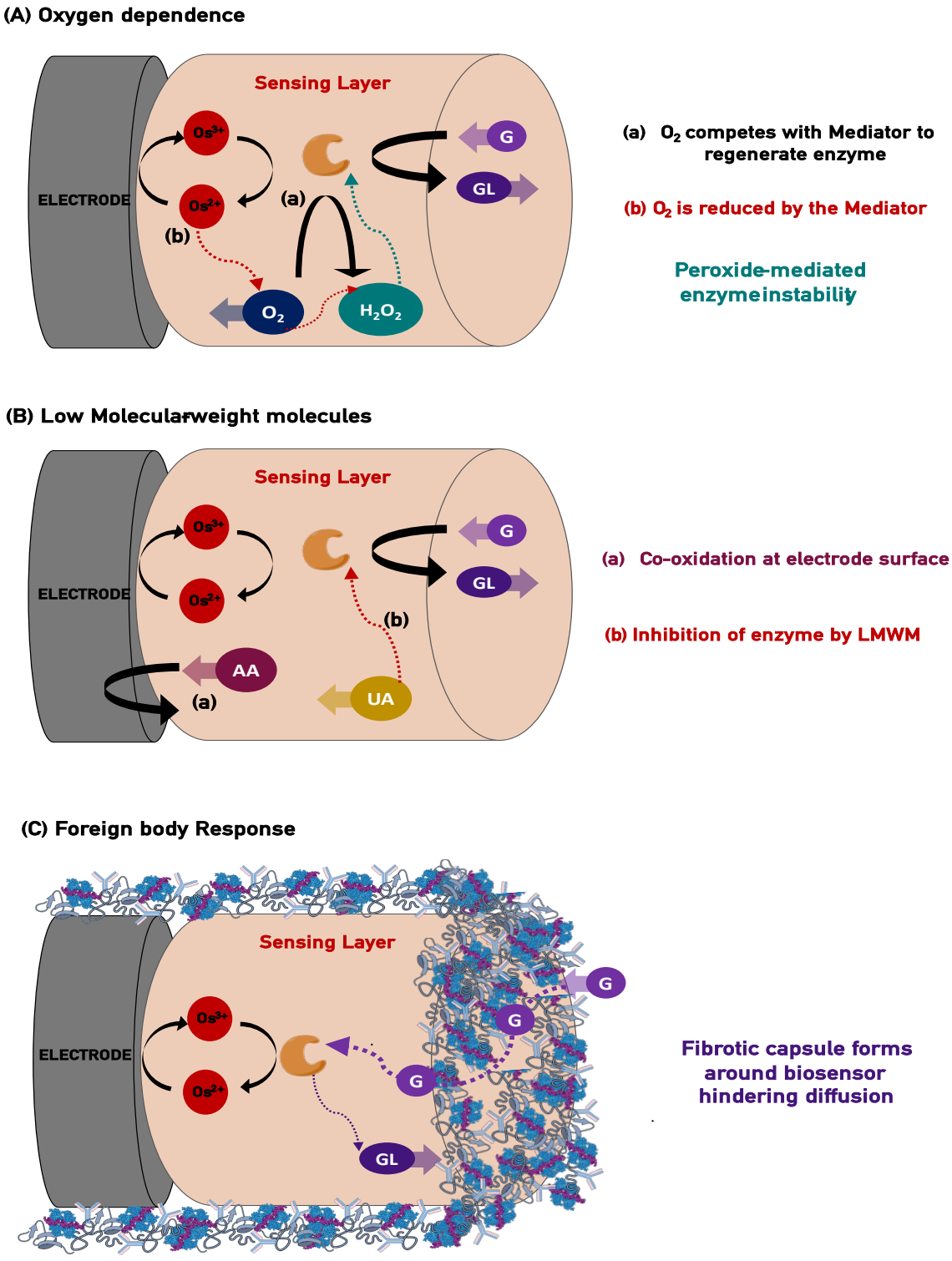

Figure 1.9: Schematic showing effect of A) oxygen dependence, B) low molecular weight materials and C) foreign body response on mediated glucose biosensors.

Second generation oxidase-based sensors can compensate for this problem by replacing the physiological electron acceptor, oxygen, with an artificial counterpart. However, the oxidation of the reduced enzyme by oxygen (Equation 1.2) can occur even in the presence of the mediator. In fact, oxygen competes with the mediator for the uptake of electrons from the reduced enzyme (Equations 1.2 and 1.4 occur simultaneously), resulting in an underestimation of glucose levels[4]. Theoretically, oxygen competition can be minimised if the rate of electron transfer across the mediator is high compared to the rate of enzyme reaction with oxygen[4]. However, it cannot be completely eliminated because oxygen diffuses freely through the matrix[4,56]. Prevoteau *et al*. have shown that oxygen can also be reduced by the osmium-based redox polymer mediators (that have redox potentials below 0.07 V vs. Ag/AgCl), which in turn leads to false glucose readings as it can now compete with the electrode for electrons from the mediator[97]. Choosing a mediator with an optimal potential range is a possible solution, but this is limited by the number of factors a mediator must meet, the complicated synthesis and, most importantly, the presence of interfering species capable of oxidation at higher potentials (0.6 V vs. Ag/AgCl). One solution is to replace oxidase-based enzymes with a dehydrogenase, e.g., glucose dehydrogenase (GDH), which does not accept oxygen as a natural electron acceptor. However, this leads to other complications as GDH does not have the high specificity of GOx and can oxidise other clinically relevant sugars such as galactose, maltose and xylose[98].

Apart from the errors caused by oxygen fluctuations, the hydrogen peroxide produced during oxygen reduction by oxidase-based biosensors also causes problems in glucose sensing as it plays a role in the instability of the enzyme. The degradation of the sensor enzyme severely limits the functional life of GOx *in vivo* and remains a major challenge in continuous glucose monitoring. Suspected causes of GOx degradation include hydrogen peroxide (H_2O_2) formed at the electrode [99–103] and intrinsic LMW materials from blood and interstitial fluid [104]. Gough and co-authors explain that GOx degradation occurs either by spontaneous inactivation or by peroxide-mediated inactivation [105–112]. They suggested that spontaneous inactivation occurs throughout the immobilised enzyme phase by an unknown mechanism. Harris *et al*. suggested that this spontaneous inactivation is due to the degradation of LMW species and the formation of epoxide within the immobilised enzyme layer (see Section 1.7.2) [96].

Glucose oxidase stability decreases over time, in part due to H_2O_2 oxidation of methionine residues in the active site to methionine sulfoxide [99–103]. Oxidative damage is a critical factor in maintaining enzyme stability. The formation of methionine sulfoxide impairs the coordination of substrate recognition, catalysis and specificity in the active site. Both soluble and immobilised GOx are susceptible to H_2O_2-mediated oxidative damage[100,101]. Bao and co-authors found that immobilised GOx was competitively inhibited by H_2O_2 [113]. The reduced form of GOx competitively binds H_2O_2 and oxygen with similar specificity. Ultimately, glucose sensor stability suffers through elimination of key active site residues by H_2O_2 or increased susceptibility to oxidative attack by H_2O_2 in the presence of glucose. When H_2O_2 concentrations reach critical levels, the sensor accuracy, substrate sensitivity and half-life of the glucose sensor decreases[96].

Enzyme engineering has gained popularity as an approach to minimising these issues. Many attempts have been made at engineering GOx to be oxygen insensitive or to engineer oxygen insensitive enzymes to accept glucose as a substrate. There has been some success but each have limitations. For example, Prevoteau *et al* managed to engineer GOx through deglycosylation to produce an oxygen insensitive variant. However, they found on integration of this enzyme into a sensor that the sensor response was greatly affected[114,115]. On the other hand, engineering of oxygen insensitive CDHs is a popular alternative. They show no decrease in glucose oxidation currents in the presence of oxygen. However, investigations showed production of minute amounts of peroxide which can affect long-term enzyme stability [50]. Enzyme engineering thus far has been able to minimise the effect of H_2O_2 but not fully eliminate it.

1.7.2 Low Molecular Weight Materials

Selectivity, an important criterion for meeting accuracy requirements, depends on the ability to eliminate reactivity to interfering LMW substances. Endogenous and exogenous LMW species such as UA, AA and acetaminophen are species that can be present in the microenvironment and limit sensor performance – either because they readily interfere with the bioelectrocatalytic activity of enzymes or because they can be co-oxidised with the analyte[116]. For example, in first generation systems using

H_2O_2 oxidation as a transduction mechanism, the relatively high polarisation voltage is also known to result in oxidation of interfering LMW species that are commonly found *in vivo*. This can be avoided through smart selection of the redox mediator, allowing selection of lower potential range. Systems with mediators whose redox potentials are poised between about −0.2 V and about 0.1 V versus Ag/AgCl will not oxidise UA or acetaminophen, the combined blood concentration of which can be as high as 0.6 mM. Nevertheless, virtually all systems in this range will still cross-react with ascorbate[56]. In addition, at potentials below 0.07 V vs Ag/AgCl the mediator can reduce oxygen, leading to a decrease in current and production of H_2O_2, which in turn causes enzyme instability. Selecting the mediator to avoid interference from LMW species and oxygen/peroxide is very difficult and limits the range of the sensor, so alternatives should be considered. Third generation sensors are likewise affected by the presence and actions of LMW species.

The other route by which LMW species affect a sensor is through their effect on the bioelectrocatalytic activity of enzymes. Kerner[117] first discovered that LMW species of < 10 kDa can lead to rapid degradation of GOx and drastically reduced sensitivity. It is difficult to pinpoint the cause of LMW species degradation of GOx because there are numerous unknown events in the surrounding tissue and in the sensor itself that can lead to gradual failure. For example, the enzyme often accumulates at the surface of the sensor, resulting in a significant concentration of GOx at the membrane-bulk interface[117–120]. This obscures the effect of oxidative degradation and prevents deconvolution of the effect of LMW species from the effect of H_2O_2[118–120]. As a result, the specific mechanisms of LMW species degradation of GOx continue to elude the scientific community.

A useful way to minimise the effect of LMW electroactive interferences is to use a permselective coating that limits the access of these components to the electrode surface[4]. Various polymers, multilayers and mixed layers with transport properties based on charge, size or polarity have therefore been used to block access of co-existing electroactive compounds[121–127]. Such layers also exclude surface-active macromolecules, protecting the surface and giving it greater stability. Wilson *et al*. eliminated interference from neutral acetaminophen and negatively charged AA and UA, respectively, by application of a multilayer permselective membrane of cellulose

acetate and Nafion[128]. Several others have developed polymeric permselective membranes, such as a sulfonated polyether- ether sulfone- polyether sulfone (SPE-ES-PES) membrane used by Vadgama *et al*.[129]. Electropolymerized films, particularly poly(phenylenediamine), polyphenol and over-oxidised polypyrrole, have been extremely useful in achieving high selectivity (by rejecting interference due to size exclusion) while confining GOx on the surface, although the final system has often not been stable enough for reliable use *in vivo*[121,123,124,130]. Other commonly used coatings include size-exclusion cellulose acetate films, the negatively charged (sulfonated) Nafion or Kodak AQ ionomers, and hydrophobic alkanethiol or lipid coatings[127]. Commercial CGM developers use proprietary membranes to create selective glucose sensors. For example, Abbott's Freestyle Navigator CGM sensor uses a cross-linked polyvinylpyridine (PVP) derivative for the coating layer [56]. It is believed that the current commercially available CGM sensors, which claim a stability of one to two weeks, employ polyurethane-based polymers in the Dexcom sensors and polyvinylpyridine- or polyvinylimidazole-based polymers in the Abbot sensors but the actual structure and composition are proprietary.

An alternative approach to minimise the effect of LMW electroactive interferences is to utilise another enzyme to consume or scavenge these interfering substances. For example, ascorbate oxidase can be co-immobilised to eliminate ascorbic acid from approaching the electrode surface [131]. In this case, however, care must be taken not to wire the enzyme scavenging systems, i.e., electrically connect them to the electrode surface. The goal is to intercept the interfering substance, and an additional polymer coating may need to be used to prevent this scavenging reaction from being detected at the electrode surface.

1.7.3 Foreign body response

Addressing the *in vivo* response to implanted sensors remains one of the greatest challenges in developing a CGM system with reasonably accurate performance for use in a closed-loop artificial pancreas. Figure 1.10 illustrates the complex inflammatory response known as the foreign body response (FBR) that occurs when a sensor is inserted subcutaneously.

The process begins immediately after contact of the implant with host fluids (e.g., blood, lymph, wound fluid) by spontaneous uncontrolled adsorption of host proteins to the implant surface. The resulting protein-conditioned surface is coated with different protein species in various conformations and adsorption states. The host cells responsible for normal wound healing encounter this unusual layer of adsorbed proteins. Within a few hours, neutrophils invade the implant tissue and react by producing cytokines, chemokines, reactive oxygen species (ROS) and other enzymes. Over the next few days, these neutrophil products recruit tissue-resident macrophages and undifferentiated monocytes to the wound site at the same time as the neutrophils exit. Macrophages respond to the implant by producing their own signalling molecules that attract fibroblasts. Fibroblasts produce excess collagen. Their presence correlates with the formation of foreign body giant cells (FBGCs), whose role in the foreign body response is poorly understood. Over time, a dense collagenous fibrotic capsule forms around the implant, physically and physiologically isolating it from the host tissue [132,133]. Due to the collagen deposition by the fibroblasts, the implant is effectively isolated from the rest of the body. This condition, in which the fibrotic capsule encapsulates the implant, together with the foreign body reaction at the interface, is called fibrosis[94].

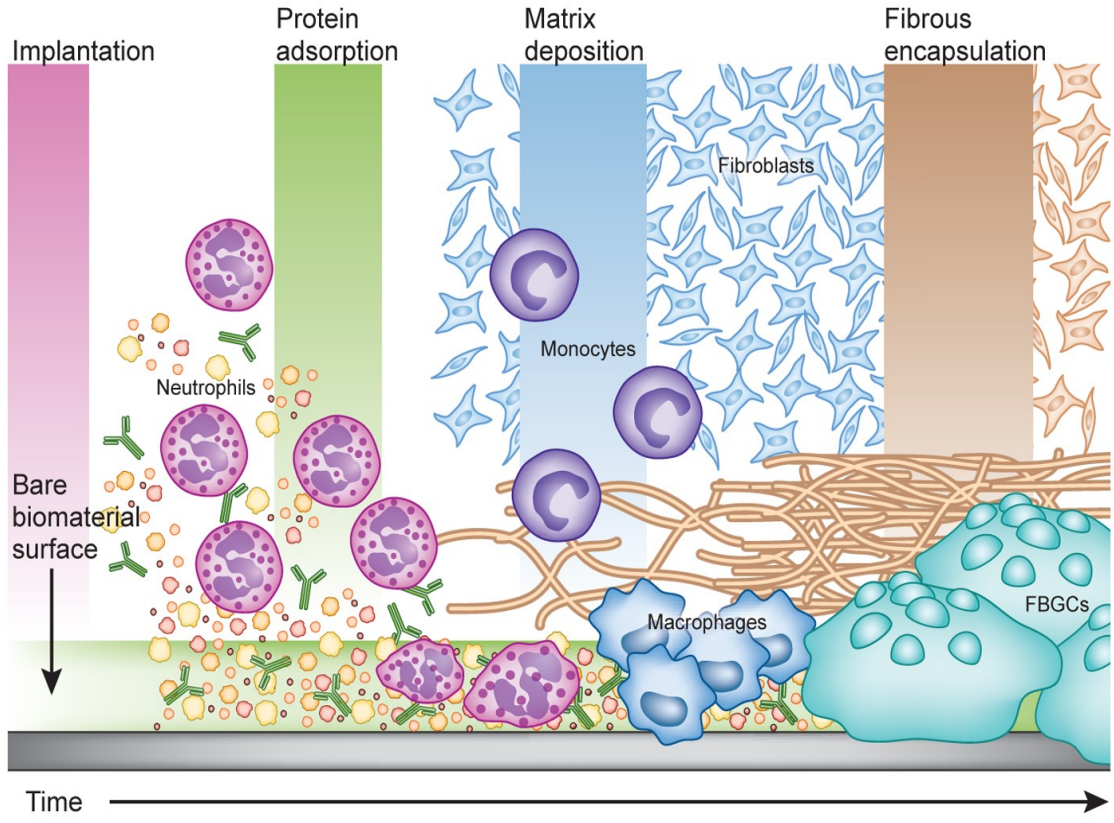

Figure 1.10: Schematic of foreign body response initiated on implantation.[132]

All stages of FBR contribute to the instability of implanted glucose sensors. These include an initial decrease in sensitivity, sensor recognition of ROS, degradation of the sensor components and consumption of oxygen and glucose by the inflammatory cells[134]. As a result, the lifetime and accuracy of the sensor is affected. The biological efforts to heal the wound and remove the foreign body in the acute phase create a highly unstable and reactive environment. The unpredictable changes in the *in vivo* microenvironment can create an unstable background response for electrochemical sensors. In FBR, the acute phase lasts about one to two weeks before a fibrotic capsule forms around the long-term implant. The capsule inhibits the diffusion of glucose and oxygen to the implant, which is not representative of "normal" tissue. The complications encountered with the first implanted devices have led many researchers to investigate the interface between the sensing function and the biological response[135]. Gerritson *et al*. and Wilson *et al*. showed that the initial cause of the loss of sensitivity was the penetration of proteins into and onto the membranes of the sensor[134,136]. Wisneiwski *et al*. characterised the "biofouling" process and worked to develop methods to circumvent the initial protein adhesion[137]. Anderson's group

contributed significantly to the understanding of the mechanism of the FBR to implants. His group provided important insights into the initial interaction of proteins with early inflammatory cells through the cascade of events that lead to the fusion of macrophages into giant cells to encapsulate an implant[138–141]. The fundamental understanding of the biological response led to specific technologies to circumvent the adverse effects, some of the first of which prevent protein adhesion. The concept is to mimic natural tissue or cellular structures to prevent protein adhesion. Naturally occurring materials such as alginate, chitin and chitosan and their derivatives are being intensively researched for application to *in-vivo* biosensors in the form of films, membranes and coatings. They offer the advantage of being comparable to natural precursors and hence the biological environment is prepared to recognise and process their metabolites [142,143]. On the other hand, modified synthetic polymers with tailored structures and coating properties are often superior to naturally occurring macromolecules, especially because of their lower immunogenicity. Zwitterionic polymers are a good example wherein the structure of the polymer facilitates the formation of a strong hydration sphere that inhibits biofouling[144–149]. Hydrogels are hydrophilic, water-insoluble three-dimensional polymer networks represented as semi-open structures with entangled chains that adsorb and store large amounts of water and are highly permeable to small molecules[70]. The use of hydrogel coatings allows glucose to diffuse through the swollen hydrogel layer. Morais *et al*. has studied a range of hydrophilic hydrogel coatings of polyethylene glycol and polyvinyl alcohol that form a protective shield of surface water (i.e. a hydration sphere) that is thought to prevent protein adhesion. Other biomimetic compositions have also been formulated to prevent protein adhesion, including collagen, chitosan, alginate, hyaluronan and phospholipids[150]. Work by Kobayashi *et al*. has demonstrated the relationship between nanofunctionalised surface properties with poly(2-hydroxyethyl methacrylate) (PHEMA) polymer brushes and the exclusion of protein adsorption on *in vivo* surfaces[151].

1.8 Overcoming sensor limitations using polymer coatings

There is a need for improved sensors that can overcome all the limitations described in Section 1.7. It is clear that polymer coatings can be used to combat issues preventing

use of glucose biosensors for long-term *in vivo* glucose monitoring. Polymer coatings used as protective shields against *in vivo* interferents must not only impart the protection but also be sufficiently permeable to glucose to ensure adequate sensor signal[152]. In addition, the polymer shields should facilitate diffusion of reaction product, gluconic acid, away from the electrode as its accumulation can alter the pH in the microenvironment thereby negatively impacting film stability and/or enzyme activity[153]. Most electrochemical glucose sensors rely on diffusion of substrate and product for sensor operation. However, use of polymer coatings results in hindered diffusion and a slower flux of glucose, impacting sensor response. For first generation sensors this slower flux of analyte can be beneficial and in fact is desired to combat the oxygen deficit[154]. However, for second and third generation sensors, hindered diffusion of glucose is counterproductive as the slower flux results in decreased sensitivity and increased sensor response times[155–158].

Diffusion is a process by which species move from one part of the system to another through random molecular motion[159]. In steady state conditions, it is governed by Fick's first law (Equation 1.17):

$$J = -D\frac{\partial c}{\partial x} \qquad \text{Equation 1.17}$$

Where J is the flux defining quantity of species diffusing across unit area of medium per unit area of time (mol cm^{-2} s^{-1}), D is the diffusion coefficient, c is the concentration and x is the distance.

In the case of using a polymer coating on a glucose biosensor mediated through a redox hydrogel, a laminate system of two successive polymer coatings is formed (Figure 1.11A)[159,160]. Diffusion slows as it passes through a polymer membrane due to the differences in diffusion coefficient and mass transfer rates depending on the medium. Taking the example of a system relying on enzymes entrapped in a redox silent polymer to scavenge interferences, the diffusion slows due to the polymer coating. However, here an additional effect is present as this system presents as a composite film containing particles (Figure 1.11B), where the particles (enzymes) create a barrier and the analyte follows a meandering path through the film to avoid them[159].

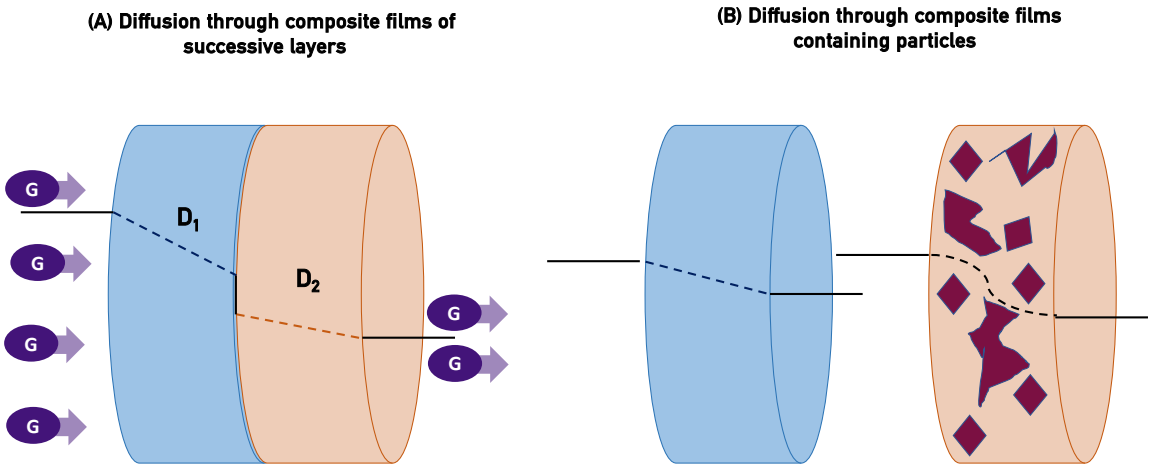

Figure 1.11: Diffusion of analyte (glucose) through A) a laminate film consisting of successive polymer layers and B) polymer films with and without particles.

Polymer coatings while necessary for protection often affect the sensor response in electrochemical systems due to diffusional barrier formation, producing decreased sensor response to a similar level as the interferences they are combating[155,160]. In addition, polymer coatings targeting one interferent will not necessarily be effective for another interferent. For example, anionic polymers as protective shields are commonly used to prevent LMW UA and AA interference but are not necessarily effective in hindering biofouling[155]. A PEG polymer shield has been shown to be useful for biofouling resistance but shows no effect against LMW species[161]. Methods to provide improved shielding against interference from LMW materials and biofouling using polymers are investigated in this thesis and presented in Chapters 4 and 5.

1.9 Electroanalytical techniques

Electrochemical characterisation methods are the essential techniques required to study the performance of enzyme electrodes. In the context of this thesis, various electroanalytical techniques are used to investigate the performance of enzyme electrodes. Therefore, a brief description of the techniques used is given in the following sections.

In electrochemical investigations, a standard three electrode cell is usually used, in which there are no membranes between the electrodes. This cell consists of a working electrode, a counter electrode and a reference electrode. The working electrode is the electrode where the redox process of interest takes place. It is usually chosen to be made of graphite, glassy carbon, platinum or gold. All the work carried out in this thesis was done with graphite working electrodes. The counter electrode is used to facilitate electron transfer in the electrolyte so that the current can be measured at the working electrode. Typical materials for counter electrodes are titanium or platinum, although a platinum mesh was used for all experimental results obtained in this work. A mesh electrode, of high conductivity and surface area was used to ensure that the counter electrode does not limit the current at the working electrode. The reference electrode is used to measure the potential applied to the working electrode. In this work an Ag/AgCl (3M KCl) reference electrode was used because it is inexpensive, easy to maintain and provides a consistently stable potential[162–165].

One of the most important electroanalytical techniques available to an electrochemist for the investigation of redox processes is cyclic voltammetry. Cyclic voltammetry is a powerful and popular electrochemical technique commonly used to study the reduction and oxidation processes of molecular species. It is also invaluable for the study of chemical reactions initiated by electron transfer, which includes catalysis[165,166]. Cyclic voltammetry has the further advantage of providing information not only on the thermodynamics of redox processes but also on the kinetics of heterogeneous electron transfer reactions and coupled chemical reactions[166]. The characteristic shapes of the voltammetric waves and their unique position on the potential scale virtually fingerprint the individual electrochemical properties of redox systems. For this reason, cyclic voltammetry is also known as "an electrochemist’s spectroscopy"[164,165].

The technique works by applying an initial potential to the working electrode, followed by a linear ramp of the potential to a predetermined inflection point where the potential is reversed linearly over the same potential range at the same rate (Figure 1.12). During this process, the electrochemical events that lead to current changes as a function of the applied potential are recorded. This results in a cyclic voltammogram (CV) in

which the applied potential is plotted on the x-axis with the current flow at the working electrode on the y-axis (Figure 1.12)[164]. If the rate of heterogeneous electron transfer at the electrode surface is fast enough to ensure that the concentrations of oxidised and reduced species are in equilibrium, the redox reaction is considered reversible, and the Nernst equation is followed (Equation 1.18)[165]. The most significant parameters in a CV are shown in Fig. 1.12. While cycling of potential through a redox process the current recorded forms two peaks, one for oxidation and one for reduction of the electroactive species, at peak potentials E_{pa} and E_{pc} respectively. These peak potentials are characteristic to each redox species and can be used to identify them, while the magnitude of the peak (peak height) gives an indication of the concentration of the electroactive species[165].

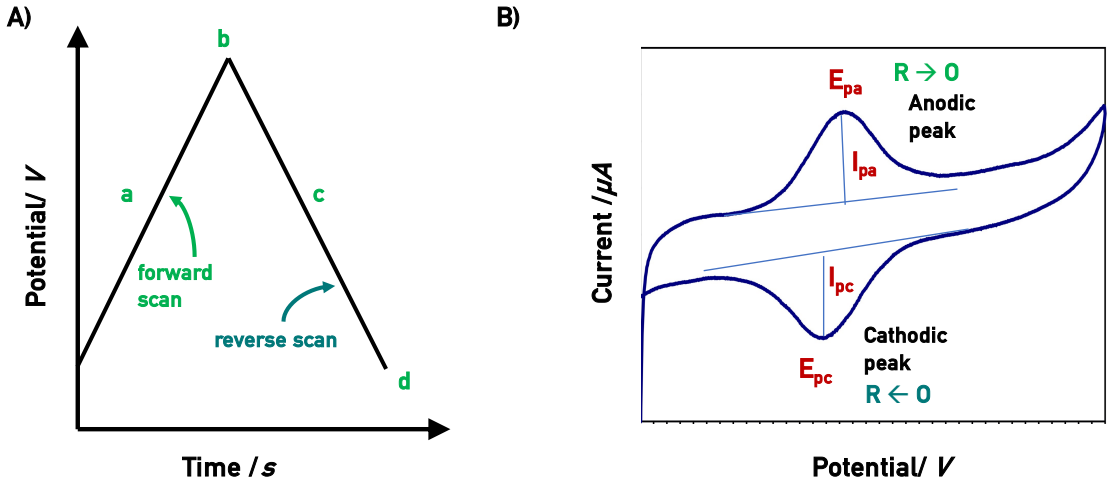

Figure 1.12: A) Typical linear waveform for cyclic voltammetry and B) A typical cyclic voltammogram of a reversible solution-phase redox reaction. The initial potential applied is shown (a), the anodic peak potential and current (E_{pa} and i_{pa}), the switching potential (b) and the cathodic peak potential and current (E_{pc} and i_{pc}).

The Nernst equation describes the relationship between the electrode potential (E), the standard reduction potential (E^o), the number of electrons involved in the process (n) and the concentration of the oxidised or reduced species ([Ox], [Red]) where R is the gas constant, T is temperature and F is Faraday's constant.

$$E = E^0 - \frac{2.303\ R\ T}{n\ F} \log \frac{[Red]}{[Ox]} \qquad \text{Equation 1.18}$$

For an electrochemically reversible process, where heterogeneous electron transfer is faster than mass transfer, the separation of the peak current potentials is given by:

$$\Delta E = E_{pa} - E_{pc} = \frac{59}{n} \text{ mV} \qquad \text{Equation 1.19}$$

The peak currents scale proportionally with the square root of the scan rate. The peak oxidation or reduction current for an electrochemically reversible reaction is given by the Randles-Sevçik equation (Equation 1.20), where i_p is the peak current for an anodic or cathodic process (in amperes, A), n is the number of electrons transferred in the process, A is the area of the electrode (cm^2), D is the diffusion coefficient of the oxidised or reduced species ($cm^2\ s^{-1}$), C is the concentration of the oxidised or reduced species (mol cm^{-3}) and v is the scan rate (V s^{-1}).

$$i_p = 0.4463\ n\ F\ A\ D^{\frac{1}{2}}\ C\ \nu^{\frac{1}{2}} \sqrt{\frac{n\ F}{R\ T}} \qquad \text{Equation 1.20}$$

Electrochemically irreversible or quasi-reversible behaviour occurs when the rate of electron transfer is slow relative to the applied scan rate. Nernst equilibrium is not maintained because electron transfer is the rate-determining step and the peak-to-peak separation is greater than 59/n mV[165]. For multilayer modified electrodes, such as enzyme electrodes, the Randles-Sevçik equation can be used to model the CV if the scan rate is quick enough to ensure semi-infinite diffusion. From this equation, the diffusion coefficient for charge transport through enzyme electrode multilayer films can be estimated. In CVs recorded at slow scan rates for thin layer cells or multilayer electrodes, finite diffusion prevails due to the expansion of a depletion layer across the entire cell or multilayer[165]. In cases where finite diffusion prevails, an estimate of the surface coverage of redox active species (Γ) confined to the electrode surface can be made (Equation 1.21) by measuring the faradaic charge (Q) passing through the film during electrolysis. This is quantified by measuring the area under the curve for an anodic or cathodic peak in a CV.

$$\Gamma = \frac{Q}{n\ F\ A} \qquad \text{Equation 1.21}$$

Each subsequent chapter of this thesis focuses on electron transfer between an electrode and an enzyme catalyst at an electrode surface. This process is called the EC' mechanism and represents electrocatalytic processes at electrodes. Catalysed electrochemical reactions, including enzyme-catalysed electrochemical processes, have attracted considerable attention because they have numerous advantages, including enhanced chemical reactivity and specificity. Typical cyclic voltammograms for EC' processes show an enhanced current response in the presence of an increased substrate concentration at the same potential[165]. The mechanism of transfer of electrons to the electrode that regenerates the enzyme catalyst for further electrocatalysis is discussed in detail in Section 1.3.

Besides CV, amperometry is a commonly used technique for electrode characterisation and evaluation of electrode performance. Amperometry is used extensively in this thesis to study the performance of enzyme electrodes. The technique works by measuring an anodic or cathodic current at a working electrode under an applied, usually fixed, potential. The current measured at the working electrode is recorded as a function of time[165].

1.10 The ImplantSens project

ImplantSens, a multidisciplinary project funded by Marie Skłodowska-Curie Actions – Innovative Training Networks (MSCA-ITN), aims to develop an implantable glucose sensor that can act as a continuous glucose monitor to improve diabetes treatment. This network comprises of 11 early stage researchers (ESRs) working across Europe on the different aspects necessary for the development of a mass-transfer independent implantable glucose biosensor. Many factors limit the sensor performance *in vivo* (as described in Section 1.7). ImplantSens follows a collaborative research approach to guarantee optimal knowledge flow to combat these and reach our final goal. The main research questions pursued were:

- Design or engineering of enzymes with specific characteristics such as switchable nature (on/off), oxygen insensitivity, etc. (ESR 8, ESR 9)

- Immobilisation of the designed enzymes on electrodes to ensure electrical contact to electrode by DET and MET pathways on different electrode architectures (ESR1, ESR2, ESR5, ESR6, ESR7)

- Modelling of sensors for optimised characteristics such as film thickness, partition coefficient (ESR7)

- Pulsed electrochemical readout methods to enable switching of enzyme between on/off states (ESR1, ESR10, ESR11)

- Design and integration of redox polymers for optimised mediation and novel polymers as protective shields (ESR1, ESR5)

- *In vitro* testing of biosensors in human physiological fluids (ESR11)

- *In vivo* studies in rats to investigate FBR and functionality of biosensors (ESR3)

The work in this thesis addresses my contributions to the ImplantSens network as ESR 5.

1.11 Thesis proposition

The aim of this thesis was to investigate methods to optimise and improve performance of mediated glucose biosensors targeting *in vivo* applications. Chapter 2 describes the optimisation of a glucose biosensor containing commercial GOx enzyme grafted onto multiwalled carbon nanotube (MWCNT) nanosupport. This optimisation was performed using a design of experiments approach pursuing multiple response optimisation of current density and operational stability. The results were compared to previously published results of a glucose biosensor based on GOx and acid treated MWCNT each encapsulated in a redox hydrogel, and the resulting optimised biosensor was used as a benchmark system by other ESRs in the ImplantSens project. In Chapter

3, the commercial GOx enzyme was replaced with an engineered CDH, the WT*Ch*CDH from Directsens produced by ESR9, and this biosensor was optimised for application to glucose detection in a DET and MET-based biosensor. The WT*Ch*CDH is specific to glucose and known to be oxygen independent, thus the sensors fabricated with this enzyme were tested to assess if the sensor can overcome the oxygen dependence effects observed for oxidase-based glucose sensors. In Chapter 4, a series of zwitterionic polymers produced by ESR1 were investigated as protective polymer coatings to minimise biofouling of the biosensor, investigated using electrochemical, enzyme-linked immunosorbent assay and cell adhesion studies. The polymers were designed to incorporate a crosslinking group to attach to the redox hydrogel sensing layer and thereby minimise the boundary between successive polymer layers, in an attempt to prevent hindered diffusion of substrate and product observed using other polymer coatings. Finally, Chapter 5 addresses whether multilayer polymer coatings or a multi-purpose single polymer layer protective shield is the better protective system by comparing performance of a multilayer of designed polymers (anionic and zwitterionic) to an enzymatic scavenging approach wherein enzymes that can scavenge LMW species are integrated into the zwitterionic polymer coating. Chapter 6 summarises the research achieved over the course of the PhD and proposes some future research directions based on the work presented in this thesis.

1.12 References

[1] A. D. Association, *Diabetes Care* **2017**, *40*, S11–S24.

[2] N. H. Cho, J. E. Shaw, S. Karuranga, Y. Huang, J. D. da Rocha Fernandes, A. W. Ohlrogge, B. Malanda, *Diabetes Res Clin Pract* **2018**, *138*, 271–281.

[3] International Diabetes Federation, *IDF Diabetes Atlas 10th Edition*, Brussels, **2021**.

[4] J. Wang, *Chem Rev* **2008**, *108*, 814–825.

[5] M. Tansey, L. Laffel, J. Cheng, R. Beck, J. Coffey, E. Huang, C. Kollman, J. Lawrence, J. Lee, K. Ruedy, W. Tamborlane, T. Wysocki, D. Xing, *Diabetic Medicine* **2011**, *28*, 1118–1122.

[6] M. Shichiri, Y. Yamasaki, R. Kawamori, N. Hakui, H. Abe, *The Lancet* **1982**, *320*, 1129–1131.

[7] I. Hirsch, *ADA Clinical Compendia* **2018**, *2018*, 1–1.

[8] H. Uchino, R. Kawamori, *Contrib Nephrol* **2001**, *134*, 106–112.

[9] A. E. G. Cass, G. Davis, G. D. Francis, H. Allen, O. Hill, W. J. Aston, I. J. Higgins, E. V. Plotkin, L. D. L. Scott, A. P. F. Turner, *Anal Chem* **1984**, *56*, 667–671.

[10] D. R. Matthews, E. Bown, A. Watson, R. R. Holman, J. Steemson, S. Hughes, D. Scott, *The Lancet* **1987**, *329*, 778–779.

[11] J. J. Mastrototaro, *Diabetes Technol Ther* **2000**, *2 Suppl 1*, S13-8.

[12] M. J. Tierney, J. A. Tamada, R. O. Potts, L. Jovanovic, S. Garg, in *Biosens Bioelectron*, Elsevier, **2001**, pp. 621–629.

[13] J. Brauker, A. Kamath, Y. Li, H. Zisser, S. Schwartz, R. Ratner, J. Wise, T. Bailey, *Diabetes* **2007**, *56*.

[14] G. McGarraugh, R. Brazg, R. Weinstein, *J Diabetes Sci Technol* **2011**, *5*, 99–106.

[15] T. Bailey, B. W. Bode, M. P. Christiansen, L. J. Klaff, S. Alva, *Diabetes Technol Ther* **2015**, *17*, 787–794.

[16] T. S. Bailey, A. Chang, M. Christiansen, *J Diabetes Sci Technol* **2015**, *9*, 209–214.

[17] M. Christiansen, T. Bailey, E. Watkins, D. Liljenquist, D. Price, K. Nakamura, R. Boock, T. Peyser, *Diabetes Technol Ther* **2013**, *15*, 881–888.

[18] M. P. Christiansen, S. K. Garg, R. Brazg, B. W. Bode, T. S. Bailey, R. H. Slover, A. Sullivan, S. Huang, J. Shin, S. W. Lee, F. R. Kaufman, *Diabetes Technol Ther* **2017**, *19*, 446–456.

[19] T. S. Bailey, A. Ahmann, R. Brazg, M. Christiansen, S. Garg, E. Watkins, J. B. Welsh, S. W. Lee, *Diabetes Technol Ther* **2014**, *16*, 277–283.

[20] P. N. Bartlett, F. A. Al-Lolage, *Journal of Electroanalytical Chemistry* **2018**, *819*, 26–37.

[21] M. W. Marinen, S. A. Schichman, S. C. Hill, H. B. Gray, *Science (1979)* **1983**, *222*, 929–931.

[22] Y. Degani, A. Heller, *Journal of Physical Chemistry* **1987**, *91*, 1285–1289.

[23] A. L. Ghindilis, P. Atanasov, E. Wilkins, *Electroanalysis* **1997**, *9*, 661–674.

[24] J. M. Goran, S. M. Mantilla, K. J. Stevenson, *Anal Chem* **2013**, *85*, 1571–1581.

[25] C. Chen, X. L. Zhao, Z. H. Li, Z. G. Zhu, S. H. Qian, A. J. Flewitt, *Sensors (Switzerland)* **2017**, *17*, 182.

[26] T. Bobrowski, W. Schuhmann, *Curr Opin Electrochem* **2018**, *10*, 112–119.

[27] M. Rasmussen, S. Abdellaoui, S. D. Minteer, *Biosens Bioelectron* **2016**, *76*, 91–102.

[28] D. Leech, P. Kavanagh, W. Schuhmann, *Electrochim Acta* **2012**, *84*, 223–234.

[29] S. C. Barton, J. Gallaway, P. Atanassov, *Chem Rev* **2004**, *104*, 4867–4886.

[30] N. Mano, *Bioelectrochemistry* **2019**, *128*, 218–240.

[31] M. Christwardana, Y. Chung, D.-H. Kim, Y. Kwon, *Journal of Industrial and Engineering Chemistry* **2019**, *71*, 435–444.

[32] R. D. Milton, F. Giroud, A. E. Thumser, S. D. Minteer, R. C. T. Slade, *Physical Chemistry Chemical Physics* **2013**, *15*, 19371–19379.

[33] D. Macaodha, P. O'Conghaile, B. Egan, P. Kavanagh, C. Sygmund, R. Ludwig, D. Leech, *Electroanalysis* **2013**, *25*, 94–100.

[34] R. Ludwig, W. Harreither, F. Tasca, L. Gorton, *ChemPhysChem* **2010**, *11*, 2674–2697.

[35] M. Zamocky, R. Ludwig, C. Peterbauer, B. Hallberg, C. Divne, P. Nicholls, D. Haltrich, *Curr Protein Pept Sci* **2006**, *7*, 255–280.

[36] F. Tasca, M. N. Zafar, W. Harreither, G. Nöll, R. Ludwig, L. Gorton, *Analyst* **2011**, *136*, 2033–2036.

[37] W. Harreither, C. Sygmund, M. Augustin, M. Narciso, M. L. Rabinovich, L. Gorton, D. Haltrich, R. Ludwig, *Appl Environ Microbiol* **2011**, *77*, 1804–1815.

[38] R. Ludwig, R. Ortiz, C. Schulz, W. Harreither, C. Sygmund, L. Gorton, *Anal Bioanal Chem* **2013**, *405*, 3637–3658.

[39] S. Scheiblbrandner, R. Ludwig, *Bioelectrochemistry* **2020**, *131*, 107345.

[40] R. Ortiz, M. Rahman, B. Zangrilli, C. Sygmund, P. O. Micheelsen, M. Silow, M. D. Toscano, R. Ludwig, L. Gorton, *ChemElectroChem* **2017**, *4*, 846–855.

[41] R. Ortiz, H. Matsumura, F. Tasca, K. Zahma, M. Samejima, K. Igarashi, R. Ludwig, L. Gorton, *Anal Chem* **2012**, *84*, 10315–10323.

[42] W. Harreither, P. Nicholls, C. Sygmund, L. Gorton, R. Ludwig, *Langmuir* **2012**, *28*, 6714–6723.

[43] W. Harreither, V. Coman, R. Ludwig, D. Haltrich, L. Gorton, *Electroanalysis* **2007**, *19*, 172–180.

[44] C. Sygmund, W. Harreither, D. Haltrich, L. Gorton, R. Ludwig, *N Biotechnol* **2009**, *25*, S115.

[45] A. Lindgren, L. Gorton, T. Ruzgas, U. Baminger, D. Haltrich, M. Schülein, *Journal of Electroanalytical Chemistry* **2001**, *496*, 76–81.

[46] F. Tasca, R. Ludwig, L. Gorton, R. Antiochia, **2013**, *177*, 64–69.

[47] M. N. Zafar, G. Safina, R. Ludwig, L. Gorton, *Anal Biochem* **2012**, *425*, 36–42.

[48] G. Henriksson, G. Johansson, G. Pettersson, *J Biotechnol* **2000**, *78*, 93–113.

[49] B. M. Hallberg, G. Henriksson, G. Pettersson, A. Vasella, C. Divne, *Journal of Biological Chemistry* **2003**, *278*, 7160–7166.

[50] A. F. Geiss, T. M. B. Reichhart, B. Pejker, E. Plattner, P. L. Herzog, C. Schulz, R. Ludwig, A. K. G. Felice, D. Haltrich, *ACS Sustain Chem Eng* **2021**, *9*, 7086–7100.

[51] G. G. Guilbault, G. J. Lubrano, *Anal Chim Acta* **1973**, *64*, 439–455.

[52] D. Wang, L. Chen, *Electrochim Acta* **2009**, *54*, 4316–4320.

[53] P. Kavanagh, D. Leech, *Physical Chemistry Chemical Physics* **2013**, *15*, 4859–4869.

[54] S. Boland, P. Kavanagh, D. Leech, *ECS Trans* **2008**, *13*, 77–87.

[55] M. V. Pishko, A. C. Michael, A. Heller, *Anal Chem* **1991**, *63*, 2268–2272.

[56] A. Heller, B. Feldman, *Chem Rev* **2008**, *108*, 2482–2505.

[57] D. Hickey, M. Meredith, D. Schmidtke, D. Glatzhofer, *ECS Meeting Abstracts* **2012**, *MA2012-01*, 1432–1432.

[58] S. M. Zakeeruddin, D. M. Fraser, M. K. Nazeeruddin, M. Grätzel, *Journal of Electroanalytical Chemistry* **1992**, *337*, 253–283.

[59] F. Mao, N. Mano, A. Heller, *J Am Chem Soc* **2003**, *125*, 4951–4957.

[60] N. Mano, F. Mao, A. Heller, *J Am Chem Soc* **2003**, *125*, 6588–6594.

[61] T. de Lumley-Woodyear, P. Rocca, J. Lindsay, A. Heller, P. Rocca, Y. Dror, A. Freeman, *Anal Chem* **1995**, *67*, 1332–1338.

[62] P. Ó Conghaile, D. MacAodha, B. Egan, P. Kavanagh, D. Leech, *J Electrochem Soc* **2013**, *160*, G3165–G3170.

[63] D. MacAodha, P. Ó. Conghaile, B. Egan, P. Kavanagh, D. Leech, *ChemPhysChem* **2013**, *14*, 2302–2307.

[64] L. Ye, M. Hämmerle, A. J. J. Olsthoorn, W. Schuhmann, H. L. Schmidt, J. A. Duine, A. Hellert, *Anal Chem* **1993**, *65*, 238–241.

[65] A. Ruff, *Curr Opin Electrochem* **2017**, *5*, 66–73.

[66] S. Alsaoub -Bochum, *Synthesis of Stable Os-Complex Modified Polymers for the Applications in Biosensors, Biofuel Cells and Biosupercapacitors*, **2017**.

[67] D. MacAodha, M. L. Ferrer, P. Ó. Conghaile, P. Kavanagh, D. Leech, *Physical Chemistry Chemical Physics* **2012**, *14*, 14667–14672.

[68] B. A. Gregg, A. Heller, *Anal Chem* **1990**, *62*, 258–263.

[69] J. W. Gallaway, S. A. Calabrese Barton, *Journal of Electroanalytical Chemistry* **2009**, *626*, 149–155.

[70] A. Heller, *Biosensors (Basel)* **2004**, *2*, 1–18.

[71] T. J. Ohara, R. Rajagopalan, A. Heller, *Anal Chem* **1993**, *65*, 3512–3517.

[72] T. J. Ohara, R. Rajagopalan, A. Heller, *Anal Chem* **1994**, *66*, 2451–2457.

[73] D. N. Blauch, J. M. Savéant, *J Am Chem Soc* **1992**, *114*, 3323–3332.

[74] P. Anderson, Mark J.; Whitcomb, *DOE Simplified: Practical Tools for Effective Experimentation With CDROM: Amazon.de: Mark J. Anderson, Patrick J. Whitcomb: Fremdsprachige Bücher*, CRC Press, **2007**.

[75] M. J. Anderson, *RSM Simplified*, Productivity Press, **2016**.

[76] R. Kumar, J. Lahann, *ACS Appl Mater Interfaces* **2016**, *8*, 16595–16603.

[77] G. D. Bowden, B. J. Pichler, A. Maurer, *Sci Rep* **2019**, *9*, 11370.

[78] V. Flexer, K. F. E. Pratt, F. Garay, P. N. Bartlett, E. J. Calvo, *Journal of Electroanalytical Chemistry* **2008**, *616*, 87–98.

[79] S. Babanova, K. Artyushkova, Y. Ulyanova, S. Singhal, P. Atanassov, *J Power Sources* **2014**, *245*, 389–397.

[80] R. Kumar, D. Leech, *Bioelectrochemistry* **2015**, *106*, 41–46.

[81] R. Bennett, I. Osadebe, R. Kumar, P. Ó. Conghaile, D. Leech, *Electroanalysis* **2018**, *30*, 1438–1445.

[82] I. Osadebe, P. Conghaile, P. Kavanagh, D. Leech, *Electrochim Acta* **2015**, *182*, 320–326.

[83] L. Liu, D. Yang, G. Liu, *Biosens Bioelectron* **2019**, *136*, 60–75.

[84] R. Gifford, *ChemPhysChem* **2013**, *14*, 2032–2044.

[85] W. J. Peveler, M. Yazdani, V. M. Rotello, *ACS Sens* **2016**, *1*, 1282–1285.

[86] K. M. Bratlie, R. L. York, M. A. Invernale, R. L. Langer, D. G. Anderson, *Adv Healthc Mater* **2012**, *1*, 267–284.

[87] D. M. Nathan, *Diabetes Care* **2014**, *37*, 9–16.

[88] D. Bruen, C. Delaney, L. Florea, D. Diamond, *Sensors (Switzerland)* **2017**, *17*, 1866.

[89] R. Badugu, J. R. Lakowicz, C. D. Geddes, *Talanta* **2005**, *65*, 762–768.

[90] P. Makaram, D. Owens, J. Aceros, *Diagnostics* **2014**, *4*, 27–46.

[91] V. D. Funtanilla, P. Candidate, T. Caliendo, O. Hilas, *P T* **2019**, *44*, 550–553.

[92] G. Cappon, G. Acciaroli, M. Vettoretti, A. Facchinetti, G. Sparacino, *Electronics (Switzerland)* **2017**, *6*, 65.

[93] Z. Zhu, L. Garcia-Gancedo, A. J. Flewitt, H. Xie, F. Moussy, W. I. Milne, *Sensors 2012, Vol. 12, Pages 5996-6022* **2012**, *12*, 5996–6022.

[94] Y. Chandorkar, K. Ravikumar, B. Basu, *ACS Biomater Sci Eng* **2019**, *5*, 19–44.

[95] N. Noskovicova, B. Hinz, P. Pakshir, *Cells* **2021**, *10*, 1794.

[96] J. M. Harris, C. Reyes, G. P. Lopez, *J Diabetes Sci Technol* **2013**, *7*, 1030–1038.

[97] A. Prévoteau, N. Mano, *Electrochim Acta* **2012**, *68*, 128–133.

[98] J. G. Hauge, *BBA - Biochimica et Biophysica Acta* **1960**, *45*, 263–269.

[99] Y. K. Cho, J. E. Bailey, *Biotechnol Bioeng* **1977**, *19*, 769–775.

[100] P. F. Greenfield, J. R. Kittrell, R. L. Laurence, *Anal Biochem* **1975**, *65*, 109–124.

[101] K. Kleppe, *Biochemistry* **1966**, *5*, 139–143.

[102] S. Krishnaswamy, J. R. Kittrell, *Biotechnol Bioeng* **1978**, *20*, 821–835.

[103] C. O. Malikkides, R. H. Weiland, *Biotechnol Bioeng* **1982**, *24*, 2419–2439.

[104] W. Kerner, M. Kiwit, B. Linke, F. S. Keck, H. Zier, E. F. Pfeiffer, *Biosens Bioelectron* **1993**, *8*, 473–482.

[105] J. C. Armour, J. Y. Lucisano, B. D. McKean, D. A. Gough, *Diabetes* **1990**, *39*, 1519–1526.

[106] D. A. Gough, *Hormone and Metabolic Research* **1988**, *20*, 30–33.

[107] D. A. Gough, L. S. Kumosa, T. L. Routh, J. T. Lin, J. Y. Lucisano, *Sci Transl Med* **2010**, *2*, DOI 10.1126/scitranslmed.3001148.

[108] J. K. Leypoldt, D. A. Gough, *Biotechnol Bioeng* **1982**, *24*, 2705–2719.

[109] P. H. S. Tse, D. A. Gough, *Biotechnol Bioeng* **1987**, *29*, 705–713.

[110] P. H. S. Tse, J. K. Leypoldt, D. A. Gough, *Biotechnol Bioeng* **1987**, *29*, 696–704.

[111] D. A. Gough, T. Bremer, *Diabetes Technol Ther* **2000**, *2*, 377–380.

[112] M. Jablecki, D. A. Gough, *Anal Chem* **2000**, *72*, 1853–1859.

[113] F. López-Gallego, L. Betancor, C. Mateo, A. Hidalgo, N. Alonso-Morales, G. Dellamora-Ortiz, J. M. Guisán, R. Fernández-Lafuente, *J Biotechnol* **2005**, *119*, 70–75.

[114] A. Prévoteau, O. Courjean, N. Mano, *Electrochem commun* **2010**, *12*, 213–215.

[115] O. Courjean, V. Flexer, A. Prévoteau, E. Suratini, O. Courjean, V. Flexer, A. Prévoteau, E. Suratini, N. M. Effect, O. Courjean, V. Flexer, A. Prøvoteau, E. Suraniti, N. Mano, **2017**.

[116] F. Wu, P. Yu, L. Mao, *Curr Opin Electrochem* **2017**, *5*, 152–157.

[117] W. Kerner, M. Kiwit, B. Linke, F. S. Keck, H. Zier, E. F. Pfeiffer, *Biosens Bioelectron* **1993**, *8*, 473–482.

[118] T. von Woedtke, U. Fischer, P. Abel, *Biosens Bioelectron* **1994**, *9*, 65–71.

[119] P. N. Bartlett, R. G. Whitaker, *Journal of Electroanalytical Chemistry* **1987**, *224*, 27–35.

[120] K. Rebrin, U. Fischer, H. Hahn von Dorsche, T. von Woetke, P. Abel, E. Brunstein, *J Biomed Eng* **1992**, *14*, 33–40.

[121] S. V. Sasso, R. J. Pierce, R. Walla, A. M. Yacynych, *Anal Chem* **1990**, *62*, 1111–1117.

[122] S. A. Emr, A. M. Yacynych, in *Electroanalysis*, John Wiley & Sons, Ltd, **1995**, pp. 913–923.

[123] C. Malitesta, F. Palmisano, L. Torsi, P. G. Zambonin, *Anal Chem* **1990**, *62*, 2735–2740.

[124] F. Palmisano, D. Centonze, A. Guerrieri, P. G. Zambonin, *Biosens Bioelectron* **1993**, *8*, 393–399.

[125] R. Sternberg, D. S. Bindra, G. S. Wilson, D. R. Thévenot, *Anal Chem* **1988**, *60*, 2781–2786.

[126] F. Moussy, S. Jakeway, D. J. Harrison, R. V. Rajotte, *Anal Chem* **1994**, *66*, 3882–3888.

[127] J. Wang, H. Wu, *Anal Chim Acta* **1993**, *283*, 683–688.

[128] D. Moatti-Sirat, F. Capron, V. Poitout, G. Reach, D. S. Bindra, Y. Zhang, G. S. Wilson, D. R. Thévenot, *Diabetologia* **1992**, *35*, 224–230.

[129] Y. Benmakroha, I. Christie, M. Desai, P. Vadgama, *Analyst* **1996**, *121*, 521–526.

[130] D. Centonze, A. Guerrieri, C. Malitesta, F. Palmisano, P. G. Zambonin, *Fresenius J Anal Chem* **1992**, *342*, 729–733.

[131] T. Xiao, F. Wu, J. Hao, M. Zhang, P. Yu, L. Mao, in *Anal Chem*, American Chemical Society, **2017**, pp. 300–313.

[132] D. W. Grainger, *Nat Biotechnol* **2013**, *31*, 507–509.

[133] C. Jiang, G. Wang, R. Hein, N. Liu, X. Luo, J. J. Davis, *Chem Rev* **2020**, *120*, 3852–3889.

[134] S. Woderer, N. Henninger, C. D. Garthe, H. M. Kloetzer, M. Hajnsek, U. Kamecke, N. Gretz, B. Kraenzlin, J. Pill, *Anal Chim Acta* **2007**, *581*, 7–12.

[135] S. Liu, J. Tang, F. Ji, W. Lin, S. Chen, *Gels* **2022**, *8*, 46.

[136] M. Gerritsen, J. A. Jansen, J. A. Lutterman, *Netherlands Journal of Medicine* **1999**, *54*, 167–179.

[137] N. Wisniewski, F. Moussy, W. M. Reichert, *Fresenius' Journal of Analytical Chemistry 2000 366:6* **2000**, *366*, 611–621.

[138] J. M. Anderson, K. M. Miller, *Biomaterials* **1984**, *5*, 5–10.

[139] S. Chen, J. A. Jones, Y. Xu, H. Y. Low, J. M. Anderson, K. W. Leong, *Biomaterials* **2010**, *31*, 3479–3491.

[140] J. M. Anderson, A. Rodriguez, D. T. Chang, *Semin Immunol* **2008**, *20*, 86–100.

[141] X. Xie, J. C. Doloff, V. Yesilyurt, A. Sadraei, J. J. McGarrigle, M. Omami, O. Veiseh, S. Farah, D. Isa, S. Ghani, I. Joshi, A. Vegas, J. Li, W. Wang, A. Bader, H. H. Tam, J. Tao, H. J. Chen, B. Yang, K. A. Williamson, J. Oberholzer, R. Langer, D. G. Anderson, *Nature Biomedical Engineering 2018 2:12* **2018**, *2*, 894–906.

[142] R. Jayakumar, M. Prabaharan, S. V. Nair, H. Tamura, *Biotechnol Adv* **2010**, *28*, 142–150.

[143] R. Jayakumar, M. Prabaharan, P. T. Sudheesh Kumar, S. V. Nair, H. Tamura, *Biotechnol Adv* **2011**, *29*, 322–337.

[144] Y. Zhang, Y. Liu, B. Ren, D. Zhang, S. Xie, Y. Chang, J. Yang, J. Wu, L. Xu, J. Zheng, *J Phys D Appl Phys* **2019**, *52*, DOI 10.1088/1361-6463/ab2cbc.

[145] M. Li, B. Zhuang, J. Yu, *Chem Asian J* **2020**, *15*, 2060–2075.

[146] Y. Liu, D. Zhang, B. Ren, X. Gong, L. Xu, Z. Q. Feng, Y. Chang, Y. He, J. Zheng, *J Mater Chem B* **2020**, *8*, 3814–3828.

[147] J. B. Schlenoff, *Langmuir* **2014**, *30*, 9625–9636.

[148] Y. Higaki, J. Nishida, A. Takenaka, R. Yoshimatsu, M. Kobayashi, A. Takahara, *Polym J* **2015**, *47*, 811–818.

[149] B. Li, B. Li, Z. Yuan, P. Jain, H. C. Hung, Y. He, Y. He, X. Lin, P. McMullen, S. Jiang, S. Jiang, *Sci Adv* **2020**, *6*, eaba0754.

[150] J. M. Morais, F. Papadimitrakopoulos, D. J. Burgess, *AAPS Journal* **2010**, *12*, 188–196.

[151] C. Yoshikawa, S. Hattori, T. Honda, C. F. Huang, H. Kobayashi, *Mater Lett* **2012**, *83*, 140–143.

[152] J. Kim, A. S. Campbell, B. E.-F. de Ávila, J. Wang, *Nat Biotechnol* **2019**, *37*, 389–406.

[153] J. Xu, H. Lee, *Chemosensors* **2020**, *8*, 1–29.

[154] R. Wilson, A. P. F. Turner, *Biosens Bioelectron* **1992**, *7*, 165–185.

[155] R. Bennett, D. Leech, *Bioelectrochemistry* **2020**, *133*, 107460.

[156] X. Xiao, X. Yan, E. Magner, J. Ulstrup, *Electrochem commun* **2021**, *124*, 106931.

[157] B. Yu, C. Wang, Y. M. Ju, L. West, J. Harmon, Y. Moussy, F. Moussy, *Biosens Bioelectron* **2008**, *23*, 1278–1284.

[158] C. A. P. Quinn, R. E. Connor, A. Heller, *Biomaterials* **1997**, *18*, 1665–1670.

[159] M. Karimi, in *Mass Transfer in Chemical Engineering Processes*, IntechOpen, **2011**.

[160] R. I. Hickson, S. I. Barry, G. N. Mercer, H. S. Sidhu, *Math Comput Model* **2011**, *54*, 210–220.

[161] O. F. Bertrand, R. Sipehia, R. Mongrain, J. Rodés, J. C. Tardif, L. Bilodeau, G. Côté, M. G. Bourassa, *J Am Coll Cardiol* **1998**, *32*, 562–571.

[162] F. Marken, A. Neudeck, A. M. Bond, in *Electroanalytical Methods: Guide to Experiments and Applications*, Springer Berlin Heidelberg, **2010**, pp. 57–106.

[163] F. Scholz, *Electroanalytical Methods: Guide to Experiments and Applications*, Springer Berlin Heidelberg, **2010**.

[164] N. Elgrishi, K. J. Rountree, B. D. McCarthy, E. S. Rountree, T. T. Eisenhart, J. L. Dempsey, *J Chem Educ* **2018**, *95*, 197–206.

[165] L. R. Faulkner, A. J. Bard, *Electrochemical Methods: Fundamentals and Applications, New York: Wiley, 2001*, John Wiley And Sons, **2008**.

[166] K. J. Lee, N. Elgrishi, B. Kandemir, J. L. Dempsey, *Nat Rev Chem* **2017**, *1*, DOI 10.1038/s41570-017-0039.

Chapter 2: Redox polymer mediated electrochemical glucose biosensor for continuous use using glucose oxidase grafted to carbon nanotubes: a design-of-experiments optimisation of current density and stability

Published as:

Redox polymer mediated electrochemical glucose biosensor for continuous use using glucose oxidase grafted to carbon nanotubes: a design-of-experiments optimisation of current density and stability

Kavita Jayakumar, Richard Bennett, Dónal Leech, Electrochimica Acta, 2021, 371, 137845

Co-author contributions:

I synthesised the PVI-bound osmium redox polymer, performed all labwork, analysis and wrote the first draft of the publication.

Richard Bennett contributed advice and guidance throughout the laboratory work and analysis.

Dónal Leech, as project supervisor, contributed through advice and guidance throughout the work and edited the first draft to provide the final version for publication.

2.1 Abstract

Enzymatic glucose electrodes based on mediated electron transfer have potential for application as semi-implantable or implantable sensors. Enzyme electrodes consisting of adsorbed osmium-based redox polymer crosslinked with a glucose oxidising enzyme are promising systems for continuous glucose monitoring, but suffer from signal output magnitude and long-term stability issues. The inclusion of carbon nanosupports such as multiwalled carbon nanotubes (MWCNTs) into these sensors tends to increase characteristics such as current density and surface coverage of enzyme or mediator. However, large quantities of nanomaterials are often necessary to see significant effects. Grafting of the enzyme to the surface of the MWCNTs improves dispersibility of the nanosupport aiding enzyme electrode fabrication and increases enzyme activity. Here we report on a design of experiments (DoE) approach to determine the optimum amount of each component in enzyme electrodes, using glucose oxidase grafted to carbon nanotube support, to maximise current density and stability for application to continuous use glucose biosensing. Using the DoE approach while considering current density and stability responses delivers a set of component amounts where both responses are optimised. Thus far stability has not been investigated as a response to be optimised using a DoE approach. The optimised enzyme electrodes show a current density of 3.18 ± 0.30 mA cm^{-2}, representing a 146 % increase in current density in 50 mM phosphate-buffered saline at 37 °C containing 5 mM glucose when compared to similar systems where enzyme and nanosupport are not covalently bound to each other. Using the predictive DoE model, component amounts were then modified to minimise the quantity of the nanoconjugate while showing similar electrochemical behaviour and current density to the optimised system, using 93% less of the nanoconjugate. The optimised operational stability under continuous use was moderate with only ≈ 50% amperometric current retained after 12 hr use. Overcoating with a Nafion protective layer improved stability to 72-75% over the same period. The coupling of adsorbed films to the electrode surface, use of additional perm-selective membranes, and/or use of pulsed potentials to implement intermittent sampling of glucose levels, rather that continuous amperometry, is proposed to improve operational stability.

2.2 Introduction

Over the past few decades there has been increased interest in electrochemical mediated enzymatic glucose sensors targeted towards semi-implantable and implantable glucose biosensors[1–7]. Of all glucose-oxidising enzymes, glucose oxidase (GOx) has been widely utilised due to its relatively low cost as well its high bioactivity and stability[8]. Electrochemical GOx-based glucose biosensors require either a high overpotential, for first-generation sensors, or the use of a mediator as an intermediate in the electron transfer process, for second-generation sensors, as the active centre of the enzyme is buried within the enzyme structure hindering direct electron transfer[9]. There has been substantial research into the use of redox hydrogels based on polymer-bound osmium complexes[5,10–12] as mediators, with polypyridyl complexes of osmium coordinatively bound to poly(N-vinylimidazole), poly(4-vinylpyridine), poly(methacrylate) or similar polymers for this purpose[13–15]. Osmium-based complexes and polymers show advantages over iron and ruthenium-based systems due to the ability to modulate the mediator redox potential by varying coordinating ligands, the relative stability of the resulting complexes in the reduced/oxidised states (Os^{II}/Os^{III}), and because the hydrogel characteristics of enzymatic electrodes based on redox-polymer films permit rapid mass and charge transport, thus generating substantial current signals[2,13,16].

The integration of nanomaterials as components of enzyme electrodes aids in increasing current capture as evidenced by reports on the effect upon inclusion of gold nanoparticles, platinum nanoparticles, carbon nanoparticles into electrodes [17–21]. In the case of enzymatic electrodes for glucose oxidation, it has been demonstrated that systems integrating carbon micro-, meso- and nano- structured materials show improved performance over those prepared without addition of such materials[13,22–24]. Inclusion of multi-walled carbon nanotubes (MWCNTs) in particular shows a distinct advantage due to fast electron transfer rate for redox reactions and high electrical conductivity, rendering them an attractive option. For instance, inclusion of MWCNTs has been shown to improve glucose oxidation currents for enzyme electrodes prepared by inclusion of the nanomaterial within crosslinked films of enzymes and osmium-based redox polymers[13,25–27], attributed to improved

retention of enzyme activity and increased surface area for retention of redox species [28].

Another consideration is the effect of the nanosupport-enzyme relationship. Immobilisation of enzyme shows advantages when compared to free enzyme, namely increased enzyme activity and improved specificity[29–31]. Considering carbon-based nanosupports, immobilisation of enzymes onto the surface on these materials has resulted in increased enzyme turnover and extension of the lifetime of the enzyme, allowing prolonged use[32–34]. On investigating the nanosupport-enzyme relationship with respect to specific enzyme activity, Campbell *et al* demonstrated higher enzymatic activity of GOx when covalently attached to MWCNTs[35]. However, when MWCNTs are used for biomedical applications, the dispersibility of the material, which impacts the stability and toxicokinetics of the CNTs, plays an important role[36–38]. Furthermore, dispersibility also plays a key role when considering fabrication of enzyme electrode biosensors as aggregation of MWCNTs in some mixtures can result in uneven dispersion of material, and lack of precision in drop-coating material onto the electrode surface. The use of a MWCNT-GOx nanoconjugate can alleviate this issue as grafting enzyme onto the surface of the MWCNTs improves nanoconjugate dispersibility[36,37].

Taking into account the multiple components of an enzyme electrode, it would be beneficial to determine how each component and the interaction of the components with one another affects parameters such as current density and the stability of these current signals on prolonged use. A comprehensive study would allow the optimisation of the components to maximise electrode performance. For this purpose, a design of experiments (DoE) approach shows distinct advantage over conventional one-factor-at-a time (OFAT) methods. Conventional OFAT methods rely on holding one variable constant, while varying the other and hence detecting one variable or factor at a time, how the response changes. Unlike OFAT, DoE explores, maps and models the behaviour of the response (or multiple responses) within a given reaction space across multiple factors simultaneously by varying all variables at once, giving a comprehensive picture of how factors and their behaviour affect the response[39]. Moreover, OFAT is unable to detect the effect of factor interactions, a shortcoming that the DoE method overcomes. The statistical optimisation process that DoE offers

has gained popularity from scientists and engineers across a variety of industries for the optimisation of a range of scientific processes[39–44].

Here we use a dual response Box Behnken design of experiments surface response approach to improve the current density and/or operational stability of enzyme electrodes. The enzyme electrodes are fabricated with osmium-based redox polymer, CNT-GOx nanoconjugate and poly(ethylene glycol) diglycidyl ether (PEGDGE) di-epoxide crosslinker and are operated under pseudo-physiological conditions. The predictive model developed was used to optimise and modify the component amounts to achieve a compromise of high current density output and high stability, at a low amount of nanoconjugate.

2.3 Experimental

2.3.1 Materials

All chemicals used in the study were from Sigma-Aldrich, unless stated otherwise. The osmium redox polymer used, $[Os(2,2'\text{-bipyridine})_2(polyvinylimidazole)_{10}Cl]^+$ structure represented in Figure S2.1 and denoted as (Os(bpy)PVI), was synthesised using literature procedures [45,46]. The glucose oxidase was from *Aspergillus niger* (GOx, EC 1.1.3.4., Sigma-Aldrich). Milli-Q water (18 MΩcm) was used to prepare all aqueous solutions. N-hydroxysulfosuccinimide (sulfo-NHS), N-ethyl-N'-(3-dimethylaminopropyl) carbodiimide hydrochloride (EDC) and 2-(N-morpholino)ethanesulfonic acid (MES) was used in the covalent attachment of enzyme onto MWCNTs, all from Sigma Aldrich. The Nafion solution (5% w/v) was from Sigma Aldrich and was diluted in ethanol to produce solutions containing 0.5% and 1% Nafion.

2.3.2 Methods

2.3.2.1 Grafting of glucose oxidase onto multi-walled carbon nanotubes

GOx was covalently attached onto the MWCNTs using literature procedures[36,40]. Briefly, MWCNTs were first oxidised by stirring (200 rpm) in an acid solution consisting of H_2SO_4 (98%, 7.5 mL) and HNO_3 (70%, 2.5 mL), at room temperature overnight. Acid-treated and oxidised MWCNTs (CNT-ox) were washed with distilled water and dried at 80 °C in a vacuum oven. CNT-ox (20 mg) was suspended in distilled water (10 mL) and then added to a mixture of MES buffer (4 mL, 500 mM, pH 6.5), sulfo-NHS aqueous solution (4 mL, 434 mM), and EDC aqueous solution (2 mL, 53 mM). After rigorous stirring at room temperature for 1 h the suspension was filtered and washed with 100 mM MES buffer (pH 6.5). Covalent attachment of the GOx onto the MWCNTs (CNT-GOx) occurred on addition of the EDC-NHS activated CNTs (2 mg) to 1 mL of GOx solution (10 mg/mL in 100 mM PBS, pH 7.0). The mixture was stirred (200 rpm) at room temperature for 1 h and then placed in the fridge at 4 °C overnight. Aliquots of this mixture were taken and stored at -20 °C until used.

2.3.2.2 Enzyme Electrode Preparation

Graphite rods (Graphite store, USA, 3.0 mm diameter, NC001295) were cut, insulated with heat shrinking tubing and polished at one end using fine grit paper to give graphite working electrodes with a geometric surface area of 0.0707 cm^2. The enzyme electrodes were assembled by drop-coating appropriate volumes of each of the components: Os(bpy)PVI redox polymer aqueous solution (5 mg mL^{-1}); CNT-GOx solution (2 mg CNT in 1 mL of 10 mg mL^{-1} GOx); and PEGDGE crosslinker solution (15 mg mL^{-1}). The deposition was allowed to dry for 24 h before the electrodes are used.

2.3.2.3 Design of Experiments

The volume of each of the components deposited on the enzyme electrodes is determined by the Design Expert Software (Version 9, STAT-EASE Inc., Minneapolis, USA) using the low, central and high values selected in Table 1. The low values of CNT-GOx and Os(bpy)PVI are selected as a minimum level requirement for the production of glucose oxidation current. The high values selected for each

component are to eliminate difficulties in co- immobilisation and retention of higher masses on the electrode surface. The central values are chosen to be around the median of the high and low limits. The design was run to optimise two responses separately, the initial amperometric current density and the short-term operational stability after 3 hr continuous polarisation in phosphate buffered saline (PBS, 0.05 M phosphate, pH 7.4, 0.15 M NaCl) solutions containing 5 mM glucose at 37°C (pseudo-physiological level).

Table 2.1: The factors and levels selected to vary for DoE

Factor	Low Value (-1)/ *μg*	Central Value (0)/ *μg*	High Value (+1)/ *μg*
CNT-GOx	10	90	150
Os(bpy)PVI	10	70	150
PEGDGE	15	75	120

2.3.2.4 Electrochemical Measurements

Electrochemical tests were conducted using a CH Instrument 1030a multichannel potentiostat (IJ Cambria) coupled with a thermostated electrochemical cell containing PBS at 37°C in the presence of ambient oxygen. The prepared enzyme electrodes were used as the working electrodes and paired with a custom-built Ag/AgCl (3M KCl) reference electrode and a platinum mesh (Goodfellow) as a counter electrode. Currents were normalised to the geometric surface area of the graphite disk electrodes to generate current density data. The stability values presented in this paper represent, unless otherwise indicated, the percentage of amperometric current density remaining at the end of a 3-hour operational period compared to that obtained 10 minutes after initial polarisation at 0.35 V.

2.3.2.5 Enzymatic Assay of Glucose Oxidase

The GOx activity was determined using an o-dianisidine, horseradish peroxidase coupled, spectrophotometric assay by monitoring absorbance change (Agilent 8453 UV-visible spectrophotometer) at 460 nm [47].

2.4 Results and Discussion

Addition of multiwalled carbon nanotubes (MWCNTs) as a nanosupport has been shown to increase the current density and redox mediator surface coverage of enzyme electrodes by providing an increased surface area for immobilisation of components[43,48]. However, in these cases, large quantities of MWCNTs have been used which can cause issues- mainly in stability and difficulties of co-immobilisation. Use of large quantities of components increases the difficulty in controlling the drop-coat on the electrode surface, affecting the precision and reproducibility. Keeping in mind future *in vivo* application, these electrodes would also require rigorous testing to ensure that the materials remain immobilised in the matrix. Grafting of enzyme onto MWCNTs has a significant effect, improving the stability of the enzyme and of the measured current density for enzyme electrodes [40,49]. Using this technique, it is possible to obtain a nanocomposite of enzyme and nanosupport (CNT-GOx) which shows current densities comparable to previous systems while using significantly smaller amounts. Here we undertake a design of experiments approach to determine the optimum amount of each component to be used to deliver either the highest current density or the highest operational stability.

Slow-scan cyclic voltammetry in the presence and absence of glucose was used to initially characterise enzyme electrodes consisting of CNT-GOx and Os(bpy)PVI redox polymer crosslinked using PEGDGE di-epoxide crosslinker. Scans recorded in the absence of glucose show peaks with redox potential centred at approximately 0.22 V vs. Ag/AgCl (3M KCl) (Figure 2.1) which agrees with previously reported values for the Os(II/III) transition of the redox polymer[10,50]. The half-wave potential recorded is negatively shifted slightly when in the presence of glucose compared to the redox potential in the absence of glucose. The basis for this shift is unclear at present, but may be indicative of substrate transport that occurs for a mixed case between substrate and kinetic-limited conditions[51,52]. At relatively slow scan rates (< 20 mV s^{-1}), peak currents vary linearly with scan rate as expected for a surface-confined redox response[53]. Peak currents vary linearly with the square root of scan rate at higher scan rates (>20 mV s^{-1}) when semi-infinite diffusion pertains for these multilayer films[53]. The osmium surface coverage (Γ_{os}) for the redox polymer,

estimated by integrating the area under the peak for CVs recorded at slow scan rates in the absence of substrate, was found to be 182 ± 12 nmol cm^{-2}, indicative of a multi-layer formation and similar to results obtained by others for the co-immobilisation of GOx with osmium-based redox polymers[28,44,48,54]. The addition of glucose to the electrochemical cell resulted in sigmoidal shaped responses characteristic of an electrocatalytic (EC') process.

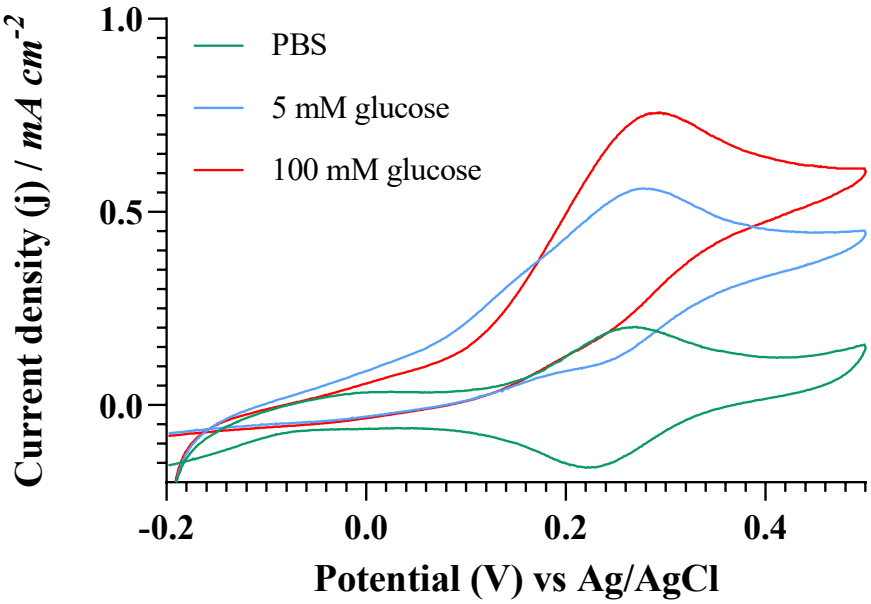

Figure 2.1: Cyclic voltammograms recorded at 1 mV s^{-1} of enzyme electrodes tested in the PBS (green) and 5 mM glucose (blue) and 100 mM glucose (red) at 37 °C. Enzyme electrodes consisted of CNT-GOx (10 µg), Os(bpy)PVI (90 µg) and PEGDGE (105 µg).

Amperometric measurements were carried out at 0.35 V vs. Ag/AgCl (3M KCl), selected as a potential 150 mV more positive than that at which a steady state current is achieved using hydrodynamic amperometry in PBS solutions containing 5 mM glucose (Appendix A.2, Figure S2.2). Amperometric glucose oxidation current density as a function of glucose concentration (Figure 2.2 with raw amperometry trace in Figure S2.3, Appendix A.2) fitted to a Michaelis-Menten model allowed the estimation of K_m^{app} values and maximum saturation current densities (j_{max}) of 3.72 ± 0.20 mM and 3.53 ± 0.10 mA cm^{-2} respectively. The obtained K_m^{app} is similar to values obtained from previous reports for GOx immobilised by Os based polymer on the electrode surface without CNTs [28] indicating good affinity towards the substrate while j_{max} correlates well with previous reports [28,43], demonstrating that the CNT-GOx based

system has comparable current density to systems with higher CNT loads. It should be noted that such a low K_m^{app} can result in a biosensor with a linear range for detection of glucose levels in saliva or sweat [55] but that the linear range will need to be expanded, for example through use of additional polymer coatings [56] to allow the detection of glucose in physiological fluids such as interstitial fluid or blood.

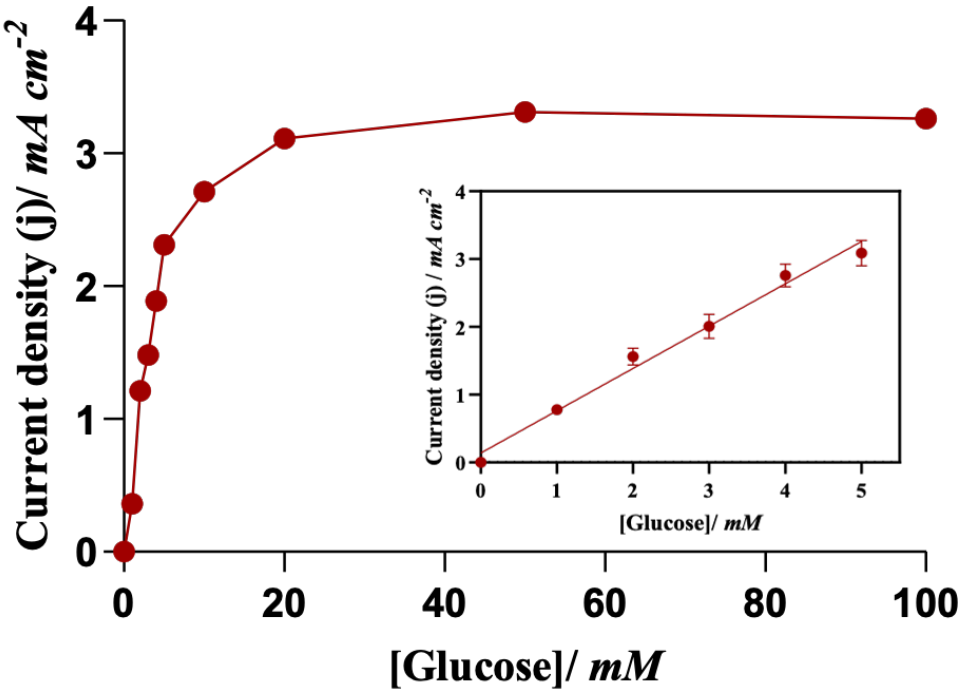

Figure 2.2: Glucose oxidation current density as a function of glucose concentration measured at 0.35 V in PBS at 37°C with stirring of the solution at 150 rpm. Enzyme electrodes consisted of CNT-GOx (10 µg), Os(bpy)PVI (90 µg) and PEGDGE (105 µg).

2.4.1 Design of Experiments

To conduct a systematic optimisation of relative amounts of each component to be used to prepare the enzyme electrode with high sensor response signal and maximum operational stability, we used a response surface factorial Box–Behnken Design (BBD) with the three design variables set at the levels summarised in Table 2.1. The design variables of the CNT-GOx, osmium redox polymer and PEGDGE component amounts form the inputs to the model while the current density in pseudo-physiological glucose and operational stability over 3 hours are the model outputs. The number of

experimental runs in a Box-Behnken design is $N=2k\ (k-1) + C_0$ [57], where k is the number of factors, and C_0 is the number of central points, i.e., the runs where each component is at the central values shown in Table 2.1. The 17 run experimental design (Table 2.2), representing a systematic sampling of combinations possible within the design space, was used to gauge the relative importance of the enzyme electrode components and their interactions. Each of the 17 experimental runs was performed on three electrodes and the average response was used in the design. The order of experimental runs was randomised to ensure independence of the data points of components and to separate the repeated central runs so as to account for human error. By analysing results from this small sample space, predictions can be made about any point in the entire experimental space, including those points about which we have no prior knowledge, if the model is found to be significant and valid.

In terms of selecting the inputs, the low levels of CNT-GOx and Os(bpy)PVI component amounts in this design were selected to be 10 µg each as this is the minimum level requirement for the production of glucose oxidation current density based on previous reports[11,43,58–60]. The CNT-GOx levels were selected keeping in mind that some amount of enzyme is required in the system to achieve glucose oxidation, but large amounts will cause difficulty in dispersing the CNT-GOx in solution to achieve reproducible co-immobilisation by drop-coating. The five runs for electrodes prepared using the central (0) component level, runs 1, 4, 6, 7 and 9 in Table 2.2, attained current density and stability responses of 2.93 ± 0.67, 2.91 ± 0.67, 2.58 ± 0.22, 2.62 ± 0.11 and 2.54 ± 0.57 mA cm^{-2} and 49, 55, 49, 59 and 50 %, respectively. When all 15 electrode responses for electrodes prepared using the central (0) component level are considered together an average current density and stability response of 2.72 ± 0.44 mA cm^{-2} and 53 ± 4 % is obtained, respectively. Replication of the central levels for the model strengthens the model and minimises the error in predictions.

After completing the experimental runs (Table 2.2), a statistical analysis of the variance (ANOVA) was undertaken on the results in order to identify the most significant sources of variation and thereby understand the roles of the three experimental variables on each response[41]. ANOVA yields F-ratios, which forms the basis for rank-ordering main effects and understanding their relative importance.

Apart from quantifying the impact of the three main effects on each response, ANOVA is also able to identify statistically significant two- and three-factor interactions. The approach in model analysis is to check if the F-values are significant, the adjusted and predicted R^2 values are within 0.2 and the adequate precision is over 4. If these criteria are met, the model is valid and makes good predictions for average responses[61,62].

Table 2.2: Design layout showing run number, component levels and responses

Run	**A:** CNT-GOx / μg	**B:** Os(bpy)PVI / μg	**C:** PEGDGE / μg	**j @ 5 mM glucose** / $mA\ cm^{-2}$	**Stability** /%
1	0	0	0	2.93 ± 0.67	49 ± 4
2	1	-1	0	2.73 ± 0.61	32 ± 4
3	1	1	0	2.50 ± 0.50	52 ± 5
4	0	0	0	2.91 ± 0.67	55 ± 5
5	-1	0	-1	1.40 ± 0.41	48 ± 4
6	0	0	0	2.58 ± 0.22	49 ± 3
7	0	0	0	2.62 ± 0.11	59 ± 1
8	1	0	1	2.93 ± 0.88	49 ± 5
9	0	0	0	2.54 ± 0.57	50 ± 2
10	0	-1	-1	1.99 ± 0.73	34 ± 5
11	-1	-1	0	2.18 ± 0.21	34 ± 2
12	1	0	-1	3.20 ± 0.50	58 ± 3
13	-1	0	1	2.22 ± 0.21	50 ± 1
14	-1	1	0	1.61 ± 0.26	46 ± 2
15	0	-1	1	1.83 ± 0.49	36 ± 4
16	0	1	-1	1.25 ± 0.11	59 ± 2
17	0	1	1	1.45 ± 0.32	54 ± 3

In the case of both current density and stability responses, the models were found to be statistically valid with significant correlation between observed and predicted responses (R^2 of 0.94 and 0.92 for current density and stability, respectively). For current density, the F-value (13.07) and p-value (0.0013) evaluated suggests that the model is statistically significant. There is therefore only a 0.13% chance that an F-value this large could occur due to noise. Furthermore, adjusted R^2 (adj-R^2, 0.87) and predicted R^2 (Q^2, 0.74) values are within 0.2, and the adequate precision (11.42) is

higher than 4, thereby suggesting that the model chosen predicts well in the chosen space and will give good predictions for average responses.
Similarly, for stability, the F-value (9.00) and p-value (0.0042) indicate the significance of the model. There is only a 0.42% chance that an F- value this large could occur due to noise. Furthermore, adjusted R^2 (adj-R^2, 0.82) and predicted R^2 (Q^2, 0.65) values are within 0.2, and the adequate precision (9) is higher than 4, indicating a valid and predictive model. The larger difference in correlation coefficients here could be due to some variability in crosslinker solution preparation. The PEGDGE is easily hydrolysed by water and thus cannot be made into one stock solution to be used for all electrodes prepared and tested. In order to use it as a crosslinker, fresh solutions must be made when preparing the electrodes, and this can cause a variability that cannot be avoided, affecting R^2 values.

Each response can be presented by a quadratic equation,

$$y = b_0 + b_1x_1 + b_2x_2 + b_3x_3 + b_{11}x_1^2 + b_{22}x_2^2 + b_{33}x_3^2 + b_{12}x_1x_2 + b_{13}x_1x_3 + b_{23}x_2x_3 \quad \text{Equation 2.1}$$

where y is the predicted response value (current density in mA cm^{-2} or percentage stability, respectively), x_1, x_2 and x_3 are the CNT-GOx, redox polymer and enzyme amounts in μg used in the enzyme electrode preparation, b_0 is the constant coefficient (intercept), b_1, b_2, b_3 and b_{12}, b_{13}, b_{23} are linear and cross product coefficients, respectively, and the quadratic coefficients are b_{11}, b_{22} and b_{33}.

The resulting response models from the 17 runs for current density (Equation 2.2) and stability (Equation 2.3) are:

$$y = 2.72 + 0.49x_1 + 0.24x_2 + 0.074x_3 + 0.17x_1^2 - 0.63x_2^2 - 0.45x_3^2 + 0.085x_1x_2 - 0.27x_1x_3 + 0.090x_2x_3 \quad \text{Equation 2.2}$$

$$y = 52.4 + 1.63x_1 + 9.38x_2 - 1.25x_3 - 2.95x_1^2 - 8.45x_2^2 + 1.80x_3^2 + 2.0x_1x_2 - 2.75x_1x_3 - 1.75x_2x_3 \quad \text{Equation 2.3}$$

The signs of the coefficients of the factors in the model equations indicate their relative effects, in which a positive sign indicates that a higher response can be obtained if the values of these factors are greater than those of the centre point[39,42,61,62]. Considering the model of current density (Equation 2.2), all three main factors were found to be significant. Additionally, the amount of Os(bpy)PVI has a synergistic factor interaction with both CNT-GOx and PEGDGE amounts. In the case of stability (Equation 2.3), the Os(bpy)PVI and CNT-GOx has significant impact on the response when taken in amounts above the central levels, and their interaction has a beneficial effect on stability in the range tested in this DoE.

The statistical model equations are depicted graphically in the form of 2-D response surface contour plots, with examples of these in Figures 2.3 and 2.4. These plots are representations of the effects of all experimental variables and their interactions. The response surface plots across the investigated ranges suggest that the optimal set of conditions can be mapped in the case of both responses. The red zones of the contour are the areas associated with high response values.

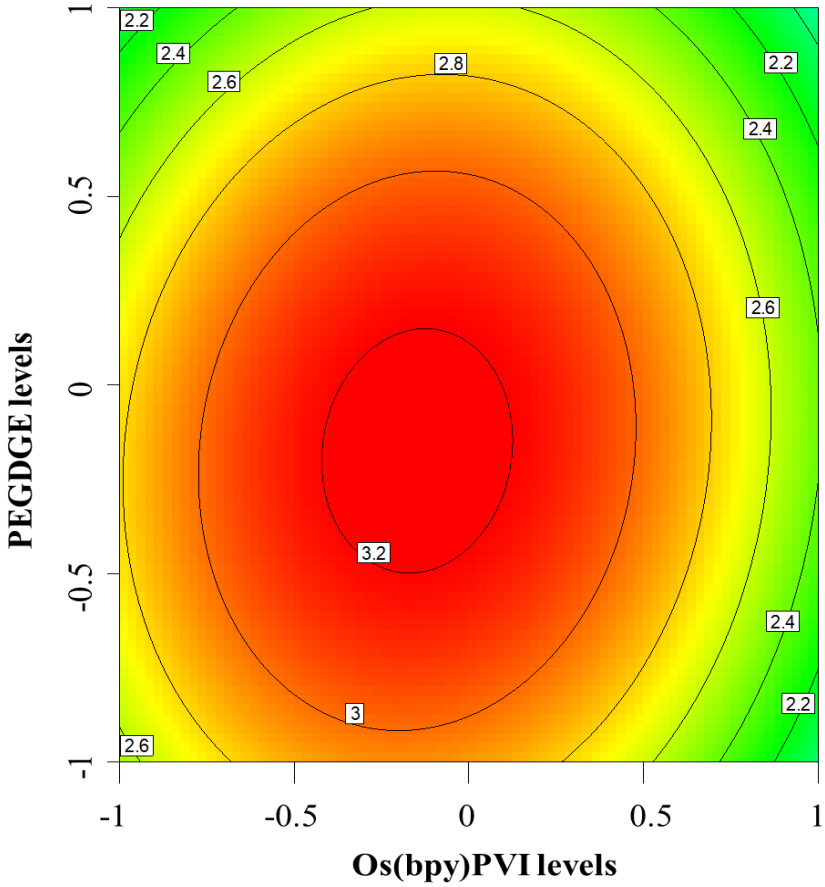

Figure 2.3: Response surface contour plots of PEGDGE vs Os(bpy)PVI levels when CNT-GOx is at 140 µg showing oxidation current density in 5 mM glucose predicted by the model (equation 2). Each contour depicts current density in mA cm^{-2}

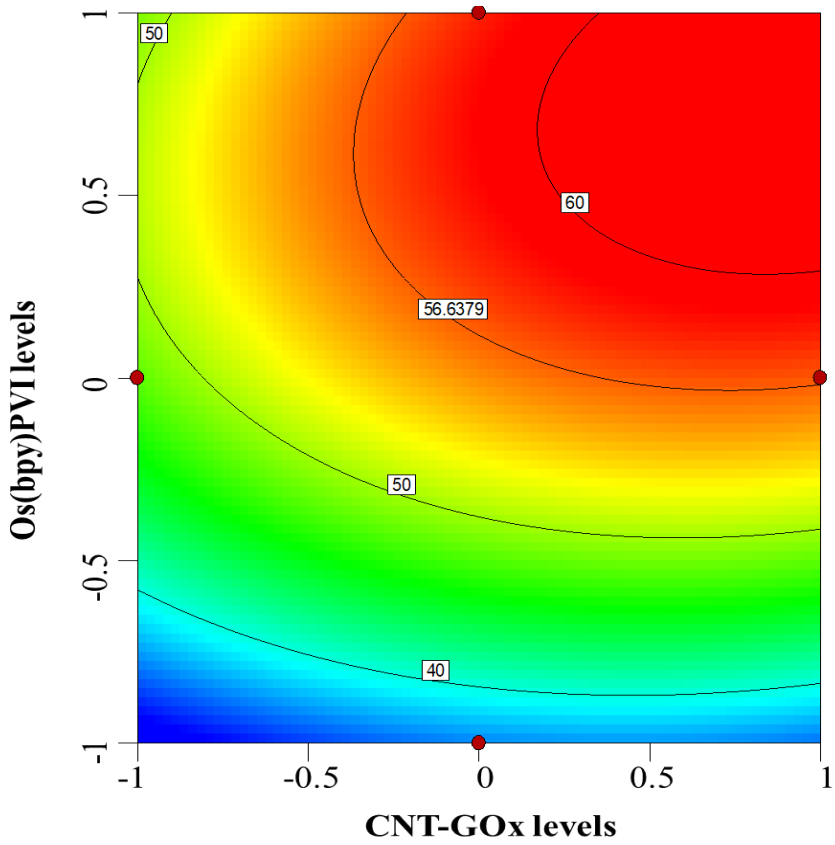

Figure 2.4: Response surface contour plots of Os(bpy)PVI vs CNT-GOx levels when PEGDGE is at 120 µg showing stability at 5 mM glucose over 3 hrs predicted by the model (equation 3). Each contour depicts stability in %.

2.4.2 Model Validation

Before a system is optimised based on a design of experiments, it is worthwhile to demonstrate that the model is a reasonable representation of the actual system and is reproducible with enough accuracy to satisfy analysis objectives. The statistical analysis gives a mathematical indication of model validity but a secondary physical validation can be done by performing more experimental runs on the system and comparing the predicted values with the observed values.

Model validation was tested based on values randomised by the model together with their predicted results under pseudo-physiological conditions of PBS solutions containing 5 mM glucose at 37°C, with the results presented in Table 2.3. Experimental values plotted against predicted values for each set of parameters (Figure 2.5), results in correlation coefficients (R^2) of 0.912 and 0.914 for current density and

stability models, respectively, indicating that the models are valid as the experimental results correlate well with statistical model predictions in all five runs. In the case of the stability validation tests, the actual stability points are systematically lower than the predicted. However, the error bars (representing the standard deviation of the experimental data points), fall on the line representing the ideal agreement ($y=x$). As stated previously, some variability is expected in stability measurements as fresh crosslinker solution must be prepared before each deposition.

Table 2.3: Model validation comparing predicted versus actual response

CNT-GOx / *µg*	**Os(bpy)PVI** / *µg*	**PEGDGE** / *µg*	**Predicted Current Density** / *mA cm^{-2}*	**Actual Current Density** / *mA cm^{-2}*	**Predicted Stability** / *%*	**Actual Stability** / *%*
90	70	75	1.84 ± 0.22	2.00 ± 0.39	53.3 ± 4	47.2 ± 4
90	70	120	1.55 ± 0.22	1.64 ± 0.33	52.1 ± 4	47.0 ± 3
150	70	120	2.03 ± 0.22	1.99 ± 0.28	50.1 ± 4	43.3 ± 4
10	70	120	1.42 ± 0.22	1.30 ± 0.23	48.8 ± 4	40.83 ± 5
90	10	75	2.34 ± 0.22	2.3 ± 0.88	52.9 ± 4	49.0 ± 6

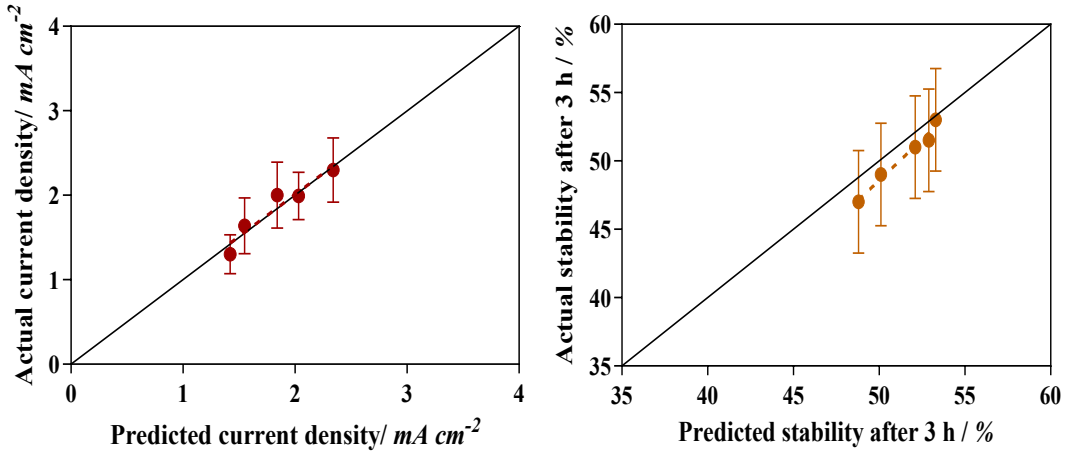

Figure 2.5: Comparison of experimental and predicted values (circles) for (A) current density and (B) stability. Vertical error bars represent standard deviation of experimental measurement. The black line is a reference representing an ideal agreement between predicted and measured values ($y = x$).

Concerning the physical validity of the models, in all five validation tests the experimental results for current density and stability are within the predicted range. Therefore, these statistical models can be considered valid mathematical representations and employed as predictive tools to find optimised component amounts.

2.4.3 Optimisation of Enzyme Electrode

The software allowed for the optimisation of the system, keeping in mind the goal to achieve high current density and high stability of response. Multi-response design optimisation is resolved by the Design Expert software using a desirability function, a weighted geometric mean that combines each individual response optimisation function into a single objective function (Appendix A.2, equation S2.1) [62]. In this case, both responses were set by the user to maximised, i.e., to have high desirability (Figure S2.7). The DoE optimum component amounts using the model equations are 150 µg CNT-GOx, 95 µg Os(bpy)PVI redox polymer and 34.2 µg PEGDGE. The biosensor formulated with these component values is predicted to deliver a current density of 3.18 ± 0.30 mA cm^{-2} and a stability of 54 ± 4 % in PBS containing 5 mM glucose. An actual measured current density of 3.10 ± 0.19 mA cm^{-2} and a stability of 51 ± 4 % (n = 3) is obtained for the enzyme electrodes prepared using the DoE

determined optimum component amounts. The current density response at physiological level from this optimised system shows a 146% or 2.4-fold increase over that of a similar system prepared using acid treated CNTs as a nanosupport with no covalent linkage between enzyme and nanosupport[54] (1.3 mA cm^{-2}). The CV response for the optimised system is shown in Figure 2.6 and the amperometric current density versus glucose concentration response is plotted in Figure 2.7 (raw amperometry trace in Appendix A.2, Figure S2.3), with maximum current density j_{max} estimated as 3.98 mA cm^{-2} and a K_m^{app} of 5.0 ± 0.10 mM. The K_m^{app} shows good agreement with literature on previous studies based on the use of redox polymer mediated glucose oxidation by GOx enzyme electrodes [28]. As stated previously, such a low K_m^{app} will give a linear range for detection of glucose levels in saliva or sweat [55] but the linear range will need to be expanded to allow the detection of glucose in physiological fluids such as interstitial fluid or blood.

The significant increase in current density over that prepared using acid treated CNTs as a nanosupport[54] may be attributed to the effect of the covalent attachment of enzyme onto the nanosupport. Covalent attachment of the GOx onto the wall of the MWCNTs should increase the activity of the enzyme [35]. In order to verify this, enzymatic activity was measured for enzyme in solution and compared to that for systems with GOx entrapped in redox hydrogel without CNTs, with CNTs (following the system investigated by us previously [54]) and with the system optimised by DoE. The average activity of 1443 U mg^{-1} was obtained for the optimised system obtained by the DoE. The activity obtained for the free enzyme solution, system with entrapped GOx in in redox hydrogel without CNTs and with CNTs was 276 U mg^{-1}, 235 U mg^{-1} and 227 U mg^{-1} which correlates well with the reported activity from Sigma-Aldrich (100–250 U mg^{-1}). This confirms that there is an increase in the enzymatic activity on covalent immobilisation of the GOx onto CNTs. This enhanced activity is responsible for the increased current density while using significantly smaller amounts of enzyme and nanosupport.

A minimisation constraint was applied to the CNT-GOx levels, as keeping the amount of this component low has two advantages: a lower amount of enzyme used makes the biosensor more cost-effective to produce and minimising amount of CNT makes electrode preparation easier. Higher electrode-to-electrode precision using lower

CNT-GOx levels is due to increased control over the drop-coating procedure, as there is better dispersibility of the components in the drop-coat mixture. The DoE optimum component amounts using the model equations, based on the previously explained constraints, are 10 µg CNT-GOx, 90 µg Os(bpy)PVI redox polymer and 105 µg PEGDGE. The biosensor formulated with these values is predicted to deliver a current density of 2.43 ± 0.30 mA cm^{-2} and a stability of 52 ± 5 % in PBS containing 5 mM glucose. An actual measured current density of 2.08 ± 0.33 mA cm^{-2} and a stability of 60 ± 3 % (n = 3) was obtained for the enzyme electrodes prepared using the selected component amounts. In terms of current density at physiological glucose levels in the presence of oxygen, the system with a minimisation constraint represents a 7.7-fold increase on the response for enzyme electrodes optimised through a OFAT method of optimisation of response (0.27 mA cm^{-2}), using the same components except where the redox polymer Os(dmobpy)PVI was used [48] and a 1.7 fold increase over a system prepared using identical components, but where enzyme was not covalently linked to nanosupport[54] (1.3 mA cm^{-2}). When comparing to results observed previously [43] for enzyme electrodes prepared by co-immobilisation of MWCNTs, GOx, osmium redox complex and carboxymethylated dextran (1.2 mA cm^{-2}) in the absence of oxygen, a 1.7 fold increase in current density response is observed. Kumar and Leech measured current density response in the absence of oxygen, a substance known to compete with the mediator and thus decrease current density whereas our tests were performed in the presence of oxygen to more accurately mimic current density response under physiological conditions.

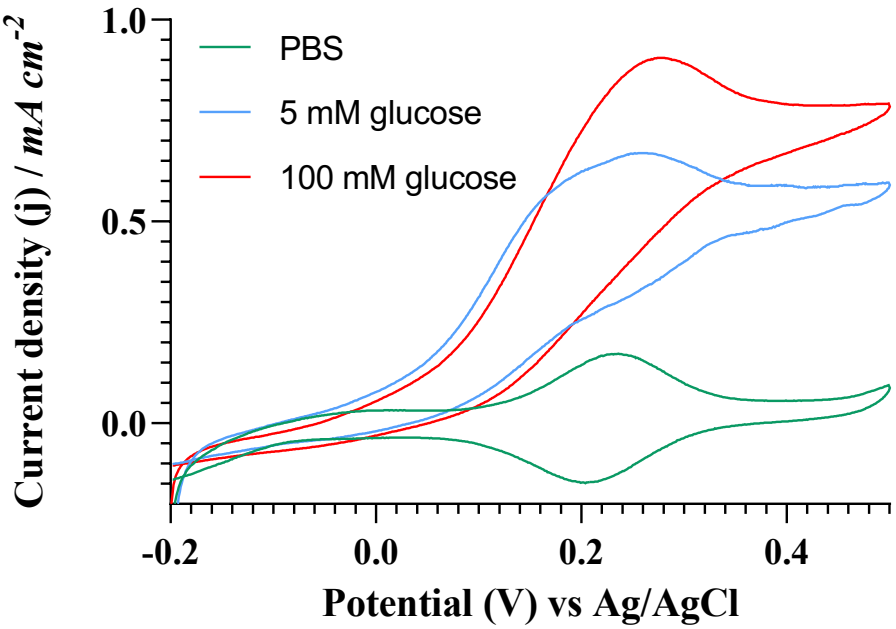

Figure 2.6: Cyclic voltammograms recorded at 1 mV s^{-1} of enzyme electrodes tested in the PBS (green) and 5 mM glucose (blue) and 100 mM glucose (red) at 37 °C. Enzyme electrodes consisted of CNT-GOx (150 µg), Os(bpy)PVI (95 µg) and PEGDGE (34.2 µg).

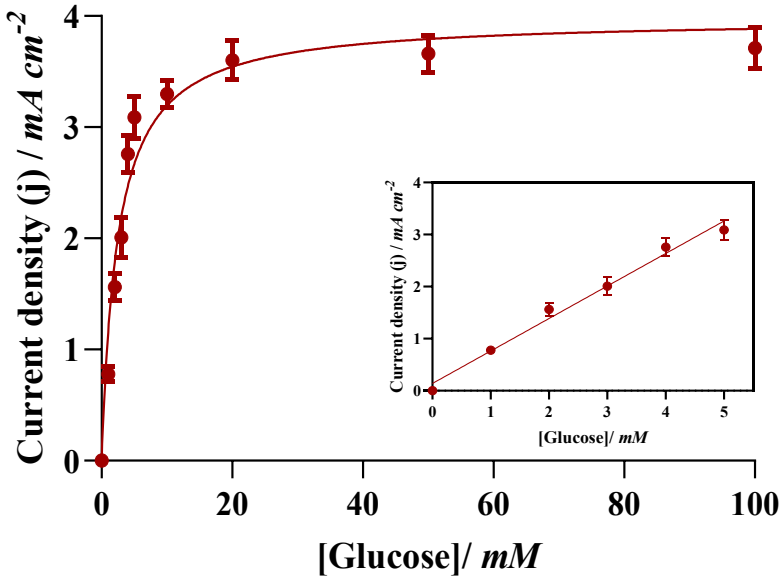

Figure 2.7: Glucose oxidation current density as a function of glucose concentration measured at 0.35 V in PBS at 37°C with stirring at 150 rpm. Enzyme electrodes consisted of CNT-GOx (150 µg), Os(bpy)PVI (95 µg) and PEGDGE (34.2 µg). Inset shows the fitting of the linear portion of the Michaelis-Menten curve selecting glucose concentration where $R^2 \geq 100$.

The stability of glucose-oxidising enzyme electrodes has not been investigated as a response in a DoE prior to this, to our knowledge. Our results show that the average stability obtained for both systems optimised by a design of experiments approach is around 50% after 3 hr continuous amperometry under physiological conditions in PBS. So, while the use of a DoE approach showed favourable results in optimising current density, the same cannot be said when considering the stability. This rapid decay could be attributed to either enzyme turnover or concentration depletion due to the low level (5 mM) of glucose present during long measurements in a static electrochemical cell under an applied potential sufficient to ensure continuous glucose oxidation.

The use of other techniques such as coupling of the layers to the electrode or the coating with protective polymer films could be useful to enhance the stability. For example, use of Nafion overcoating has been proven to increase the stability of the electrode while protecting it from interferents such as uric acid and ascorbic acid[54]. Overcoating of enzyme electrodes using a 0.5 wt% Nafion solution, following the protocol previously used [54], showed a marked improvement in the stability for both the electrodes prepared using the optimised component amounts and electrodes prepared using the amounts selected with the minimisation constraint applied (Figure 2.8). Another possibility is the electrochemical crosslinking through co-deposition. This has been investigated by the Schuhmann group showing that in the co-deposition of poly(benzoxazine) and Os-based redox polymer, optimising the ratio of the two polymers showed an improvement in stability[14].

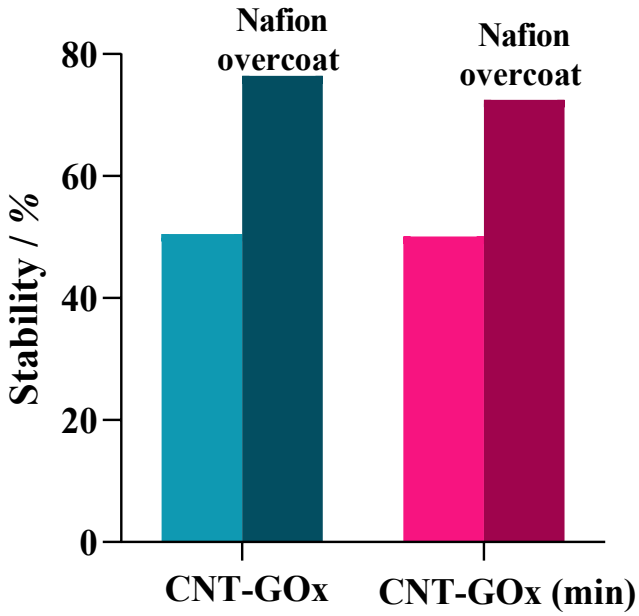

Figure 2.8: Stability at 5 mM glucose level after 12 h amperometry of the optimised system, CNT-GOx, and the optimised system with a minimisation constraint, CNT-GOx (min), with and without a 0.5 wt% Nafion overcoat.

2.5 Conclusions

Immobilisation of glucose oxidase and MWCNTs for preparation of glucose biosensors was replaced by use of a covalently-bound nanoconjugate of GOx and MWCNTs (CNT-GOx), permitting lower amounts of nanoconjugate to be used in the preparation of sensors compared to amounts of MWCNT used previously. A DoE optimisation approach, while considering two responses (current density and stability) allowed the discovery of a set of component amounts where both responses could be maximised. Thus far stability has not been investigated as a response to be optimised using a DoE approach. The successful use of this predictive model in the optimisation of enzyme electrode components indicates its potential for further applications in this field. Furthermore, the current densities obtained for the optimised systems, even when a minimisation constraint is applied, are significantly higher than those obtained in a system where enzyme and nanosupport are not covalently bound. This indicates that the manipulation of the enzyme-nanosupport relationship can enhance enzyme activity and thus, current density, allowing the use of significantly lower amounts of active components. Stability obtained for the systems was moderate at only ≈ 50% after 12

hr continuous use, but use of a Nafion protective layer improved stability to 72–75%. Approaches, not tested in this work, that could further improve stability include coupling of adsorbed films to the electrode surface through covalent bonds, use of additional perm-selective membranes, and/or use of pulsed potentials to implement intermittent sampling of glucose levels, rather that continuous amperometry

2.6 Acknowledgement

This publication is part of a project that has received funding from the European Union's Horizon 2020 research and innovation programme under grant agreement Nº813006.

2.7 References

[1] T. Bobrowski, W. Schuhmann, Curr Opin Electrochem. 10 (2018) 112–119.

[2] A. Heller, B. Feldman, Acc Chem Res. 43 (2010) 963–973.

[3] P. D'Orazio, Clinica Chimica Acta. 334 (2003) 41–69.

[4] A. Ruff, Curr Opin Electrochem. 5 (2017) 66–73.

[5] P. Pinyou, A. Ruff, S. Pöller, S. Ma, R. Ludwig, W. Schuhmann, Chemistry - A European Journal. 22 (2016) 5319–5326.

[6] A. Prévoteau, N. Mano, Electrochim Acta. 68 (2012) 128–133.

[7] C. Chen, Q. Xie, D. Yang, H. Xiao, Y. Fu, Y. Tan, S. Yao, RSC Adv. 3 (2013) 4473–4491.

[8] R. Wilson, A.P.F. Turner, Biosens Bioelectron. 7 (1992) 165–185.

[9] P.N. Bartlett, F.A. Al-Lolage, Journal of Electroanalytical Chemistry. 819 (2018) 26–37.

[10] T.J. Ohara, R. Rajagopalan, A. Heller, Anal Chem. 65 (1993) 3512–3517.

[11] F. Mao, N. Mano, A. Heller, J Am Chem Soc. 125 (2003) 4951–4957.

[12] P.A. Jenkins, S. Boland, P. Kavanagh, D. Leech, Bioelectrochemistry. 76 (2009) 162–168.

[13] D. MacAodha, M.L. Ferrer, P.Ó. Conghaile, P. Kavanagh, D. Leech, Physical Chemistry Chemical Physics. 14 (2012) 14667–14672.

[14] S. Barwe, C. Andronescu, S. Pöller, W. Schuhmann, Electroanalysis. 27 (2015) 2158–2163.

[15] S. Alsaoub, S. Barwe, C. Andronescu, S. Pöller, A. Ruff, W. Schuhmann, Chempluschem. 80 (2015) 1178–1185.

[16] A. Prévoteau, N. Mano, Electrochim Acta. 112 (2013) 318–326.

[17] K.P. Prasad, Y. Chen, P. Chen, ACS Appl Mater Interfaces. 6 (2014) 3387–3393.

[18] R. Tel-Vered, I. Willner, Isr J Chem. 50 (2010) 321–332.

[19] O. Yehezkeli, R. Tel-Vered, S. Raichlin, I. Willner, ACS Nano. 5 (2011) 2385–2391.

[20] P.P. Joshi, S.A. Merchant, Y. Wang, D.W. Schmidtke, Anal Chem. 77 (2005) 3183–3188.

[21] Y. Choi, G. Wang, M.H. Nayfeh, S.T. Yau, Biosens Bioelectron. 24 (2009) 3103–3107.

[22] S.C. Barton, H.H. Kim, G. Binyamin, Y. Zhang, A. Heller, J Am Chem Soc. 123 (2001) 5802–5803.

[23] R. Antiochia, L. Gorton, Biosens Bioelectron. 22 (2007) 2611–2617.

[24] C. Kang, H. Shin, A. Heller, Bioelectrochemistry. 68 (2006) 22–26.

[25] P. Ó Conghaile, D. MacAodha, B. Egan, P. Kavanagh, D. Leech, J Electrochem Soc. 160 (2013) G3165–G3170.

[26] B. Reuillard, A. Le Goff, C. Agnès, M. Holzinger, A. Zebda, C. Gondran, K. Elouarzaki, S. Cosnier, Physical Chemistry Chemical Physics. 15 (2013) 4892–4896.

[27] P. Kavanagh, D. Leech, Physical Chemistry Chemical Physics. 15 (2013) 4859–4869.

[28] I. Osadebe, D. Leech, ChemElectroChem. 1 (2014) 1988–1993.

[29] C. Mateo, J.M. Palomo, G. Fernandez-Lorente, J.M. Guisan, R. Fernandez-Lafuente, Enzyme Microb Technol. 40 (2007) 1451–1463.

[30] R.C. Rodrigues, C. Ortiz, Á. Berenguer-Murcia, R. Torres, R. Fernández-Lafuente, Chem Soc Rev. 42 (2013) 6290–6307.

[31] C. Garcia-Galan, Á. Berenguer-Murcia, R. Fernandez-Lafuente, R.C. Rodrigues, Adv Synth Catal. 353 (2011) 2885–2904.

[32] C.Z. Dinu, G. Zhu, S.S. Bale, G. Anand, P.J. Reeder, K. Sanford, G. Whited, R.S. Kane, J.S. Dordick, Adv Funct Mater. 20 (2010) 392–398.

[33] N. Grover, M.P. Douaisi, I. V. Borkar, L. Lee, C.Z. Dinu, R.S. Kane, J.S. Dordick, Appl Microbiol Biotechnol. 97 (2013) 8813–8821.

[34] P. Asuri, S.S. Bale, R.C. Pangule, D.A. Shah, R.S. Kane, J.S. Dordick, Langmuir. 23 (2007) 12318–12321.

[35] A.S. Campbell, C. Dong, F. Meng, J. Hardinger, G. Perhinschi, N. Wu, C.Z. Dinu, ACS Appl Mater Interfaces. 6 (2014) 5393–5403.

[36] B.C. Kim, I. Lee, S.J. Kwon, Y. Wee, K.Y. Kwon, C. Jeon, H.J. An, H.T. Jung, S. Ha, J.S. Dordick, J. Kim, Sci Rep. 7 (2017) 1–10.

[37] H. Ali-Boucetta, K. Kostarelos, Adv Drug Deliv Rev. 65 (2013) 2111–2119.

[38] J. Simon, E. Flahaut, M. Golzio, Materials. 12 (2019) 624.

[39] G.D. Bowden, B.J. Pichler, A. Maurer, Sci Rep. 9 (2019) 11370.

[40] X. Wang, S.B. Kim, D. Khang, H.H. Kim, C.J. Kim, Biochem Eng J. 112 (2016) 20–31.

[41] G. Chen, J. Chen, C. Srinivasakannan, J. Peng, Appl Surf Sci. 258 (2012) 3068–3073.

[42] R. Kumar, J. Lahann, ACS Appl Mater Interfaces. 8 (2016) 16595–16603.

[43] R. Kumar, D. Leech, Bioelectrochemistry. 106 (2015) 41–46.

[44] R. Bennett, I. Osadebe, R. Kumar, P.Ó. Conghaile, D. Leech, Electroanalysis. 30 (2018) 1438–1445.

[45] E.M. Kober, J. V Caspar, B. Patrick Sullivan, T.J. Meyer, J. Am. Chem. Soc. 27 (1988) 7405.

[46] R.J. Forster, J.G. Vos, Macromolecules. 23 (1990) 4372–4377.

[47] N.T. Crosby, Methods of enzymatic analysis, Vol. VII, TrAC Trends in Analytical Chemistry. 5 (1986) XXIV.

[48] I. Osadebe, P. Conghaile, P. Kavanagh, D. Leech, Electrochim Acta. 182 (2015) 320–326.

[49] S. Gupta, C.N. Murthy, C.R. Prabha, Int J Biol Macromol. 108 (2018) 687–703.

[50] H. Ju, D. Leech, Anal Chim Acta. 345 (1997) 51–58.

[51] B. Limoges, J. Moiroux, J.M. Savéant, Journal of Electroanalytical Chemistry. 521 (2002) 8–15.

[52] P.N. Bartlett, K.F.E. Pratt, Journal of Electroanalytical Chemistry. 397 (1995) 61–78.

[53] A.J. Bard, L.R. Faulkner, Electrochemical Methods: Fundamentals and Applications, 2nd Edition | Wiley, 2001.

[54] R. Bennett, D. Leech, Bioelectrochemistry. 133 (2020) 107460.

[55] D. Bruen, C. Delaney, L. Florea, D. Diamond, Sensors 2017, Vol. 17, Page 1866. 17 (2017) 1866.

[56] X. Xiao, P. Conghaile, D. Leech, E. Magner, ChemElectroChem. 6 (2019) 1344–1349.

[57] B. Qi, X. Chen, F. Shen, Y. Su, Y. Wan, Ind Eng Chem Res. 48 (2009) 7346–7353.

[58] A. Heller, AIChE Journal. 51 (2005) 1054–1066.

[59] A. Heller, Physical Chemistry Chemical Physics. 6 (2004) 209–216.

[60] E.J. Calvo, C. Danilowicz, L. Diaz, Journal of the Chemical Society, Faraday Transactions. 89 (1993) 377–384.

[61] P. Anderson, Mark J.; Whitcomb, CRC Press, 2007.

[62] M.J. Anderson, RSM Simplified, Productivity Press, 2016.

Chapter 3: An oxygen insensitive amperometric glucose biosensor based on an engineered cellobiose dehydrogenase: direct versus mediated electron transfer responses

Published as:

An oxygen insensitive amperometric glucose biosensor based on an engineered cellobiose dehydrogenase: direct versus mediated electron transfer responses

Kavita Jayakumar, Thomas M.B. Reichhart, Christopher Schulz, Roland Ludwig, Alfons K.G. Felice, and Dónal Leech, ChemElectroChem, 2022, 9, e20220041

Co-author contributions:

I synthesised the PVI-bound osmium redox polymer, performed all labwork, analysis and wrote the first draft of the publication.

Thomas Reichhart provided the WT*Ch*CDH enzyme used in this study.

Christopher Schulz and Alfons K.G Felice contributed advice and guidance throughout the laboratory work and analysis.

Roland Ludwig helped to edit the first draft of this publication.

Dónal Leech, as project supervisor, contributed through advice and guidance throughout the work and edited the first draft to provide the final version for publication.

3.1 Abstract

Cellobiose dehydrogenase (CDH) is capable of oxidizing cellobiose and related carbohydrates and generating electrical current at carbon-based electrodes through direct electron transfer (DET) or mediated electron transfer (MET) mechanisms. As a result, CDHs have been utilized as biocatalysts in biosensors and biofuel cell anodes. A novel, engineered ascomycetous Class II CDH with enhanced glucose activity was tested as a bioelectrocatalyst for application to DET or MET-based glucose biosensors with the electrode component amount selection optimized for maximum current in 5 mM glucose solutions. The optimised DET biosensor showed a similar sensitivity and 3-fold lower $K_{M,app}$ when compared to non-optimised DET sensor based on the same engineered CDH. The optimized MET biosensor had a similar $K_{M,app}$ to non-optimized MET biosensor. However, it showed 15-fold improvement in j_{max} and 17-fold improvement in sensitivity over the DET biosensor. The sensor signals are not affected by the presence of oxygen, although operation in artificial serum results in 43% and 28% lower sensitivity for the DET and MET sensors, respectively. While no individually tested potential interferent breaches a mean absolute relative difference of 20% of the current, the cumulative co-operative effect in complex media, such as artificial serum, decreases the glucose oxidation current signal.

3.2 Introduction

Diabetes is a common chronic disease affecting 1 in 11 people[1]. Recent projections by the International Diabetes Federation show that the global diabetes prevalence, estimated to be 9.3% (463 million) in 2019, is expected to rise to 10.9% (700 million) by 2045[1,2]. This indicates the need to measure blood glucose in a cheap, fast and miniaturized way due to the dramatic increase in diabetes patients. There has been substantial investment in rapid and sensitive glucose biosensors since the concept of glucose biosensors was proposed by Clark and Lyons[3]. While non-enzymatic glucose sensors have been researched intensively, it has not led to breakthrough developments compared to their enzymatic counterparts that now dominate the market[4,5]. The majority of commercial glucose biosensors are based on glucose oxidase (GOx) with amperometric or coulometric measurements[5]. However, use of

GOx in such biosensors has some drawbacks due to its affinity to oxygen and its inability to establish direct electron transfer (DET) to electrodes[4,6,7].
For an amperometric biosensor, redox enzymes should exhibit efficient electronic communication to electrodes under sample conditions. Amperometric glucose biosensors based on GOx operate through oxidation of H_2O_2, produced by the oxidation of glucose and reduction of oxygen as co-substrate, at the electrode (1st generation) or O_2 is replaced by an alternate co-substrate, a mediator, as the electron acceptor in mediated electron transfer (MET)-based biosensors (2nd generation)[4,8,9]. First generation biosensors have the disadvantage of high overpotential and electrode poisoning, usually overcome by use of a redox mediator characterized by a lower redox potential. However the resulting 2nd generation biosensors tend to have more complicated sensor constructions and possible leaking of mediators[5,10]. The 3rd generation biosensors are based on DET between enzyme and electrode. While desirable due to the simplicity of electrode architecture and the avoidance of potentially hazardous mediators, DET biosensors still require more research to overcome low electron transfer rates to have comparable analytical characteristics to MET sensors[4,5,11,12].

Only a few enzymes can establish DET to electrode surfaces. The use of cellobiose dehydrogenases (CDHs)[13] has attracted significant interest due to capacity to undergo DET and thus potential applicability in bioelectronics[14]. The CDHs consist of a multidomain protein composed of a FAD-containing dehydrogenase (DH) domain connected via a flexible linker to a cytochrome (CYT) domain with a heme *b* type cofactor[15]. CDHs can oxidize various sugars, including cellobiose or lactose[16,17] and, in some instances even glucose, at the FAD cofactor in the DH domain. Re-oxidation of $FADH_2$ can occur directly by interdomain electron transfer to the heme group in the CYT domain, which acts as a built-in mediator and can pass on electrons to various terminal electron acceptors such as electrode surfaces[13].

CDH-based biosensors have been realized using carbon[18] and gold[19] as electrode material. Engineering of CDH has been performed to generate CDH variants for several purposes[10,20,21]. For instance, de-glycosylation of CDH can increase the faradaic efficiency[22–24] while amino acid substitutions in the active site can be used to change the substrate specificity of CDH[25–27]. A prominent example of the latter

is an engineered CDH variant with enhanced glucose specificity[10] that can be used to construct biosensors for biomedical applications such as glucose measurements for diabetes management[28]. The engineering of CDH substrate specificity affects not only the glucose turnover rate, but also interdomain electron transfer rate and DET.

In this work, we demonstrate the use of an engineered CDH, equipped with glucose activity-enhancing mutations, incorporated into DET and MET-based sensors. A CDH from *Crassicarpon hotsonii* equipped with glucose activity-enhancing mutations C291Y and W295R was recombinantly produced in *Komagatella phaffii* as described previously.[25] The enzyme is referred to as wild-type (WT*Ch*CDH) to enable comparison to data published on the enzyme[26]. In the MET biosensor, the WT*Ch*CDH is encapsulated in an osmium complex-based polymer hydrogel, which acts as the mediator. These sensors are characterized electrochemically, and components used to prepare the electrodes optimized. The sensors are further tested in artificial serum to demonstrate their behaviour in complex media, and an interference study is conducted with the known interferents present in artificial serum.

3.3 Experimental

3.3.1 Materials

All chemicals were purchased from Sigma-Aldrich, unless otherwise stated. Milli-Q water (18 MΩ.cm) was used to prepare all aqueous solutions unless otherwise stated. The redox polymer $[Os(2,2'\text{-bipyridine})_2(\text{poly-vinyl-imidazole})_{10}Cl]^+$ (Os(bpy)PVI) was synthesized by modification of published procedures[4,61].

3.3.2 Methods

3.3.2.1 Enzyme Production

A CDH from *Crassicarpon hotsonii (*syn. *Myriococcum thermophilum*) equipped with glucose activity-enhancing mutations C291Y and W295R was used in this study. The mutations are both located in the active site of the DH domain responsible for substrate

activity and specificity. C291Y was designed to provide an additional hydroxyl group for hydrogen bonding to stabilize the reducing sugar moiety and enhance glucose binding and oxidation. W295R was created to spatially constrain the binding of the non-reducing sugar moiety to improve glucose specificity and decrease maltose activity.

The CDH was recombinantly produced in *Komagatella phaffii* (syn. *Pichia pastoris*) as described previously[20] via methanol induction of the AOX promoter according to the manufacturer's instructions (Invitrogen). The enzyme was subsequently purified using hydrophobic interaction chromatography and anion exchange chromatography as previously established[62]. All purification steps were performed on an ÄKTA Pure FPLC system (GE Healthcare). Purified enzymes were concentrated and rebuffered to 1 mM phosphate buffer, pH 7.4, with centrifugal filters (Amicon; 30 kDa mass cutoff) to a concentration of approximately 15 mg mL^{-1} and stored at 4 °C. The enzyme is referred to as wild-type (WT*Ch*CDH) throughout this text to enable comparison to previously published data on the enzyme[21].

3.3.2.2 Enzyme Electrode Preparation

Graphite rods (Graphite store, USA, 4.0 mm diameter, NC001300) were cut, insulated with heat shrink tubing and polished at one end using fine grit paper to give graphite working electrodes with a geometric surface area of 0.126 cm^2. The MET biosensors were assembled by drop-coating 30 µL of Os(bpy)PVI aqueous solution (5 mg mL^{-1}), 16 µL of WT*Ch*CDH aqueous solution (10 mg mL^{-1}) and 7.4 µL of poly(ethylene glycol) diglycidyl ether (PEGDGE) crosslinker aqueous solution (15 mg mL^{-1}). The deposition was allowed to dry for 24 h at ambient temperature before the electrodes were used. The electrode amounts are based on amounts optimized to produce the highest glucose oxidation current density in 5 mM glucose solution using a design of experiments approach (Appendix A.3, Figure S3.2).

Electrodes for use as DET biosensors were first pre-treated in 1% v/v ethylene glycol diglycidyl ether (EGDGE) in 0.1 M NaOH at 60 ºC for 1 h. The electrodes were then rinsed in water and ethanol and dried with nitrogen. Electrodes were drop-coated with either 16 µL or 18 µL of WT*Ch*CDH aqueous solution (10 mg mL^{-1}) and placed in an

oven at 60 ºC for 1 h before use. The 18 µL WT*Ch*CDH volume is the amount optimized to produce the highest glucose oxidation current density in 5 mM glucose solution using a one-factor-at-a-time optimization approach (Appendix A.3, S3.1). The 16 µL WT*Ch*CDH volume was selected to benchmark the response of the 3rd generation biosensor to that of the MET biosensors that are prepared using this volume of enzyme solution.

3.3.2.3 Electrochemical Measurements

Electrochemical tests were conducted using a CH Instruments 1030a multichannel potentiostat (IJ Cambria). The enzyme electrodes were used as working electrodes, with a custom-built Ag|AgCl (3 M KCl) as reference electrode and a platinum mesh (Goodfellow) as a counter electrode. Electrodes were placed in a thermostated electrochemical cell containing phosphate buffered saline (50 mM phosphate, 120 mM NaCl, pH 7.4) at 37 °C with experiments conducted, unless otherwise stated, in the presence of ambient oxygen. Current signals are normalised to the geometric surface area of the graphite disk electrodes to generate current density data. Stability values represent, unless otherwise indicated, the percentage of amperometric current density remaining at the end of a 12 h operational period compared to that obtained 20 minutes after initial polarization. The applied potential is 0.35 V for the MET biosensor and 0.1 V for the DET biosensor. Square wave voltammetry (SWV) in a voltage window of –0.4 V to 0.4 V with an amplitude of 30 mV, frequency of 2 Hz and step amplitude of 5 mV was used to characterise the DET biosensor electrochemical response.

Artificial serum was prepared based on an aqueous solution containing uric acid (68.5 mg L^{-1}), ascorbic acid (9.5 mg L^{-1}), fructose (36 mg L^{-1}), lactose (5.5 mg L^{-1}), urea (267 mg L^{-1}), cysteine (18 mg L^{-1}), sodium chloride (6.75 g L^{-1}), sodium bicarbonate (2.138 g L^{-1}), calcium sulfate (23.8 mg L^{-1}), magnesium sulfate (104.5 mg L^{-1}) and bovine serum albumin (7 g L^{-1})[63].

Oxygen dependency of the sensors was evaluated by recording glucose-responsive amperometry at 0.35 V for the MET biosensor or 0.1 V for the DET biosensor in PBS

at 37 ºC containing ambient oxygen. The PBS was then replaced, and the glucose additions repeated after the solution was purged with nitrogen for 30 mins.

Biosensor response (i.e., amperometry at 0.35 V or 0.1 V for MET or DET, respectively) to 5 mM glucose in the presence of interferent was compared to biosensor response to glucose without interferent. Interference testing used solutions of fructose (1000 mg L^{-1})[64], lactose (2000 mg L^{-1})[65] mannose (2000 mg L^{-1})[66], glycerol (3000 mg L^{-1})[67], acetaminophen (200 mg L^{-1}), ascorbic acid (60 mg L^{-1}) or uric acid (120 mg L^{-1})[59]. The test concentration of sugars and glycerol is chosen based on a maximum blood concentration reported for these substances[59,64-67]. The test concentration chosen for each of the electroactive interferents is based on the guidelines provided in the Clinical and Laboratory Standards Institute (CLSI) document EP7-A2 section 5.5 “Interferent Test Concentrations”; these recommended concentrations vary according to the specific substance, but all substances were tested at a concentration above the highest blood concentration expected in the intended patient population[37].

Interference screening data was analysed by calculating the mean absolute relative difference (MARD) between the mean baseline glucose concentration reading without interferent (M_0) and the mean glucose reading value with interferent present (M_I) as:

$$\text{MARD (M)} = \frac{|M_I - M_0|}{M_0} \times 100 \qquad (1)$$

In this study, interference was defined as an absolute MARD ≥ 20% as defined by Boehm *et al.* previously [58].

3.4 Results and Discussion

3.4.1 Electrochemical characterization of the sensors

Cyclic voltammetry (CV) was used to initially characterize DET biosensor response (Figure 1). Redox peaks of the cytochrome domain (usually present around –0.1 V[18,39,40]) were not visible in CV. This could be due to the high charging current

relative to the signal, or oxygen reduction current obscuring the cytochrome domain signal on the electrode surface[18,40,41]. To verify the presence of WT*Ch*CDH on the electrode surface, SWV (Figure 3.1b) was also performed. Peaks in SWV between –0.2 to 0 V are attributed to the CYT domain[40] and the increase in SWV oxidation current in this potential range in the presence of 5 mM glucose (Figure 3.1, red trace) supports this attribution. The origin of the peak at 0.3 V is not yet clear, and has been attributed to surface quinones usually present on carbon surfaces as a peak at around the same potential is observed in the SWV of bare graphite electrodes[42].

Slow-scan CV in the presence and absence of glucose was used to characterize MET biosensors prepared by co-immobilization of WT*Ch*CDH and Os(bpy)PVI redox polymer using PEGDGE di-epoxide cross-linker. Scans recorded in the absence of glucose display peaks with redox potential centred at 0.22 V vs. Ag|AgCl (3 M KCl) (Figure 3.2) which agrees with previously reported values for the Os(II/III) transition of the redox polymer[8,43]. At slow scan rates < 20 mVs^{-1} peak currents vary linearly with scan rate as expected for a redox response controlled by finite diffusion within thin films on a surface[44]. The peak current varies linearly with the square root of scan rate at higher scan rates when semi-infinite diffusion within the film limits the current response[34]. The surface coverage (Γ_{os}) of the redox polymer, estimated by integrating the area under the peak for CVs recorded at slow scan rate in the absence of glucose, is 144 ± 3 nmol cm^{-2}, which confirms multi-layer formation, similar to results obtained by others for the co- immobilization of enzymes and osmium-based redox polymers[35–38]. On addition of glucose to the electrochemical cell, sigmoidal shaped responses characteristic of an electrocatalytic (EC') process are observed. The half-wave potential is negatively shifted by 20 mV in the presence of glucose substrate compared to the redox potential in the absence of substrate, indicative of substrate transport limitation under these conditions[39,40].

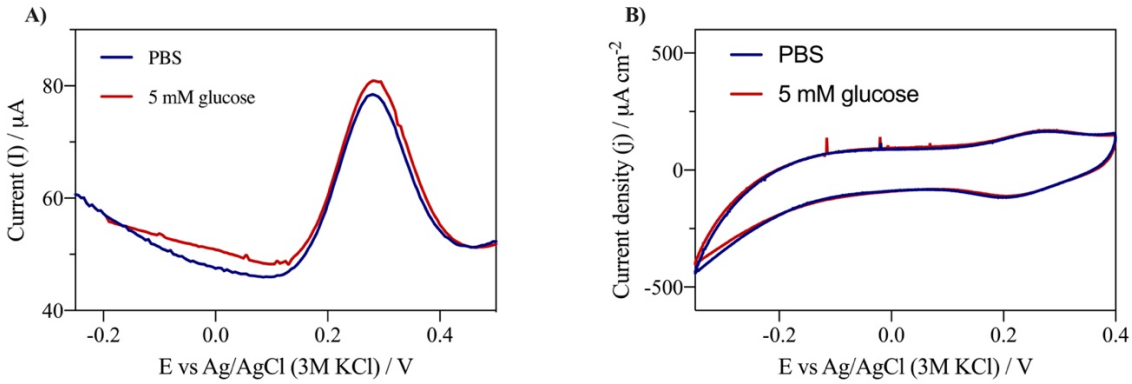

Figure 3.1: Cyclic voltammogram recorded at 1 mV s^{-1} (top) in PBS (blue) and square wave voltammogram (bottom) in PBS (blue) and in PBS including 5 mM glucose (red) of DET biosensors containing 1 µg immobilized WT*Ch*CDH. Electrolyte temperature 37 °C.

Amperometric measurements were carried out at 0.35 V vs. Ag|AgCl (3 M KCl) for the MET biosensor and 0.1 V for the DET biosensor to further characterize responses. The 0.35 V applied potential for the MET system is the same as that reported previously for the Os-based polymer, selected based on hydrodynamic voltammetry and confirmed as appropriate for glucose oxidation[41]. For the DET biosensor, as the peaks for WT*Ch*CDH appeared in the range of –0.2 to 0 V, a potential that was 0.1 V more positive than 0 V was selected. Amperometric glucose oxidation current density response as a function of glucose concentration (Figure 3.3) was fitted to the Michaelis-Menten equation to provide an estimate of the apparent Michaelis-Menten affinity constant, $K_{M,app}$, and the maximum saturation current density (j_{max}) for glucose. Sensitivity, Table 3.1, is obtained from the slope of the linear section of the Michaelis-Menten curve and indicates the ability of the sensor to respond to changes in glucose concentration.

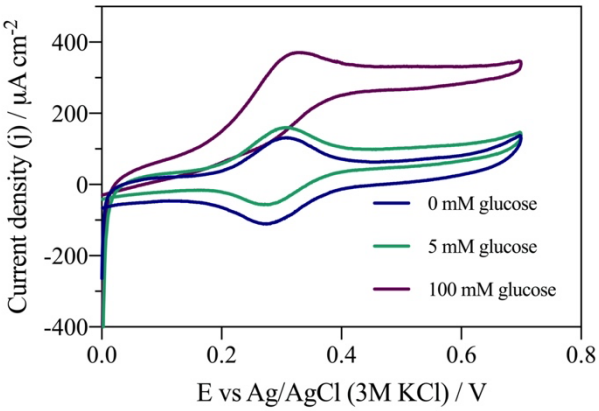

Figure 3.2: Cyclic voltammograms recorded at 1 mV s^{-1} for MET-based enzyme electrodes tested in PBS (red) and in PBS including 5 mM glucose (green) or 100 mM glucose (blue) at 37 °C. Enzyme electrodes consisted of WT*Ch*CDH (160 µg), Os(bpy)PVI (90 µg) and PEGDGE (105 µg).

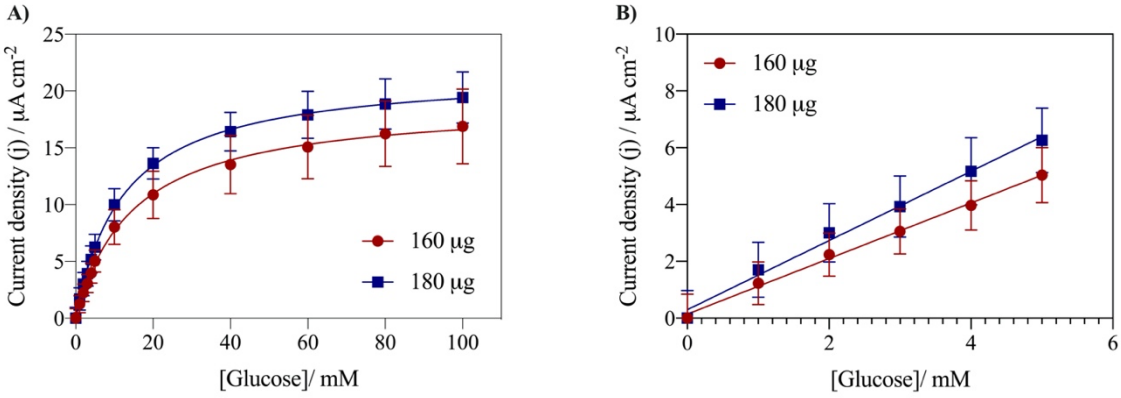

Figure 3.3: Glucose response curves for the DET system with 160 µg and 180 µg WT*Ch*CDH drop-coated onto the electrodes (top) and the linear plot for 0-5 mM glucose (bottom) based on amperometry at 0.1 V in PBS at 37 ºC, where n=4. The error bars represent the standard deviation.

Values of $K_{M,app}$ of 14.7 ± 1.2 mM and 12.4 ± 0.6 mM, are obtained for use of volumes of 16 µL or 18 µL, respectively, of a 10 mg mL^{-1} WT*Ch*CDH solution in the preparation of DET biosensors. Alteration of the amount of WT*Ch*CDH drop-coated on the surface was optimized to maximize glucose oxidation current density in 5 mM glucose solutions. This is achieved using 18 µL volume of enzyme solution (Appendix A.3, Supplementary Fig S3.1). While $K_{M,app}$ values for biosensors are influenced by the physicochemical properties of the films on the surface and the differences in

enzyme immobilization methods, the $K_{M,app}$ value for the WT*Ch*CDH DET biosensor is nearly 3-fold lower than the value of 36 ± 1 mM reported for a WT*Ch*CDH DET biosensor prepared by drop-coating 1 µL of a 15 mg mL^{-1} WT*Ch*CDH solution on electrodes[21]. As a consequence, the linear range of 0-5 mM and j_{max} of 21.8 ± 0.3 µA cm^{-2} for the DET biosensor based on an enzyme volume of 18 µL (180 µg), Figure 3 and Table 1, are lower than the 0-10 mM and 47 µA cm^{-2} obtained at the WT*Ch*CDH DET biosensor from a previous report[21]. Signal sensitivity is, however, similar for both type of electrodes at ~1 µA cm^{-2} mM^{-1} (Table 3.1). The sensitivity using the WT*Ch*CDH, however, is at least threefold higher than that reported using other CDH DET glucose biosensors operating in PBS (Table 3.1). The optimized WT*Ch*CDH DET biosensor has a relative standard deviation of 10.1% and a stability in current signal of 57.4 ± 0.4 % initial current remaining after 12 h of continuous application.

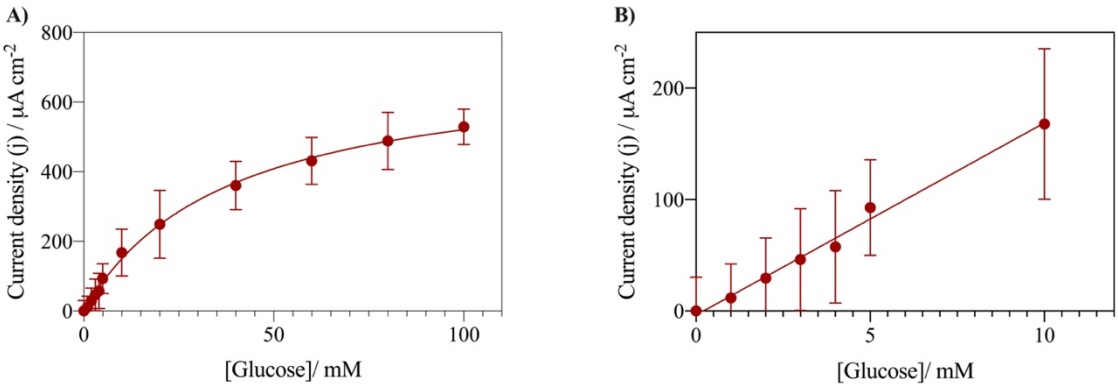

Figure 3.4: Glucose response curves for the MET system (top) and the linear plot for 0-5 mM glucose (bottom) based on amperometry at 0.35 V in PBS at 37 ºC, where n=4. The error bars represent the standard deviation

For the MET sensors, the amount of each component drop-coated on the surface was optimized using a Box-Behnken design-of-experiments approach (Appendix A.3, Supporting Information Figure S3.2) to maximize glucose oxidation current density in 5 mM glucose solutions, as described previously[41]. The $K_{M,app}$ of 37.9 ± 5.4 mM obtained for the optimized MET biosensor is similar to the value of 36 ± 1 mM reported for a WT*Ch*CDH DET biosensor[21]. However, the j_{max} value of 719 ± 43 µA cm^{-2} achieved with the MET biosensor is 15-fold higher than the 47 µA cm^{-2} obtained for that DET biosensor[21], and more than 30-fold higher than that obtained for the optimized WT*Ch*CDH DET biosensor reported on here. This higher j_{max} value

results in 17-fold increased sensitivity, and a wider linear range, to glucose for the MET biosensor over the WT*Ch*CDH DET biosensor operating in PBS (Table 3.1). On comparing DET to MET biosensor performance, the lower $K_{M,app}$ and j_{max} values for DET suggests that interdomain electron transfer is rate limiting and affects the measured kinetic constants.

The MET biosensors reported on here display higher sensitivity than the DET biosensors. The biosensor sensitivity is similar, or better, than that of other MET biosensors based on GOx, apart from those that include nanostructured supports within the film matrix to enhance current density (see data in Table 3.1).

The MET biosensor has a reproducibility relative standard deviation (RSD) of 5.8% (n=6) and a stability of 53.04 ± 1.1 % (n=4) over 12 h of continuous amperometry. Comparison of operational stability is difficult as there are variations in how this is measured. However, considering that over 12h of continuous operation the half-life of the enzyme has not been reached, the MET sensor performance is comparable to that of other glucose biosensors (Table 3.1). The MET biosensor linear range of 0-10 mM encompasses a range that includes clinical glucose levels for diabetes monitoring.[47].

Table 3.1: Analytical parameters of the glucose sensors

Sensor	Sensitivity[a] /μA cm^{-2} mM^{-1}	Linear Range[b] / mM	Detection Limit[c] / mM	Reproducibility RSD[d]/ %	Operational Stability[e] / %	J @ 5 mM glucose / μA cm^{-2}	Reference
Operation in PBS: selected DET-based sensors							
WT*Ch*CDH/graphite (160 μg)	0.99 ± 0.22	0-5	1.8	12.1	54± 1	5.0 ± 1.0	This work
WT*Ch*CDH/graphite (180 μg)	1.22 ± 0.17	0-5	1.7	10.7	57 ± 1	6.3 ± 1.1	This work
WT*Ch*CDH/graphite	1.00	0-10	-	-	-	5.0	[21]
[(f)]*Ct*CDH/graphite	0.030	0.002-2	0.001	-	-	-	[42]
*Ct*CDH/SPE	0.12	0.025-30	0.01	3.3	90 {7 h}	-	[42]
Engineered *Ct*CDH/graphite	0.21	0.1-1.0	0.1	-	-	-	[43]
Engineered *Ct*CDH/graphite	0.30	0.002-2.0	0.001	-	-	-	[10]
Operation in PBS: selected MET-based sensors							
WT*Ch*CDH/OsPolymer/graphite	17.3 ± 3.9	0-10	1.9	5.8	53± 1	93 ± 11	This work
GOx/OsPolymer/GC	5	0-10	-	-	-	-	[44]
GOx/PEI-Fc/GC	18	0-5		17		90	[45]
GOx/MWCNT-Fc/CS/GC	25	0.012-3.8	0.003	-	-	-	[46]
*Ct*CDH/OsPolymer/ MWCNT/graphite	90	0-40	-	-	86	-	[48]
GOx/OsPolymer/ MWCNT/graphite	250	0-10	-	-	70	-	[48]
[(g)]FADGDH/OsPolymer/MWCNT/graphite	250	0-10	-	-	72	1500	[48]
GOx-CNT/OsPolymer/ graphite	400	0-4	-	-	60	2080	[41]
Operation in Artificial Serum							
DET WT*Ch*CDH/graphite (180 μg)	0.70	0-5	2.0	15.1	54± 2	3.7 ± 1.1	This work
MET WT*Ch*CDH/OsPolymer/graphite	12.4	0-10	1.7	7.4	52 ± 1	72 ± 12	This work

[a] Sensitivity is obtained from the slope of the linear section of the Michaelis-Menten curve and indicates the ability of the sensor to respond to changes in glucose concentration. [b] Linear range is the range where current density is a linear function of glucose concentration and R^2=0.99. [c] Detection limit is the lowest value at which glucose can be detected and is defined as 3σ where σ is the standard deviation of the sensor at 0 mM glucose. [d] Reproducibility RSD is derived from the standard deviation on repeating a measurement a fixed number of times. [e] Operational stability

is defined as the current retained after 12 h of continuous amperometric measurement, unless otherwise indicated [f] *Ct* is *Corynascus thermophilus*. [g] FADGDH is FAD dependent glucose dehydrogenase.

3.4.2 Effect of Oxygen on Sensor Performance

Glucose determination using GOx-based biosensors is complicated by the effect of oxygen on sensor performance, as oxygen is the natural electron acceptor for GOx oxidation of glucose and therefore competes with the mediator for electrons. Furthermore, oxygen can be reduced by the enzyme or mediator, producing hydrogen peroxide which can inhibit the enzyme[48–50]. As CDH has low activity with oxygen[51], a major benefit of using CDH in sensors is that sensor response should be less dependent on oxygen. This is important for glucose sensing applications as a biosensor sensitive to oxygen would show fluctuations and errors in glucose measurement due to the variation in oxygen concentration. One approach is to modify the structure of GOx through enzyme engineering to mitigate oxygen sensitivity. For example, Prévoteau *et al.* [52] used semi-rational engineering of GOx to enhance the electron transfer to the enzyme active site. However, while higher glucose oxidation current compared to native enzyme was achieved, it was due to improved enzyme and redox polymer interaction rather than a decrease in oxygen sensitivity. Horaguchi *et al.* [53] introduced mutations within the putative residues involved in the GOx oxidative half-reaction to decrease less oxygen sensitivity. However, the mutation affects the reductive half-reaction also and resulted in a decrease in enzyme activity and stability. The WT*Ch*CDH biosensors developed do not display a significant change in sensor response in the presence of oxygen (Figure 3.5). However, WT*Ch*CDH turnover stability in the presence of oxygen and excess glucose is negatively affected by the presence of oxygen, most likely related to the susceptibility of methionine residues to oxidation given that replacement of methionine residues results in improved turnover stability[21].

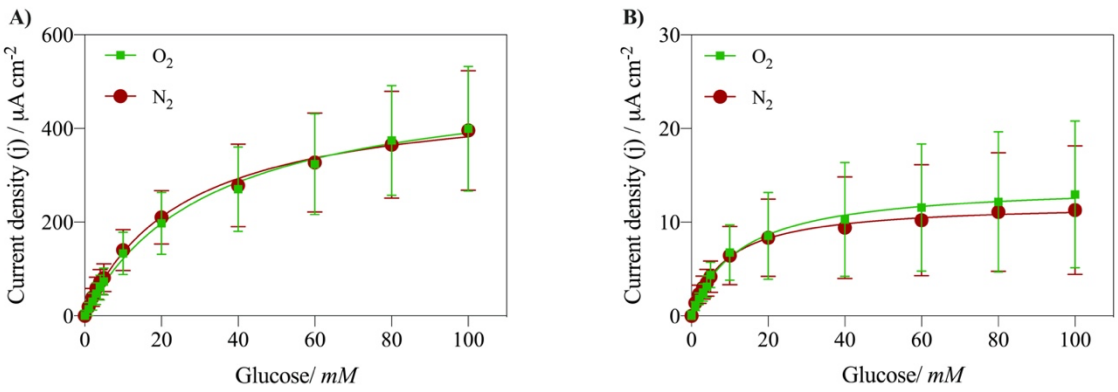

Figure 3.5: Glucose response curves for the MET system based on amperometry at 0.35 V (A) and for the DET system with 180 µg WT*Ch*CDH drop-coated onto the electrodes based on amperometry at 0.1 V (B) in the presence (green) and absence (red) of ambient oxygen in PBS at 37 ºC, where n=4. The error bars represent the standard deviation.

3.4.3 Operation under sample conditions

In order to test practical application of the oxygen insensitive DET and MET-based glucose biosensors in physiological fluids, the amperometric response to glucose in artificial serum was measured. Glucose oxidation current responses increase with increasing glucose concentrations for all sensors and the analytical parameters for the sensors are presented in Table 3.1. The current density obtained for a glucose level of 5 mM, representing a normal blood glucose level, is lower in artificial serum compared to the response in PBS, an effect previously observed and attributed to electrochemical interferences and protein adsorption[38,54–56]. The operational stability of all the sensors is ~ 50% and does not seem to be affected by the additional components present in the artificial serum over that present in PBS. In the presence of artificial serum, $K_{M,app}$ values were found to be 23.0 ± 3. mM and 7.4 ± 0.7 mM while j_{max} values were 393.8 ± 39.1 and 9.5 ± 1.1µA cm^{-2} for the MET and DET biosensor, respectively. While further research is required to determine the exact mechanism(s), the decrease of both $K_{M,app}$ and j_{max} values in the presence of serum components suggests that there is a uncompetitive inhibitor for WT*Ch*CDH present in this complex media[57]. This decrease in both $K_{M,app}$ and j_{max} values could also be explained by passivation of the electrode or film, for example by protein adsorption. While this does not seem to adversely affect the operational stability of the sensors, the sensitivities are lower, and

the reproducibility RSD's are higher for both types of sensors in artificial serum compared to operation in PBS.

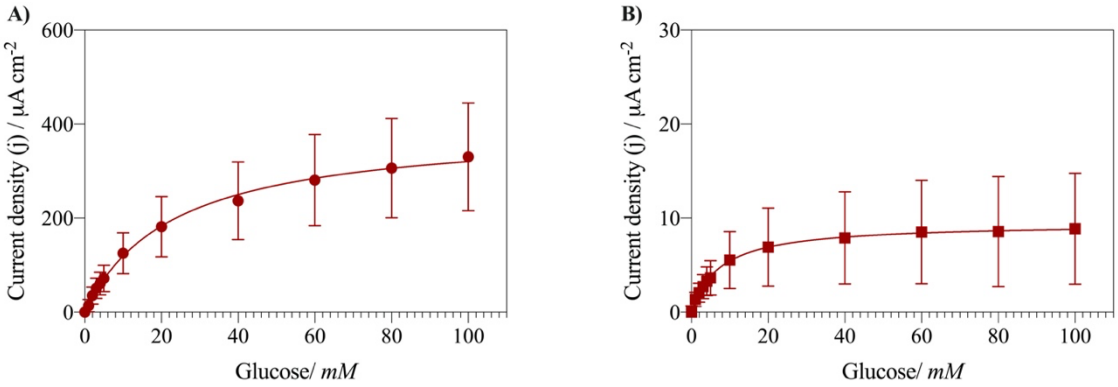

Figure 3.6: Glucose response curves for the MET system based on amperometry at 0.35 V (A) and for the DET system based on amperometry at 0.1 V (B) in the artificial serum buffer at 37 °C (n=4). The error bars represent the standard deviation.

3.4.4 Interferent screening

In order to evaluate the specificity of the engineered WT*Ch*CDH to glucose as a substrate as well as to verify that the loss in current density, sensitivity and increase in RSD when testing in artificial serum does not occur due to the presence of other sugars or an electrochemical interferent present in the complex media, an interference study was conducted. Interference is calculated using a MARD threshold of 20% in the presence of 5 mM glucose (equation 3.1). From the data in Figure 3.7, none of the other sugars or sugar alcohols result in a MARD greater than 20%. However, lactose shows the highest MARD which is close to the 20% threshold classifying interference. This is likely due to the structure of lactose, which is very similar to cellobiose, the preferred substrate of CDH-type enzymes[14]. Overall, while it may seem that lactose is just under the limit of interference, it must be considered that all the non-glucose sugars were tested at the maximum concentration in blood plasma to accurately depict a worst-case scenario. Thus, in artificial serum, lactose would likely not interfere in the signal and may not be the sole component responsible for the difference in the analytical parameters between PBS and artificial serum. Glycerol also affects glucose oxidation currents, especially for the MET biosensor system. It should be noted that solution properties may change sensor film swelling and mass transport of glucose to the electrode surface.

While lactose was the only sugar to cause significant interference, it is reported that the sugar mannose causes the most significant interference for biosensors based on GOx[58] and *Ch*CDH[13,18]. To fully account for potential interference of electroactive substances it is recommended to use 2-3 times their highest blood concentrations while testing in order to depict the worst-case scenario[59,60]. Therefore, ascorbic acid, uric acid and acetaminophen were studied as interferents at concentrations higher than their usual blood concentrations (Figure 3.8). Even under these extreme conditions the MARD response for all three electroactive interferents remains below the 20% threshold, and they are not therefore classified as interferents. Uric acid shows the highest MARD in the sensor current response. Uric acid has been reported to act as a non-competitive inhibitor of *Ct*CDH and affect the stability of the enzyme over time[61]. In general, the electroactive substances can cause deviations in glucose reading due to co-oxidation (Figure 8). Overall, while the presence of uric acid and lactose alone do not exceed the MARD threshold to be classified as interferences, their combined presence, as is the case in artificial serum, may work co-operatively. The MARD calculated for artificial serum is 40-50% when compared to sensor response in PBS. Finally, while taking into account the cooperative effect of the *in vivo* sugars and the electrochemical interferents, the presence of BSA in the artificial serum may also introduce non-specific protein adsorption that could contribute to increase the MARD in artificial serum.

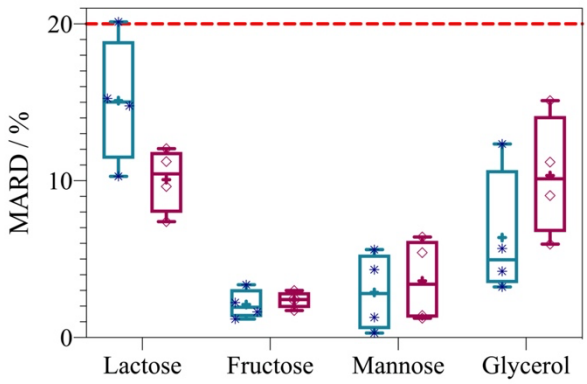

Figure 3.7: Box plot showing the mean absolute relative difference (MARD, %) of the current signal in 5 mM glucose (PBS, pH 7.4, 37ºC) for DET (pink) and MET (blue) sensors in the presence of sugars or glycerol. The line inside the box = mean, box limits = standard deviation

(n=4); * and ◇ represent individual data points; lower and upper error bars = 5% and 95% limits, respectively; red line = 20% MARD threshold for definition of interference.

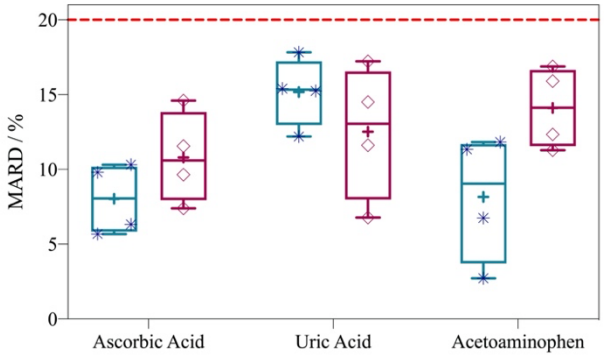

Figure 3.8: Box plot showing the mean absolute relative difference (MARD, %) of the current signal in 5 mM glucose (PBS, pH 7.4, 37ºC) for DET (pink) and MET (blue) sensors in the presence of common electrochemical interferents found in the blood. The line inside the box = mean, box limits = standard deviation (n=4); * and ◇ represent individual data points; lower and upper error bars = 5% and 95% limits, respectively; red line = 20% MARD threshold for definition of interference.

3.5 Conclusions

Recombinantly produced WT*Ch*CDH containing glucose-activity enhancing mutations was used to produce DET and MET-based glucose biosensors. The biosensor component amounts were optimized for sensor current response in 5 mM glucose. Biosensor operation was characterized electrochemically in PBS and artificial serum. The MET biosensor showed high sensitivity on the same order of magnitude to systems containing other glucose-oxidising enzymes [44,45]. This shows the potential of the engineered enzyme for application to glucose biosensing. While the MET biosensor shows higher sensitivity than the DET biosensor, the DET biosensor based on recombinantly produced WT*Ch*CDH offers a substantial improvement in sensitivity over other DET-based glucose biosensors. Moreover, both DET and MET sensors showed no change in glucose response when measured in the absence and presence of oxygen. Operation in artificial serum results in a decrease in glucose oxidation current density attributed to electrochemical interferences and protein

adsorption, but the operational stability is not affected by operation in artificial serum. An interference study conducted with sugars and common electrochemical interferents that can be present *in vivo* demonstrated that no individual component crosses the threshold to become an interferent alone, but in complex media such as artificial serum, they may have a cooperative effect.

3.6 Acknowledgements

This publication is part of a project that has received funding from the European Union's Horizon 2020 research and innovation programme under grant agreement Nº813006.

3.7 References

[1] P. Saeedi, I. Petersohn, P. Salpea, B. Malanda, S. Karuranga, N. Unwin, S. Colagiuri, L. Guariguata, A.A. Motala, K. Ogurtsova, J.E. Shaw, D. Bright, R. Williams, Diabetes Res Clin Pract. 157 (2019) 107843.

[2] N.H. Cho, J.E. Shaw, S. Karuranga, Y. Huang, J.D. da Rocha Fernandes, A.W. Ohlrogge, B. Malanda, Diabetes Res Clin Pract. 138 (2018) 271–281.

[3] L.C. Clark, C. Lyons, Ann N Y Acad Sci. 102 (1962) 29–45..

[4] A. Heller, B. Feldman, Chem Rev. 108 (2008) 2482–2505.

[5] K.E. Toghill, R.G. Compton, Int J Electrochem Sci. 5 (2010) 1246–1301.

[6] P.N. Bartlett, F.A. Al-Lolage, Journal of Electroanalytical Chemistry. 819 (2018) 26–37.

[7] R. Wilson, A.P.F. Turner, Biosens Bioelectron. 7 (1992) 165–185.

[8] T.J. Ohara, R. Rajagopalan, A. Heller, Anal Chem. 65 (1993) 3512–3517.

[9] A.E.G. Cass, G. Davis, G.D. Francis, H. Allen, O. Hill, W.J. Aston, I.J. Higgins, E. v. Plotkin, L.D.L. Scott, A.P.F. Turner, Anal Chem. 56 (1984) 667–671.

[10] R. Ortiz, M. Rahman, B. Zangrilli, C. Sygmund, P.O. Micheelsen, M. Silow, M.D. Toscano, R. Ludwig, L. Gorton, ChemElectroChem. 4 (2017) 846–855.

[11] A. Heller, Physical Chemistry Chemical Physics. 6 (2004) 209–216.

[12] C. Chen, Q. Xie, D. Yang, H. Xiao, Y. Fu, Y. Tan, S. Yao, RSC Adv. 3 (2013) 4473–4491.

[13] S. Scheiblbrandner, R. Ludwig, Bioelectrochemistry. 131 (2020) 107345.

[14] R. Ludwig, W. Harreither, F. Tasca, L. Gorton, ChemPhysChem. 11 (2010) 2674–2697.

[15] T.C. Tan, D. Kracher, R. Gandini, C. Sygmund, R. Kittl, D. Haltrich, B.M. Hällberg, R. Ludwig, C. Divne, Nat Commun. 6 (2015) 1–11.

[16] F. Tasca, R. Ludwig, L. Gorton, R. Antiochia, Sens Actuators B Chem. 177 (2013) 64–69.

[17] P. Bollella, F. Mazzei, G. Favero, G. Fusco, R. Ludwig, L. Gorton, R. Antiochia, Biosens Bioelectron. 88 (2017) 196–203.

[18] W. Harreither, V. Coman, R. Ludwig, D. Haltrich, L. Gorton, Electroanalysis. 19 (2007) 172–180.

[19] A. Lindgren, L. Gorton, T. Ruzgas, U. Baminger, D. Haltrich, M. Schülein, Journal of Electroanalytical Chemistry. 496 (2001) 76–81.

[20] M. Zámocký, C. Schümann, C. Sygmund, J. O'Callaghan, A.D.W. Dobson, R. Ludwig, D. Haltrich, C.K. Peterbauer, Protein Expr Purif. 59 (2008) 258–265.

[21] A.F. Geiss, T.M.B. Reichhart, B. Pejker, E. Plattner, P.L. Herzog, C. Schulz, R. Ludwig, A.K.G. Felice, D. Haltrich, ACS Sustain Chem Eng. 9 (2021) 7086–7100.

[22] R. Ortiz, H. Matsumura, F. Tasca, K. Zahma, M. Samejima, K. Igarashi, R. Ludwig, L. Gorton, Anal Chem. 84 (2012) 10315–10323.

[23] S.C. Feifel, R. Ludwig, L. Gorton, F. Lisdat, Langmuir. 28 (2012) 9189–9194.

[24] M. Shao, M.N. Zafar, M. Falk, R. Ludwig, C. Sygmund, C.K. Peterbauer, D.A. Guschin, D. MacAodha, P.Ó. Conghaile, D. Leech, M.D. Toscano, S. Shleev, W. Schuhmann, L. Gorton, ChemPhysChem. 14 (2013) 2260–2269.

[25] A. Hildebrand, E. Szewczyk, H. Lin, T. Kasuga, Z. Fan, , Appl Environ Microbiol. 81 (2015) 597–603.

[26] Desriani, S. Ferri, K. Sode, Biochem Biophys Res Commun. 391 (2010) 1246–1250.

[27] F.A.J. Rotsaert, V. Renganathan, M.H. Gold, Biochemistry. 42 (2003) 4049–4056.

[28] C. Sygmund, W. Harreither, D. Haltrich, L. Gorton, R. Ludwig, N Biotechnol. 25 (2009) S115.

[29] F. Mao, N. Mano, A. Heller, J Am Chem Soc. 125 (2003) 4951–4957.

[30] U. Baminger, S.S. Subramaniam, V. Renganathan, D. Haltrich, Appl Environ Microbiol. 67 (2001) 1766–1774.

[31] C.A. Burtis, E.R. Ashwood, D.E. Bruns, Tietz Elsevier Health Sciences, 2012.

[32] M. Miller, J.W. Craig, W.R. Drucker, H. Woodward, Yale J Biol Med. 29 (1956) 335–60.

[33] J.G. Blanco, Journal of Biological Chemistry. 79 (1928) 667–672.

[34] T. Bailey, A. Chang, P.D. Rosenblit, L. Jones, G. Teft, S. Setford, J. Mahoney, Diabetes Technol Ther. 14 (2012) 701–709.

[35] F.C. Wood, G.F. Cahill, J Clin Invest. 42 (1963) 1300–1312.

[36] R. Guisado, W.W. Tourtellotte, A.I. Arieff, U. Tomiyasu, S.K. Mishra, M.C. Schotz, J Neurosurg. 42 (1975) 226–228.

[37] EP07 Interference Testing in Clinical Chemistry, 2017.

[38] R. Boehm, J. Donovan, D. Sheth, A. Durfor, J. Roberts, I. Isayeva, J Diabetes Sci Technol. 13 (2019) 82–95.

[39] G. Kovacs, R. Ortiz, V. Coman, W. Harreither, I.C. Popescu, R. Ludwig, L. Gorton, Bioelectrochemistry. 88 (2012) 84–91.

[40] P. Bollella, L. Gorton, R. Ludwig, R. Antiochia, Sensors (Switzerland). 17 (2017) 1912.

[41] W. Harreither, P. Nicholls, C. Sygmund, L. Gorton, R. Ludwig, Langmuir. 28 (2012) 6714–6723.

[42] C. Schulz, R. Ludwig, L. Gorton, Anal Chem. 86 (2014) 4256–4263.

[43] H. Ju, D. Leech, Anal Chim Acta. 345 (1997) 51–58.

[44] Bard Allen J., Faulkner Larry R., A.J. Bard, Faulkner Larry R., John Wiley and Sons, 2001.

[45] L.R. Faulkner, A.J. Bard, John Wiley and Sons, 2008.

[46] I. Osadebe, D. Leech, ChemElectroChem. 1 (2014) 1988–1993.

[47] I. Osadebe, P. Conghaile, P. Kavanagh, D. Leech, Electrochim Acta. 182 (2015) 320–326.

[48] R. Bennett, D. Leech, Bioelectrochemistry. 133 (2020) 107460.

[49] R. Bennett, I. Osadebe, R. Kumar, P.Ó. Conghaile, D. Leech, Electroanalysis. 30 (2018) 1438–1445.

[50] B. Limoges, J. Moiroux, J.M. Savéant, Journal of Electroanalytical Chemistry. 521 (2002) 8–15.

[51] P.N. Bartlett, K.F.E. Pratt, Journal of Electroanalytical Chemistry. 397 (1995) 61–78.

[52] K. Jayakumar, R. Bennett, D. Leech, Electrochim Acta. 371 (2021) 137845.

[53] V. Mani, B. Devadas, S.M. Chen, Biosens Bioelectron. 41 (2013) 309–315.

[54] A.K.G. Felice, C. Sygmund, W. Harreither, R. Kittl, L. Gorton, R. Ludwig, J Diabetes Sci Technol. 7 (2013) 669–677.

[55] R. Rajagopalan, A. Aoki, A. Heller, Journal of Physical Chemistry. 100 (1996) 3719–3727.

[56] S.A. Merchant, D.T. Glatzhofer, D.W. Schmidtke, Langmuir. 23 (2007) 11295–11302.

[57] J.D. Qiu, W.M. Zhou, J. Guo, R. Wang, R.P. Liang, Anal Biochem. 385 (2009) 264–269.

[58] V.B. Juska, M.E. Pemble, Sensors. 20 (2020).

[59] A. Prévoteau, N. Mano, Electrochim Acta. 112 (2013) 318–326.

[60] A. Prévoteau, N. Mano, Electrochim Acta. 68 (2012) 128–133.

[61] N. Mano, Bioelectrochemistry. 128 (2019) 218–240.

[62] C. Sygmund, P. Santner, I. Krondorfer, C.K. Peterbauer, M. Alcalde, G.S. Nyanhongo, G.M. Guebitz, R. Ludwig, Microb Cell Fact. 12 (2013) 38.

[63] A. Prévoteau, O. Courjean, N. Mano, Electrochem Commun. 12 (2010) 213–215.

[64] Y. Horaguchi, S. Saito, K. Kojima, W. Tsugawa, S. Ferri, K. Sode, Electrochim Acta. 126 (2014) 158–161.

[65] V. Coman, R. Ludwig, W. Harreither, D. Haltrich, L. Gorton, T. Ruzgas, S. Shleev, Fuel Cells. 10 (2010) 9–16

[66] T. Siepenkoetter, U. Salaj-Kosla, X. Xiao, P. Conghaile, M. Pita, R. Ludwig, E. Magner, Chempluschem. 82 (2017) 553–560.

[67] R.D. Milton, K. Lim, D.P. Hickey, S.D. Minteer, Bioelectrochemistry. 106 (2015) 56–63.

[68] A. Cornish-Bowden, Fundamentals of Enzyme Kinetics, 1979.

[69] S. Scheiblbrandner, R. Ludwig, Bioelectrochemistry. 131 (2020) 107345.

[70] M.N. Zafar, G. Safina, R. Ludwig, L. Gorton, Anal Biochem. 425 (2012) 36–42.

[71] R. Bennett, E. Blochouse, D. Leech, Electrochim Acta. 302 (2019) 270–276.

[72] P. Rafighi, M. Tavahodi, B. Haghighi, Sens Actuators B Chem. 232 (2016) 454–461.

[73] K.Y. Hwa, B. Subramani, Biosens Bioelectron. 62 (2014) 127–133.

Chapter 4: Tethering zwitterionic polymer coatings to mediated glucose biosensor enzyme electrodes can decrease sensor foreign body response yet retain sensor sensitivity to glucose

Published as:

Tethering zwitterionic polymer coatings to mediated glucose biosensor enzyme electrodes can decrease sensor foreign body response yet retain sensor sensitivity to glucose

Kavita Jayakumar[†], Anna Lielpetere[†], Daniel A. Domingo-Lopez, Ruth E. Levey, Garry P. Duffy[3], Wolfgang Schuhmann[2*], Dónal Leech, Biosensors and Bioelectronics, 219, 114815

[†]These authors contributed equally to the research

Co-author contributions:

I synthesised the PVI-bound osmium redox polymer, performed all labwork, analysis and wrote the first draft of the publication.

Anna Lielpetere synthesised the zwitterionic polymers and co-wrote the first draft of the publication.

Daniel A. Domingo-Lopez and Ruth E. Levey guided and contributed to protein adsorption and cell adhesion study labwork.

Garry P. Duffy provided valuable guidance and feedback for protein adsorption and cell adhesion study laboratory work and analysis of results.

Wolfgang Schuhmann, as project supervisor of Anna Lielpetere, contributed through advice and guidance throughout the work and edited the first draft of the publication.

Dónal Leech, as my project supervisor, contributed through advice and guidance throughout the work and edited the first draft to provide the final version for publication.

4.1 Abstract

Foreign body response (FBR) is a major challenge that affects implantable biosensors and medical devices, including glucose biosensors, leading to a deterioration in device response over time. Polymer shields are often used to mitigate this issue. Zwitterionic polymers (ZPs) are a promising class of materials that reduce biofouling of implanted devices. A series of ZPs each containing tetherable epoxide functional groups was synthesised for application as a polymer shield for eventual application as implantable glucose biosensors. The polymer shields were initially tested for the ability to resist fibrinogen adsorption and fibroblast adhesion. All synthesised ZPs showed comparable behaviour to a commercial Lipidure ZP in resisting fibrinogen adsorption. Nafion, a common anionic shield used against electrochemical interferents, showed higher protein adsorption and comparable cell adhesion resistance as uncoated control surfaces. However, a poly(2-methacryloyloxyethyl phosphorylcholine-*co*-glycidyl methacrylate (MPC)-type ZP showed similar behaviour to Lipidure, with approximately 50% reduced fibrinogen adsorption and 80% decrease in fibroblast adhesion compared to uncoated controls. An MPC-coated amperometric glucose biosensor showed comparable current density and a 1.5-fold increase in sensitivity over an uncoated control biosensor, whereas all other polymer shields tested, including Lipidure, Nafion and a poly(ethylene glycol) polymer, resulted in lower sensitivity and current density. Collectively, these characteristics make MPC-polymer shield coatings an appealing possibility for use in CGMS glucose sensors and other implanted devices with the aim of reducing FBR while maintaining sensor performance.

4.2 Introduction

Modern healthcare offers a wide range of implantable medical devices to improve the quality of life [1–4]. However, the host's foreign-body response (FBR) which encases the implant in a fibrotic membrane frequently impairs the intended function of these devices [5]. For example, commercial continuous glucose monitoring systems (CGMS) based on amperometric glucose sensors have an operational lifespan of up to 14 days [6,7] due to the significant hurdles of sensor long-term stability and sensor

calibration concerns, which are exacerbated by the hostile environment inside the human body [3–5,7–9].

The FBR process initiates immediately upon implant contact with host fluids (e.g., blood, lymph, wound fluids) by spontaneous uncontrolled adsorption of host proteins to the implant surface [2]. This surface biofouling can cause device contamination, loss of specificity and overall surface passivation, all of which can lead to device failure. In order to overcome this, research is required on minimising the adherence of molecules and systems to surfaces [10,11], particularly in preventing the *in vivo* and *in vitro* adhesion of biomolecules, cells and bacteria to objects [12–16]. To this end, anti-fouling coatings are a promising solution [17–22]. Generally, good anti-fouling layers have polar functional groups (i.e., are hydrophilic), are hydrogen bond acceptors, have no hydrogen bond donors and have zero net charge [15,23]. Surface coatings based on poly(ethylene glycol) (PEG) or oligo(ethylene glycol) (OEG) and their derivatives have been widely used in biomedical applications [24]. However, their anti-fouling activity depends on many factors and is directly proportional to the degree of polymerisation and the density of surface coating [23] which can often limit their application depending on the requirements of the biomedical implant.

The hydrophilicity of most polymer/biopolymer coatings is the primary anti-fouling mechanism that operates by producing a highly hydrated environment within the anti-fouling coating and establishing a steric repulsive barrier that fouling molecules must overcome before adhesive connections can be formed with the surface [25]. Despite the fact that PEG and OEG are considered the "gold standard" of anti-fouling coatings, research into zwitterionic polymer (ZP) alternatives has gained traction in the last decade due to their stronger hydration effects that result in enhanced anti-fouling properties [1,15,16,26]. The ZP mechanism of action is related to the ability to balance charge and therefore impair electrostatic interactions, as well as to form a strong hydration sphere as a physical and entropic barrier to approaching biomolecules [27]. Because of their ease of synthesis, carboxybetaine (CB) and sulfobetaine (SB)-based ZPs are the most widely employed zwitterionic coatings for surfaces [28,29]. However, phosphocholine-based (PC) polymers are the only FDA-approved and commercially available zwitterionic anti-fouling materials utilised to improve the performance of medical devices: commercially known as Lipidure [30]. However, PC-

based ZP materials are rarely the topic of systematic studies, probably due to challenging material synthesis [30].

One of the key advantages of using anti-fouling polymer coatings on implant surfaces is the wide range of monomers and end-group functional structures that can be selected to form polymers with tuneable anti-fouling mechanisms. However, despite the many types of anti-fouling coatings, the coating specifications vary depending on the application. For example, a stent requires an anti-fouling coating where the main concern would be biocompatibility and thus a wide variety of coatings could be utilised. On the other hand, a sensor for application as in a CGM requires a mechanism to limit the FBR while also permitting analyte (glucose) access to the sensing system or surface. In this case, a suitable anti-fouling shield should not only resist biofouling of the sensor, but also must be permeable to the enzyme substrate, e.g., glucose, as well as allow diffusion of reaction products [31]. In the case of glucose biosensor enzyme electrodes, accumulation of the reaction product gluconic acid changes the local pH which can impact film stability or deactivate the enzyme [21]. A PEG shield may not be suitable, despite its anti-fouling capability, as this capability is dependent on the density of the coating itself [32] and a dense coating may limit substrate or product diffusion. Moreover, in the case of electrochemical glucose biosensors, one significant issue with anti-fouling coatings is electrode passivation, where coatings grafted to an electrode surface occupy a portion of the electroactive surface area thus reducing the amount of surface capable of participating in electrochemical reactions or charge transfer processes [31]. This has the same effect on biosensors as surface fouling, in that the total electrochemical signal magnitude is lowered due to reduced electrode surface accessibility for the electron or charge transfer carrier [33–35].

For a successful implantable glucose biosensor enzyme electrode, the primary challenge is to devise a coating which prevents fouling without simultaneously passivating the electrode surface or hindering substrate or product diffusion. Multiple coatings have been tested for this purpose including Nafion [33], PEG [36], polyaniline [37] and poly(2-hydroxyethyl methacrylate) (polyHEMA) [38]. While coatings shield the sensor from (bio)molecular interference, they also result in a decrease in glucose current density due to the restricted diffusion of glucose through the polymer shield [33–35]. Deploying a polymer shield usually results in a multi-layer architecture,

where diffusion of the analyte is hindered as it passes through each layer, resulting in decreased sensitivity and signal [3–5,7–9].

The interface between the sensing and anti-fouling layers plays a critical role. When the boundary between the layers is defined, they act as two distinct layers (Scheme 4.1C) and the analyte has different diffusion characteristics as it passes through each layer [39,40]. Computational studies predict that minimising the boundary between the layers can create a unique case where diffusivities equalise and the polymer shield does not hinder diffusion [40]. In an attempt to minimise the boundary between layers, we synthesised ZPs with a reactive epoxy functional group. This functional group acts as a tether and can react with compatible groups on the sensor surface or with the polymer backbone of a redox polymer layer in a mediated glucose biosensor enzyme electrode. This may allow the anti-fouling ZP layer to merge with the sensing layer at the interface between the two, minimising the boundary between the layers (Scheme 4.1B). In this study, the anti-fouling response of surfaces coated with the synthesised ZPs was evaluated using a two-part biological screening to check the ability to resist fibrinogen protein and fibroblast cell adhesion to the coated surfaces. The ZP providing the best anti-fouling response was then applied as an anti-fouling coating on an amperometric glucose biosensor enzyme electrode and device operation was tested and compared to the same glucose biosensor enzyme electrode coated with commercial polymer shields (Nafion and Lipidure).

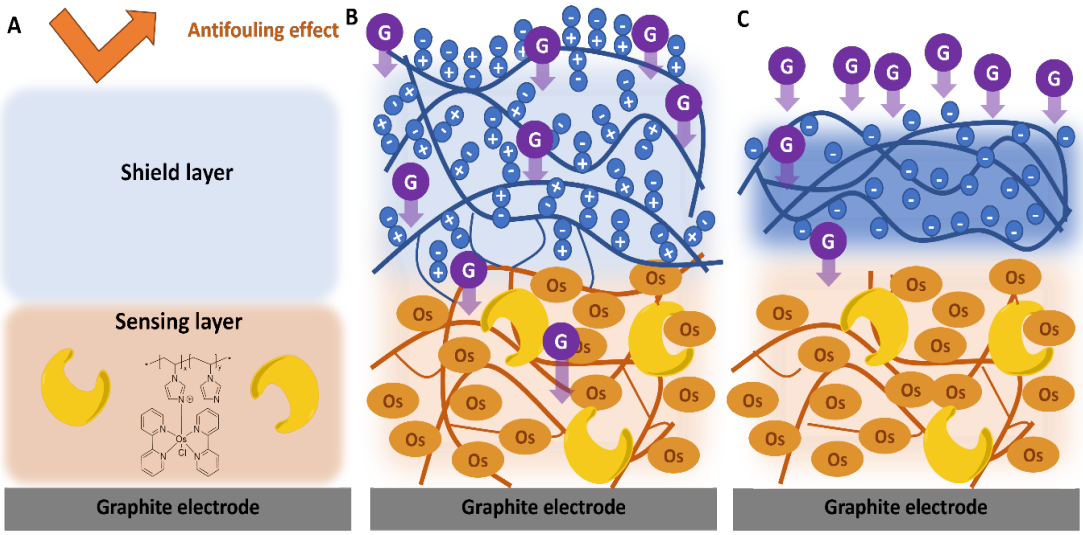

Scheme 4.1: Schematic of A) a glucose biosensor enzyme electrode used for the evaluation of anti-fouling, with sensing layer consisting of an osmium-complex based redox polymer [poly(1-vinylimidazole)Os(bpy)$_2$Cl]$^+$, an engineered cellobiose dehydrogenase enzyme (represented by **C** icon); B) a mixed boundary that can occur due to the presence of the epoxide crosslinking group in the ZP anti-fouling layer leading to un-hindered glucose (G) diffusion through the layers; C) multi-layer with rigid boundary at the interface between anti-fouling and sensing layer resulting in hindered glucose diffusion.

4.3 Materials and methods

4.3.1 Chemicals

All chemicals were purchased from Sigma-Aldrich, Alfa Aesar, Acros Organics, TCI, and Roth and used as received unless otherwise noted. Deuterated solvents were from Deutero or Eurisotop and were stored at 4°C: dimethyl sulfoxide (DMSO)-d_6 was stored at room temperature. Glycidyl methacrylate and butyl acrylate were passed through a column containing the corresponding inhibitor remover (Sigma-Aldrich) and stored at –20°C. The polymerisation initiator azobisisobutyronitrile (AIBN) was recrystallised from hot toluene and stored at –20 °C. All aqueous solutions were prepared using water purified and deionised with a Milli-Q system. The redox polymer [poly(1-vinylimidazole)Os(bpy)$_2$Cl]$^+$ (Os(bpy)PVI), structure depicted in Scheme 1A where x = 1 and y = 9, was synthesised by modification of published procedures (Heller and Feldman, 2008; Mao et al., 2003). A cellobiose dehydrogenase (CDH)

from *Crassicarpon hotsonii (*syn. *Myriococcum thermophilum*) equipped with glucose activity-enhancing mutations C291Y and W295R, provided by DirectSens GmbH [42], was used in this study.

4.3.2 Synthesis

All reactions and manipulations were conducted using the standard Schlenk technique under argon atmosphere. Polymer structure and nomenclature are presented in Figure 4.1A, based on the monomer selection and reaction depicted in Figure 4.1B. Details of synthesis of each polymer and their characterisation by NMR is provided in Supplementary information.

4.3.3 Protein and cell adhesion assays

4.3.3.a Fibrinogen ELISA

24-Well microtiter plates were coated with 180 µL of 0.5 wt/v% of the different polymer solutions, six wells for each polymer, and allowed to cure overnight. Six uncoated wells of a 24-well plate of the same surface area were used as the control. Each well was incubated with 1 mL of fibrinogen (0.5 mg/mL in phosphate buffered saline: 50 mM phosphate, 120 mM NaCl, pH 7.4, PBS) for 1 hour, followed by five washes with pure PBS buffer. They were then incubated with 1 mL of horseradish peroxidase (HRP)–conjugated anti-fibrinogen antibody (0.5 µg/ml) in PBS buffer for 1 h followed by five washes with PBS buffer. Next, 1 mL of *o*-phenylenediamine (1 mg/ml) and 0.1 M citrate phosphate (pH 5.0) solution, containing 0.03% hydrogen peroxide was added. After 15-min incubation, the enzymatic reaction was stopped by adding an equal volume of 1 M HCl. The absorbance value at 492 nm was recorded by a plate reader (Hidex Sense Microplate Reader) and was normalised to that for the uncoated well.

4.3.3.b Cell adhesion study

The WPMY-1 myofibroblast cell line (ATCC CRL-2845) was cultured in high glucose Dulbecco's modified Eagle's medium D5671 (Sigma) supplemented with 5% fetal

bovine serum, 1% penicillin-streptomycin and 0.05% L-glutamine and passaged at 70-80% confluency.

For the cell adherence assay, glass coverslips (22 mm × 22 mm) were coated with 180 µL of 0.5 wt/v% of the different polymer solutions investigated. A set of uncoated coverslips was used as control. After allowing polymers to cure for 24 h, all coverslips were placed in 6 well plates and sterilised by two 30 min UV cycles, followed by two washing steps with PBS. Myofibroblast cells were seeded on top of the coated coverslips and uncoated controls at 1×10^5 cells/mL density, using 2 mL per well to fully cover the sample surface. Samples were cultured for 72 h (37°C, 5% CO_2) and cell attachment was monitored daily using an optical microscope. Slides were then stained with Alexa Fluor 488 Phalloidin (A12379, Thermo Scientific), counterstained with Hoechst, as documented by Dolan *et al.* [41], and were then mounted using fluoromount. Hoechst dyes are a fluorescent stains that bind to AT-rich regions of the minor grove in DNA and can be used to stain nuclei of cells. The nuclei are visible in blue in the fluorescence images and are used to provide cell counts. Alexa Fluor 488 Phalloidin is a highly selective bicyclic peptide used for staining actin filaments and is used to image cell body, giving accurate visual of cell adhesion on slides. Slides were imaged using an Olympus FluoView FV 3000 Confocal Laser Scanning Microscope. The relative cell counts were determined using the "Analyse Particles" tool in FIJI ImageJ where each sample had $n = 3$ with 5 images per replicate. All counts were normalised with respect to the uncoated control.

4.3.4 Electrode modification

Graphite rods (Graphite store, USA, 4.0 mm diameter, NC001300) were cut, insulated with heat shrink tubing and polished at one end using fine grit paper, to give graphite working electrodes with a geometric surface area of 0.126 cm^2. The biosensors were assembled by drop-coating 30 µL of Os(bpy)PVI aqueous solution (5 mg mL^{-1}), 16 µL of CDH aqueous solution (10 mg mL^{-1}) and 7.4 µL of poly(ethylene glycol) diglycidyl ether (PEGDGE) crosslinker aqueous solution (15 mg mL^{-1}). The deposition was allowed to dry for 3 h before a 10 µL aliquot of 0.5 wt./v% of the respective polymer shield was applied to the electrodes. The electrodes were allowed to cure overnight at ambient temperature before the electrodes were used. The biosensor component amounts are based on amounts optimised to produce the highest

glucose oxidation current density in 5 mM glucose solution using a design of experiments approach [42].

4.3.5 Electrochemical measurements

Electrochemical tests were conducted using a CH Instruments 1030a multichannel potentiostat (IJ Cambria). The enzyme electrodes were used as working electrodes, with a custom-built Ag|AgCl (3 M KCl) as a reference electrode and a platinum mesh (Goodfellow) as a counter electrode. Electrodes were placed in a thermostated electrochemical cell containing PBS at 37 °C with experiments conducted, unless otherwise stated, in the presence of ambient oxygen. Current signals are normalised to the geometric surface area of the graphite disk electrodes to generate current density data.

4.4 Results and Discussion

4.4.1 Design of zwitterionic polymers

The selection of methacrylate and acrylate-based monomers allows the design and synthesis of a range of polymers with easily tuneable properties produced by changing the nature and the ratio of the monomers. A restricted series of ZPs with designed composition was synthesised (Figure 4.1A a-d). The commercially available ZP Lipidure (Figure 4.1A e) was selected as a control to assess the performance of the new ZPs.

The polymers were synthesised in a one-step free radical polymerisation procedure initiated by AIBN using the initial molar ratios of the monomers shown in Figure 4.1B. As it was not possible to determine the monomer ratio in the isolated polymers due to signal overlap in NMR spectra (Appendix A.4,Figures S4.1-4.4) the polymer structure is depicted assuming retention of the initial monomer ratio in the synthesised polymers. The synthesised polymers are all water soluble.

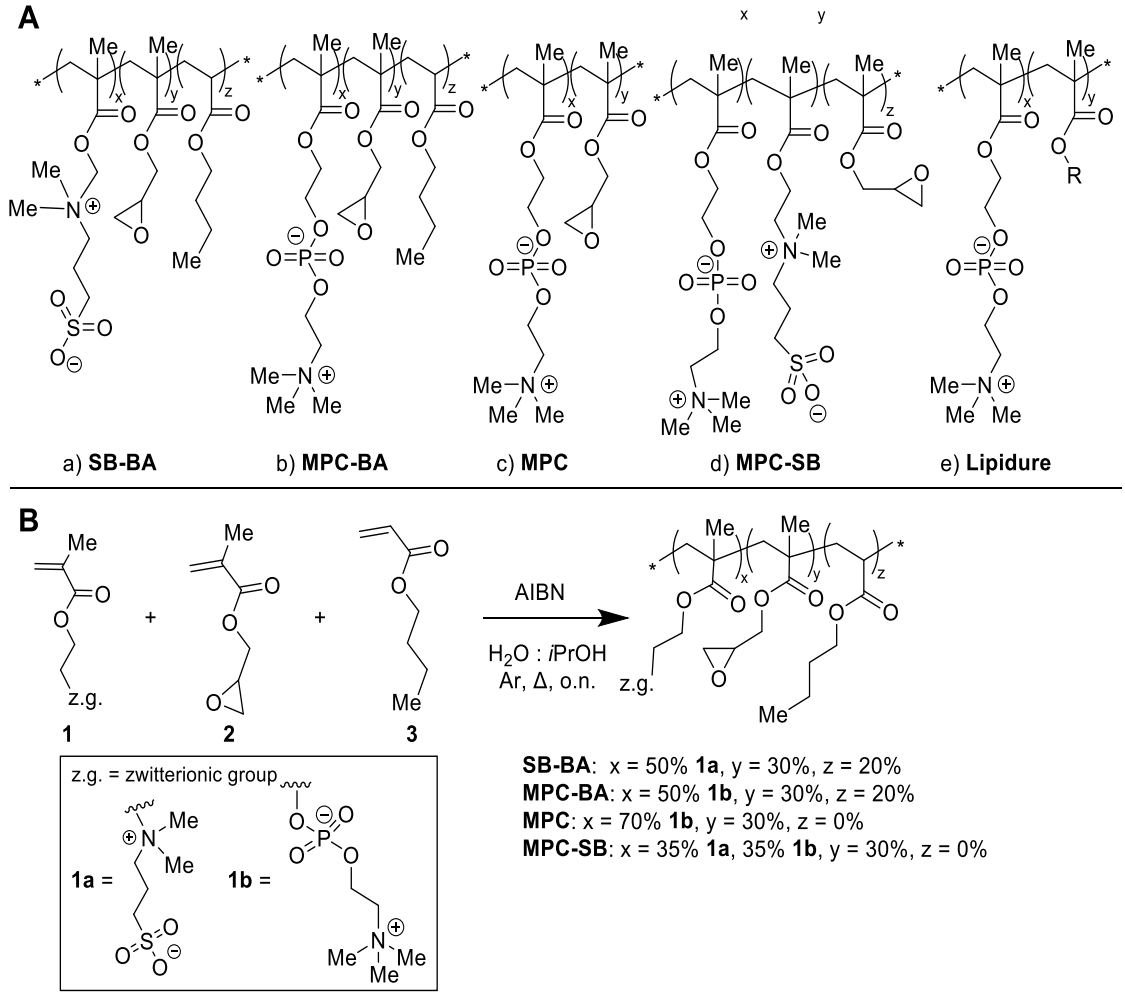

Figure 4.1: A) Structures of the synthesised ZPs and of the commercial Lipidure ZP. a) **SB-BA:** poly(sulfobetaine methacrylate-*co*- glycidyl methacrylate-*co*-butyl acrylate); b) **MPC-BA:** poly(2-methacryloyloxyethyl phosphorylcholine-*co*-glycidyl methacrylate-*co*-butyl acrylate); c) **MPC**: poly(2-methacryloyloxyethyl phosphorylcholine-*co*-glycidyl methacrylate); d) **MPC-SB**: poly(sulfobetaine methacrylate-*co*-2-methacryloyloxyethyl phosphorylcholine-*co*-glycidyl methacrylate); e) **Lipidure**. **B**) Monomers used for the synthesis of ZP series and the general synthesis scheme for ZPs combining zwitterionic groups (**1**, with the z.g. structure defined in the box as **1a** or **1b**), crosslinker group structure **2** and/or a hydrophobic group structure **3**.

Several criteria were factored into the selection of monomers in the design of ZPs for coating glucose biosensors to be deployed as CGMS. First, two different zwitterionic groups, SB and MPC, were selected, to compare their performance as an anti-fouling shield. The SB monomer (Figure 4.1B, structure **1a**) and MPC monomer (Figure 4.1B structure **1b**) were chosen due to their commercial availability and the good anti-fouling performance of coatings based on these monomers [14,16,20,28,43,44]. The

mole ratio of zwitterionic monomers was kept high at 50% or 70% since a clear correlation between the loading of zwitterionic moiety in polymers and anti-fouling properties has been reported [14]. For example, Ueda et al. have investigated P(MPC-BMA) polymers with various monomer ratios where polymers with higher MPC loading show reduced protein adsorption [45]. Similar trends have been obtained with other zwitterionic groups. A combination of both SB and MPC in the same polymer backbone was also investigated (Fig. 4.1B, structure d MPC-SB).

Secondly, the hydrophobicity of the polymer was varied by either including or excluding a hydrophobic BA monomer (Figure 4.1B, structure **3**) into the polymer backbone. The inclusion of hydrophobic interactions is one strategy used to ensure the stability of coatings [1,46]. The polymer should contain sufficient loading of hydrophobic groups to permit processing. For example, Watanabe et al. developed poly(MPC-*co*-butyl methacrylate) with an MPC : butyl methacrylate (BMA) mole ratio 30:70 that was optimised to be soluble in ethanol [20]. The commercially available MPC-based polymer Lipidure was developed from poly(MPC-BMA). However, coating biosensors with alcohol solutions can affect enzyme activity, change the properties of the film [43] and require time for the film to reorient on hydration and achieve equilibrium [30]. Our polymer design strategy, therefore, sought to obtain water-soluble polymers by synthesis of MPC-BA and SB-BA polymers containing 30% mole ratio of BA (Fig. 4.1B, structure **3**): a lower loading of the hydrophobic groups than that used by Watanabe et. al. [20].

The introduction of high loading of hydrophobicity to improve film stability decreases the water solubility of the polymer and the loading of zwitterionic groups. As an alternate approach to improve coating stability zwitterionic coatings can be covalently attached to surfaces, achieved through two main pathways. With “grafting to” methods, the polymer is attached to a surface after preparation, whereas with “grafting from” methods, the polymer is directly synthesised on a modified surface [18]. While it has been reported that “grafting from” methods can provide better anti-fouling protection [47], “grafting to” methods benefit from easier preparation and can be used for large-scale applications [1]. Therefore, “grafting to” was our chosen approach, achieved by introducing a crosslinking group through 30% loading of glycidyl methacrylate monomer (Fig. 4.1B, structure **2**) to covalently attach the anti-fouling

coating to the sensor. The glycidyl methacrylate was selected because the epoxy group can react with a range of nucleophiles. As our end goal was to apply the anti-fouling polymers as a shield over a mediated glucose biosensor enzyme electrode (Scheme 4.1A), an epoxide functionality is an appropriate choice. The sensing layer contains a redox polymer with an imidazole backbone and an enzyme with amino-functional groups, both of which react with the epoxide functionality at ambient temperature resulting in ring-opening of the epoxide and covalent bond formation [48]. The covalent bond formation between the layers can result in a less rigid boundary between the two layers (Scheme 4.1B). This may minimise the diffusional barrier that leads to loss of current response and sensitivity often seen with polymer coatings, such as Nafion, on amperometric biosensors (Scheme 4.1C).

In addition to the commercially available Lipidure and newly synthesised ZPs, Nafion was selected for testing since it is widely used as a coating for amperometric glucose biosensors. Nafion consists of hydrophilic sulfonic acid groups dispersed in a hydrophobic matrix of tetrafluoroethylene and perfluoroalkyl ethers [49]. Nafion is a chemically inert negatively charged polymer that is soluble in an ethanol/water mixture, but not in water. Nafion is often used as an anti-interference layer to prevent access to the electrode surface of negatively charged species like ascorbic acid or uric acid [33]. It has also been shown that Nafion can increase the stability of a biosensor and increase the linear range of analyte detection [50]. Finally, poly(ethylene glycol) (PEG) was also included for testing in our study as it is recognised as the ‘gold standard’ coating for biocompatibility.

4.4.2 Resistance to protein adsorption and cell adhesion

Anti-fouling has been a critical property to prevent biomaterials from failure in complex biological environments. In order to study the anti-fouling properties of the range of ZPs involved in this study, a two-part screening was performed. First, a conventional enzyme-linked immunosorbent assay (ELISA) was used to check resistance to non-specific protein adsorption of fibrinogen, a plasma protein involved in platelet aggregation, blot clot formation, and fibrotic formation [51]. This is important because protein adsorption is considered a key step to initiating the FBR [2]. Subsequently, a study was conducted using WPMY-1 myofibroblast to determine

resistance to cell adhesion [41]. Myofibroblasts were used due to their significant role in fibrotic capsule formation, through the excessive deposition of new extracellular matrix [52].

The polymer coatings tested, include the synthesised ZPs (MPC, MPC-SB, SB-BA and MPC-BA), the commercial ZP (Lipidure), PEG and Nafion. Conventionally, electrochemical glucose biosensors are coated with anionic or negatively charged polymers such as Nafion to minimise effects on sensor signal of electrochemical interferents such as ascorbic acid or uric acid [33,34]. There have not, however, been many investigations into the ability of Nafion to prevent fouling by proteins or cells. The PEG coating has been included, as surface coatings based on its derivatives have been widely used in biomedical applications [24]. Lipidure, a commercial ZP polymer, was used as a control to determine how the synthesised ZPs performed in comparison to this FDA-approved ZP. Compared to the uncoated control, all synthesised ZPs show approximately 50% reduced fibrinogen adsorption (Figure 4.2), displaying comparable behaviour to the commercial Lipidure polymer. ZPs are known to resist biofouling through the formation of a strong hydration sphere [27]. The entropy required to break this hydration sphere is quite high, and thus proteins are hindered in their ability to adsorb onto the surface. The different structural modifications made to the ZPs do not alter their ability to resist fibrinogen protein adsorption as the small differences in relative fibrinogen adsorption are not statistically significant. However, Nafion shows an increase in fibrinogen adsorption producing 1.8 times higher adsorption compared to the uncoated control. The fibrinogen adsorption to Nafion is 3.5 times higher than the adsorption at the ZP coatings. Nafion is incapable of forming a hydration sphere of the same strength as a ZP [15,53]. Additionally, it has a strong negative charge which can induce an electrostatic attraction on the positive domains of fibrinogen leading to increased protein adsorption. PEG shows intermediate behaviour with a 20% decrease in fibrinogen adsorption compared to the uncoated control. This is likely due to the weaker hydration sphere formed when compared to its ZP counterparts.

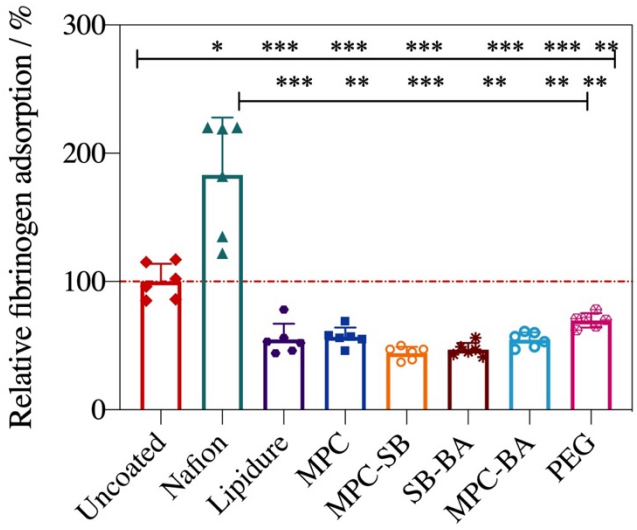

Figure 4.2: Relative fibrinogen adsorption onto wells coated with Nafion, Lipidure, MPC, MPC-SB, SB-BA, MPC-BA and PEG measured by ELISA. All values were normalised to the uncoated control. Mean ± SD (n= 6); *p<0.03, **p< 0.002, ***p<0.0002

The results of the fibrinogen adsorption study indicate that all the synthesised ZPs have the potential for application in anti-fouling at interfaces. Moreover, as a group they have comparable behaviour to the FDA-approved Lipidure despite differences in structure and loading of the zwitterionic moiety. Thus, an *in vitro* cell adhesion study was conducted to see if anti-fouling behaviour to protein adsorption persisted in prevention of adhesion of biological cells implicated in FBR. To test for this WPMY-1 myofibroblast cells were utilised and were seeded onto coated and uncoated glass coverslips. The number of adhered cells after 3-day incubation at 37ºC was counted, after staining, by means of imaging with a fluorescence microscope (Figure 4.3). A large number of myofibroblasts was observed forming a confluent layer on the uncoated control and on the Nafion-coated coverslip. This difference in the behaviour between cell adhesion and protein adsorption for Nafion versus the control, where fibrinogen adsorbs more on the Nafion surface than the control but cell adhesion is the same for both, might indicate that the charge on the Nafion polymer film does not significantly contribute to differences in cell adhesion. Moreover, the mixed hydrophobic and hydrophilic groups and the resulting poor hydration sphere [53] of Nafion may also contribute to the similarity in cell count to the control. A recent study by Higaki et al. demonstrated that, in terms of anti-fouling ability, polymers had the following trend: zwitterionic polyelectrolytes > hydrophobic polymers > charged

polyelectrolytes [12,13] indicating that it might be a combination of hydrophobicity and charge that yields the high cell count on the control and Nafion-coated surfaces.

Coverslips coated with Lipidure and MPC showed much better resistance to cell adhesion than coverslips coated with the other synthesised ZPs, with approximately 80% reduction in cell adhesion compared to the control. This may be due to the structural similarity between MPC and Lipidure, in comparison with the other synthesised ZPs. Despite the presence, within the MPC polymer, of a crosslinking group loaded at 30%, the anti-fouling behaviour of MPC remains similar to that of the commercial polymer. The ZPs synthesised to contain hydrophobic groups (MPC-BA and SB-BA) show higher cell adhesion than the MPC and Lipidure coatings. This is likely due to the hydrophobicity induced by the presence of the BA groups, leading to the formation of a weaker hydration sphere when compared to MPC. While the BA groups do not render the film fully hydrophobic, their inclusion does decrease film hydrophilicity when compared to MPC films, as evident from contact angles of 88.6° for MPC-BA films and 49.0° for MPC films (Appendix A.4, Figure S4.7, Table S4.1). The cell count for BA-containing coatings was not statistically significantly different to the uncoated control. Interestingly, there are domains in the images for both MPC-BA and SB-BA where there is no cell adhesion. This indicates that the polymer may orient itself in the film for the zwitterionic groups and hydrophobic groups to present separate domains, inducing some degree of phase separation. In the case of the mixed ZP MPC-SB, containing 35% of MPC and 35% of SB zwitterionic groups, the resistance to cell adhesion shows a ~40% reduction compared to the control, while the image also shows domains with no cell adhesion and domains with cell colonies. This may be attributed to the different cell adhesion behaviour of MPC and SB. For example, Liu et al. report that MPC surfaces show stronger anti-fouling characteristics than SB surfaces [54].

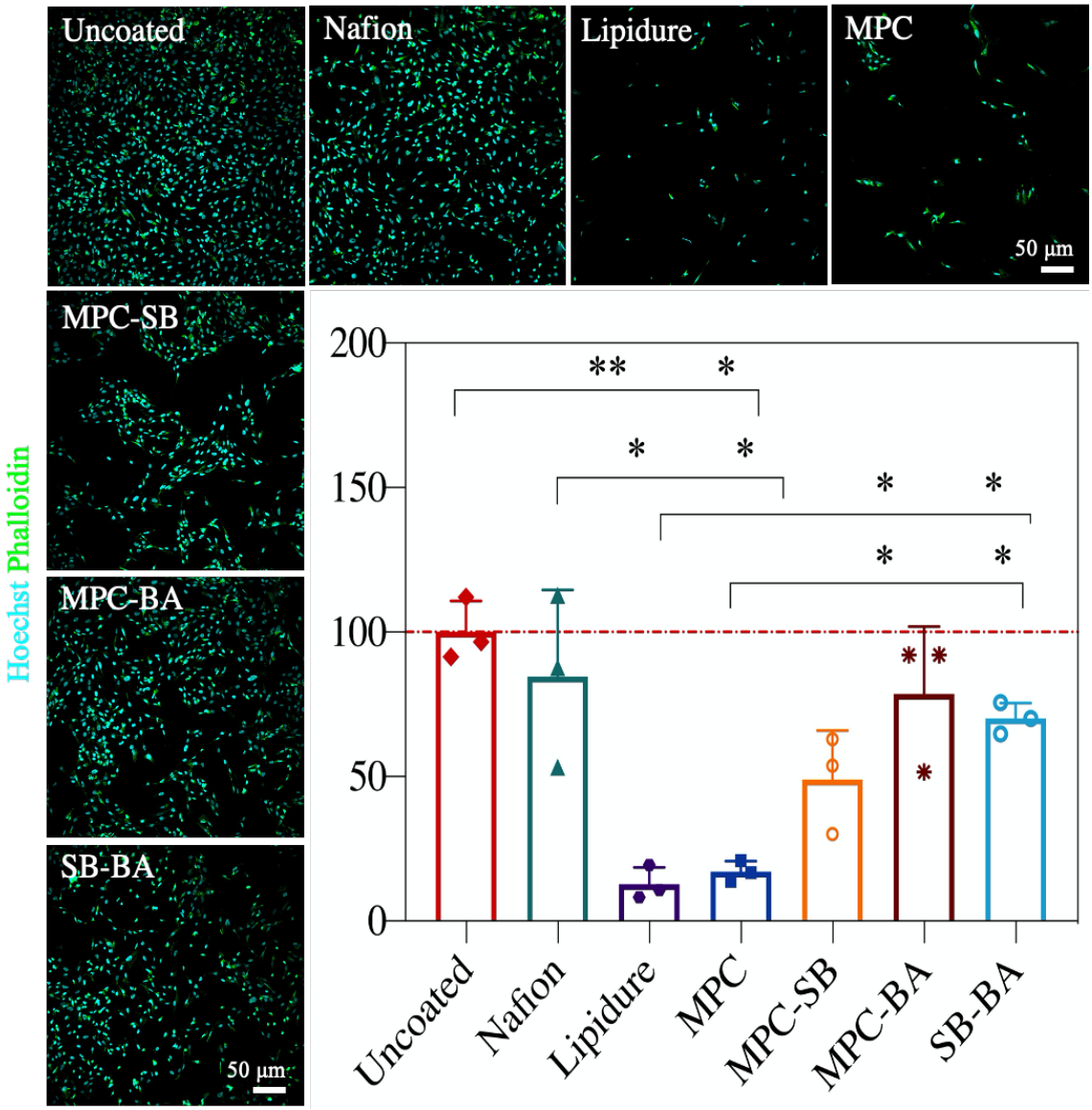

Figure 4.3: Cell adhesion study. (a) Fluorescence imaging of myofibroblast cells adhered to glass slides after incubation for 3 days. Phalloidin (green, cell body), Hoechst (nucleus). Scale bars: 50 µm. (b) Relative cell count, as percentage of uncoated control, for the polymer coated slides. Mean ± S.E.M. (n= 3); *p<0.03, **p< 0.002, ***p<0.0002

Overall, the biological screening demonstrates that structural modifications to ZPs affect the anti-fouling behaviour of surfaces coated with the ZPs. Attaching a zwitterionic functional group to the polymer backbone results in a decrease in non-specific protein adsorption, regardless of the other functional groups present in the copolymers. However, cell adhesion is not significantly different to the control when the ZPs are also loaded with 30% hydrophobic BA functional group. Therefore, while the addition of hydrophobic groups can contribute to improved film stability [20,44], it does not improve resistance to cell adhesion compared to the control. In these tests,

the mass of polymer used to make the coatings was low to minimise the effect on the signal response in glucose biosensors, our target application. For alternate applications increasing the mass of polymer coating could decrease the protein adsorption further for all ZPs, as we observed for coatings using Lipidure (Appendix A.4, Figure S4.5). The MPC coating shows identical behaviour to the commercial polymer for resisting both fibrinogen adsorption and myofibroblast cell adhesion. This ability indicates that the MPC ZP could have applications in anti-fouling coatings at interfaces and for minimisation of FBR at *in-vivo* medical devices. The added advantage, over the commercially available Lipidure, is that the ZPs were synthesised to contain an epoxide group that allows crosslinking and attachment to a surface, tethering the coatings onto the medical device surface for a range of applications.

4.4.3 Effect of polymer shield on mediated glucose biosensor

Protein adsorption can affect sensor response, often resulting in lower signal response and sensitivity [26,31,55,56], as has been observed for amperometric glucose biosensors using *in vitro* testing in complex media [26,44,56–58]. In order to overcome this, a protective layer (a shield) must be utilised to minimise non-specific protein adsorption. Implantation of sensors as CGMS requires more stringent protection to counter alteration to signals due to FBR. In this study, an MPC or Lipidure protective polymer shield represents the best option to minimise both protein adsorption and cell adhesion (indicative of the potential to invoke FBR). We, therefore, tested the use of MPC and Lipidure as polymer shields for a mediated glucose biosensor [42] to examine how each shield affects the electrochemical response. Nafion was included in this study as it is often used as a polymer shield for electrochemical glucose biosensors to minimise response from electrochemical interferents such as uric acid and ascorbic acid [57]. PEG was also included, as it is often used as a coating to improve medical device biocompatibility.

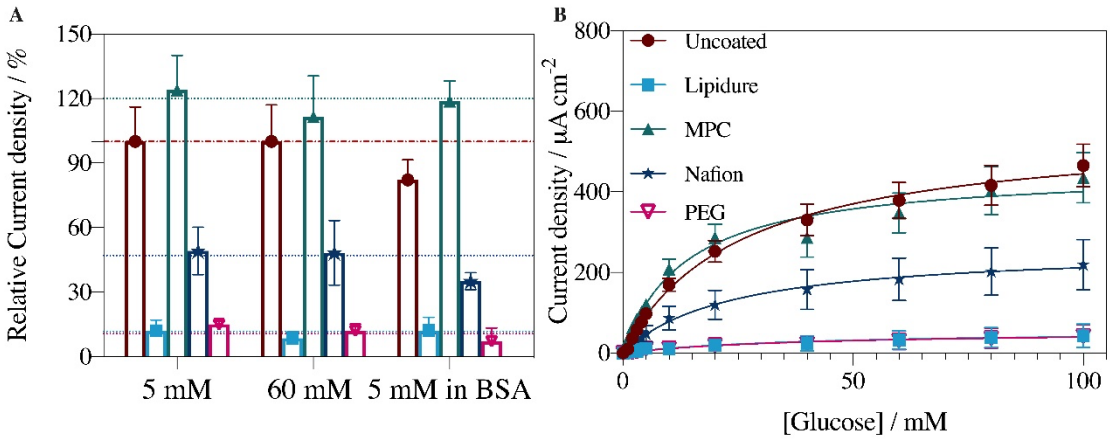

Figure 4.4: Glucose response of amperometric biosensors, tested at a constant applied potential of 0.35 V vs Ag/AgCl (3 M KCl) in phosphate buffered saline (0.05 M phosphate buffer, 150 mM NaCl) at 37 ºC presented as A) current density for coated electrodes relative to that of an uncoated electrode in 5 mM or 60 mM glucose solutions, and 5 mM glucose in PBS containing BSA (7 g L^{-1} and B) current density versus glucose concentration in phosphate buffered saline.

The amperometric current response to glucose (Figure 4.4) for sensors coated with a polymer shield of Lipidure, PEG or Nafion all show a significantly lower glucose oxidation current density compared to that of sensors coated with the MPC polymer shield or sensors that are not coated with a polymer shield. This lower current signal for a polymer shield coated system is usually attributed to hindering of glucose mass transport through the coating [26,44,55–57]. The sensor coated with the MPC polymer shield shows an almost identical response for glucose compared to the uncoated sensor. This may be due to the swelling of ZPs, thus permitting un-hindered mass transport to and away from the electrode surface. However, in that case, Lipidure should show similar electrochemical behaviour due to similarity in the polymer structure. The presence of an epoxide group in the MPC ZP results in the polymer shield chemically reacting with the sensing layer with crosslinks between the two layers leading to inter-layer mixing at the interface. This may result in the formation of a more uniform hydrogel when MPC is used as the shield (as depicted in Scheme 4.1B). The similar glucose oxidation current densities obtained with the MPC coated sensor and the uncoated sensor support the hypothesis that inter-layer mixing allows the formation of a hydrogel that behaves as a single layer with low diffusional barrier [59]. When Lipidure or Nafion is utilised the decreased glucose oxidation current density

response signifies that there is a higher diffusional barrier, possibly because of low inter-layer mixing (Scheme 4.1C) resulting in two distinct layers being formed [40,49,57,60]. To attempt to evaluate whether differences in diffusion play a role in the differences in the sensor response, a charge transport diffusion parameter, $D^{1/2}C$ (where D is the charge transport diffusion co-efficient within the sensor film and C is the concentration of redox complex in the sensor film volume), was extracted from the voltammetric response of the sensor in the absence of glucose substrate (Table 4.1 and Appendix A.4, Figure S4.6). The uncoated and MPC-coated sensors yield similar $D^{1/2}C$ values, higher than the values obtained for the Lipidure, Nafion or PEG-coated sensors tested. The MPC ZP as a polymer shield, where epoxide groups form crosslinks between the shield and the sensor layer, does not lead to an additional charge transport diffusional barrier over that obtained using the uncoated sensor layer, whereas an additional charge transport diffusional barrier is introduced for sensors coated with Lipidure, Nafion or PEG polymer shields. The mass of MPC coating can be doubled, from 50 to 100 μg, with negligible loss in signal (Appendix A.4, Figure S4.5) should a thicker film coating be required to achieve improved sensor stability or anti-fouling performance.

Table 4.1: Analytical parameters for glucose biosensor

Sensor	**K_M^{app} / mM**	**j_{max} / μA cm^{-2}**	**Sensitivity /μA cm^{-2} mM^{-1}**	**LOD / mM**	**J_{rel}/P_{rel}**	**$D^{1/2}C$ /10^{-11} mol cm^{-2} s$^{-1/2}$**
Uncoated	23.4	557.1	12.8 ± 1.1	1.9	1	2.6
Lipidure	38.1	55.9	2.4 ± 0.3	5.2	0.2	1.3
MPC	23.7	455.4	20.1 ± 1.2	2.7	2.5	2.7
Nafion	25.2	261.4	6.0 ± 0.6	4.1	0.3	1.9
PEG	40.9	55.8	2.2 ± 0.4	3.5	0.2	1.1

This is supported by comparison of the apparent Michaelis-Menten constant, K_M^{app}, the maximum current density, j_{max}, and the sensitivity parameters, presented in Table 4.1, extracted from the glucose response of each of the sensors (Figure 4.4). The MPC-coated sensor shows a similar K_M^{app} and j_{max} to that for the uncoated sensor, different to the parameters extracted for the Lipidure, Nafion and PEG-coated sensors. We again

attribute this to crosslinking and inter-layer mixing at the interface between the MPC and sensor layers resulting in a low diffusional barrier to mass and charge transport for the MPC-coated sensor compared to the other coated sensors. In addition, the MPC sensor sensitivity is several-fold higher than other coated sensors and is 1.5-fold higher than that of the uncoated sensor. For hydrogel-based amperometric biosensors, the ionic conductivity can influence the sensitivity of biosensors. ZPs are known for their high ionic conductivity, which may allow fast counter-ion movement [14,16]. The high measured charge transport parameter, $D^{1/2}C$, for the MPC coated sensors relative to the other coated sensors (Table 4.1) supports the hypothesis that MPC biosensors display higher charge transport.

To compare polymer shield coating performance the ratio of the relative current density for coated sensors to uncoated sensors in 5 mM glucose (J_{Rel} extracted from Figure 4.4A) to the relative fibrinogen protein adsorption response for coated sensors to uncoated sensors (P_{Rel}, extracted from Figure 4.2) was computed (Table 4.1 J_{rel}/P_{rel}). The J_{rel}/P_{rel} ratio for the uncoated control is, by definition, 1. The J_{rel}/P_{rel} ratio for the Lipidure, Nafion and PEG-coated sensors are 0.2, 0.3 and 0.2, all significantly lower than 1, indicating that there is a loss in sensor performance relative to the uncoated control due to either lower current density and/or increased protein adsorption. A J_{rel}/P_{rel} of 2.5 for the MPC-coated sensor signifies that the coating combines the advantage of high glucose sensor sensitivity, due to the low diffusional barrier, and low protein adsorption, compared to the other coated sensors and the uncoated control.

This is confirmed from the current density measured for all the sensors at 5 mM glucose in PBS containing bovine serum albumin (BSA, 7 g L^{-1}) relative to the response of the uncoated sensor in a solution of 5 mM glucose in PBS (Figure 4.4A). The uncoated sensor and the Nafion-coated sensor both show decreased response as a result of BSA protein adsorption. Although Lipidure and PEG do not show a substantial decrease in current density in the presence of BSA, ultimately there is an ~85% loss in signal compared to an uncoated sensor due to the higher diffusional barrier presented by the coating. The MPC-coated sensor is the only sensor that shows high glucose current response that is unaffected by BSA.

4.5 Conclusions

Four new ZPs, containing epoxide groups that are amenable to crosslinking, have been synthesised for use as polymer coatings on amperometric glucose biosensors. Films of all the synthesised ZPs can lower fibrinogen adsorption compared to an uncoated control and therefore show promise for use as anti-fouling coatings at interfaces. However, only the MPC coating performed as well as the commercial ZP, Lipidure, in hindering cell adhesion. The MPC ZP, therefore, has potential use in mitigating FBR of implanted medical devices. The MPC ZP was tested as a polymer coating on an amperometric glucose biosensor. The MPC coated sensor demonstrates 1.5-fold higher sensitivity than an uncoated sensor, while sensors coated with Lipidure, Nafion and PEG show lower sensitivity. The epoxide crosslinking group in the MPC ZP allowed the coating to be tethered to the sensing layer, leading to inter-layer mixing at the boundary between the two layers and resulting in a low diffusional barrier to mass and charge transport for the MPC-coated sensor compared to the other coated sensors. Thus, the MPC ZP not only shows anti-fouling and cell adhesion resistance responses comparable to the commercial Lipidure ZP but also has the advantage of higher glucose sensor sensitivity. An important benefit of the MPC ZP is the possibility to increase the polymer coating thickness to achieve improved sensor stability or anti-fouling performance while retaining sufficient sensor signal. Although the MPC ZP shows potential for application as a polymer coating on implanted biomedical devices, more comprehensive *in-vitro* tests using biological species involved in FBR are planned

4.6 Acknowledgements

This project has received funding from the European Union's Horizon 2020 research and innovation program under the Marie Skłodowska-Curie MSCA-ITN “ImplantSens” [813006]. Donation of the CDH by Thomas Reichhart and Roman Kittl (DirectSens GmbH, Klosterneuburg, Austria) and Roland Ludwig, Universität für Bodenkultur Wien (BOKU) Vienna, Austria is gratefully acknowledged. We would like to thank prof. Axel Rosenhahn and Jana Karthäuser from Ruhr University Bochum for the opportunity to perform contact angle measurements.

4.7 References

[1] S.H. Chen, Y. Chang, K. Ishihara, Langmuir 33 (2017) 611–621.

[2] D.W. Grainger, Nat. Biotechnol. 31 (2013) 507–509.

[3] Y.J. Heo, S. Takeuchi, Y.J. Heo, S. Takeuchi, Adv. Healthcare Mater. 2 (2013) 43–56.

[4] C. Chen, X.L. Zhao, Z.H. Li, Z.G. Zhu, S.H. Qian, A.J. Flewitt, Sensors 17 (2017) 182.

[5] J.M. Anderson, A. Rodriguez, D.T. Chang, Semin. Immunol. 20 (2008) 86–100.

[6] T. Bailey, B.W. Bode, M.P. Christiansen, L.J. Klaff, S. Alva, Diabetes Technol. Ther. 17 (2015) 787–794.

[7] G. Cappon, G. Acciaroli, M. Vettoretti, A. Facchinetti, G. Sparacino, Electronics (Switzerland) 6 (2017) 65.

[8] A. Barfidokht, J.J. Gooding, Electroanalysis 26 (2014) 1182–1196.

[9] J. Wang, Chem. rev. 108 (2008) 814–825.

[10] J.A. Callow, M.E. Callow, Nat. Commun. 2 (2011).

[11] S. Dobretsov, R.M. Abed, M. Teplitski, Biofouling 29 (2013) 423–441.

[12] Y. Higaki, J. Nishida, A. Takenaka, R. Yoshimatsu, M. Kobayashi, A. Takahara, Polym. J. (Tokyo, Jpn.) 47 (2015) 811–818.

[13] M. Li, B. Zhuang, J. Yu, Chem. - Asian J. 15 (2020) 2060–2075.

[14] S. Liu, J. Tang, F. Ji, W. Lin, S. Chen, Gels 8 (2022) 46.

[15] J.B. Schlenoff, Langmuir 30 (2014) 9625–9636.

[16] Y. Zhang, Y. Liu, B. Ren, D. Zhang, S. Xie, Y. Chang, J. Yang, J. Wu, L. Xu, J. Zheng, J. Phys. D: Appl. Phys. 52 (2019).

[17] O.F. Bertrand, R. Sipehia, R. Mongrain, J. Rodés, J.-C. Tardif, L. Bilodeau, G. Côté, M.G. Bourassa, J. Am. Coll. Cardiol. 32 (1998) 562–571.

[18] S. Chen, L. Li, C. Zhao, J. Zheng, Polymer 51 (2010) 5283–5293.

[19] Y. Su, C. Luo, Z. Zhang, H. Hermawan, D. Zhu, J. Huang, Y. Liang, G. Li, L. Ren, Journal of the Mechanical Behavior of Biomedical Materials 77 (2018) 90–105.

[20] J. Watanabe, K. Ishihara, Colloids Surf., B 65 (2008) 155–165.

[21] J. Xu, H. Lee, Chemosensors 8 (2020) 1–29.

[22] Z. Zhang, T. Chao, S. Chen, S. Jiang, Langmuir 22 (2006) 10072–10077.

[23] Q. Wei, T. Becherer, S. Angioletti-Uberti, J. Dzubiella, C. Wischke, A.T. Neffe, A. Lendlein, M. Ballauff, R. Haag, Angew. Chem., Int. Ed. 53 (2014) 8004–8031.

[24] J.D. Andrade, Springer, New York, NY, 1985.

[25] S. Lowe, N.M. O'Brien-Simpson, L.A. Connal, Polym. Chem. 6 (2014) 198–212.

[26] X. Xie, J.C. Doloff, V. Yesilyurt, A. Sadraei, J.J. McGarrigle, M. Omami, O. Veiseh, S. Farah, D. Isa, S. Ghani, I. Joshi, A. Vegas, J. Li, W. Wang, A. Bader, H.H. Tam, J. Tao, H.J. Chen, B. Yang, K.A. Williamson, J. Oberholzer, R. Langer, D.G. Anderson, Nat. Biomed. Eng. 2 (2018) 894–906.

[27] T. Goda, K. Ishihara, Y. Miyahara, CJ. Appl. Polym. Sci. 132 (2015) 41766.

[28] J. Ning, G. Li, K. Haraguchi, Macromolecules 46 (2013) 5317–5328.

[29] Z. Zhang, H. Vaisocherová, G. Cheng, W. Yang, H. Xue, S. Jiang, Biomacromolecules 9 (2008) 2686–2692.

[30] Y. Iwasaki, K. Ishihara, Sci. Technol. Adv. Mater. 13 (2012) 64101.

[31] M.J. Russo, M. Han, P.E. Desroches, C.S. Manasa, J. Dennaoui, A.F. Quigley, R.M. Kapsa, S.E. Moulton, R.M. Guijt, G.W. Greene, S.M. Silva, ACS Sensors 6 (2021) 1482–1507.

[32] G. McGarraugh, Diabetes Technol. Ther. 11 (2009) S-17-S-24.

[33] C.P. Andrieux, P. Audebert, B. Divisia-Blohorn, S. Linquette-Maillet, J. Electroanal. Chem. 353 (1993) 289–296.

[34] C.P. Andrieux, P. Audebert, B. Divisia-Blohorn, S. Linquette-Maillet, P. Bacchi, J. Electroanal. Chem. 394 (1995) 141–148.

[35] T.J. Ohara, R. Rajagopalan, A. Heller, Anal. Chem. 66 (1994) 2451–2457.

[36] C.A. Quinn, R.E. Connor, A. Heller, Biomaterials 18 (1997) 1665–1670.

[37] N. Mano, E.Y. Joung, J. Tarver, Y.L. Loo, A. Heller, J. Am. Chem. Soc. 129 (2007) 7006–7007.

[38] B. Yu, C. Wang, Y.M. Ju, L. West, J. Harmon, Y. Moussy, F. Moussy, Biosens. Bioelectron. 23 (2008) 1278–1284.

[39] G. Cencetti, F. Battiston, New J. Phys. 21 (2019) 35006.

[40] R.I. Hickson, S.I. Barry, G.N. Mercer, H.S. Sidhu, Math. Comput. Model. 54 (2011) 210–220.

[41] E.B. Dolan, C.E. Varela, K. Mendez, W. Whyte, R.E. Levey, S.T. Robinson, E. Maye, J. O'Dwyer, R. Beatty, A. Rothman, Y. Fan, J. Hochstein, S.E. Rothenbucher, R. Wylie, J.R. Starr, M. Monaghan, P. Dockery, G.P. Duffy, E.T. Roche, Science Robotics 4 (2019).

[42] K. Jayakumar, T.M. Reichhart, C. Schulz, R. Ludwig, A.K. Felice, D. Leech, ChemElectroChem.

[43] A.L. Lewis, P.D. Hughes, L.C. Kirkwood, S.W. Leppard, R.P. Redman, L.A. Tolhurst, P.W. Stratford, Biomaterials 21 (2000) 1847–1859.

[44] H. Wu, C.J. Lee, H. Wang, Y. Hu, M. Young, Y. Han, F.J. Xu, H. Cong, G. Cheng, Chem. Sci. 9 (2018) 2540–2546.

[45] T. Ueda, H. Oshida, K. Kurita, K. Ishihara, N. Nakabayashi, Polym. J. (Tokyo, Jpn.) 24 (1992) 1259–1269.

[46] K. Ishihara, J. Biomed. Mater. Res., Part A 107 (2019) 933–943.

[47] J.J. Wu, J. Zhou, J.Q. Rong, Y. Lu, H. Dong, H.Y. Yu, J.S. Gu, Chin. J. Polym. Sci. 36 (2018) 528–535.

[48] A. Heller, B. Feldman, Chem. rev. 108 (2008) 2482–2505.

[49] K. Ito, M. Harada, N.L. Yamada, K. Kudo, H. Aoki, T. Kanaya, Langmuir 36 (2020) 12830–12837.

[50] X. Xiao, X. Yan, E. Magner, J. Ulstrup, Electrochem. Commun. 124 (2021) 106931.

[51] Q. Liu, A. Singh, R. Lalani, L. Liu, Biomacromolecules 13 (2012) 1086–1092.

[52] N. Noskovicova, B. Hinz, P. Pakshir, Cells 10 (2021) 1794.

[53] R. Hammer, M. Schönhoff, M.R. Hansen, J. Phys. Chem. B 123 (2019) 8313–8324.

[54] Y. Liu, D. Zhang, B. Ren, X. Gong, L. Xu, Z.Q. Feng, Y. Chang, Y. He, J. Zheng, J. Mater. Chem. B 8 (2020) 3814–3828.

[55] Y. Hu, B. Liang, L. Fang, G. Ma, G. Yang, Q. Zhu, S. Chen, X. Ye, Langmuir 32 (2016) 11763–11770.

[56] W. Yang, H. Xue, L.R. Carr, J. Wang, S. Jiang, Biosens. Bioelectron. 26 (2011) 2454–2459.

[57] R. Bennett, D. Leech, Bioelectrochemistry 133 (2020) 107460.

[58] R.D. Milton, K. Lim, D.P. Hickey, S.D. Minteer, Bioelectrochemistry 106 (2015) 56–63.

[59] S.E. Solovyov, A.Y. Goldman, E-Polymers.

[60] K.E. Toghill, R.G. Compton, International Journal of Electrochemical Science 5 (2010) 1246–1301.

Chapter 5: Cross-linkable polymer-based multi-layers for protecting electrochemical glucose biosensors against uric acid, ascorbic acid and biofouling interferences

Published as:

Cross-linkable polymer-based multi-layers for protecting electrochemical glucose biosensors against uric acid, ascorbic acid and biofouling interferences

Anna Lielpetere[†], Kavita Jayakumar[†], Dónal Leech and Wolfgang Schuhmann, ACS Sensors, 2023

[†]These authors contributed equally to the research

Co-author contributions:

I synthesised the PVI-bound osmium redox polymer, performed all labwork, analysis and wrote the first draft of the publication.

Anna Lielpetere synthesised the zwitterionic polymer and anionic polymer and co-wrote the first draft of the publication.

Wolfgang Schuhmann, as project supervisor of Anna Lielpetere, contributed through advice and guidance throughout the work and edited the first draft of the publication.

Dónal Leech, as my project supervisor, contributed through advice and guidance throughout the work and edited the first draft to provide the final version for publication.

5.1 Abstract

The lifetime of implantable electrochemical glucose monitoring devices is limited due to the foreign body response and detrimental effect of low molecular weight interferents which are components of the physiological media. Polymer coatings can be used to shield from these interferences and prolong the functional lifetime of biosensors. This work explored several approaches to protect redox polymer-based glucose biosensors against biological and low molecular weight interferences by designing six targeted multi-layer sensor architectures. Biological interferents, like cells and proteins, and low molecular weight interferents, like ascorbic acid and uric acid, were found to have individual effects on current density and operational stability of glucose biosensors requiring individual protection. In a previous study, protection against biofouling has been realised by using poly(2-methacryloyloxyethyl phosphorylcholine-*co*-glycidyl methacrylate) (MPC) zwitterionic polymer coating. This study focused on expanding this protection to low molecular weight interferents as well. For protecting against low molecular weight interferences, an enzymatic approach was compared to electrostatic repulsion by negatively charged polymers. A system consisting of polyvinylimidazole-polysulfostyrene copolymer and MPC zwitterionic polymer, together called polymer design (PD), showed the highest resistance against both low molecular weight and biological interferences. Sensor protected with PD shield shows low MARD values for interferences and low variability in sensor readings in complex media. For sensor measurements in artificial plasma, PD extends the linear range (R^2 =0.99) of the sensor from 0–10 mM for the control to 0–20 mM, shows a smaller decrease in sensitivity and retains high current densities. The application of PD multi-target coating improves both sensor performance and operational stability in complex media and shows promise for the use in sensors operating in real conditions.

5.2 Introduction

Due to the prevalence of diabetes in society, there has been an increasing need for devices that monitor glucose levels in blood[1]. Research efforts and advances in technology over the past decade have seen the progression of these monitoring devices

from fledgling fingerprick devices, relying on test strips inserted into a detector[2-3], to sub-cutaneous or fully implantable continuous glucose monitors (CGMs)[4-5]. Of the commercially available CGMS, those based on electrochemical biosensing dominate the market due to their specificity, fast response time, sensitivity, and low detection limit[6-7]. While they provide an alternative to daily fingerprick tests, CGMs present a few challenges mostly originating from the hostile environment on implantation and the complexity of physiological fluids. Foreign body response (FBR) is the host's immune reaction to an implanted device that results in inflammation and, ultimately, encapsulation of the device by a fibrotic capsule which negatively affects the accuracy, sensitivity, and lifetime of *in vivo* glucose biosensors[8]. Electrochemical biosensors, in particular, suffer losses in sensitivity, accuracy and sensor drift as sensor operation relies upon the diffusion of analyte to-and-from sensor surface – a process affected by the progressive growth of the fibrotic capsule over time[9]. The lifetime of currently available electrochemical CGMs does not exceed 14 days after implantation[10]. Hindered diffusion of the product due to the fibrotic capsule can lead to accumulation of gluconic acid, resulting in a drop in the local pH influencing the enzyme's stability and thereby sensor lifetime. Additionally, the biological cells consume glucose, leading to a local decrease in glucose concentration affecting sensor response. Moreover, inflammation leads to the degradation of the implant components and further reduces its lifetime[11].

New materials are being developed to reduce the effects of foreign body response and prolong the functional lifetime of biosensors[8,10,12]. A promising class of materials are zwitterionic polymers that reduce non-specific protein adsorption by impairing electrostatic interactions and forming a hydration layer[13]. We recently reported that a 2-methacryloyloxyethyl phosphorylcholine-based zwitterionic polymer (MPC) coating, containing crosslinking epoxy functional groups, decreases fibrinogen adsorption and fibroblast adhesion in *in vitro* tests, while improving the performance and operational stability of glucose biosensors when used as a protective coating[14].

Endogenous and exogenous small molecule interferences can also affect the sensor signal[6,15]. Low molecular weight (LMW) species like ascorbic acid (AA) and uric acid (UA) can be directly oxidised at the electrode and/or inhibit the enzyme affecting its bioelectrocatalytic activity[16]. Uric acid has also been reported to act as an

uncompetitive inhibitor to commonly used glucose-converting enzymes such as glucose oxidase (GOx), *FAD*-dependent glucose dehydrogenase (FAD-GDH) and cellobiose dehydrogenase (CDH)[17]. Several strategies have been developed for improving the sensitivity and performance of glucose biosensors, including coating with permselective membranes that discriminate against LMW species either by size or charge, or layers to remove oxidisable species as well as coatings that release anti-inflammatory agents to attempt to prevent FBR[15]. The majority of these approaches rely on integration of a polymeric shield into sensor architecture. Protective membranes have been used on glucose biosensors since the first commercial glucose biosensor employed an inner cellulose acetate and an outer polycarbonate membrane[3]. Anionic membranes such as Nafion or poly(ester-sulfonic acid)[18-19], that repel the negatively charged AA and UA interferents, are often used. Multi-layer membranes consisting of Nafion and cellulose acetate or polyurethane can protect against a wider range of interferents[18,20]. These membranes are mainly useful to protect first-generation glucose biosensors, that detect hydrogen peroxide, due to low permeability of the multi-layers to larger molecules such as the glucose target analyte. Thus, application of coatings is detrimental to amperometric biosensor response as they lead to formation of a diffusional barrier[21]–[23]. A major challenge that remains is to improve the selectivity of amperometric glucose biosensors while maintaining high sensitivity and response time[24].

Integration of enzyme layers to remove oxidisable species in the sensing strategy has been used in biosensing applications. Introduction of a combination of glucose oxidase and catalase has been successful to remove glucose as an interferent in electrochemical enzymatic biosensors detecting another analyte, such as sucrose or lactose[25-26]. Horseradish peroxidase (HRP) can oxidize ascorbate, urate and acetaminophen interference in the presence of hydrogen peroxide[27-28]. In addition, HRP in combination with lactate oxidase (LOx) has been used in the commercial FreeStyle Navigator sensor to generate peroxide *in situ* for oxidation of these interferents, though the drawback of this method is the reliance on dissolved oxygen as the LOx co-substrate[3]. Ascorbate oxidase (AsOx) can also selectively remove ascorbate, in the presence of oxygen co-substrate, and has been employed for sample treatment[29–31]. AA interference has also been minimised by incorporation of bovine serum albumin (BSA) or phospholipids in poly(*o*-phenylenediamine)-containing GOx glucose

biosensor on platinum used for *in vivo* brain monitoring. The AA interferent was blocked by the non-enzyme proteins because they increased the density of the films without increasing the demand for oxygen that would be the case if the loading of GOx was increased[32]. Enzyme integration for use as a scavenging system has one limitation-there is a possibility of wiring AsOx to the electrode either via mediator or DET. AsOx layers must therefore be separate from the mediated sensing layer, usually achieved by application of a redox-silent polymer between the layers. This again leads to formation of a diffusional barrier. Moreover, the efficiency and duration of the interferent-removal layer is limited by enzyme activity and lifetime.

It is important to note that each of the protective measures detailed above is not multi-purpose, i.e., a protective coating may target minimising either biological interference or endogenous LMW interference but not both. Protection can be either a single layer system with a multi-purpose effect – minimising biological and LMW interference – or a multi-layer sensor architecture wherein each consecutive layer has its own role in minimising a specific interferent. Regardless of which of these architectures is successful, it should minimise the loss in sensor signal due to the application of the coating. In this work, we explore and report on approaches to protect redox polymer-based glucose biosensors against biological and LMW interferences by designing targeted multi-layer sensor architectures. Protection against biofouling is realised by using a previously designed zwitterionic polymer incorporating crosslinking sites. Two different strategies, an enzymatic approach and a polymer layer approach, are examined for the removal of interferences from LMW – AA and UA.

5.3 Materials and methods

5.3.1 Chemicals

All chemicals were purchased from Sigma-Aldrich, Alfa Aesar, Acros Organics, TCI, or Roth and used as received unless otherwise noted. Glycidyl methacrylate and butyl acrylate were passed through a column containing the corresponding inhibitor remover (Sigma-Aldrich) and stored at –20°C. 1-Vinylimidazole and 4-styrene sulfonic acid sodium salt hydrate were used as received. The polymerisation initiator azobisisobutyronitrile (AIBN) was recrystallised from hot toluene and stored at –20°C.

All aqueous solutions were prepared using water purified and deionised with a Milli-Q system. The redox polymer [poly(1-vinylimidazole)Os(bpy)$_2$Cl]$^+$ (Os(bpy)PVI), structure depicted in Scheme 1A where x = 1 and y = 9, was synthesised by modification of published procedures[33],[34]. A cellobiose dehydrogenase (CDH) from *Crassicarpon hotsonii (*syn. *Myriococcum thermophilum*) modified with glucose activity-enhancing mutations C291Y and W295R, provided by DirectSens GmbH[35], was used as the glucose oxidising enzyme in this study. Uricase from *Bacillus fastidiosus* (specific activity ~9 U/mg) and ascorbate oxidase from *Cucurbita* species (specific activity ≥1500 U/mg) were purchased from Sigma Aldrich.

5.3.2 Synthesis

All reactions and manipulations were conducted using the standard Schlenk technique under argon atmosphere. The co-polymer structure and nomenclature is presented in Figure S5.1 (Appendix A.5). Polymers were characterised by NMR, with results provided in Figure S5.2-5.4 (Appendix A.5). Synthesis of the P(SS^5-GMA^3-BA^2) was described previously[26].

5.3.2.1 Poly(1-vinylimidazole-co-4-styrene sulfonic acid sodium salt hydrate) P(VI12-SSNa1)

The synthesis procedure has been published previously[36]. Briefly, 1-vinylimidazole (3.31 mL, 37 mmol) and 4-styrene sulfonic acid sodium salt hydrate (0.62 g, 3 mmol) were dissolved in DMSO:H_2O 1:1 (4 mL) in a round bottom-flask equipped with a condenser, deaerated by argon bubbling and then AIBN (0.25 g, 1.5 mmol) was added. The reaction mixture was heated to 70 °C. After 30 min, a yellow gel was obtained, and heating stopped. After cooling to room temperature, the crude product was dissolved in 20 mL of EtOH and 3 mL H_2O. The solution was poured into stirred acetone (80 mL) and the white precipitate was separated by centrifugation and dried under reduced pressure for 24 h. Off-white solid (3.11 g). ^{1}H-NMR (200.13 MHz, D_2O) δ/ppm: 6.71-7.69 (overlapping signals, broad, imidazole, benzene), 3.88 (s, broad, CH-N), 3.23 (s, broad, CH), 2.12 (s, broad, CH_2, CH_3).

5.3.2.2 Poly(1-vinylimidazole-co-4-styrene sulfonic acid sodium salt hydrate) P(VI[1]-SSNa[1])

1-vinylimidazole (453 µL, 5 mmol) and 4-styrene sulfonic acid sodium salt hydrate (1.03 g, 5 mmol) were dissolved in DMSO:H_2O 1:1 (10 mL) in a round-bottom flask equipped with a condenser, deaerated by argon bubbling and then AIBN (0.25 g, 1.5 mmol) was added. The reaction mixture was heated to 70 °C for 1 h. After cooling down, the product was precipitated by pouring into stirred acetone (~150 mL), separated by centrifugation, washed with acetone and freeze-dried under high vacuum. White solid (1.24 g). ^{1}H-NMR (300 MHz, D_2O) δ/ppm: 7.89 – 7.21 (m, 2H), 7.05 – 6.21 (m, 2H), 2.15 – 0.98 (m, 3H).

5.3.3 Electrode modification

Graphite rods (Graphite store, USA, 4.0 mm diameter, NC001300) were cut, insulated with heat shrink tubing and polished at one end using fine grit paper, to give graphite working electrodes with a geometric surface area of 0.126 cm^2. The biosensors were assembled by drop-coating 30 µL of Os(bpy)PVI aqueous solution (5 mg mL^{-1}), 16 µL of CDH aqueous solution (10 mg mL^{-1}) and 7.4 µL of poly(ethylene glycol) diglycidyl ether (PEGDGE) crosslinker aqueous solution (15 mg mL^{-1}). The biosensor component amounts are based on amounts optimised using a design of experiments approach[35] to produce the highest glucose oxidation current density in 5 mM glucose solution. The deposition was allowed to dry for 3 h before a 10 µL aliquot of 0.5 wt./v% of the selected polymer coating was applied to the electrodes. The electrodes were allowed to cure overnight at ambient temperature before being used. For multi-layer systems, an additional coating of 10 µL aliquot of 0.5 wt./v% of the selected polymer was applied 1 h after addition of the first polymer coating. For the enzyme layer, uricase (15 µg, 9 U/mg) and ascorbate oxidase (15µg, ≥1500 U/mg) were mixed with 8 µL of MPC aliquot. First, 2 µL of MPC was added as a coating and allowed to dry before addition of enzyme/MPC mixture.

5.3.4 Electrochemical measurements

Electrochemical tests were conducted using a CH Instruments 1030a multichannel potentiostat (IJ Cambria). The enzyme electrodes were used as working electrodes,

with a custom-built Ag|AgCl (3 M KCl) as a reference electrode and a platinum mesh (Goodfellow) as a counter electrode. Electrodes were placed in a thermostated electrochemical cell containing phosphate buffered saline (PBS), artificial plasma, bovine serum albumin (BSA, 7 g L^{-1}) in PBS or uric acid (UA, 68.5 mg L^{-1}) in PBS at 37 °C with experiments conducted, unless otherwise stated, in the presence of ambient oxygen. Current signals are normalised to the geometric surface area of the graphite disk electrodes to generate current density data.

Artificial plasma was prepared based on an aqueous solution recipe of uric acid (68.5 mg L^{-1}), ascorbic acid (9.5 mg L^{-1}), fructose (36 mg L^{-1}), lactose (5.5 mg L^{-1}), urea (267 mg L^{-1}), cysteine (18 mg L^{-1}), sodium chloride (6.75 g L^{-1}), sodium bicarbonate (2.138 g L^{-1}), calcium sulfate (23.8 mg L^{-1}), magnesium sulfate (104.5 mg L^{-1}) and bovine serum albumin (7 g L^{-1})[37].

Interference screening data was analysed by calculating the mean absolute relative difference (MARD) between the mean baseline glucose concentration reading without interferent (M_0) and the mean glucose reading value with interferent present (M_I) as:

$$\text{MARD (M)} = \frac{|M_I - M_0|}{M_0} \times 100 \qquad (1)$$

In this study, interference was defined as an absolute MARD ≥ 20%[38]. Testing levels for UA, BSA and AA was set at their concentrations in artificial plasma. The effect of UA and AA on the biosensor signal was tested using amperometry at 0.35 V in 5 mM glucose with injections of UA or AA into the electrochemical cell. The effect of BSA on the biosensor signal was tested using amperometry in 5 mM glucose prior to, and then 10 min after adding BSA into the electrochemical cell.

5.4 Results and discussion

We previously reported that a zwitterionic 2-methacryloyloxyethyl phosphorylcholine (MPC) based co-polymer, containing crosslinkable epoxy functional groups in the co-polymer, is the most effective coating over a glucose biosensor to prevent fibrinogen adsorption and biological cell adsorption while maintaining good sensor performance and improved sensitivity in buffer solution and in the presence of BSA[14]. Here, we explore the design of complex sensor architectures to control not only the adsorption

of biological molecules, but also to limit LMW UA and AA interference to the sensor signal while preserving efficient substrate and product mass transport to maintain high sensor signal.

5.4.1 Design of protective systems

Three characteristics were considered in the design of glucose sensors with resistance to interferents present in physiological media: (i) resistance to biofouling; (ii) resistance to LMW interference from AA and UA; and (iii) efficient mass transport of substrate and product through the layers as presented in Scheme 5.1 and Table 5.1.

A glucose biosensor consisting of an enzyme embedded in a crosslinked redox polymer hydrogel (Case I) is susceptible to non-specific protein adsorption and cell adhesion when operating in physiological fluids. This occurs within minutes to hours, and the adsorbed and adhered biological film creates a diffusional barrier to glucose, leading to sensor signal drift consistent with the changes in glucose diffusivity[39]. Additionally, LMW species such as AA and UA can diffuse through the sensing layer (Table 5.1, Case I) to be oxidised at the electrode causing sensor interference.

A protective overcoat consisting of a zwitterionic MPC polymer (Case II) limits non-specific protein adsorption and cell adhesion while presenting a low diffusional barrier to glucose and charge transport. This is due to inter-layer mixing between the MPC and the sensing layer driven by epoxy crosslinking[14]. However, zwitterionic polymers may not hinder the diffusion of ascorbic acid and uric acid as the swellability and high ionic conductivity of zwitterionic hydrogels enables rapid diffusion[40]. Protection against negatively charged LMW UA and AA interferences can by realised by electrostatic repulsion provided by a negatively charged polymer layer (Case III and Case IV). To test for this a selection of polymers was chosen that included Nafion (Case III) and three polymers containing styrene sulfonate groups in various loadings and chemical compositions: a poly(styrene sulfonate-*co*-glycidyl methacrylate-*co*-butylacrylate) (P($SSNa^5$-GMA^3-BA^2), ratio SSNa:GMA:BA 50:30:20)) and two poly(1-vinylimidazole-*co*-styrene sulfonate) polymers P(VI^{12}-$SSNa^1$) and P(VI^1-$SSNa^1$) (see Appendix A.5, Figure S5.1), where the superscripts indicate the monomer molar ratio. The P($SSNa^5$-GMA^3-BA^2) polymer was previously used as a capping

layer for improving the stability of bioelectrodes[41]. High loading of sulfonate groups ensures good solubility in water to aid film deposition and swelling of the coating in aqueous solution to aid substrate and product diffusion,[42-43] while the presence of epoxy crosslinking sites and hydrophobic methacrylate groups can be used to form stable coating on surfaces. A (P(VI^{12}-$SSNa^{1}$)) was prepared to provide a polymer with a high loading of 1-vinylimidazole groups and therefore structural similarity to the Os(bpy)PVI redox polymer. Due to its nucleophilicity, 1-vinylimidazole can react with the PEGDGE crosslinker used to crosslink the redox polymer and enzyme to covalently anchor the polyvinylimidazole polymer film to the sensing layer. This may minimise the diffusional barrier introduced by the additional polymer layer[14]. The P(VI^{1}-$SSNa^{1}$) had similar properties, but a lower loading of 1-vinylimidazole groups and higher loading of the negatively charged styrene sulfonate groups. Amperometric tests with injections of the LMW UA and AA interferents showed that P(VI^{1}-$SSNa^{1}$) coated sensor was the most selective for glucose (Appendix A.5, Figure S5.5), and it was therefore chosen as the negatively charged polymer for further tests (Case IV). While polymer coating of negatively charged polymers such as Nafion and P(VI^{1}-$SSNa^{1}$) can protect against interference from negatively charged substances such as AA and UA, they do not protect against protein adsorption or cell adhesion[14]. Coatings with polymers such as Nafion has also been shown to limit glucose diffusion[14,20–23,44].

Table 5.1: Predicted performance of glucose biosensor systems

Case	Protection against biological interference	Protection against UA and AA weight interference	Efficient glucose and gluconic acid transport
I (Non-coated control)	–	–	+
II (MPC)	+	–	+
III (Nafion)	–	+	–
IV (P(VI^{1}-$SSNa^{1}$))	–	+	+
V (Enzyme layer)	+	+	+
VI (Nafion+MPC)	+	+	–
VII (Polymer Design)	+	+	+

An enzymatic approach based on *L*-ascorbic oxidase (AsOx) and uricase (UOx) (Case V) crosslinked in the MPC layer was also tested to protect from LMW AA and UA interference by converting AA to 2-dehydroascorbate (by AsOx) and UA to 5-hydroxyisourate (by UOx) which further decomposes into allantoin. It is proposed that the MPC would minimise biofouling resistance while retaining efficient glucose transport due to crosslinkable groups and that the enzymes would scavenge UA and AA, providing protection from these LMW interferents. An alternative polymer multi-layer approach, integrating a negatively charged polymer layer between the sensing layer and zwitterionic MPC layer, was tested to protect against AA and UA as well as protein and cell adhesion interferences in sensor signal. Both Nafion (Case VI) and the P(VI^{1}-SSNa^{1}) polymer (Case VII) were selected for testing as the interlayer. As Nafion layers are known to limit glucose diffusion, it is predicted that the Case VI system would provide protection from interference but have a lowered glucose sensor response. The polymer design in Case VII on the other hand, is predicted to show protection from interference but with efficient mass transport of glucose to retain a strong glucose sensor response.

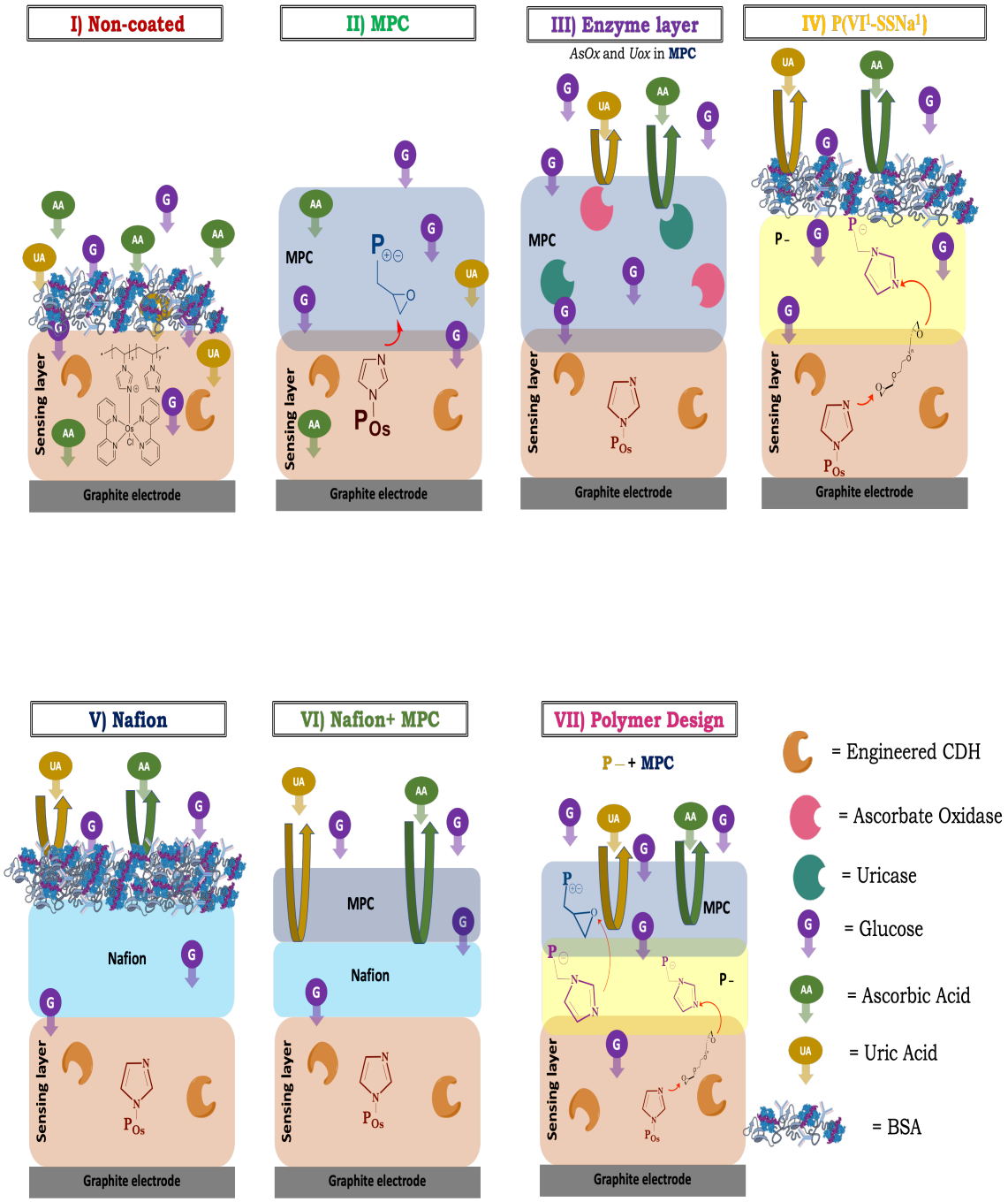

Scheme 5.1: Schematic of different sensor architectures and their proposed behaviour in complex media

5.4.2 Individual effect of low molecular weight and biological interferents in complex media

Biosensors coated with the protective layers were investigated in PBS, artificial plasma and PBS containing UA or BSA. BSA is known to adsorb non-specifically on sensors, mimicking the effect of human serum albumin (HSA) on biosensor current and UA is

known to affect the current response of enzymatic biosensors[44]. All coated biosensors were compared to a non-coated electrode, Case I, that contained only the sensing layer of Os(bpy)PVI, CDH and PEDGDE, heretofore labelled as 'control'.

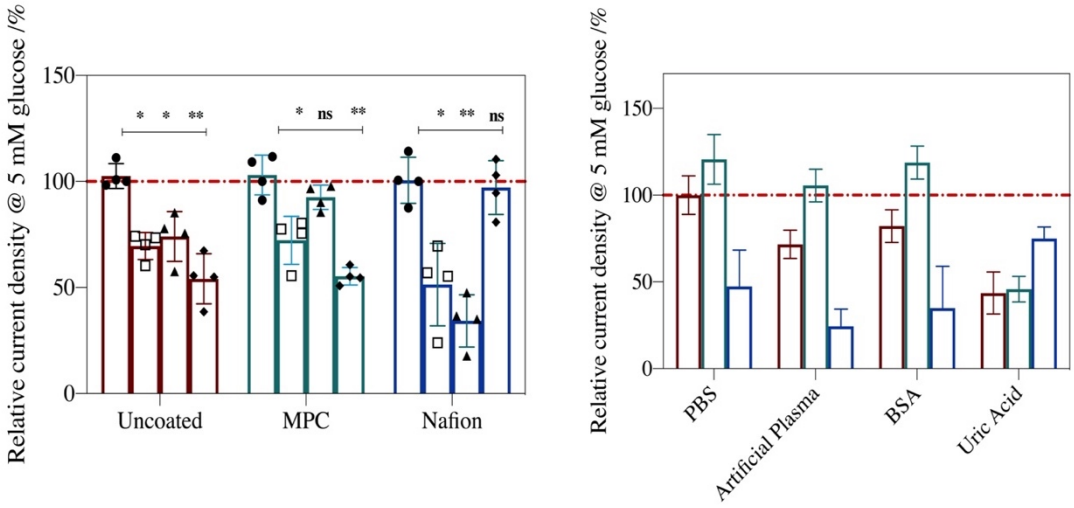

Figure 5.1: Relative current density for detection of 5 mM glucose at 37 ºC where A) current density in PBS (●), artificial plasma (□), BSA (▲) and uric acid (◆) is normalised to that of each system in PBS (0.05M, pH 7.4). B) Current density for detection of 5 mM glucose is normalised to the non-coated control (Case I) in PBS at 37 ºC. Responses are for non-coated control (Case I, maroon), MPC-coated (Case II, green) and Nafion-coated (Case III, dark blue). Mean ± SD. (n = 4); *p<0.03, **p< 0.002, ***p<0.0002

Current densities for glucose oxidation at sensors coated with polymer coatings in PBS, artificial plasma, and PBS with BSA or UA relative to the response of sensor in PBS (A) or to the response of the non-coated control in PBS (B) are presented in Figure 5.1. The non-coated control (Case I) displays a significant drop in current density in uric acid (50%) and a 25% and 20% loss in artificial plasma and BSA, respectively. Current density decrease in uric acid was greater than in artificial plasma with the same uric acid concentration. This may be because protein adsorption in artificial plasma hinders the diffusion of UA to the sensing layer. The same trend of current density decrease was previously observed for redox polymer-based enzyme electrodes prepared using either an FAD-GDH or CDH enzyme[17]. The current decrease in the presence of uric acid could originate from accumulation of uric acid oxidation product allantoin in case of direct oxidation of uric acid at the electrode, or from inhibition of the enzyme by UA. The simultaneous decrease in K_m^{app} and j_{max} (Appendix A.5, Table S5.1) indicates that it is likely uncompetitive inhibition of CDH by UA that leads to

current decrease. Additionally, the baseline current in the absence of glucose is higher when UA is present (Appendix A.5, Figure S5.6), implying that oxidation of UA occurs.

On application of a protective polymer coating, current density usually decreases due to the formation of a diffusional barrier, as reported on previously[14,44]. This is observed (Table S5.1) when Nafion (Case III) is used as a coating. The MPC coating (Case II) results, however, in an increase in current density relative to the response of the control sensor (Figure 5.1B) and a decrease in K_m^{app} (Table S5.1). This is likely due to the high ionic conductivity of the zwitterionic polymers and the interlayer mixing because of epoxy crosslinking with the sensing layer[14]. In Case II, the sensor retains glucose oxidation current density in BSA with a statistically insignificant decrease of 8% but shows significant sensor signal decrease in UA (45%) and artificial plasma (28%). This confirms that while the zwitterionic functionality of MPC enables protection from protein adsorption, the swellable nature does not inhibit diffusion of and interference from LMW species such as UA.

For a Nafion coating, Case III, there is a statistically insignificant change in glucose oxidation current density (-3%) in UA but a significant decrease in artificial plasma (49%) and BSA (65%). Nafion has a mixed hydrophilic/hydrophobic structure and is unable to form a strong hydration sphere to repel protein adsorption[45-46]. Moreover, it is anionic and can electrostatically interact with positive domains of the proteins, increasing protein adsorption. Thus, higher protein adsorption occurs,[14] forming an additional layer which hinders diffusion of glucose substrate. The K_m^{app} and j_{max} remain the same in UA indicating that in Case III, UA does not behave as an inhibitor. This shows that in Case III, Nafion coating hinders UA diffusion to the extent that UA concentration in the sensing layer is insufficient to cause enzyme inhibition.

Coatings targeting minimisation of biofouling operate via formation of a strong hydration sphere that forms an entropic barrier that proteins and cells must overcome for adsorption to occur[40],whereas protective coatings against LMW UA interference rely on electrostatic repulsion and similarity of charges to hinder interference[15]. An efficient protective system for complex media will need to confer the properties of both Case II and Case III to be successful.

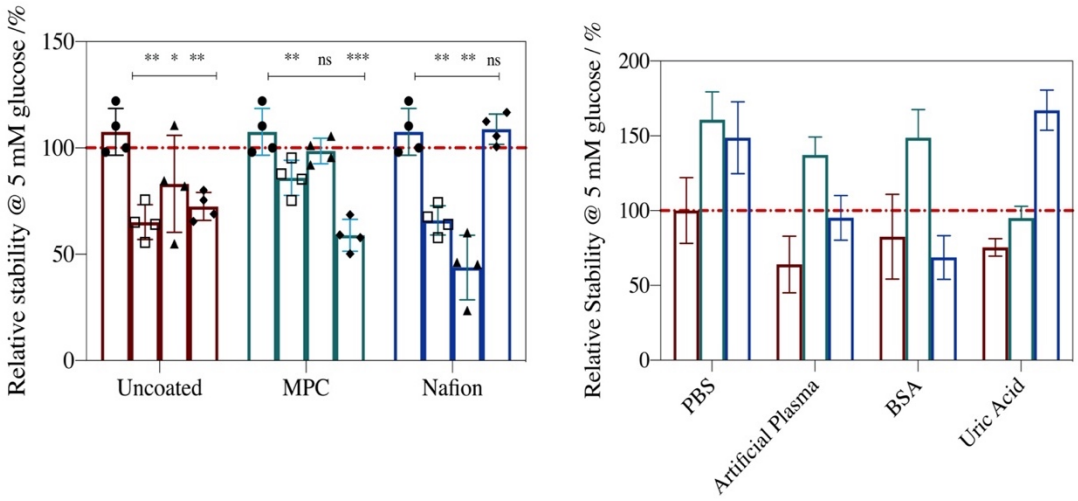

Figure 5.2: Relative stability after 12 h continuous polarisation in 5 mM glucose where A) stability for PBS (●), artificial plasma (□), BSA (▲) and uric acid (◆) is normalised to that of each system in PBS (0.05 M, pH 7.4). B) Stability is normalised to the control in PBS at 37 ºC for non-coated control (Case I, maroon), MPC (Case II, green) and Nafion (Case III, dark blue). Mean ± SD. (n= 4); *p<0.03, **p< 0.002, ***p<0.0002

Considering the glucose oxidation sensor signal stability, each system shows a lower stability in complex media relative to that in PBS alone (Figure 5.2A). For example, the non-coated control (Case I) shows stability decrease of 35%, 17% and 28% in artificial plasma, BSA and UA, respectively. The MPC (Case II) retains current in BSA showing statistically insignificant decrease but shows significant decreases of 40% in UA and 15% in artificial plasma. On the contrary, Nafion (Case III) shows statistically insignificant stability decrease in UA with a significant decrease of 57% in BSA and 35% in artificial plasma. For each case, the presence of polymer coating improves the glucose oxidation sensor signal stability compared to that of the control in PBS (Figure 5.2B).

5.4.3 Multi-purpose protection from protein and LMW interferents

An interference screening was performed in different Case systems to evaluate if the multi-purpose Case IV-VII coatings can minimise protein, AA and UA interference compared to Case I-III coatings. Interference is calculated using a MARD threshold of 20% in the presence of 5 mM glucose (equation 1). MARD was selected as a measure to portray effect of an interference as it quantifies the mean absolute difference in

presence of interference to the mean sensor response in absence of interference. Additionally, the size of the box in Figure 5.3A represents the standard deviation across 4 electrodes. The wider the box, the more the response of the biosensor varies in a particular media. This variability can negatively affect the sensitivity of the sensor or its ability to distinguish between successive glucose concentrations. The desired response is therefore a Case system that does not cross the 20% MARD threshold and has a compact box indicating low variability in sensor readings across a sample size of 4.

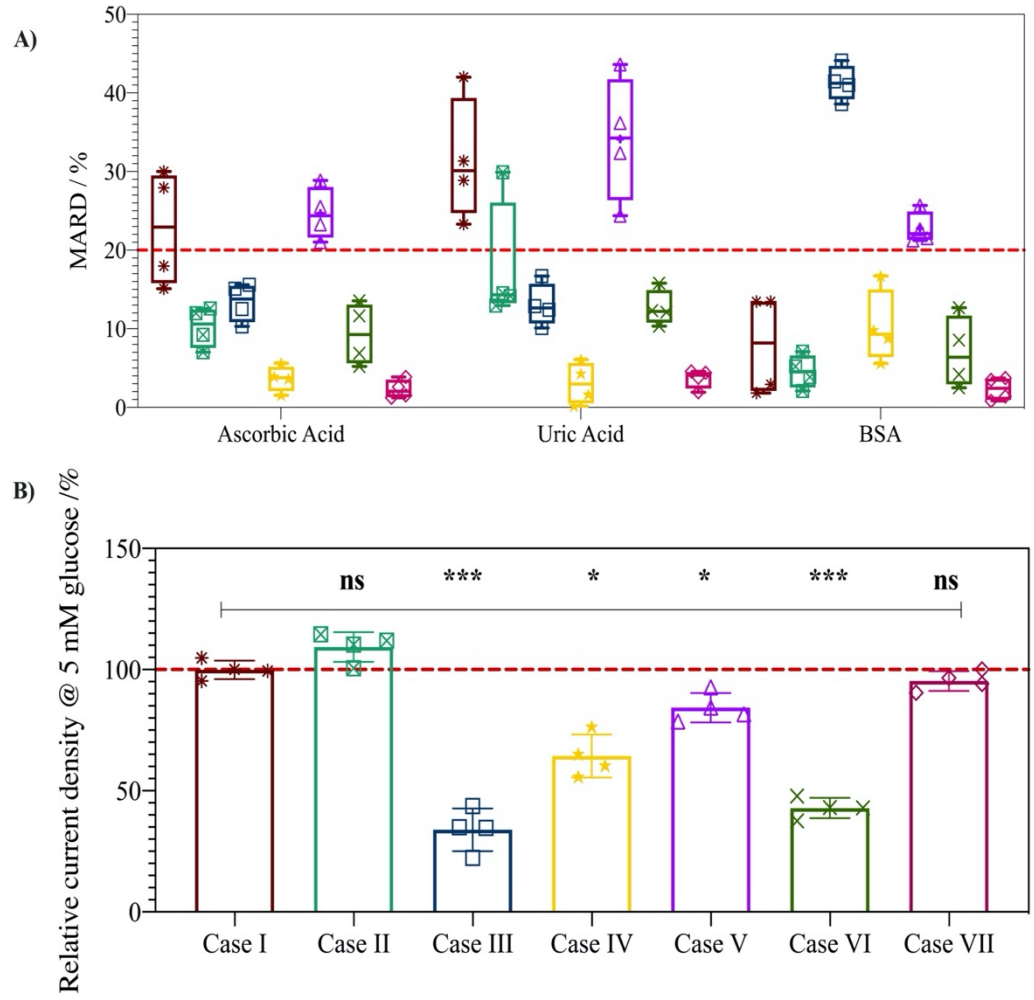

Figure 5.3: A) Box plot showing the mean absolute relative difference (MARD, %) of the current signal in 5 mM glucose (PBS, pH 7.4, 37 ºC) in the presence of ascorbic acid, uric acid and BSA for Case I (maroon,*), Case II (green, ☒), Case III (dark blue,□), Case IV (yellow,★), Case V (violet,△), Case VI (dark green, ×) and Case VII (pink,◇). The line inside the box = mean, box limits = standard deviation (n=4); * and the symbols represent individual data points; lower and upper error bars = 5% and 95% limits, respectively; red line = 20% MARD threshold for definition of interference. B) relative current densities of Case I-VII in PBS (0.05 M, pH 7.4). Mean ± SD. (n= 4); *p<0.03, **p< 0.002, ***p<0.0002.

The addition of AA and UA, as expected, acts as interferents at the non-coated control (Case I) with MARD of 23 ± 7% and 31 ± 8%, respectively. While protein adsorption may occur in BSA, the effect on the current is insufficient to breach the 20% threshold to be classified as an interferent (MARD = 8 ± 6%). However, the standard deviation is high. Moreover, as protein adsorption can increase with time, further protein adsorption may occur should a non-coated control sensor be used over longer periods in complex media. For MPC-coated system (Case II), UA acts as an interferent for Case II (MARD = 18 ± 8%) but AA and BSA have MARD of 10 ± 2% and 5 ± 2%, respectively, and are not classified as interferents. Nafion system (Case III) protects against interference from UA and AA (MARD = 13 ± 2%) but shows high interference from BSA (MARD = 41 ± 2%). This again can be attributed to the mixed hydrophobic/hydrophilic structure and anionic nature of Nafion[47]. The new P(VI^1-$SSNa^1$) co-polymer used in Case IV shows protection from UA, AA and BSA interference with MARD of 4 ± 2%, 3 ± 2% and 10 ± 5%, respectively. While protein adsorption does occur, similar to the non-coated control, the effect on the current is insufficient for BSA to be classified as an interferent. The difference in the effect protein adsorption for Case IV versus Case III is likely due to the more hydrophilic nature of P(VI^1-$SSNa^1$) compared to Nafion, as hydrophobic films show greater biofouling than hydrophilic films[45,48]. Nevertheless, as in Case I, the P(VI^1-$SSNa^1$) Case IV system response in BSA shows high variability and considering the prolonged timescale of protein adsorption, this anionic coating might be problematic as a shield for biofouling. The enzyme scavenging Case V approach results in interference from UA, AA and BSA with MARD of 25 ± 3%, 34 ± 8% and 22 ± 7% respectively. The interference from UA is likely due to the low enzymatic activity of UOx (9 U/mg), which limits the efficiency of the enzymatic scavenging mechanism. While the AsOx enzyme has good specific activity (1500 U/mg), amperometric tests (Appendix A.5, Figure S5.7) confirm that the ASOx system does not sufficiently protect against interference from AA, as injection of AA leads to an increase in sensor current. It is interesting to note that the MARD in the presence of BSA is higher for enzyme scavenging case V system where enzymes are in the MPC layer, compared to case II (MPC alone). It is possible that the enzymes affect the surface chemistry sufficiently to hinder the protective effect against protein adsorption offered by a zwitterionic polymer.

The multi-layer architectures (Nafion+ MPC, Case VI and polymer design, Case VII), both show good protection from interference by UA, AA and BSA with MARD of 9 ± 4%, 12 ± 2% and 7 ± 5% for Case VI and 2 ± 1%, 3 ± 1% and 2 ± 1% for Case VII, respectively. Thus, from the results in Figure 5.3A, P(VI^1-$SSNa^1$) (Case IV), Nafion + MPC (Case VI) and the polymer design (Case VII) show the most promise as polymer shields for protection from both LMW interference such as AA, UA and biological interferences such as BSA. However, the glucose oxidation current density is significantly lower than that observed at the non-coated Case I for Case IV (36% decrease) and VI (58% decrease) compared to that for the polymer design Case VII (Figure 5.3B). In addition, the polymer design Case VII system shows the lowest MARD and variability in signal. Therefore, the polymer design (Case VII) shows statistically insignificant loss in current density compared to control the best ability to protect against AA, UA and BSA interference and the lowest signal variability.

5.4.4 Polymer design-based sensor performance and operational stability

The response in 5 mM glucose of the polymer design Case VII sensor, covered with the negatively charged polymer P(VI^1-$SSNa^1$) as the interlayer and MPC as the outer layer is compared to a Case I sensor without protective overcoats operating in PBS and artificial plasma (Figure 5.4). To prepare the Case VII sensors, both overcoats were applied in equal amounts (10 µg). The glucose oxidation amperometric current response of the polymer design Case VII showed slightly higher current density (20%) than the uncoated Case I sensor in PBS. This can be attributed to the high ionic conductivity of zwitterionic polymers which enables rapid counterion movement. Additionally, the ability of the multi-layer sensor to retain high current densities shows that glucose transport through the P(VI^1-$SSNa^1$) and MPC films encounters a low diffusional barrier. This is similar to that reported on previously, proposed to be due to the chemical crosslinkage between layers leading to interlayer mixing [14].Application of the polymer design multi-layer does not significantly affect the current density or sensitivity of the biosensors in PBS, displaying 12% improvement in sensitivity (Table 5.2). The Case VII system thus performs better than a system containing Os(bpy)PVI and coated with 0.5 w/v% Nafion[44] as the Nafion overcoat on biosensors containing GOx and FAD-GDH resulted in 67% and 72% loss in sensor signal.

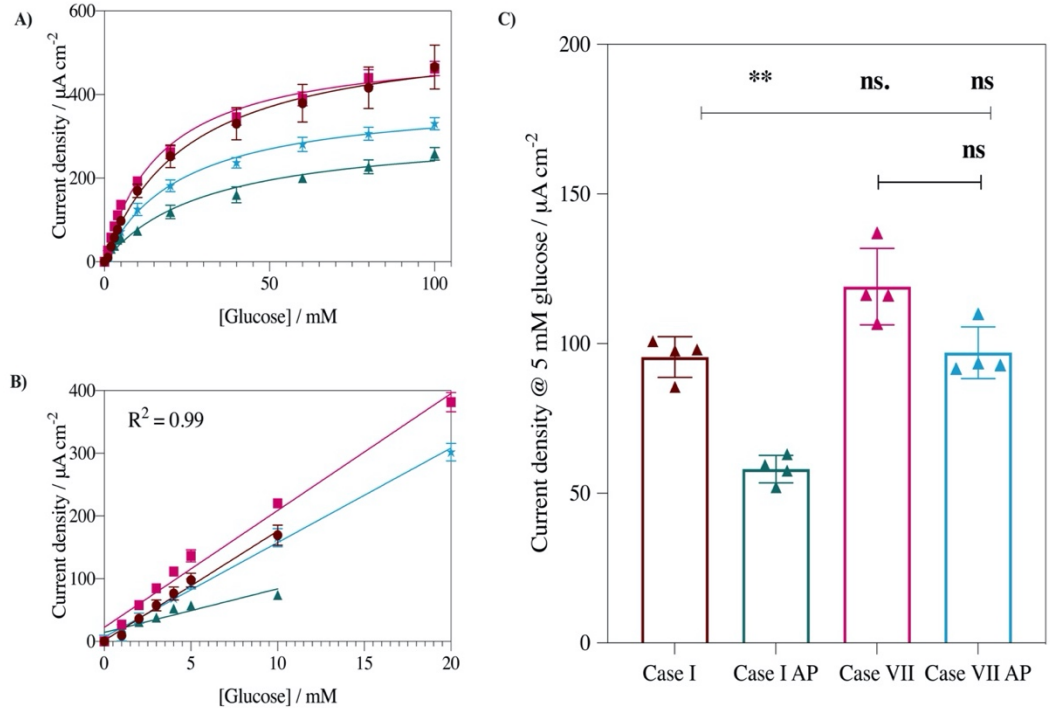

Figure 5.4: Glucose response for the amperometric biosensors, tested at a constant applied potential of 0.35 V vs Ag/AgCl (3 M KCl) at 37 ºC in PBS (0.05 M, pH 7.4) and artificial plasma (AP) presented as A) current density versus glucose concentration from 0-100 mM B) response over glucose concentration linear range where R^2= 0.99 C) current density for coated sensors in 5 mM glucose relative to that of the non-coated sensor. Case I in PBS (maroon), Case I in AP (green), Case VII in PBS (pink), Case VII in AP (blue). Mean ± SD. (n= 4); *p<0.03, **p< 0.002, ***p<0.0002

Table 5.2: Analytical parameters for glucose biosensor

Sensor	**K_M^{app} / mM**	**j_{max} / µA cm^{-2}**	**Sensitivity /µA cm^{-2} mM^{-1}**	**LOD / mM**	**S_{AP}/S_{PBS}**
Case I in PBS	25.2 ± 4.7	557.1 ± 8.3	17.5 ± 1.9	2.9	0.6
Case I in artificial plasma	30.7 ± 3.8	315.2 ± 12.3	6.9 ± 1.3	5.3	
Case VII in PBS	17.2 ± 5.1	520.5 ± 11.2	19.7 ± 0.9	1.7	0.9
Case VII in artificial plasma	23.1 ± 6.2	393.8 ± 30.2	15.1 ± 0.6	4.5	

The advantage of using the polymer design system is highlighted by the differences between the Case VII coated and Case I control sensor performance measured in

artificial plasma. Some loss in the current densities is expected when switching to complex media, however, the loss is significantly less pronounced for the Case VII sensor with the multi-layer protective shield. Case I shows a 39% loss in current density in AP compared to that in PBS whereas Case VII shows a statistically insignificant loss of 9% under the same conditions (Figure 5.4C). Multi-layer coating also extends the linear range (R^2 =0.99) of the sensor, extending the range to 20 mM compared to 10 mM for Case I control (Figure 5.4B). Finally, the sensitivity data extracted from the slope of the linear range (Table 5.2) indicates that Case VII sensor displays higher sensitivity than Case I both in PBS and in artificial plasma. The Case I sensor shows 60% loss in sensitivity operating in artificial plasma compared to in PBS whereas the Case VII sensor shows only 23% loss in sensitivity. It should be noted that the Case VII sensor shows similar sensitivity in artificial plasma to that of the Case I control sensor in PBS despite being in complex media. A study reporting on use of Nafion coatings over Os(bpy)PVI-based enzyme electrodes[44] does not report sensitivities in artificial plasma and thereby the loss in sensitivity due to complex media, but the slopes from Michaelis-Menten curves clearly indicate that operation in artificial plasma results in a significant loss in sensitivity. For their sensor with GOx and FAD-GDH, non-coated biosensors register higher current densities and sensitivities in artificial plasma (visualised by the slope) than their Nafion-coated counterparts. A similar study of GOx encapsulated in poly(3,4-ethylenedioxythiophene) (PEDOT) along with another system where PEDOT was functionalised with polysulfobetaine (PSPEDOT), showed results similar to what was observed in this study[49]. Tests in PBS and plasma showed that zwitterionic polymer systems had higher current and sensitivity compared to their non-zwitterionic counterparts, likely due to influence of high ionic conductivity. The sensitivities for PSPEDOT and PEDOT were 12.63 μA cm^{-2} mM^{-1} and 7.54 μA cm^{-2} mM^{-1}, respectively, in PBS which decreased by 13% and 40% in plasma. While introduction of a sulfobetaine zwitterionic moiety into the coating increased sensor sensitivity, similar to that observed in this report, however, the sensitivity of Case VII sensor is higher than that of PSPEDOT sensor. While many other studies target application of glucose sensor as CGMs [50,51,52] and include testing in complex media, the changes in analytical parameters and sensitivity in the complex media are not reported.

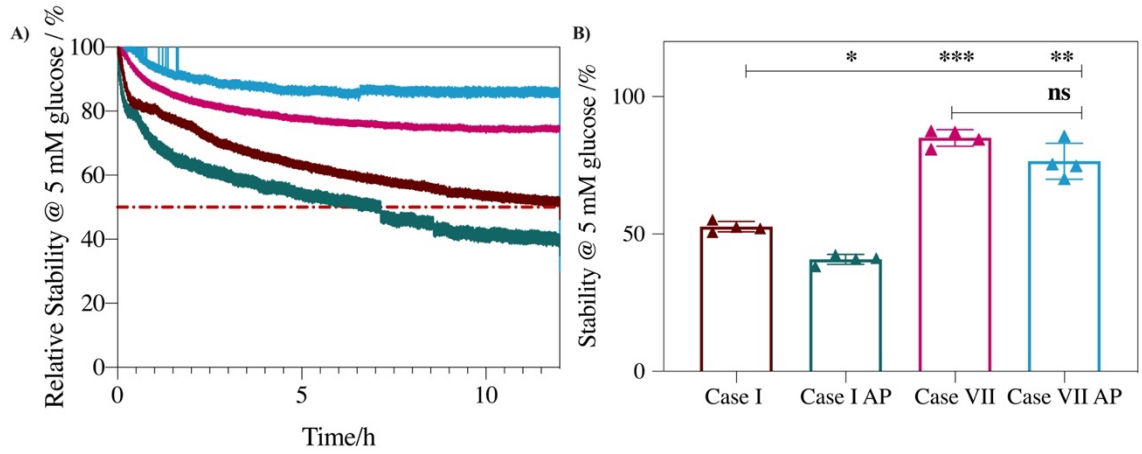

Figure 5.5: Operational stability over 12 h of amperometric response to 5 mM glucose for non-coated (Case I) and polymer design (Case VII) systems in PBS (0.05 M, pH 7.4) and artificial plasma (AP) presented containing 5 mM glucose as A) Relative stability over time and B) Stability after 12 h. Case I in PBS (maroon), Case I in AP (green), Case VII in PBS (pink), Case VII in AP (blue). Mean ± SD. (n= 4); *p<0.03, **p< 0.002, ***p<0.0002.

The results on operational stability measured in PBS and artificial plasma and presented in Figure 5.5, confirm that multi-layer coating enhances the stability of the sensor. This is likely due to the stabilising effect the polymer overcoats can have on the redox polymer sensing layer. The Case VII sensor shows better stability, with 85% signal retained after 12 h of continuous operation in PBS and 77% in artificial plasma, than the Case I non-coated control which had 54% stability in PBS and 38% in artificial plasma. A ratio of stability in complex media to stability in PBS of 0.6 for Case I and 0.9 for Case VII, respectively, shows that coatings ameliorate operational stability. Moreover, on comparing stability for Case VII to that of individual polymer coatings (Case II and Case III, Figure 5.2) it is evident that multi-layer coating improved protection over that provided by individual layers for sensors operating in artificial plasma, due to complexity of interactions between LMW species and BSA in complex media. Comparing with the results of Nafion-coated systems studied by Bennett et al,[17] the use of a multi-layer coatings in Case VII provides similar stability to that of a GOx/MWCNT based biosensor despite lack of use of nanosupport in PBS and complex media.

5.5 Conclusions

Single-layer and multi-layer polymer coatings based on various protection mechanisms were investigated as anti-interference shields for a second-generation glucose biosensor. The sensor architectures were designed to target either biological and low molecular weight interferences individually or both. Study of the effect of the most detrimental interferents, BSA and uric acid, showed that low molecular weight and biological interferents have individual effects on current density and operational stability that are compounded in complex media like artificial plasma, therefore, they require individual protections. For targeting negatively charged low molecular weight interferences, the effectiveness of negatively charged polymer layers for electrostatic repulsion of the interferents was compared to a protective layer containing enzymes that consume the interfering species. Due to the low activity of enzymes, electrostatic repulsion of the low molecular weight interferences was found to be more effective. An interference screening was performed in different complex media for the designed single- and multi-target protection systems. Most of the single-target coatings showed that at least one of the plasma components examined in this study acted as an interferent. Both multi-target architectures where the outer layer consisted of antifouling zwitterionic polymer (MPC) and interlayer of either Nafion or synthesised polyvinylimidazole-polysulfostyrene copolymer (P(VI^1-$SSNa^1$)) showed good resistance against interferences. Polymer design architecture consisting of P(VI^1-$SSNa^1$) and MPC was found to be superior due to very low MARD values for all the tested interferences, low variability in the obtained results and significantly better glucose permeability compared to the multi-layer system with Nafion interlayer. In contrast to other reports using polymer coatings, application of the polymer design multi-layer did not negatively affect the current density or sensitivity of the biosensors. Additionally, the linear range of the sensor was two times wider for the multi-layer system than the control. Overall, a multi-layer protective coating system consisting of the newly designed P(VI^1-$SSNa^1$) and MPC shows promise for potential application in biosensor development. Further studies in physiological samples are needed.

5.6 Acknowledgments

This project has received funding from the European Union's Horizon 2020 research and innovation program under the Marie Skłodowska-Curie MSCA-ITN "ImplantSens" [813006]. Donation of the CDH by Thomas Reichhart and Roman Kittl (DirectSens GmbH, Klosterneuburg, Austria) and Roland Ludwig, Universität für Bodenkultur Wien (BOKU) Vienna, Austria is gratefully acknowledged.

5.7 References

[1] P. Saeedi, I. Petersohn, P. Salpea, B. Malanda, S. Karuranga, N. Unwin, S. Colagiuri, L. Guariguata, A.A. Motala, K. Ogurtsova, J.E. Shaw, D. Bright, R. Williams, Diabetes research and clinical practice 157 (2019) 107843.

[2] L.C. Clark, C. Lyons, Ann. N. Y. Acad. Sci. 102 (1962) 29–45.

[3] S.K. Vashist, D. Zheng, K. Al-Rubeaan, J.H.T. Luong, F.-S. Sheu, Anal. Chim. Acta 703 (2011) 124–136.

[4] U. Gebhardt, G. Luft, G.J. Richter, F. von Sturm, Bioelectrochem. Bioenerg. 5 (1978) 607–624.

[5] E.M. Lonsdale, J.W. Steadman, W.L. Pancoe, IEEE Trans. Biomed. Eng. 13 (1966) 153–159.

[6] Y. Wang, M. Hu, in: S. Peteu, J.F. Rusling, P. Vadgama (Eds.), Detection Challenges in Clinical Diagnostics, Royal Society of Chemistry, Cambridge, 2013, pp. 65–88.

[7] J. Wang, J. Pharm. Biomed. Anal. 19 (1999) 47–53.

[8] O. Didyuk, N. Econom, A. Guardia, K. Livingston, U. Klueh, J. Diabetes Sci. Technol. 15 (2021) 676–683.

[9] U. Klueh, J.T. Frailey, Y. Qiao, O. Antar, D.L. Kreutzer, Biomaterials 35 (2014) 3145–3153.

[10] T. Bobrowski, W. Schuhmann, Curr. Opin. Electrochem. 10 (2018) 112–119.

[11] A. Koh, S.P. Nichols, M.H. Schoenfisch, J. Diabetes Sci. Technol. 5 (2011) 1052–1059.

[12] O. Veiseh, A.J. Vegas, Adv. Drug Delivery Rev. 144 (2019) 148–161.

[13] J. Xu, H. Lee, Chemosensors 8 (2020) 66.

[14] K. Jayakumar, A. Lielpetere, D.A. Domingo-Lopez, R.E. Levey, G.P. Duffy, W. Schuhmann, D. Leech, Biosens. Bioelectron. 219 (2022) 114815.

[15] W.-Z. Jia, K. Wang, X.-H. Xia, TrAC, Trends Anal. Chem. 29 (2010) 306–318.

[16] J.M. Harris, C. Reyes, G.P. Lopez, J. Diabetes Sci. Technol. 7 (2013) 1030–1038.

[17] R. Bennett, E. Blochouse, D. Leech, Electrochim. Acta 302 (2019) 270–276.

[18] T. Kulkarni, G. Slaughter, Membranes 6 (2016).

[19] S. Kuwabata, Chem. Lett. 37 (2008) 230–235.

[20] Y. Zhang, Y. Hu, G.S. Wilson, D. Moatti-Sirat, V. Poitout, G. Reach, Anal. Chem. 66 (1994) 1183–1188.

[21] C.P. Andrieux, P. Audebert, B. Divisia-Blohorn, S. Linquette-Maillet, Journal of Electroanalytical Chemistry 353 (1993) 289–296.

[22] C.P. Andrieux, P. Audebert, P. Bacchi, B. Divisia-Blohorn, J. Electroanal. Chem. 394 (1995) 141–148.

[23] T.J. Ohara, R. Rajagopalan, A. Heller, Anal. Chem. 66 (1994) 2451–2457.

[24] J.I. Njagi, S.M. Kagwanja, in: Interfaces and Interphases in Analytical Chemistry (2011), pp. 225–247.

[25] F. Scheller, R. Renneberg, Anal. Chim. Acta 152 (1983) 265–269.

[26] F. Lopez, S. Ma, R. Ludwig, W. Schuhmann, A. Ruff, Electroanalysis 29 (2017) 154–161.

[27] R. Maidan, A. Heller, J. Am. Chem. Soc. 113 (1991) 9003–9004.

[28] R. Maidan, A. Heller, Anal. Chem. 64 (1992) 2889–2896.

[29] J. Anzai, H. Takeshita, Y. Kobayashi, T. Osa, T. Hoshi, Anal. Chem. 70 (1998) 811–817.

[30] G. Nagy, M.E. Rice, R.N. Adams, Life Sciences 31 (1982) 2611–2616.

[31] R. Kurita, K. Hayashi, X. Fan, K. Yamamoto, T. Kato, O. Niwa, Sens. Actuators, B 87 (2002) 296–303.

[32] K. McAteer, R.D. O'Neill, Analyst 121 (1996) 773.

[33] F. Mao, N. Mano, A. Heller, J. Am. Chem. Soc. 125 (2003) 4951–4957.

[34] A. Heller, B. Feldman, Chem. Rev. 108 (2008) 2482–2505.

[35] K. Jayakumar, T.M.B. Reichhart, C. Schulz, R. Ludwig, A.K.G. Felice, D. Leech, ChemElectroChem 9 (2022).

[36] S. Alsaoub, Synthesis of Stable Os-Complex Modified Polymers for the Applications in Biosensors, Biofuel Cells and Biosupercapacitors. PhD thesis, Bochum, 2017.

[37] N. Rifai, Tietz Textbook of Clinical Chemistry and Molecular Diagnostics, Elsevier, 2018.

[38] R. Boehm, J. Donovan, D. Sheth, A. Durfor, J. Roberts, I. Isayeva, J. Diabetes Sci. Technol. 13 (2019) 82–95.

[39] J.R. Roberts, J. Park, K. Helton, N. Wisniewski, M.J. McShane, J. Diabetes Sci. Technol. 6 (2012) 1267–1275.

[40] J.B. Schlenoff, Langmuir 30 (2014) 9625–9636.

[41] J. Szczesny, N. Marković, F. Conzuelo, S. Zacarias, I.A.C. Pereira, W. Lubitz, N. Plumeré, W. Schuhmann, A. Ruff, Nat. Commun. 9 (2018) 4715.

[42] M.J. Molina, M.R. Gómez-Antón, I.F. Piérola, J. Polym. Sci. B Polym. Phys. 42 (2004) 2294–2307.

[43] T. Kothe, S. Pöller, F. Zhao, P. Fortgang, M. Rögner, W. Schuhmann, N. Plumeré, Chem. - Eur. J. 20 (2014) 11029–11034.

[44] R. Bennett, D. Leech, Bioelectrochemistry 133 (2020) 107460.

[45] Y. Higaki, J. Nishida, A. Takenaka, R. Yoshimatsu, M. Kobayashi, A. Takahara, Polym. J. 47 (2015) 811–818.

[46] M. Li, B. Zhuang, J. Yu, Chem. - Asian J. 15 (2020) 2060–2075.

[47] K. Ito, M. Harada, N.L. Yamada, K. Kudo, H. Aoki, T. Kanaya, Langmuir 36 (2020) 12830–12837.

[48] R. Hammer, M. Schönhoff, M.R. Hansen, J. Phys. Chem. B 123 (2019) 8313–8324.

[49] H. Wu, C.-J. Lee, H. Wang, Y. Hu, M. Young, Y. Han, F.-J. Xu, H. Cong, G. Cheng, Chem. Sci. 9 (2018) 2540–2546.

[50] Y. Wang, X. Qing, Q. Zhou, Y. Zhang, Q. Liu, K. Liu, W. Wang, M. Li, Z. Lu, Y. Chen, D. Wang, Biosens. Bioelectron. 95 (2017) 138–145.

[51] Y. Cai, B. Liang, S. Chen, Q. Zhu, T. Tu, K. Wu, Q. Cao, L. Fang, X. Liang, X. Ye, Biosens. Bioelectron. 165 (2020) 112408.

[52] Y. Song, Y. Shen, C. Gong, J. Chen, M. Xu, L. Wang, L. Wang, ChemElectroChem 4 (2017) 1457–1462.

Chapter 6 : Conclusions and Future directions

6.1 Conclusions

The main objective of this thesis was to investigate strategies that can improve the performance of mediated glucose biosensors for application as continuous glucose monitors (CGMs) by combating the performance limitations of existing systems. Chapter 1 provides a literature review encompassing the history of diabetes treatment with glucose monitoring, the mechanism of electrochemical glucose sensing with enzymes, the use of enzymes as catalysts and overview of glucose biosensing advances and the current limitations that afflict sensor performance. Currently, biosensor performance of CGMs is limited by their oxygen dependence, interference from low molecular weight (LMW) species and from the foreign body response (FBR). Chapter 2 describes the development of a biosensor using commercial glucose oxidising enzyme that is then optimised for maximum current density and operational stability under conditions that mimic the *in vivo* operational conditions. This was important as most CGMs that rely on electrochemical transduction utilise glucose oxidase (GOx) as the biorecognition element. In order to minimise amount of nanosupport used to enhance current response and stability, the enzyme was grafted onto the nanosupport forming a nanoconjugate. The optimisation performed enabled fabrication of biosensors with 146% improvement in current density response compared to similar systems where enzyme and nanosupport are not covalently bound to each other. On application of a minimisation constraint, biosensors with comparable current response to the optimised systems while using 93% less of enzyme-nanosupport nanoconjugate were realised. However, enzyme electrodes fabricated with oxidase-based enzymes do suffer from the limitation of oxygen dependence, which is usually compensated for in CGMs using algorithms [1].

Due to constantly varying oxygen concentrations *in vivo*, oxidase-based enzymes can give errors in glucose sensing readings, either by competition of oxygen with mediator to regenerate enzyme or competition with electrode to steal electrons from the mediator. In addition, peroxide produced during oxygen reduction results in the oxidation of methionine residues of enzyme, causing enzyme instability. To overcome these detrimental effects, the investigation of an oxygen-insensitive engineered cellobiose dehydrogenase (WT*Ch*CDH), that can be used in MET and DET

biosensors, was used to fabricate enzyme electrodes for glucose sensing, as discussed in Chapter 3. The MET biosensor showed high sensitivity on the same order of magnitude to systems containing other glucose-oxidising enzymes [2–4]. This shows the potential of the engineered enzyme for application to glucose biosensing. While the MET biosensor shows higher sensitivity than the DET biosensor, the DET biosensor based on WT*Ch*CDH offers a substantial improvement in sensitivity over other DET-based glucose biosensors. Moreover, both DET and MET sensors showed no change in glucose response when measured in the absence and presence of oxygen. Previous characterisation of engineered WT*Ch*CDH showed production of some peroxide which can oxidise methionine residues, but to a substantially lower degree than GOx which uses oxygen to regenerate enzyme[5].

Other significant limitations considering the long-term goal of implantation are the foreign body response (FBR), that affects implanted devices due to the host's hostile environment, and the presence of low molecular weight (LMW) species (See Chapter 1, Figure 1.9). Polymer coatings that mitigate these limitations (Nafion, PEG, etc) have a limitation of their own as they induce a diffusional barrier hindering mass transport of the analyte and product to-and-from the electrode surface. This impairs the sensor performance. In order to mitigate against this, a novel strategy was explored in Chapter 4 wherein crosslinking sites were introduced into the polymer backbone of the protective coatings. This approach was based on the theory that the crosslinking sites would allow crosslinks to form with the redox polymer of the underlying sensing layer, minimising the boundary at the interface between sensing and protection layers, thereby minimising and/or removing the diffusional barrier. Using zwitterionic polymers as a protective coating against biological interferents and epoxy functionality as the crosslinking group, a series of novel ZPs was investigated to reduce biofouling by fibrinogen and fibroblasts. The developed MPC polymer showed comparable behaviour to a FDA approved ZP, Lipidure, in minimising fibrinogen adsorption and fibroblast adhesion. On application as a protective coating on the glucose biosensor optimised in Chapter 3, the sensor showed glucose sensing behaviour comparable to a non-coated sensor in phosphate buffered saline with no diminishment in current density and a 1.5-fold increase in sensitivity. On the contrary, coatings of commercial polymers Nafion, PEG and Lipidure resulted in current density decreases of 50-70% compared to a non-coated sensor in phosphate buffered saline confirming that only

MPC was able to overcome the diffusional barrier limitation of polymer coatings. Moreover, from testing in PBS containing bovine serum albumin (7 g L^{-1}) at concentrations to mimic human serum albumin, the MPC coated sensor showed no loss in sensor performance contrary to the non-coated biosensor which lost 40% of the current signal. This proved that through specific design of polymers as protective coatings it was possible to create a protective system that could impart the desired function while retaining current signals.

In order to expand this protection, Chapter 5 explored a range of architectures to simultaneously protect the sensor from biological and LMW electroactive species. To this end, two main approaches were investigated – enzymatic scavenging and multi-layer polymer coating. Enzymatic scavenging relied on the use of enzymes integrated into the MPC protective coating that targeted oxidation of the LMW species UA and AA. The MPC was selected to impart resistance to biofouling for the biosensor, creating a single protective layer with multipurpose protection. For comparison, multi-layer polymer coatings relying on the use of successive polymer coatings of an anionic interlayer to repel anionic LMW electroactive species UA and AA and of MPC as the outerlayer to impart resistance to biofouling were also investigated. The presence of the crosslinking sites allows each layer to chemically crosslink with each other, minimising the boundaries at the each interface and therefore the diffusional barriers. The multi-purpose enzymatic scavenging and MPC polymer approach did not remove UA and AA interference due to the low activity of the scavenging enzymes, while the anionic polymer coatings proved effective in hindering access of LMW UA and AA to the sensor. The multi-layer polymer coating systems effectively protected the sensor from the LMW UA and AA, and from the biological interferences when tested in an interference screening method, while maintaining current density comparable to a non-coated control in PBS. The multi-layer coating showed higher current density and sensitivity and extended linear range of the biosensor in PBS and artificial plasma compared to non-coated control, showing therefore promise as an effective protective architecture for glucose biosensors. To conclude, biosensors fabricated using the improvements described in this thesis have great potential for application as sensors in CGMs.

6.2 Future directions

6.2.1 ImplantSens

The continuation of this work presented in this thesis would entail *in vitro* testing of the sensors systems in human physiological fluids such as human plasma and blood. These experiments are planned, and fall within the purview of ESR 11. In addition, in order to evaluate potential application of fabricated biosensors in CGMs, *in vivo* tests using rat models can simultaneously gauge biocompatibility and functionality. The *in vitro* biological tests in Chapter 4 of this thesis only tests for two aspects of the FBR – fibrinogen and fibroblasts adsorption. Further *in vivo* tests are required to determine if minimisation of biofouling is achieved over extended time periods and if the sensing ability of the biosensor is affected during this process. Such experiments are planned and fall within the purview of ESR 3. Results presented in this thesis have been used by other ESRs to produce and examine different electrode and sensor architectures. For example, The redox polymer used in this thesis has been distributed to ESRs to be used in conjunction with the coating described in Chapters 4-5 to be used on different electrode architectures. This has led to the optimised sensing layer components described in Chapter 3 being deposited on nanoporous gold electrodes, tubular electrodes, pencil graphite microneedle and on nanoband array electrodes to form sensors. *In vitro* and *in vivo* testing of the sensors resulting from these depositions on different electrodes are to be tested by ESR 3 and ESR 11.

Another future research path is the use of pulsed potential sensing regimes. Pulsed regimes proposed are based on use of a positive potential (0.35 V vs Ag/AgCl in this thesis) to measure glucose oxidation current and then a negative potential, where no glucose oxidation occurs, to switch "off" the enzyme electrode. This is one of the long-term goals of the ImplantSens network and one of the main reasons (apart from minimising detrimental effects of oxygen dependence) that oxygen insensitivity was targeted in the Implantsens consortium, and in this thesis. For example, an oxygen-sensitive enzyme switched to a negative potential regime can still utilise oxygen as co-substrate instead of the redox polymer mediator to regenerate the enzyme and prevent the system from being switched 'off'. The results from Chapter 3 show promise that

an oxygen-insensitive system can be achieved to be investigated using pulsed potential regimes. This allows a sensor to measure glucose at predetermined time intervals and then stay switched off, which could aid in having an equilibrium-based sensing mechanism [6] and extending sensor lifetime.

6.2.2 Beyond ImplantSens

The importance of monitoring blood glucose levels for diabetes treatment has been previously described (See Chapter 1). The CGMs are the latest iteration of blood glucose monitors, where the continuous nature of the device enables personalisation of medical treatment [7]. Hyper- and hypoglycaemic periods can be detected and/or predicted (depending on the algorithms used) and corrective measures such as administration of exogenous insulin, exercise or consumption of food can be taken. CGMs effectiveness is limited by the lower lifetime and accuracy, depending on their transduction mechanism. Electrochemical transduction systems such as FreeStyle Libre have high accuracy but a limited sensor lifetime of 14 days whereas optical transduction systems such as that provided by Eversense have longer sensor lifetimes of 30 days but lower accuracy due to the transduction mechanism[8]. Thus far, these systems have been deployed based on an understanding of their limitations. The research results provided in this thesis aims to contribute towards improvement of electrochemical sensors and aid in prolonging sensor lifetime on implantation for application to CGMs. The research required to reach this goal is described in Section 6.2.1. However, what happens beyond this stage?

At present, effective diabetes treatment relies on monitors (management devices) used in conjunction with delivery devices, forming an open-loop system (Figure 6.1). Common delivery systems include insulin injections, insulin pens, insulin pumps and insulin patches[9]. Open-loop systems of CGMs paired with insulin pumps minimise the burden of treatment on the patient compared to previous systems of fingerprick glucose monitors paired with insulin injections. However, the patient must still make decisions regarding actions to counter hyper/hypoglycaemic periods indicated by CGM either by activating the insulin pump or consuming food. On the other hand, a closed-loop system interconnects a CGM, an insulin pump, and an algorithm to fully automate insulin delivery. To reach this goal, there is a need for significant

technological advances and development of smart algorithms that can anticipate the patient's needs.

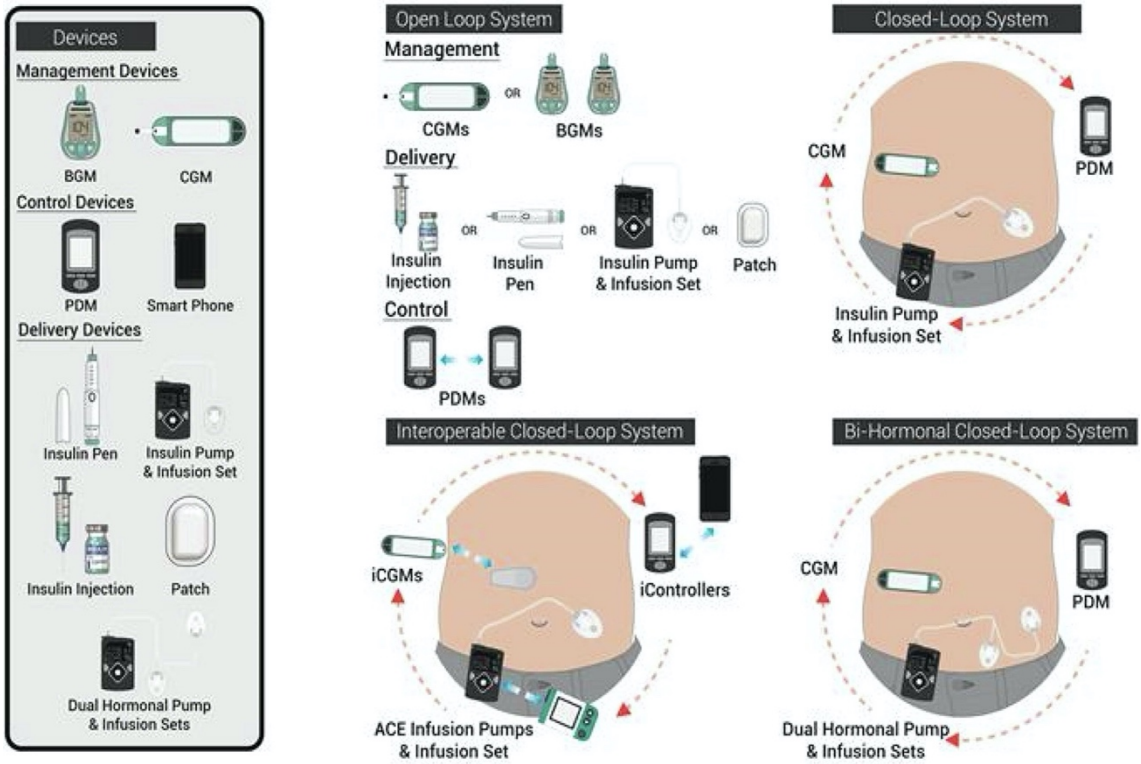

Figure 6.1: Main devices used in diabetes treatment, and their coupling to form open loop systems, closed-loop systems (hybrid or fully automated), interoperable closed-loop systems and bi-hormonal closed-loop systems[9].

6.3 References

[1] R. Gifford, ChemPhysChem. 14 (2013) 2032–2044.

[2] P. Rafighi, M. Tavahodi, B. Haghighi, Sens Actuators B Chem. 232 (2016) 454–461.

[3] V. Mani, B. Devadas, S.M. Chen, Biosens Bioelectron. 41 (2013) 309–315.

[4] K.Y. Hwa, B. Subramani, Biosens Bioelectron. 62 (2014) 127–133.

[5] A.F. Geiss, T.M.B. Reichhart, B. Pejker, E. Plattner, P.L. Herzog, C. Schulz, R. Ludwig, A.K.G. Felice, D. Haltrich, ACS Sustain Chem Eng. 9 (2021) 7086–7100.

[6] A. Muhs, T. Bobrowski, A. Lielpētere, W. Schuhmann, Angew. Chemie Int. Ed. 61 (2022)

[7] J. Wang, Chem Rev. 108 (2008) 814–825.

[8] T. Bobrowski, W. Schuhmann, Curr Opin Electrochem. 10 (2018) 112–119.

[9] D.A. Domingo-Lopez, G. Lattanzi, L. H. J. Schreiber, E.J. Wallace, R. Wylie, J. O'Sullivan, E.B. Dolan, G.P. Duffy, Adv Drug Deliv Rev. 185 (2022) 114280.

APPENDIX

Supplementary Information for Chapter 2-5 in thesis

A.1 Publications

K. Jayakumar, R. Bennett, D. Leech, Electrochemical glucose biosensor based on an osmium redox polymer and glucose oxidase grafted to carbon nanotubes: A design-of-experiments optimisation of current density and stability, Elsevier Ltd, 2021. https://doi.org/10.1016/j.electacta.2021.137845.

K. Jayakumar, T.M.B. Reichhart, C. Schulz, R. Ludwig, A.K.G. Felice, D. Leech, An Oxygen Insensitive Amperometric Glucose Biosensor Based on An Engineered Cellobiose Dehydrogenase: Direct versus Mediated Electron Transfer Responses, ChemElectroChem. 9 (2022). https://doi.org/10.1002/celc.202200418.

K. Jayakumar, A. Lielpetere, D.A. Domingo-Lopez, R.E. Levey, G.P. Duffy, W. Schuhmann, D. Leech, Tethering zwitterionic polymer coatings to mediated glucose biosensor enzyme electrodes can decrease sensor foreign body response yet retain sensor sensitivity to glucose, Biosens. Bioelectron. 219 (2023) 114815. https://doi.org/10.1016/j.bios.2022.114815.

A.2 Chapter 2 Supplementary Information : A design-of-experiments optimisation of current density and stability for mediated glucose-oxidising enzyme electrodes stabilised using enzyme grafting to carbon nanotube

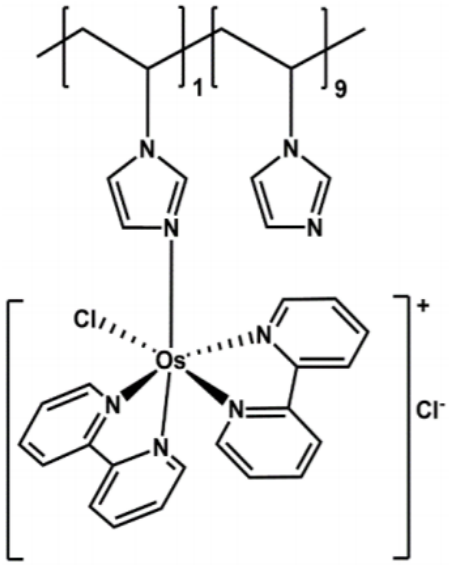

Figure S2.1: Proposed structure of $[Os(2,2'\text{-bipyridine})_2(polyvinylimidazole)_{10}Cl]^+$ (Os(bpy)PVI)

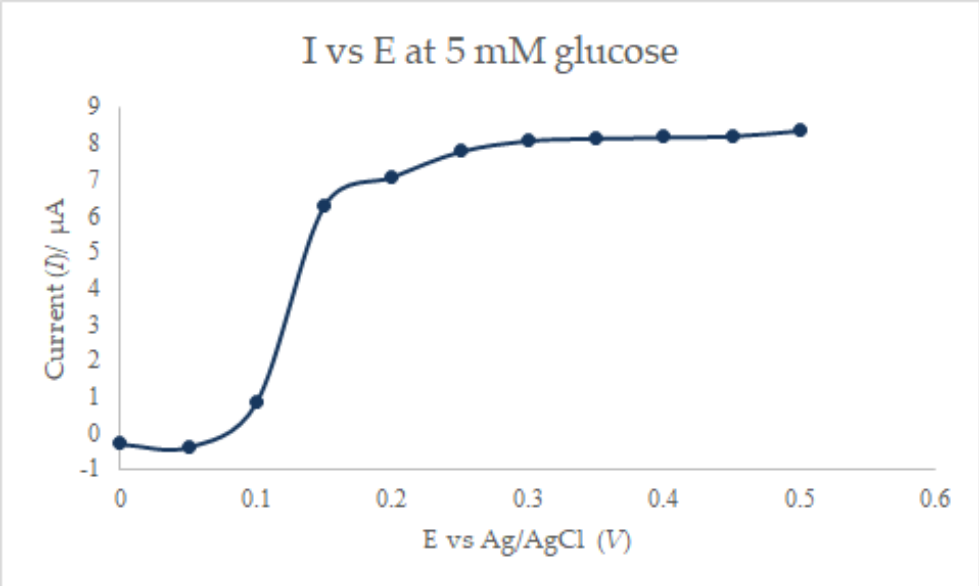

Figure S2.2: Hydrodynamic voltammetry at 5 mM glucose from 0-0.5 V for a system containing Os(bpy)PVI, GOx in 0.5 M PBS.

The hydrodynamic voltammetry experiment was performed with enzyme electrodes prepared using co-immobilised (with PEGDGE) Os-based polymer (5 µL of a 5 mg/mL solution) and GOx (10 µL of a 10 mg/mL solution) on graphite electrodes, and placed in phosphate buffered saline to determine the potential at which the system is in a catalytic current generation regime. In the hydrodynamic voltammetry experiment, the electrolyte was agitated at 150 rpm and potential steps from 0-0.5 volts were applied for 2 mins each. The steady-state current was extracted from each of these runs and plotted against potential to give a hydrodynamic voltammogram. From this experiment, it was determined that an applied potential of 0.35 V would be sufficient for amperometry studies.

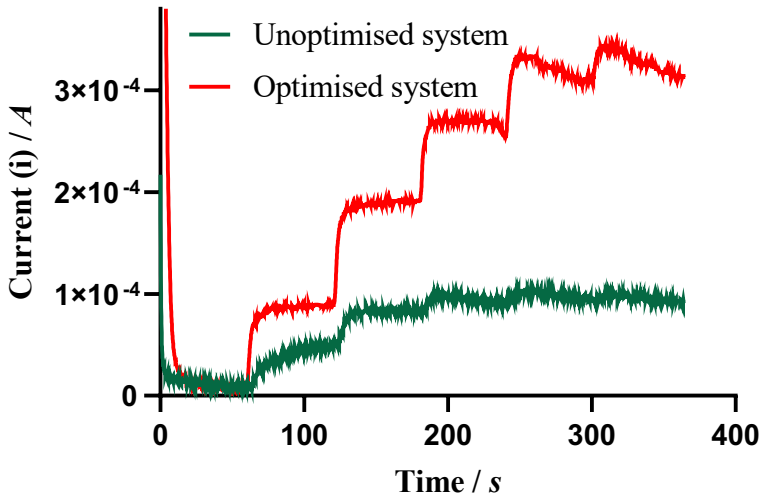

Figure S2.3: Raw amperometry traces of addition of solutions containing 0-5 mM glucose (step changes of 1 mM each) for electrodes used to obtain results displayed in Figures 1-2 (green trace) and Figures 6-7 (red trace).

Figure S2.3 depicts the raw amperometry traces of the systems shown in Figures 2.1, 2.2, 2.6 and 2.7. The green trace shows the raw amperometry obtained from one of the electrodes using unoptimised component amounts in Figures 2.1-2.2 while the red traces show the same for one of the electrodes from the final optimised system in Figures 2.6-2.7. The significant difference in current represents the merit of the DoE optimisation process.

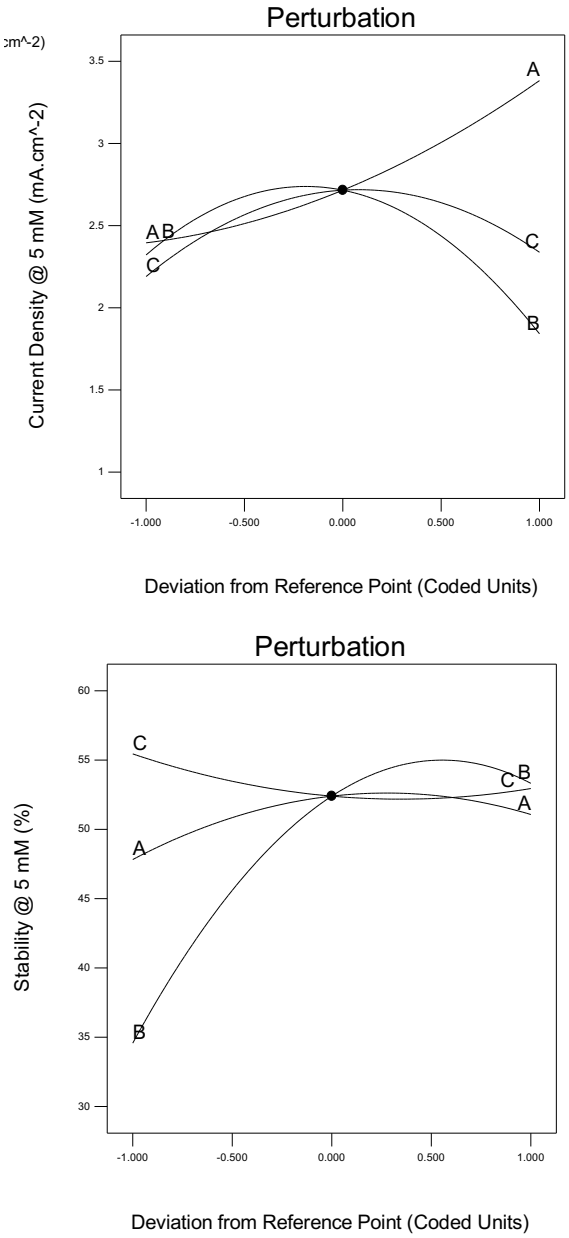

Figure S2.4: Deviation graph of a) predicted current density (mA cm^{-2}) and b) stability (%) versus the deviation of process parameters (A: CNT-GOx, B: Os(bpy)PVI, C: PEGDGE).

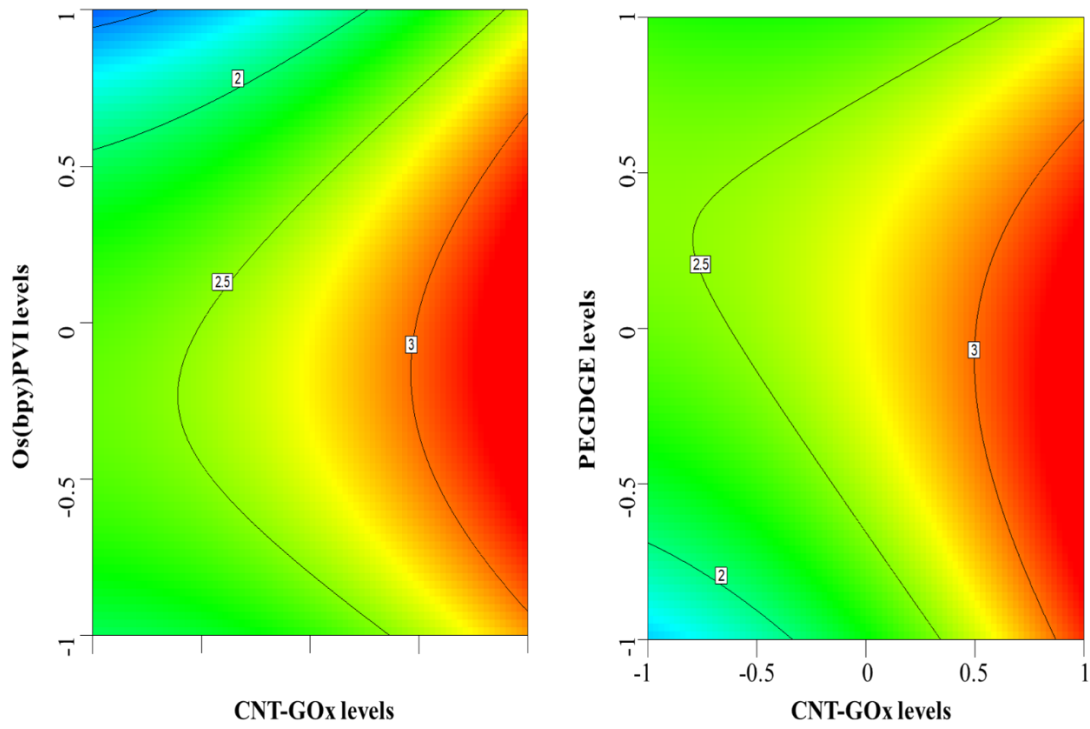

Figure S2.5: Response surface contour plots of a) Os(bpy)PVI vs CNT-GOx levels when PEGDGE is at 72 µg and b) a) PEGDGE vs CNT-GOx levels when Os(bpy)PVI is at 49 µg showing oxidation current density in 5 mM glucose predicted by the model (equation 2). Each contour depicts current density in mA cm^{-2}.

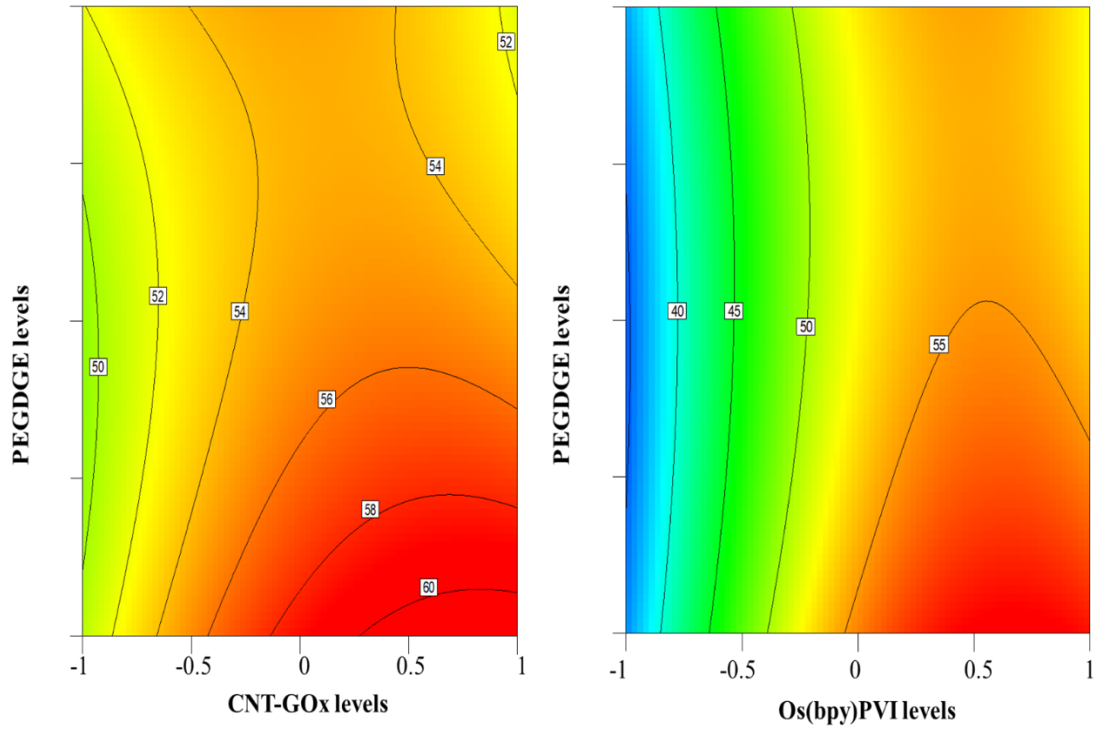

Figure S2.6: Response surface contour plots of a) PEGDGE vs CNT-GOx levels when Os(bpy)PVI is at 75 µg and b) PEGDGE vs Os(bpy)PVI when CNT-GOx is at 93 µg showing

stability at 5 mM glucose over 3 hrs predicted by the model (equation 3). Each contour depicts stability in %.

The contour plots depicted in supplementary Figures S2.5 and S2.6 represent saddlepoints. As the optimum responses or hotspots in these cases are off-centre, it is much more difficult to extract the composition of the parameters that would give an optimum response from these figures.

$$\text{Desirability (D)} = \left(\prod_{i=1}^{n} d_i \right)^{1/n} \qquad \text{Supplementary equation } \mathbf{S2.1}$$

Where D is the overall objective desirability function of the system; d_i, which ranges from 0 to 1 (least to most desirable, respectively), represents the desirability of each individual (i) response; and n is the number of responses being optimized.

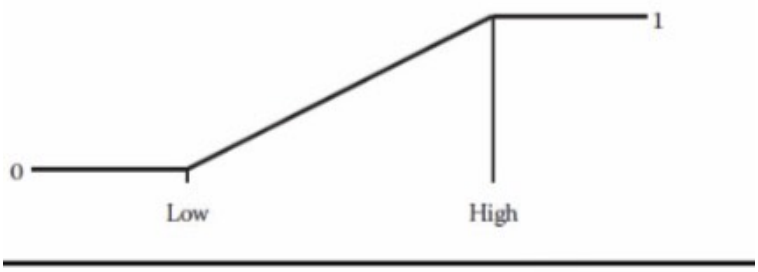

Figure S2.7 : Desirability ramp shown by the Design Expert software when the goal assigned to a response is maximisation.

The individual desirability functions are realised by assigning a goal of maximising or minimising the response within the range investigated by the design. Factors can be assigned a goal of being maximised, minimised or in range, where in range means the full range of the design is accessible during the optimisation. The overall desirability D can be plotted with contours or in 3D using the same tools as those used for the response surface methodology analysis for single responses.

A.3 Chapter 3 Supplementary Information: An Oxygen Insensitive Amperometric Glucose Biosensor Based on An Engineered Cellobiose Dehydrogenase : Direct versus Mediated Electron Transfer Responses

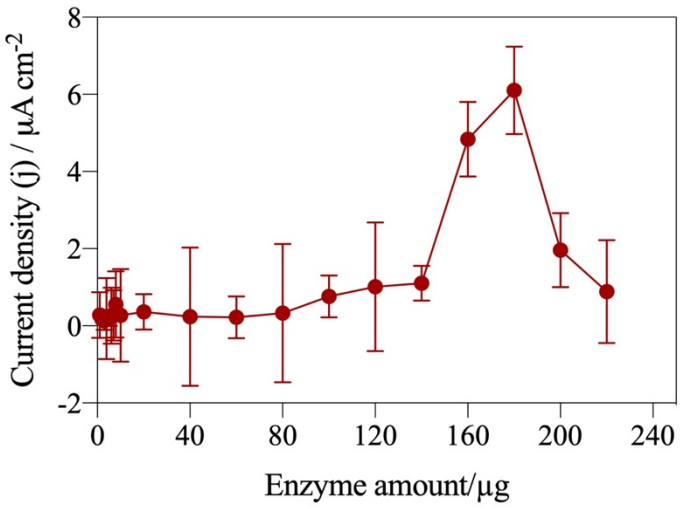

Fig. S3.1: Current density at 5 mM glucose across a range of CDH enzyme amounts

The current density at 5 mM was extracted and plotted as a function of CDH amount (Figure S3.1). An optimum was found at 160 µg and 180 µg. Electrodes were made with these enzyme amounts and delivered current densities of 5.04 ± 0.97 µA cm^{-2} (n = 4) and 6.26 ± 1.13 µA cm^{-2} (n = 4) respectively. The sensors had K_m^{app} values of 14.8 mM (n = 4) and 12.4 mM (n = 4) and operational stabilities of 54.6 ± 0.7 % (n = 4) and 57.4 ± 0.4 % (n = 4) over a 12h time period.

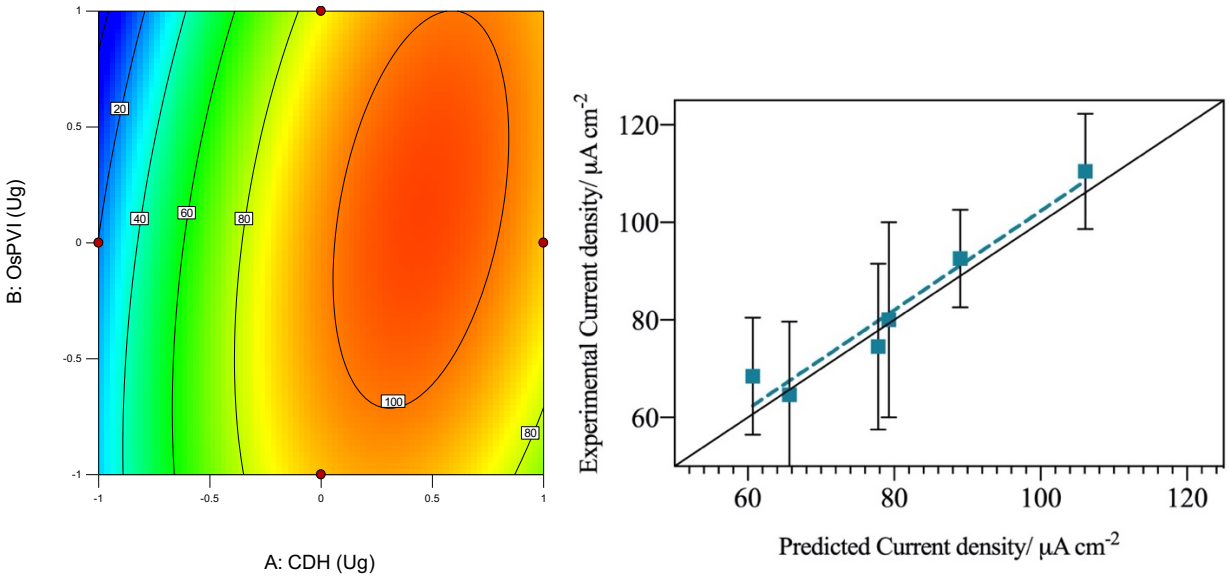

Fig. S3.2: A) Response surface contour plots of OsPVI vs CDH levels when PEGDGE is at 15 µg showing glucose oxidation current density in 5 mM glucose predicted by the model. Each contour depicts current density in µA cm^{-2}. B) Validation of the model through confirmation runs.

The DoE optimum component amounts using the model equations are 160 µg CDH, 150 µg Os(bpy)PVI redox polymer and 111 µg PEGDGE. The biosensor formulated with these component values is predicted to deliver a current density of 113.20 ± 17.21 µA cm^{-2} in PBS containing 5 mM glucose. An actual measured current density of 97.67 ± 11.12 µA cm^{-2} (n = 4) is obtained for the enzyme electrodes prepared using the DoE determined optimum component amounts. The experimental value is lower than the predicted response but well within the standard deviation. The sensor had a K_m^{app} value of 37.9 mM (n = 4) and operational stability of 53.04 ± 1.10 % (n = 4) over a 12h time period.

A.4 Chapter 4 Supplementary Information: Tethering zwitterionic polymer coatings to mediated glucose biosensor enzyme electrodes can decrease sensor foreign body response yet retain sensor sensitivity to glucose

S4.1. Materials and methods

S4.1.1 Spectroscopy

^{1}H-NMR spectra were recorded with a DPX200 spectrometer from Bruker. The residual solvent peak was used as an internal standard for the determination of chemical shifts.

S4.1.2 Synthesis

All reactions and manipulations were conducted using the standard Schlenk technique under argon atmosphere. Polymer structure and nomenclature are presented in Figure 4.1, based on the monomer selection and reaction depicted in Figure 4.2.

S4.1.2a Synthesis of SB-BA, P(DMAPS^{50}-GMA^{30}-BA^{20})

Under an argon atmosphere, DMAPS ([2-(methacryloyloxy)ethyl] dimethyl-(3-sulfopropyl) ammonium hydroxide) monomer **1a** (1.355 g, 4.85 mmol, 50%) was dissolved in 7 mL water and GMA (glycidyl methacrylate) monomer **2** (397 µL, 414 mg, 2.91 mmol, 30%) and BA (butyl acrylate) monomer **3** (279 µL, 249 mg, 1.94 mmol, 20%) were dissolved in 10 mL of isopropanol. The mixture was deaerated with extensive argon bubbling for 7 min. Radical initiator AIBN (2.5 mg, 0.015 mmol) was then added. The reaction mixture was stirred for 21 h (overnight) at 70°C. After cooling down to RT, the reaction mixture was quenched with 10 mL THF. The precipitated polymer was separated by centrifugation (4000 rpm, 15 min) and lyophilised for dryness (in HV, 30 min).

^{1}H-NMR (200.13 MHz, D_2O): δ/ppm 4.54 (broad, -CH_2O- of DMAPS), 4.06 (broad, epoxide), 3.84 (broad, -CH_2O- of BA), 3.63 (broad, -CH_2CH_2-N^+ of DMAPS), 3.27 (broad, $(CH_3)_3N^+$-), 3.02 (broad, overlapping, -$CH_2SO_3^-$ & epoxide), 2.31 (broad,

overlapping, epoxide & -$N^+(CH_2)_2\mathbf{CH_2}SO_3^-$), 2.04 (broad, CH_3 of the backbone), 1.73 & 1.03 (broad, overlapping, -CH_2- of the backbone & BA).

S4.1.2.b Synthesis of MPC-BA P(MPC^{50}-GMA^{30}-BA^{20})

Under an argon atmosphere, MPC (2-methacryloyloxyethyl phosphorylcholine) monomer **1b** (200 mg, 0.68 mmol, 50%) was dissolved in 1 mL H_2O and GMA monomer **2** (56 µL, 58 mg, 0.41 mmol, 30%) and BA monomer **3** (39 µL, 34.6 mg, 0.27 mmol, 20%) were dissolved in 1.4 mL of isopropanol. The mixture was deaerated with extensive argon bubbling for 7 min. AIBN (0.5 mg, 0.003 mmol) was then added. The reaction mixture was stirred for 21 h (overnight) at 70°C. After cooling down to RT, the reaction mixture was quenched with 10 mL THF. The precipitated polymer was separated by centrifugation (4000 rpm, 15 min) and lyophilised for dryness (in HV, 30 min).

^{1}H-NMR (200.13 MHz, D_2O): δ/ppm 4.5 (broad, -CH_2O-), 4.3 and 4.1 (2x -CH_2-PO_4^-), 3.69 (-CH_2-N^+-) 3.43 (epoxide), 3.24 (3x CH_3N^+-), 3.0 and 2.85 (epoxide), 1.97, 1.65 and 1.46 (broad, -CH_2- of BA and -CH_2- groups of the backbone), 0.93 (broad, -CH_3 of BA and -CH_3 groups of the backbone)

S4.1.2.c Synthesis of MPC, P(MPC^{70}-GMA^{30})

Under an argon atmosphere, MPC monomer **1b** (200 mg, 0.68 mmol, 70%) was dissolved in 1 mL H_2O and GMA monomer **2** (40 µL, 41.37 mg, 0.29 mmol, 30%) was dissolved in 0.6 mL isopropanol. The mixture was deaerated with extensive argon bubbling for 10 min. AIBN (0.5 mg, 0.003 mmol) was then added. The reaction mixture was stirred for 21 h (overnight) at 70°C. After cooling down to RT, the reaction mixture was quenched with 12 mL THF. The precipitated polymer was separated by centrifugation (4000 rpm, 15 min) and lyophilised for dryness (in HV, 30 min).

^{1}H-NMR (200.13 MHz, D_2O): δ/ppm 4.51 (broad, -CH_2O-), 4.31 and 4.10 (2x -CH_2-PO_4^-), 3.70 (broad, 3x-CH_2-N^+-) 3.45 (epoxide), 3.24 (broad, 5x CH_3N^+-), 3.01 (-CH_2-SO_3^-), 2.83 (epoxide), 2.28 (-$^+NCH_2$-$\mathbf{CH_2}$-$CH_2SO_3^-$), 2.01 (broad, -CH_2- groups of the backbone), 0.93 (broad, -CH_3 groups of the backbone)

S4.1.2.d Synthesis of MPC-SB P(MPC^{35}-DMAPS^{35}-GMA^{30})

Under an argon atmosphere, MPC monomer **1b** (200 mg, 0.68 mmol, 35%) was dissolved in 1.3 mL H_2O, DMAPS monomer **1a** (190 mg, 0.68 mmol, 35%) dissolved in 0.7 mL H_2O and GMA monomer **2** (79 µL, 82.7 mg, 0.58 mmol, 30%) dissolved in 1.2 mL of isopropanol. The mixture was deaerated with extensive argon bubbling for 7 min. AIBN (0.9 mg, 0.0055) was then added. The reaction mixture was stirred for 21 h (overnight) at 70°C. After cooling down to RT, the reaction mixture was quenched with 25 mL THF. The precipitated polymer was separated by centrifugation (4000 rpm, 15 min) and lyophilised for dryness (in HV, 50 min).
^{1}H-NMR (200.13 MHz, D_2O): δ/ppm 4.51 (broad, -CH_2O-), 4.31 and 4.10 (2x -CH_2-PO_4^-), 3.70 (broad, 3x-CH_2-N^+-) 3.45 (epoxide), 3.24 (broad, 5x CH_3N^+-), 3.01 (-CH_2-SO_3^-), 2.83 (epoxide), 2.28 (-$^+NCH_2$-**CH_2**-$CH_2SO_3^-$), 2.01 (broad, -CH_2- groups of the backbone), 0.93 (broad, -CH_3 groups of the backbone)

S4.1.3 Statistical methods

Statistical significance was determined by one-way ANOVA with a Tukey multiple comparisons test. These statistical analyses were performed using GraphPad Prism 9 (GraphPad software). Statistical significance was set at $p < 0.03$.

S4.1.4. Contact angle measurements

Static WCAs of the polymer coatings were determined using a custom-built goniometer equipped with a CCD camera. A droplet of MilliQ water was applied (n = 3) on the coating and its shape measured after 5s was fitted using contact angle program in ImageJ.

S4.2 NMR data

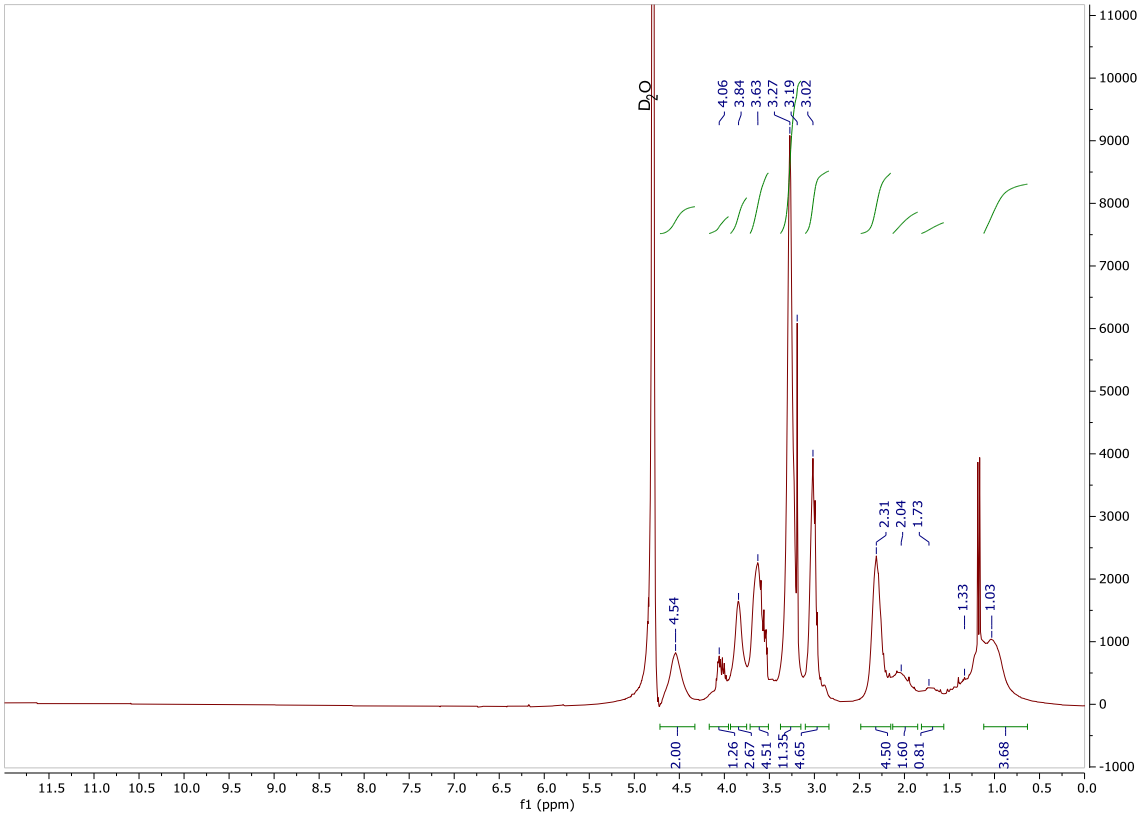

Figure S4.1: ^{1}H-NMR (200 MHz, D_2O) spectrum of the **SB-BA** polymer

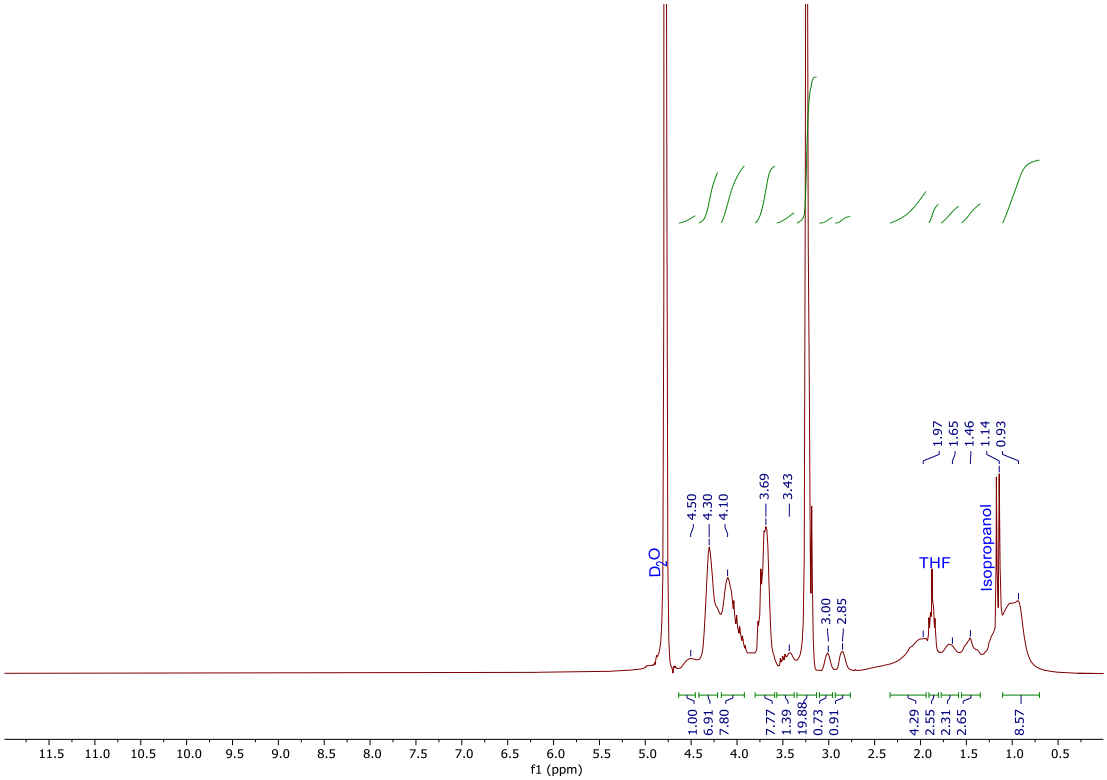

Figure S4.2: ^{1}H-NMR (200 MHz, D_2O) spectrum of the **MPC-BA** polymer

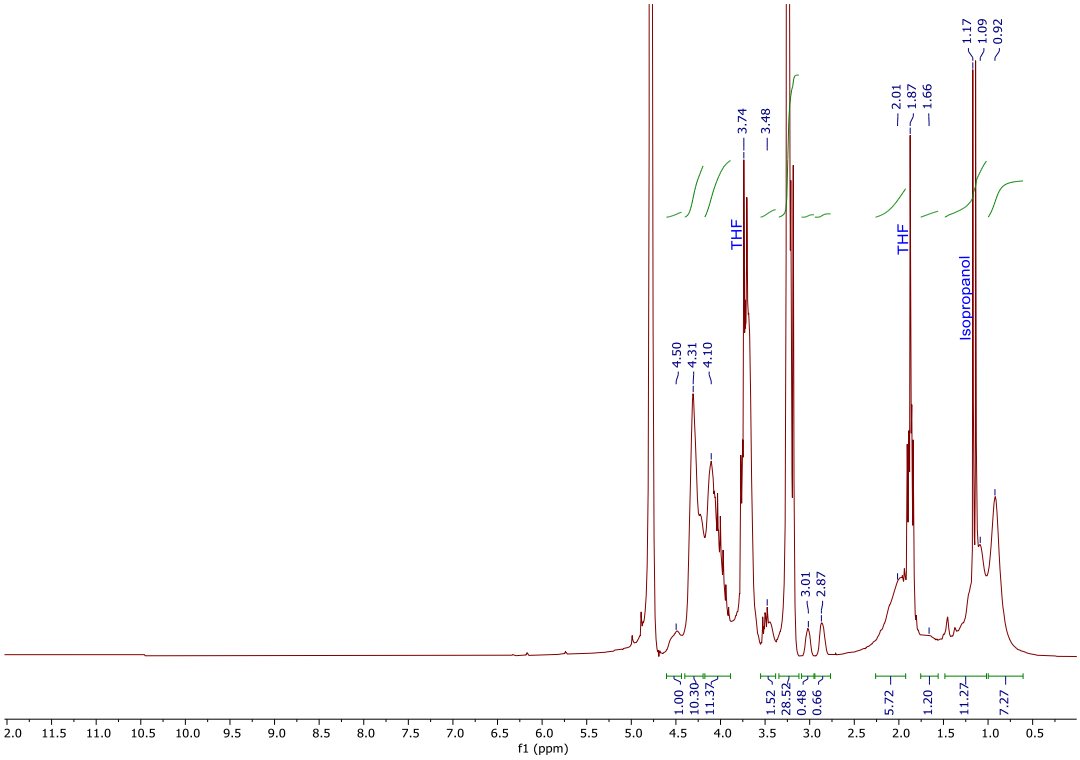

Figure S4.3: ^{1}H-NMR (200 MHz, D_2O) spectrum of the **MPC** polymer

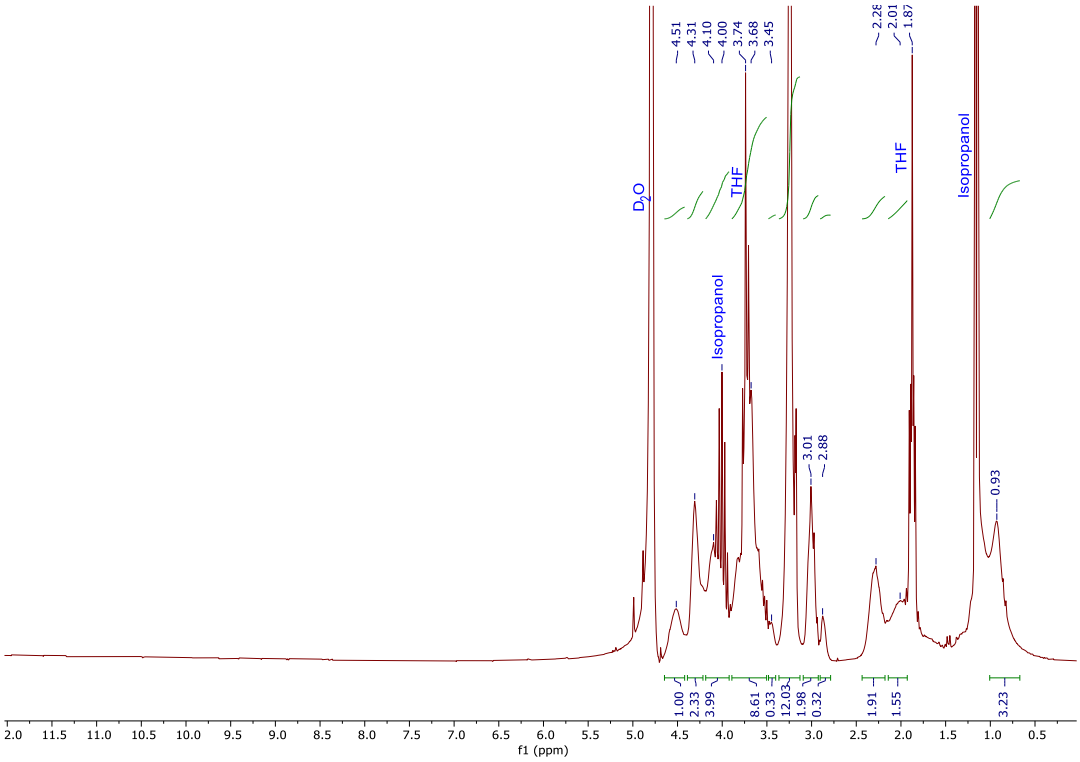

Figure S4.4: ^{1}H-NMR (200 MHz, D_2O) spectrum of the **MPC-SB** polymer

S4.3 Effect of polymer film thickness

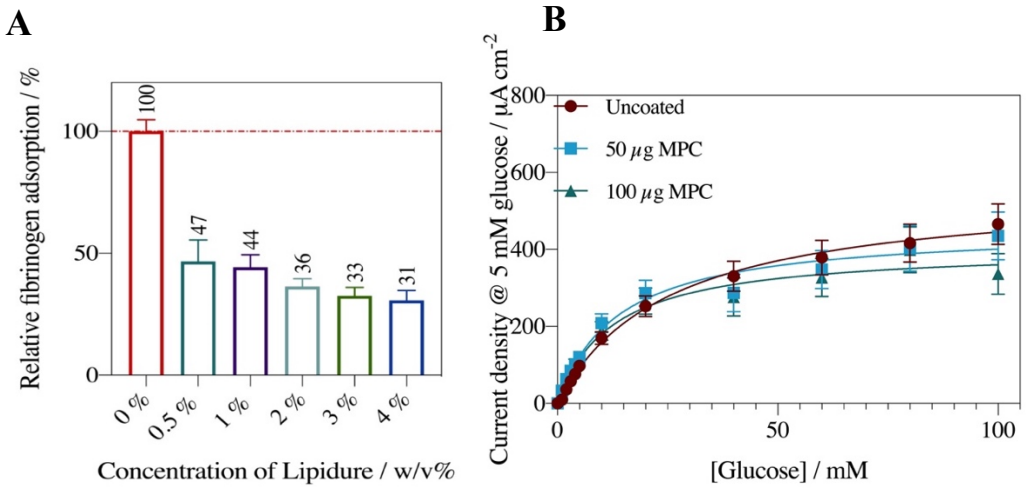

Figure S4.5: A) Effect of Lipidure amount on the relative fibrinogen adsorption B) Effect of MPC film thickness (in μg) on the current density in PBS.

S4.4 $D^{1/2}C$ calculation

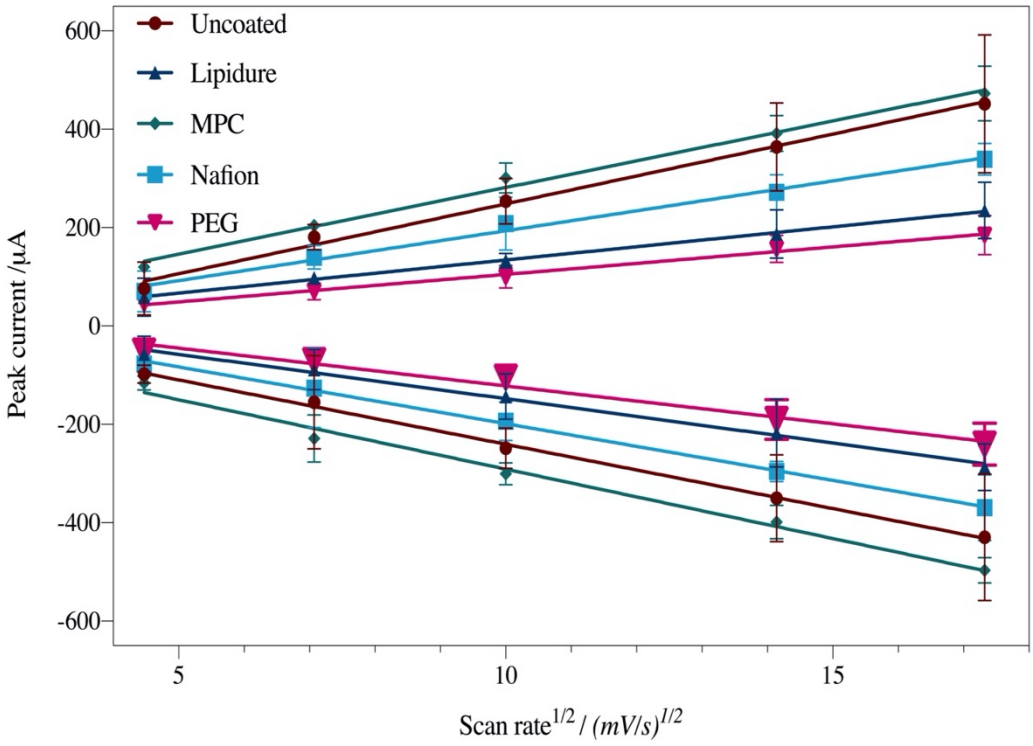

Figure S4.6: Peak current vs scan rate$^{1/2}$ for biosensors in PBS, no glucose substrate, where the slope of the plot is used to extract the $D^{1/2}C$ parameter.

S4.5 Contact angle measurements

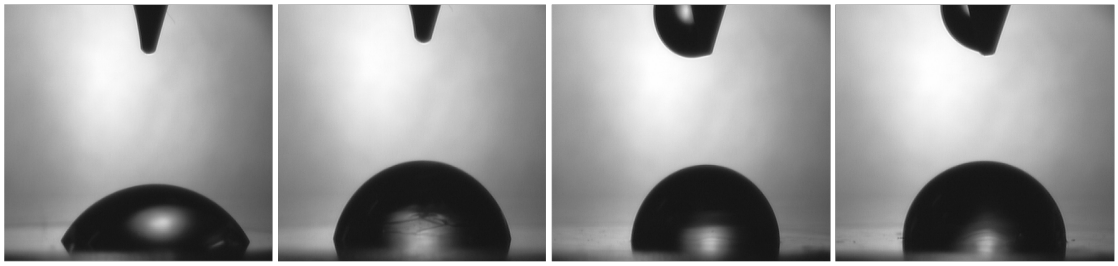

Figure S4.7: Representative image of contact angle measurements of MPC, MPC-SB, MPC-BA and SB-BA (left to right) after 5 s contact with water.

Table S4.1. Contact angle measurements of ZP coated glass slides after 5 s. (n = 3, Mean ± SD)

	MPC	MPC-SB	MPC-BA	SB-BA
Contact angle	49.0 ± 1.3	70.1 ± 8.0	88.6 ± 1.2	86.9 ± 0.7

A.5 Chapter 5 Supplementary Information: Polymer-based multilayer shield for protecting glucose biosensors against interferences and biofouling

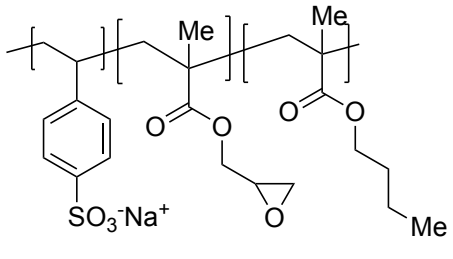

P(SS-GMA-BMA)

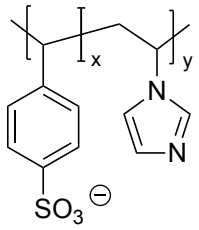

P(VI^{12}-SSNa^{1}) / P(VI^{1}-SSNa^{1})

Figure S5.1: Chemical structures for the negatively charged polymers tested. Monomer ratio in P(SS-GMA-BA) SSNa:GMA:BA 50:30:20; in P(VI^{12}-SSNa^{1}) x = 12, y = 1; in P(VI^{1}-SSNa^{1}) x = 1, y= 1.

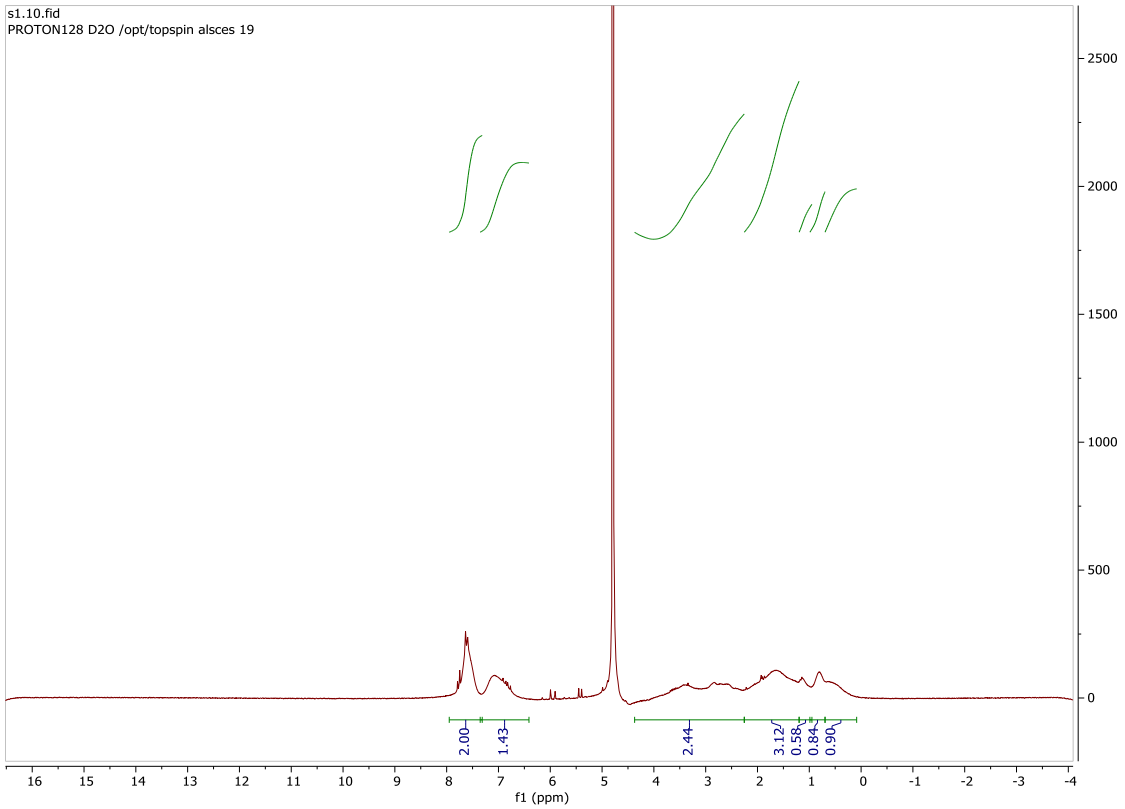

Figure S5.2: ^{1}H-NMR (200 MHz, D_2O) spectrum of the P(SSNa-GMA-BA) polymer

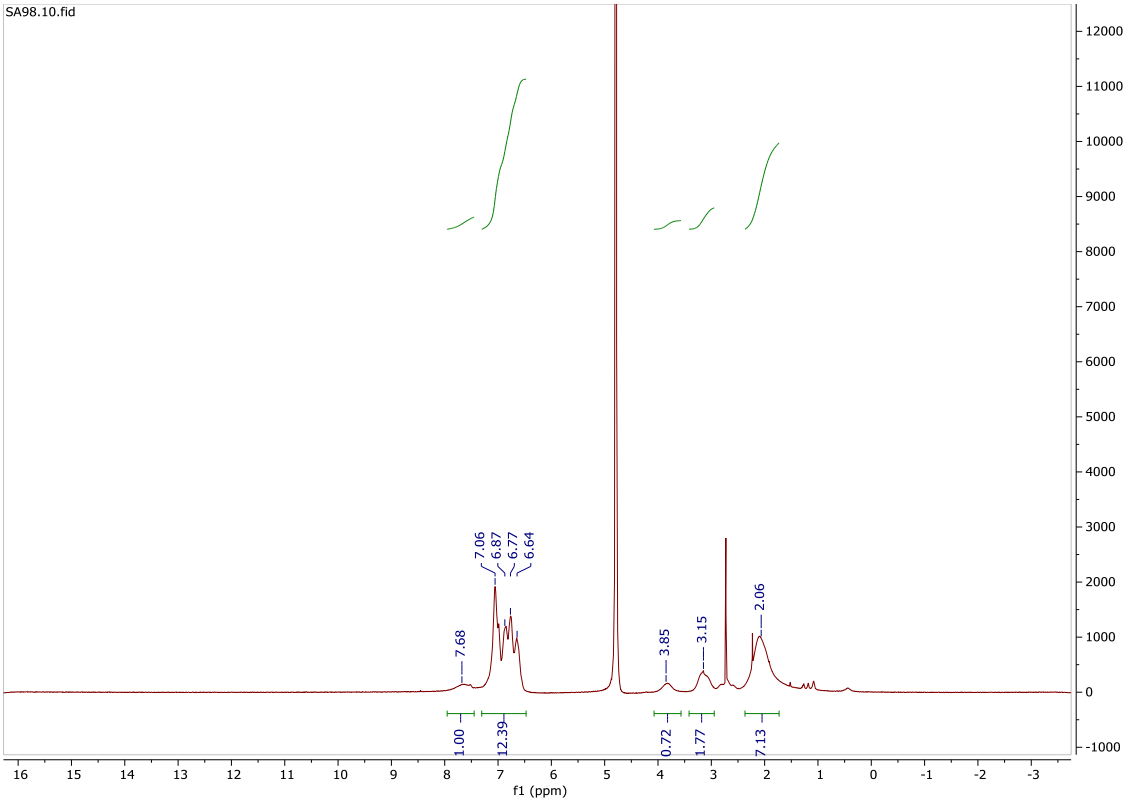

Figure S5.3: ^{1}H-NMR (200 MHz, D_2O) spectrum of the P(SSNa^{1}-VI^{12}) polymer

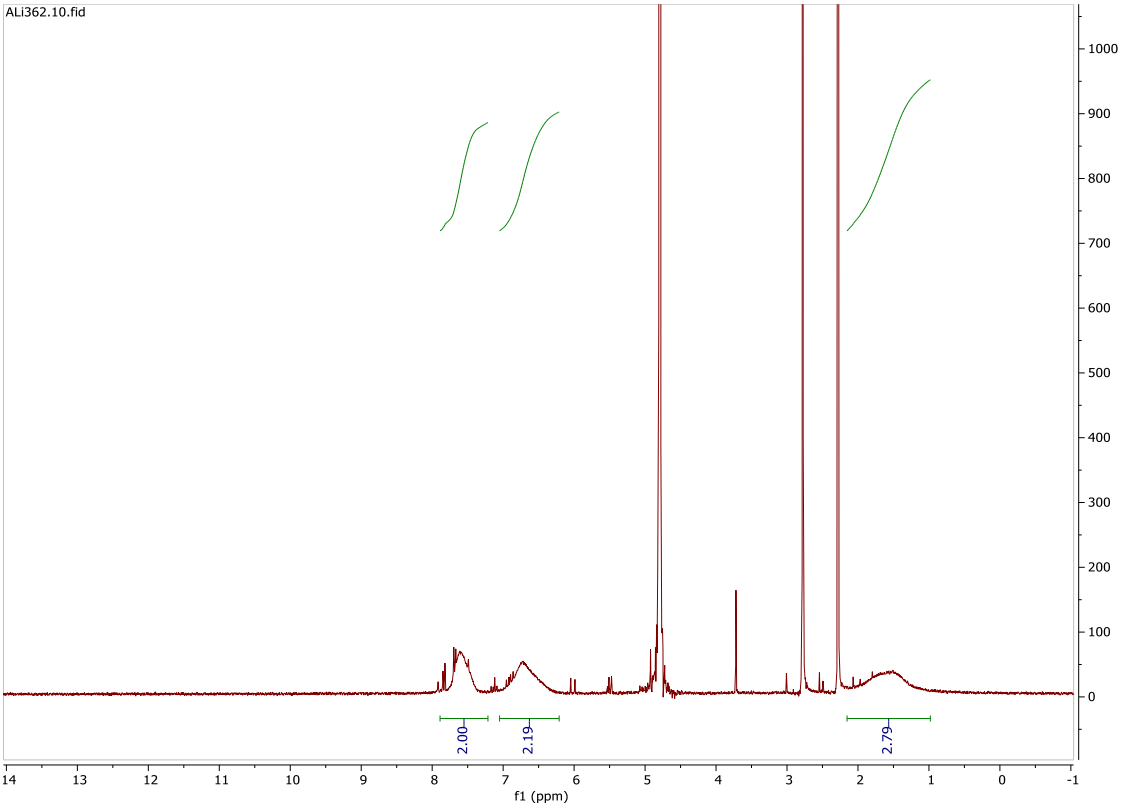

Figure S5.4: ^{1}H-NMR (200 MHz, D_2O) spectrum of the P(SSNa^{1}-VI^{1}) polymer

Table S5.1: K_M^{app} and j_{max} for non-coated control, and systems coated with Lipidure, MPC and Nafion in PBS and artificial plasma. (n = 3, Mean ± SD)

Media	Non-coated control		Lipidure		MPC		Nafion	
	K_M^{app} / mM	j_{max} / µA cm$^-$	K_M^{app} / mM	j_{max} / µA cm$^-$	K_M^{app} / mM	j_{max} / µA cm$^-$	K_M^{app} / mM	j_{max} / µA cm$^-$
PBS	26.2 ± 1.1	557.1 ± 10.5	38.1 ± 7.5	55.9 ± 4.1	13.7 ± 3.1	455.4 ± 12.7	23.4 ± 4.7	261.4 ± 13.1
Artificial Plasma	23.0 ± 1.4	393.8 ± 7.5	24.9 ± 3.9	41.4 ± 11.2	15.5 ± 0.1	427.4 ± 13.2	80.9 ± 10.2	217.5 ± 11.2
BSA	7.3 ± 1.2	291.6 ± 8.2	37.8 ± 12.1	52.2 ± 8.1	14.6 ± 4.8	486.2 ± 19.9	69.8 ± 5.1	278.4 ± 8.1
Uric Acid	14.3 ± 4.5	285.2 ± 14.3	29.5 ± 10.1	40.5 ± 7.4	10.9 ± 1.2	249.2 ± 2.1	20.1 ± 3.2	296.4 ± 11.2

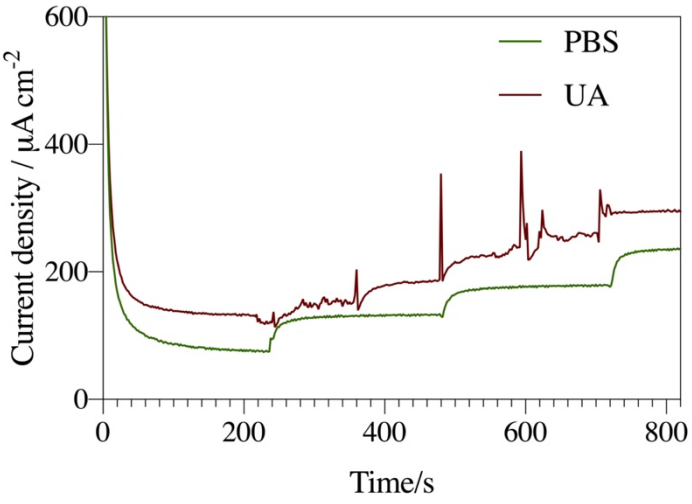

Figure S5.5: Amperometry at 350 mV for the non-coated control in PBS (0.05 M, pH 7.4) and PBS containing uric acid at physiological concentration.

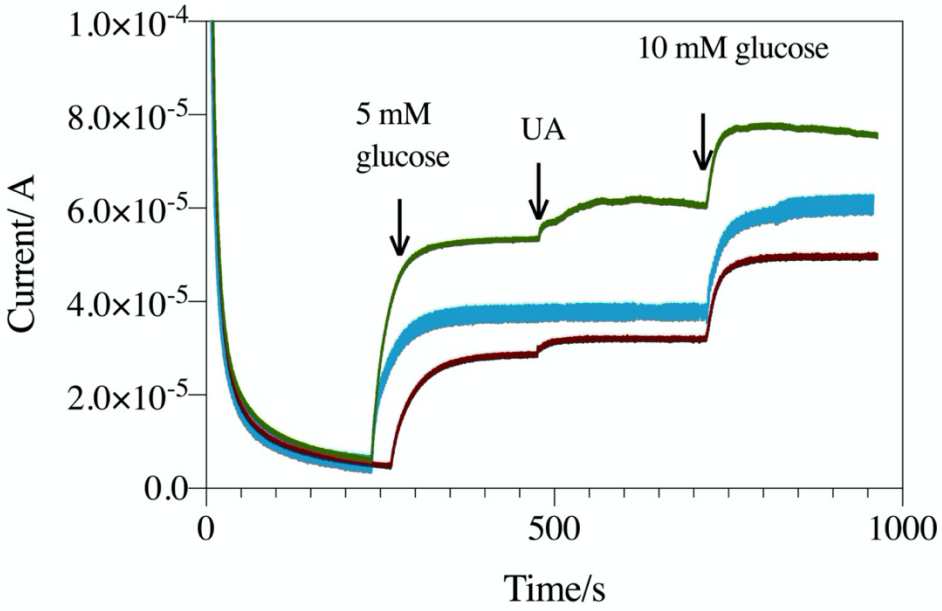

Figure S5.6: Amperometry at 350 mV for the system coated with P(SSNa-GMA-BA) (green), P(VI^{12}-$SSNa^{1}$) (red) and P(VI^{1}-$SSNa^{1}$) (blue) in PBS (0.05 M, pH 7.4).

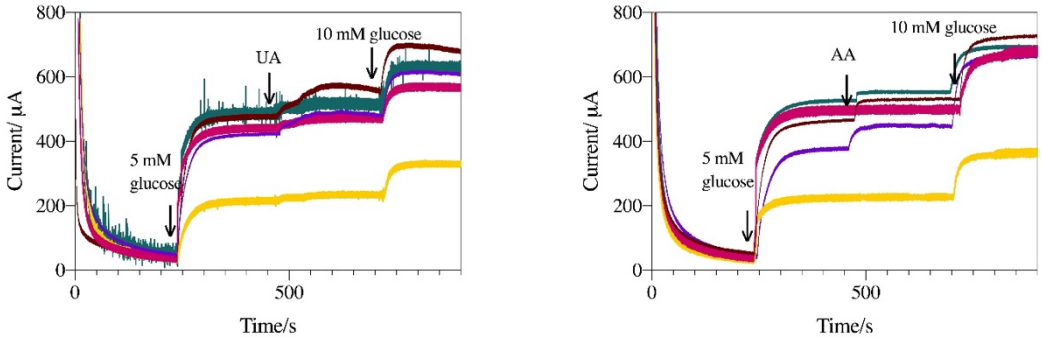

Figure S5.7: Amperometry at 350 mV for the non-coated control (red), system coated with enzyme layer (violet), MPC (green), polymer design (pink) and P(VI^{1}-$SSNa^{1}$) (yellow) in PBS (0.05 M, pH 7.4) with injections of A) uric acid and B) ascorbic acid.

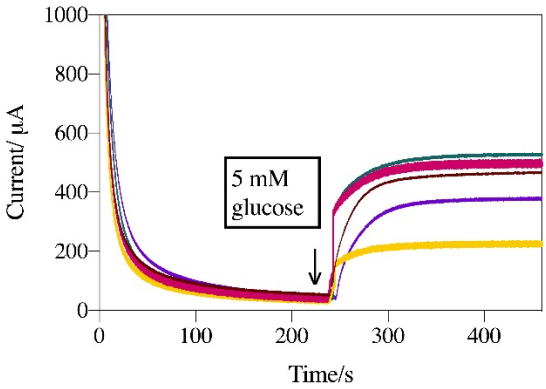

Figure S8: Expanded view of figure S7 amperometric response at 350 mV for the uncoated control Case I (dark red), MPC Case II (green), P(VI^{1}-SSNa^{1}) Case IV (yellow), enzyme layer Case V (violet) and novel polymer design Case VII (pink) in PBS (0.05 M, pH 7.4) with injections 5 mM glucose.